

Supporting Information for

Exploring Copper β -Diketimate Complexes for Heterogeneous Ammonia Oxidation Anchored on Graphitic Surfaces via CH- π and π - π Interactions

*Josep A. Gutiérrez-Orgaz¹, Marco Nicaso¹, Anna M. Beiler¹, Marta
Martínez-Belmonte¹, Jordi Benet-Buchholz¹, Mireia Segado-Centellas^{1,3},
Xavier Sala², Carles Bo^{1,2}, and Antoni Llobet^{*,1}*

¹ Institute of Chemical Research of Catalonia (ICIQ), Barcelona Institute of Science and Technology (BIST), Avda. Països Catalans 16, 43007 Tarragona, Spain

² Departament de Química, Universitat Autònoma de Barcelona (UAB), 08193 Cerdanyola del Vallès, Spain.

³ Departament de Química Física i Inorgànica, Universitat Rovira i Virgili (URV), Marcel·lí Domingo s/n, 43007 Tarragona, Spain

*Corresponding author email: allobet@iciq.cat

Table of Contents

1. General Procedure	4
2. Materials.....	4
3. Electrochemistry	4
3.1. Preparation of Ammonia Solutions	5
4. Synthesis and Characterization	7
4.1. Preparation of 1	7
4.2. Preparation of 2	8
4.3. Preparation of 3	9
4.4. Preparation of HL1	11
4.5. Preparation of HL2	12
4.6. Preparation of HL3	14
4.7. Preparation of HL4	16
4.8. Preparation of HL5	19
4.9. Preparation of HL6	22
4.10. Preparation of HL7	25
4.11. Preparation of HL8	29
4.12. Preparation of HL9	32
4.13. Preparation of HL10	34
4.14. Preparation of [Cu ^I (L1)(MeCN)]	36
4.15. Preparation of [Cu ^{II} (L1)(AcO)].....	37
4.16. Preparation of [Cu ^{II} (L3)(AcO)].....	37
4.17. Preparation of [Cu ^{II} (L3) ₂].....	39
4.18. Preparation of [Cu ^{II} (L4) ₂].....	39
4.19. Preparation of [Cu ^I (L2)(MeCN)]	40
4.20. Preparation of [Cu ^I (L7)(MeCN)]	42
4.21. Preparation of [Cu ^I (L10)(MeCN)]	46
5. Electrochemical Studies	49
5.1. Electrochemistry of HL1	49
5.2. Electrochemistry of HL2	50
5.3. Electrochemistry of HL3	51
5.4. Electrochemistry of HL4	52
5.5. Electrochemistry of Cu ^{II} (AcO) ₂	53
5.6. Electrochemistry of [Cu ^I (MeCN) ₄]CF ₃ SO ₃	54
5.7. Electrochemistry of [Cu ^{II} (L1)(AcO)].....	55
5.8. Electrochemistry of [Cu ^{II} (L3)(AcO)].....	57
5.9. Electrochemistry of [Cu ^{II} (L3) ₂].....	58

5.10. Electrochemistry of [Cu ^{II} (L4) ₂]	59
5.11. Electrochemistry of [Cu ^I (L1)(MeCN)]	60
5.12. Electrochemistry of [Cu ^I (L10)(MeCN)]	68
5.13. Electrochemistry of [Cu ^I (L2)(MeCN)]	73
5.14. Electrochemistry of [Cu ^I (L7)(MeCN)]	78
5.15. Comparative Studies	93
6. Spectroscopical Studies	94
6.1. UV-Vis Studies	94
6.2. NMR Studies	95
7. Crystallographic Details	96
7.1. Data Collection	96
7.2. Structure Solution and Refinement	96
7.3. ORTEP Structures and Comments	97
8. Computational Studies	104
8.1. General Procedure	104
8.2. Structure Optimization and Anchoring	104
9. References	114

1. General Procedure

Synthetic and electrochemical investigations were performed under a dry inert atmosphere by utilizing an MBraun glovebox and/or Schlenk techniques unless otherwise stated. Water content in self-prepared dry solvents was monitored via Karl-Fischer titration. ^1H , $^{13}\text{C}\{^1\text{H}\}$, and ^{19}F NMR spectra were recorded at room temperature (RT) on 300 MHz Bruker Avance Neo or 400 MHz Bruker Avance I spectrometers in appropriate deuterated solvents, with residual protons as internal reference. Multiplicities are reported using the following abbreviations: s = singlet, br s = broad singlet, d = doublet, t = triplet, hept = heptuplet, m = multiplet. **p-XRD** data were collected on a Bruker D8 Advance Powder Diffractometer with a vertical 2θ - θ goniometer in transmission mode, equipped with a $K\alpha_1$ germanium monochromator for Cu radiation ($\lambda = 1.5406$ Å), fixed divergence slits and a diffracted beam radial Soller slit. The system is equipped with a VANTEC single photon counting PSW detector with a 12° overture in 2θ , and a ninety positions auto charger sample stage. **UV-vis** spectra were acquired using a Varian Cary 50 Bio UV-Vis Spectrophotometer. **IR** spectra were recorded on a Cary 640 FTIR-ATR spectrometer. Elemental analysis (**EA**) was conducted in Universidad de Santiago de Compostela; CHNS analyses were performed using a Thermo FlashSmart instrument, and sample weights were measured on an XPR2U microbalance under air. In some cases, the EA results are consistent with the possible incorporation of small amounts of water, likely due to the hygroscopic nature of the samples. Nominal mass measurements by mass spectrometry (**MS**) were obtained using an Agilent 6130 Single quadrupole LC/MS via direct injection.

2. Materials

All chemicals and solvents were purchased from common suppliers (e.g., Sigma-Aldrich, Acros Organics, abcr GmbH, TCI, Carlo Erba Reagents) and used without further purification unless otherwise noted. When reagent purity was not absolute, the purity level is indicated in parentheses. Titanium tetrachloride (Acros Organics) was stored and handled under an inert atmosphere using a Straus flask. Anhydrous THF, DCM, MeCN, hexane, toluene, and Et₂O were obtained by passing them through a solvent purification system (Innovative Technology or MBraun). Other solvents, such as MeOH or TFE, were dried by using activated 3 Å molecular sieves.^{1,2} Electrodes and other accessories were sourced from IJ Cambria Scientific Ltd, while carbon fiber paper (Sigracet 39 AA – 10 x 10 cm) was supplied by Fuel Cell Store. Analytical thin-layer chromatography (TLC) was performed using aluminum sheets coated with silica gel 60 (Merck, 10554). Chromatograms were visualized under UV light. Silica gel (Sigma Aldrich, 717185) with a pore size 60 Å, 230-400 mesh, and 40-63 μm particle size was used for column chromatography. Celite[®] 545 (Merck, 102693), with a particle size of 0.02-0.1 mm, was also used for certain filtrations.

3. Electrochemistry

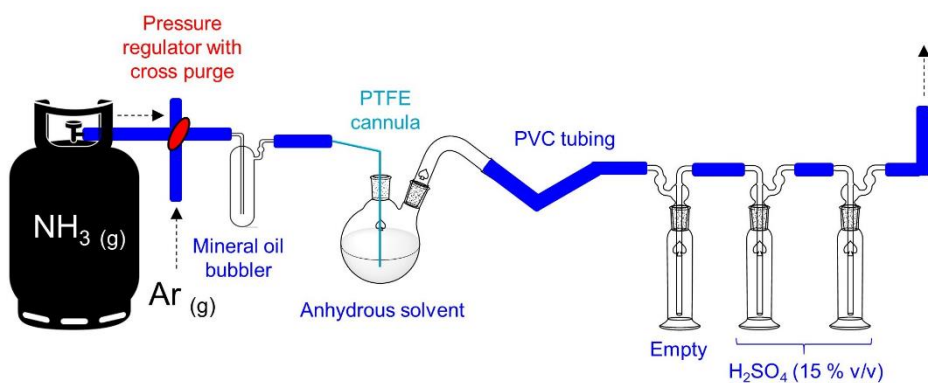
Electrochemical measurements were performed on IJ-Cambria CHI-660C or CHI-730D potentiostats using custom-built, one-compartment glass cells with a three-electrode configuration at RT unless otherwise specified. Glassy carbon disk (GC_{disk} ; $S = 0.07$ cm²) or carbon fiber paper (C_{FP} ; 0.5 cm x 0.5 cm; geometric $S = 0.25$ cm²) were used as working electrodes (WE) for homogeneous or heterogeneous electrochemistry, respectively. A Pt Electrode Clamp (ANR Tech) was used to hold the C_{FP} electrodes. C_{FP} electrodes were approximately 2 cm x 0.5 cm in size, with a 0.5 cm x 0.5 cm area used for soaking functionalization and electrochemical studies. Current densities were calculated based on the 0.25 cm² geometric area. Generally, functionalized C_{FP} electrodes prepared inside a glovebox were rapidly connected to the Pt Electrode Clamp in air and then used in a custom glass cell under an inert atmosphere. A Pt wire

or disk served as the counter electrode (CE). A pseudo-reference electrode was prepared by coating a sanded Ag wire with AgCl: the Ag wire was soaked in bleach for 30 seconds to form the AgCl layer, rinsed with water and acetone, dried with nitrogen, and immersed in the same electrolyte solution as the working electrode, separated by a frit. This Ag/AgCl electrode provided a relatively stable reference potential with a shift of ≤ 10 mV, verified against the ferrocene/ferrocenium ($\text{Fc}^{+/0}$) couple before and after experiments.³ Cyclic voltammetry (CV) experiments were carried out at a scan rate of 100 mV s^{-1} unless otherwise noted. All the electrochemical experiments in this work were iR-compensated at 85%, except for controlled potential electrolysis (CPE) experiments. TBAPF₆ ($\geq 98\%$, Sigma Aldrich) was recrystallized from absolute EtOH (Bp/RT), isolated via vacuum filtration, washed with absolute EtOH, and dried under vacuum overnight at RT.

3.1. Preparation of Ammonia Solutions

The preparation of ammonia solutions in organic solvents started by purging the anhydrous solvent (typically 20-50 mL) with Ar for 5 mins using a 2-neck round-bottom flask (Figure S1) or a commercially available bottle sealed with a septum.

(a)



(b)



Figure S1. Setup for the preparation of NH_3 solutions in organic solvents.

Ammonia gas (Air Liquide, 99.96%) was then sparged into the anhydrous, air-free solvent (typically for 10-30 min) at RT. The outgas was neutralized by passing it through an aqueous sulfuric acid solution (15% v/v). Finally, Ar was passed through the headspace for 5 min, and the resulting solution was stored under an inert atmosphere at RT. Straus flasks were used to introduce the prepared NH_3 solutions into the glovebox.

The concentration of NH_3 in the prepared solutions was determined before each electrochemical experiment by adding 1 part of the ammonia solution (in MeOH, propylene carbonate [PC], MeCN or TFE [2,2,2-trifluoroethanol]) to 19 parts of water and titrating the miscible mixture with a 0.1 M HCl aqueous solution, which had been previously standardized using a 0.05 M sodium carbonate aqueous solution (Figure S2). The titrations were repeated three times, using either a pH meter or methyl orange indicator to determine the equivalence point.

Commercially available 0.5 M NH_3 in THF (Acros Organics) and 2 M NH_3 in MeOH (Aber Chemicals) solutions were also used.

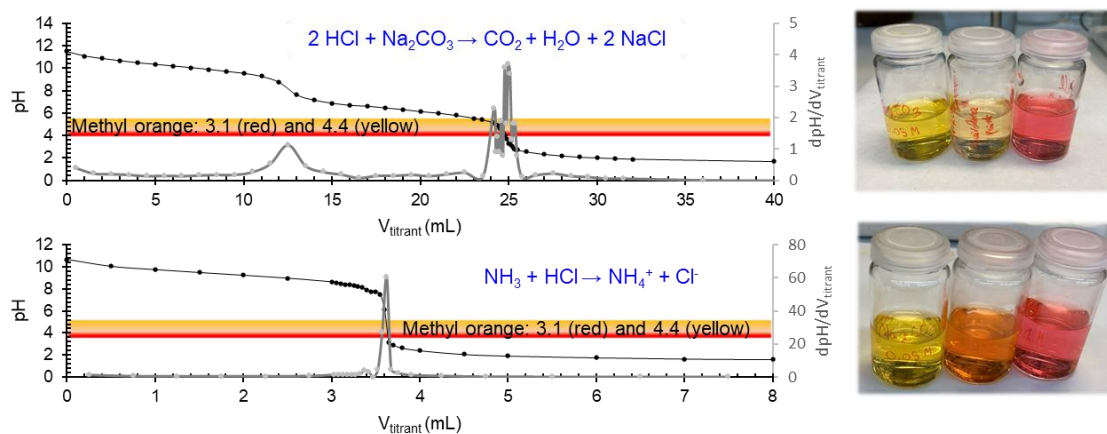
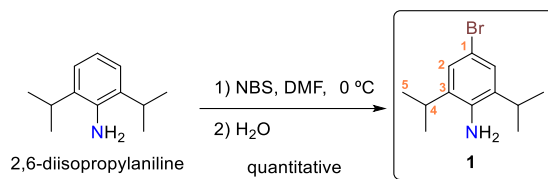


Figure S2. Representative example of HCl standardization and NH_3 titration using methyl orange and a pH meter.

4. Synthesis and Characterization

4.1. Preparation of **1**



The preparation of **1** has been previously reported in the literature.⁴ A solution of *N*-bromosuccinimide (NBS) (20.7 g, 114 mmol, 98%) in anhydrous DMF (50 mL) was added dropwise over 30 min to a stirred solution of 2,6-diisopropylaniline (19.7 g, 100 mmol, 97%) in anhydrous DMF (100 mL) at 0 °C under an inert atmosphere. The reaction mixture was stirred at 0 °C for 1 h, after which water (150 mL) and brine (50 mL) were added. The resulting mixture was extracted with EtAcO (3 x 200 mL), and the combined organic layers were washed with saturated NH₄Cl solution (3 x 100 mL), followed by water (100 mL) and brine (100 mL), and then dried over anhydrous Na₂SO₄. After solvent removal, **1** was obtained as a dark red oil in quantitative yield and used without further purification. ¹H NMR (400 MHz, CDCl₃) δ (ppm): 7.11 (s, 2H, **H2**), 3.71 (br s, 2H, **NH₂**), 2.88 (hept, $J_{\text{H4-H5}} = 7.0$ Hz, 2H, **H4**), 1.25 (d, $J_{\text{H5-H4}} = 7.0$ Hz, 12H, **H5**).

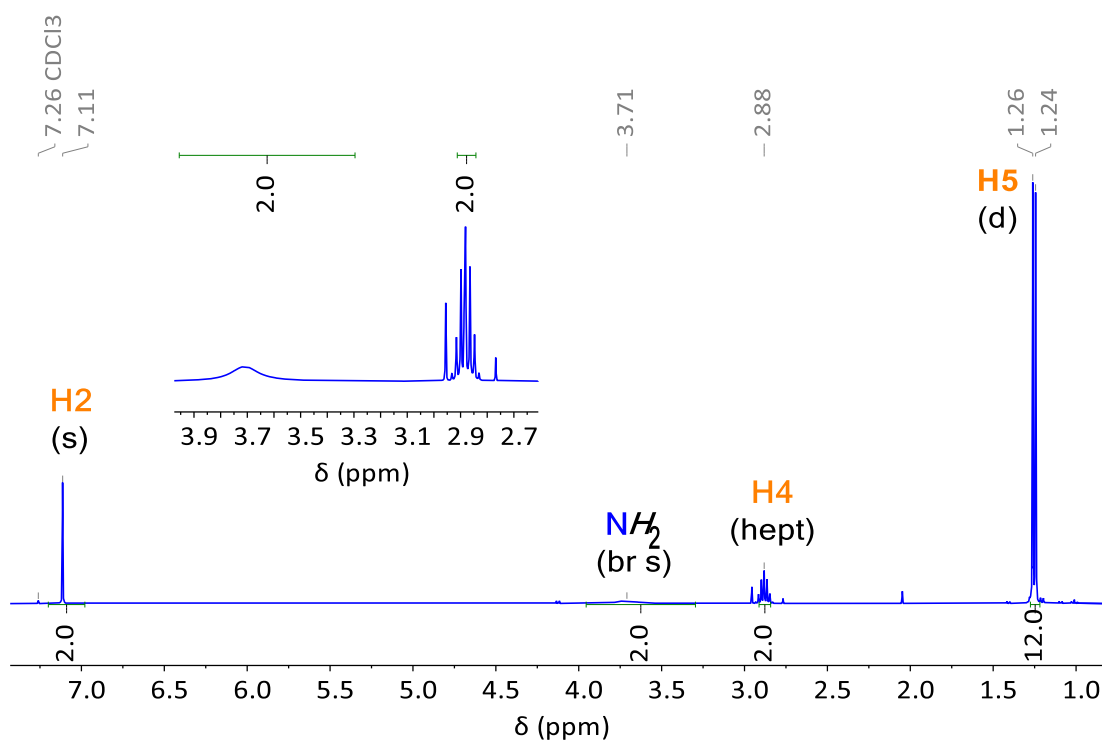
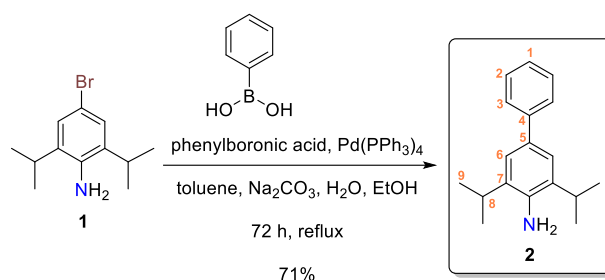


Figure S3. ¹H NMR spectrum (400 MHz, CDCl₃) of **1**.

4.2. Preparation of **2**

The preparation of **2** has been previously reported in the literature.^{5,6} **1** (8.0 g, 31 mmol), phenylboronic acid (5.74 g, 47 mmol) and $\text{Pd}(\text{PPh}_3)_4$ (1.81 g, 1.55 mmol, 99%) were dissolved in toluene (200 mL) and EtOH (50 mL). The mixture was purged with inert gas for 30 min. Meanwhile, Na_2CO_3 (80 mL, 2 M solution in water) was also purged with inert gas for 30 min, and then added to the reaction mixture. The biphasic reaction mixture was slowly heated to reflux, during which an exothermic reaction occurred, causing the reaction mixture to turn black. The resulting mixture was maintained under reflux for 3 days under an inert atmosphere. After cooling to RT, the organic layer was separated and filtered through toluene-rinsed Celite pad. The filtrate was dried over anhydrous Na_2SO_4 , and the solvent was removed under vacuum. The residue was purified by column chromatography (wet loading in eluent, silica gel, hexane/DCM 1:1, $R_f \sim 0.4$) to yield **2** (5.67 g, 22 mmol, 71%) as a colorless oil. $^1\text{H NMR}$ (400 MHz, CDCl_3) δ (ppm): 7.59 (m, 2H, **H3**), 7.43 (t, 2H, $J_{\text{H2-H1}} = J_{\text{H2-H3}} = 8.0$ Hz, **H2**), 7.31 (m, 3H, **H1 + H6**), 3.81 (br s, 2H, **NH**), 3.01 (hept, $J_{\text{H8-H9}} = 7.0$ Hz, 2H, **H8**), 1.36 (d, $J_{\text{H9-H8}} = 7.0$ Hz, 12H, **H9**).

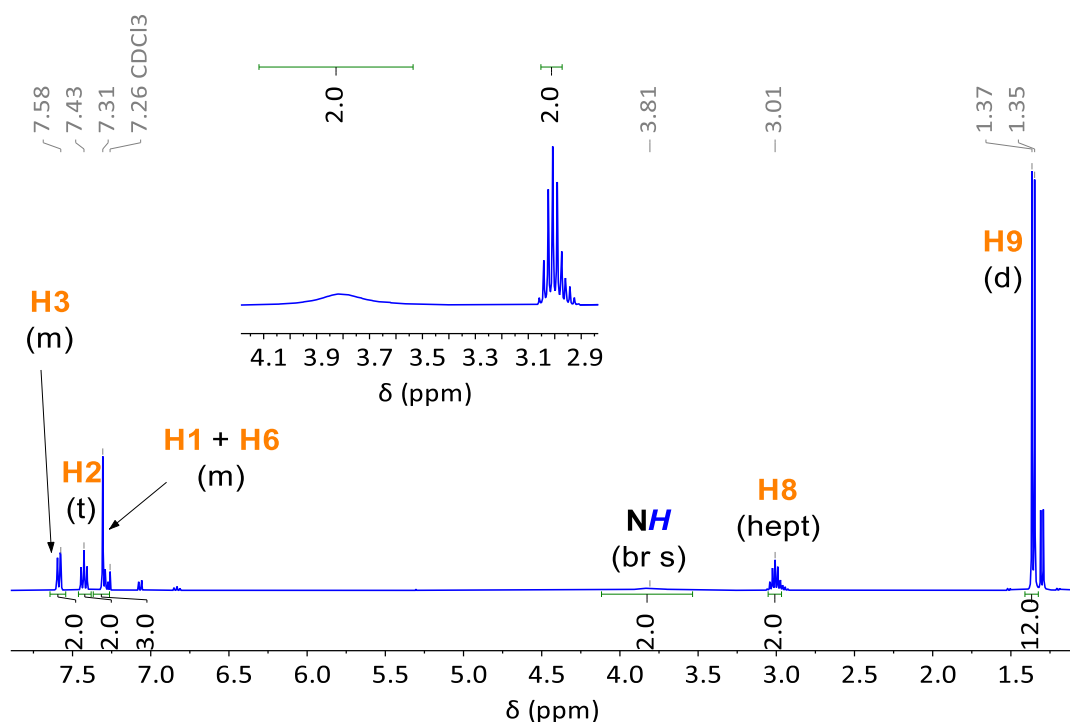
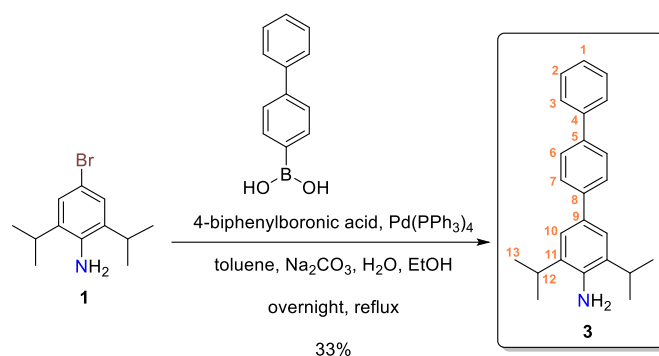


Figure S4. $^1\text{H NMR}$ spectrum (400 MHz, CDCl_3) of **2**.

4.3. Preparation of **3**

1 (18.0 g, 70 mmol), 4-biphenylboronic acid (21.3 g, 106 mmol, 98%) and Pd(PPh₃)₄ (4.10 g, 3.51 mmol, 99%) were dissolved in toluene (200 mL) and EtOH (50 mL). The mixture was purged with inert gas for 30 min. Meanwhile, Na₂CO₃ (80 mL, 2 M solution in water) was also purged with inert gas for 30 min, and then added to the reaction mixture. The biphasic reaction mixture was slowly heated to reflux, during which an exothermic reaction occurred, causing the reaction mixture to turn black. The resulting mixture was maintained under reflux overnight under an inert atmosphere. After cooling to RT, this was filtered through toluene-rinsed Celite pad, and the dark organic layer was separated and dried over anhydrous Na₂SO₄. The solvent was removed under reduced pressure and a brown/purple solid was obtained as a residue, which was purified by column chromatography (silica gel, wet loading in DCM, hexane/DCM 8:2 to DCM, *R_f* ~ 0.1) and triturated in hexane to obtain pure **3** (7.55 g, 22.9 mmol, 33%) as a white solid. ¹H NMR (400 MHz, CDCl₃) δ (ppm): 7.70-7.63 (m, 6H, **Ar**), 7.50-7.44 (m, 2H, **Ar**), 7.41-7.31 (m, 3H, **Ar**), 3.84 (br s, 2H, **NH**₂), 3.01 (hept, *J*_{H12-H13} = 7.0 Hz, 2H, **H12**), 1.36 (d, *J*_{H13-H12} = 7.0 Hz, 12H, **H13**). ¹³C{¹H} NMR (101 MHz, CDCl₃) δ (ppm): 141.39, 141.07, 140.12, 138.94, 132.80, 130.86, 128.86, 127.42, 127.16, 127.07, 121.79, 28.20, 22.60. **MS** (APCI⁺, MeOH) *m/z* calcd for C₂₄H₂₈N [M+H]⁺: 330.2; found: 330.3. **Anal. Calcd** for C₂₄H₂₇N·0.2H₂O: C, 86.50; H, 8.29; N, 4.21. Found: C, 86.75; H, 8.82; N, 4.38. The **SC-XRD** structure is shown in Figure S103.

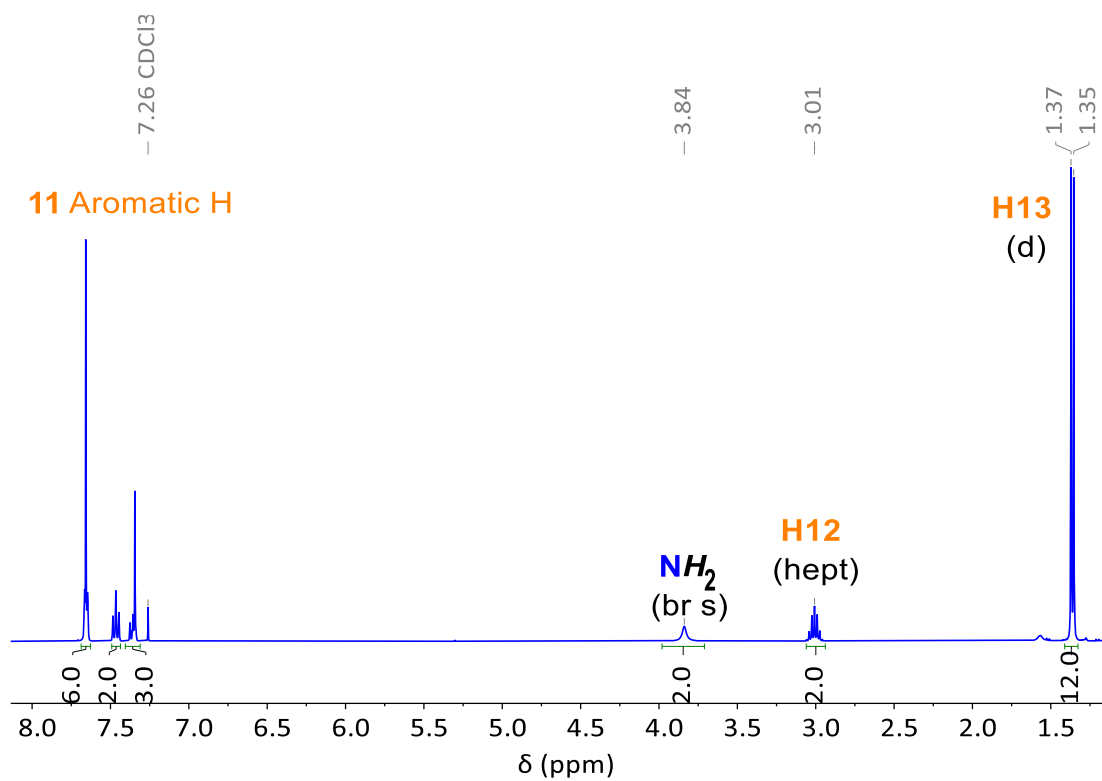


Figure S5. ^1H NMR spectrum (400 MHz, CDCl_3) of **3**.

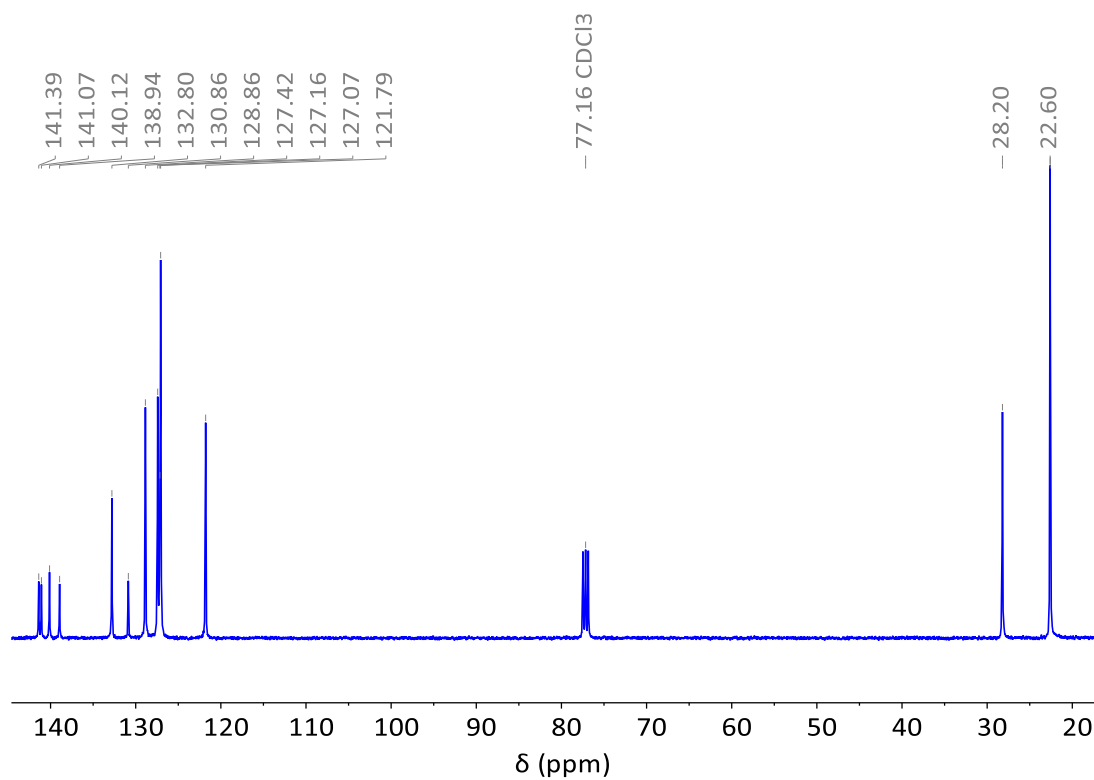
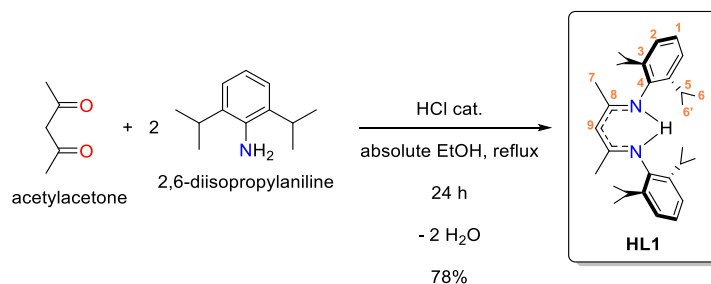


Figure S6. $^{13}\text{C}\{^1\text{H}\}$ NMR spectrum (101 MHz, CDCl_3) of **3**.

4.4. Preparation of **HL1**

The preparation of **HL1** was based on previously reported procedures.⁷ A solution of acetylacetone (4.1 mL, 40 mmol, 99%) and 2,6-diisopropylaniline (16.6 mL, 85 mmol, 97%) in absolute EtOH (30 mL) was purged with inert gas for 15 min. Then, concentrated HCl (3.3 mL, 40 mmol, 37%) was added dropwise to the solution, and the mixture was refluxed for 24 h under an inert atmosphere. After this time, the hydrochloride salt H(**L1**)·HCl formed as a white solid. The reaction mixture was cooled to 0 °C, and the salt was filtered, washed with cold EtOH, and dried under vacuum. This salt was deprotonated by dissolving it in DCM (150 mL) and mixing with saturated Na₂CO₃ (100 mL). The aqueous layer was discarded, the organic layer was washed with brine, dried over anhydrous Na₂SO₄ and filtered, and the solvent was removed under vacuum to leave **HL1** (13.0 g, 31 mmol, 78%) as a white solid. ¹H NMR (400 MHz, CDCl₃) δ (ppm): 12.12 (br s, 1H, **NH**), 7.13 (m, 6H, **H1 + H2**), 4.88 (s, 1H, **H9**), 3.11 (hept, $J_{\text{H5-H6}} = J_{\text{H5-H6}'} = 7.0$ Hz, 4H, **H5**), 1.73 (s, 6H, **H7**), 1.22 (d, $J_{\text{H6-H5}} = 7.0$ Hz, 12H, **H6**), 1.12 (d, $J_{\text{H6'-H5}} = 7.0$ Hz, 12H, **H6'**).

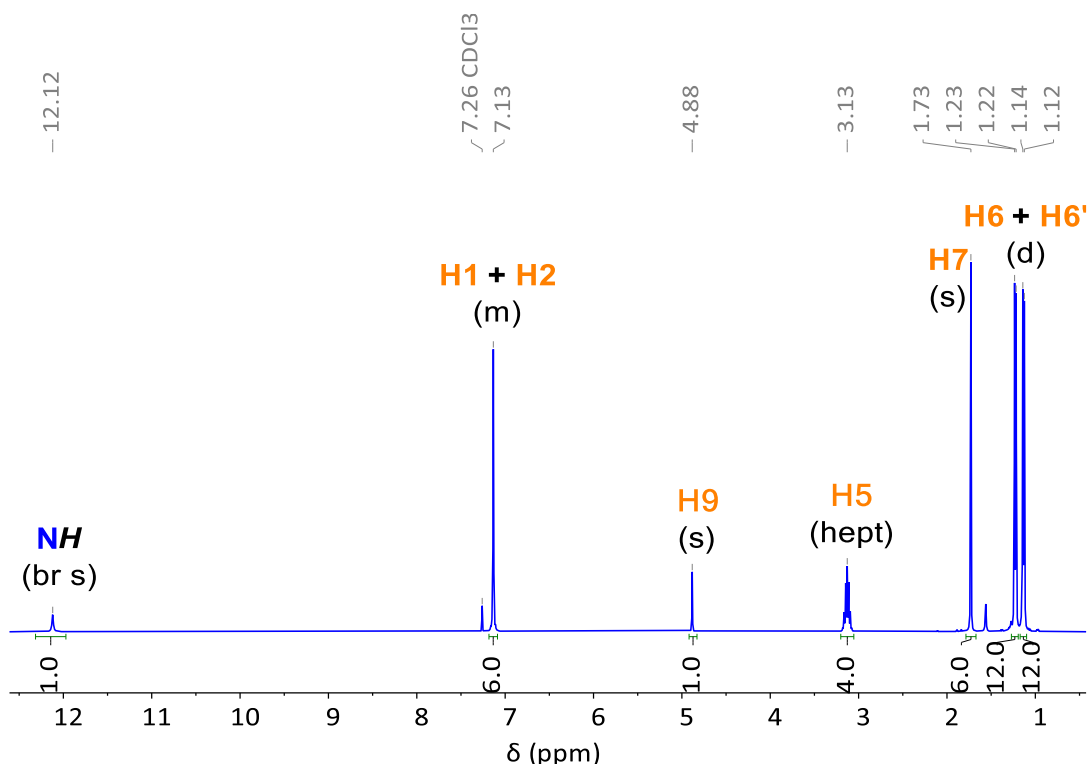
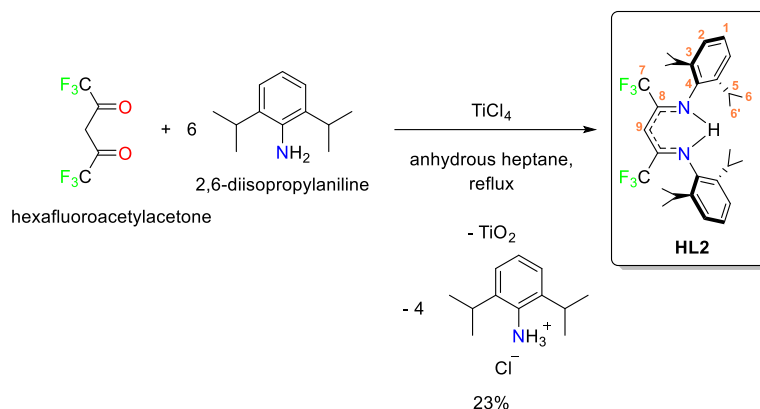


Figure S7. ¹H NMR spectrum (400 MHz, CDCl₃) of **HL1**.

4.5. Preparation of **HL2**

The preparation of **HL2** was based on previously reported procedures.^{8,9} Under an inert atmosphere, titanium tetrachloride (6.0 mL, 55 mmol) was added dropwise to a vigorously stirring solution of 2,6-diisopropylaniline (29.55 g, 150 mmol, 90%) in anhydrous heptane (150 mL). A dense orange precipitate formed immediately. After stirring the reaction mixture for 2 h at RT, hexafluoroacetylacetone (3.6 mL, 25 mmol, 99%) was added. The resulting reaction mixture was refluxed overnight, during which the color of the solution turned light yellow, and a significant amount of precipitate consisting of titanium dioxide and 2,6-diisopropylanilinium chloride formed. The yellow solution was isolated by vacuum filtration, and *n*-pentane was used to rinse the reaction flask. Then, the filtrate was washed with water (x 3) and brine (x 1). The orange layer was dried over anhydrous MgSO₄, and the solvent was removed under reduced pressure to afford an orange oil. MeOH (50 mL) was added, and the mixture was stirred at RT to form shiny yellow crystals of **HL2**, which were isolated by vacuum filtration and washed with MeOH. The mother liquor was stored at -35 °C overnight to give a second crop of crystals. Total yield: 2.97 g, 5.64 mmol, 23%. ¹H NMR (300 MHz, C₆D₆) δ (ppm): 11.55 (br s, 1H, **NH**), 7.12 (d, 2H, **H1**), 7.06 (d, 4H, **H2**), 6.02 (s, 1H, **H9**), 3.10 (hept, $J_{\text{H5-H6}} = J_{\text{H5-H6}'} = 7.0$ Hz, 4H, **H5**), 1.22 (d, $J_{\text{H6-H5}} = 7.0$ Hz, 12H, **H6**), 1.04 (d, $J_{\text{H6'-H5}} = 7.0$ Hz, 12H, **H6'**). ¹⁹F NMR (282 MHz, C₆D₆) δ (ppm): -65.23 (s, **CF₃**). IR-ATR: 1642 cm⁻¹ (s, $\nu(\text{C=N})$) [reported]; 1640 cm⁻¹ (s, $\nu(\text{C=N})$) [found].

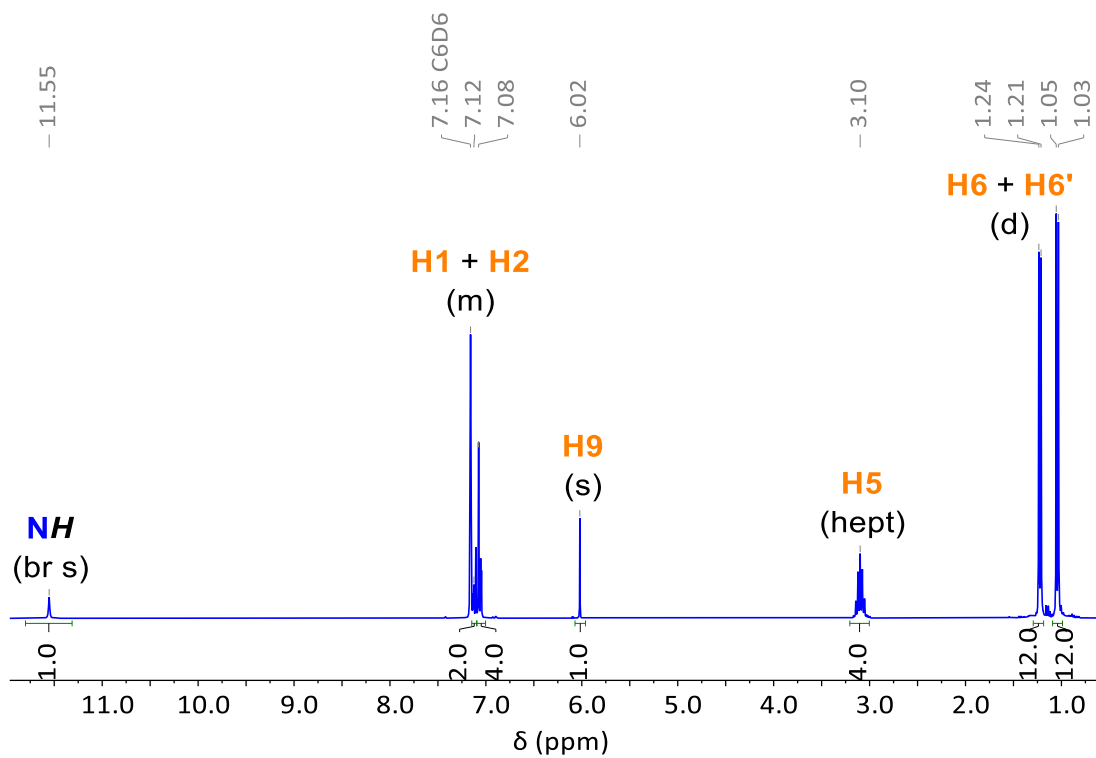


Figure S8. ^1H NMR spectrum (300 MHz, C_6D_6) of HL2.

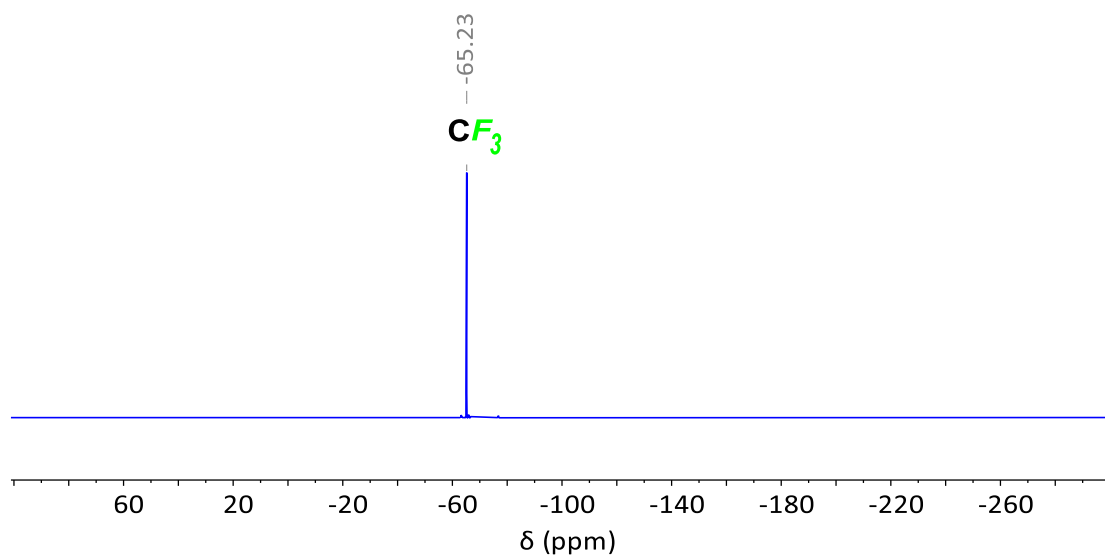
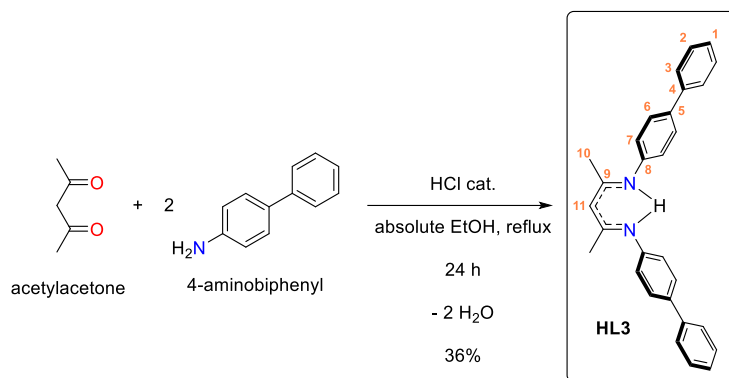


Figure S9. ^{19}F NMR spectrum (282 MHz, C_6D_6) of HL2.

4.6. Preparation of **HL3**

Acetylacetone (1.5 mL, 14.4 mmol, 99%) and 4-aminobiphenyl (5.13 mg, 29.7 mmol, 98%) were dissolved in absolute EtOH (130 mL) under an inert atmosphere. Then, concentrated HCl (1.2 mL, 14.4 mmol) was added dropwise to the solution, and the resulting mixture was refluxed for 24 h under an inert atmosphere. After this time, the hydrochloride salt **H(L3)**·HCl formed as a yellow solid. The salt was filtered, washed with cold EtOH, and dried under vacuum. This salt was deprotonated by dissolving it in CHCl₃ (150 mL) and mixing with saturated Na₂CO₃ (100 mL). The aqueous layer was discarded, the organic layer was washed with brine, dried over anhydrous Na₂SO₄ and filtered. Evaporation of the solvent gave a yellow residue, which was recrystallized from 1:1 THF/heptane to obtain pure **HL3** as a yellow solid. A second crop of crystals was obtained from recrystallizing the residue of the mother liquor. Total yield: 2.07 g, 5.14 mmol, 36%. ¹H NMR (400 MHz, CDCl₃) δ (ppm): 12.87 (br s, 1H, **NH**), 7.61 (d, $J_{\text{H3-H2}} = 7.6$ Hz, 4H, **H3**), 7.56 (d, $J_{\text{H6-H7}} = 8.0$ Hz, 4H, **H6**), 7.44 (t, $J_{\text{H2-H3}} = J_{\text{H2-H1}} = 7.6$ Hz, 4H, **H2**), 7.33 (tt, $J_{\text{H1-H2}} = 7.6$ Hz, $J_{\text{H1-H3}} = 1.5$ Hz, 2H, **H1**), 7.07 (d, $J_{\text{H7-H6}} = 8.0$ Hz, 4H, **H7**), 4.96 (s, 1H, **H11**), 2.10 (s, 6H, **H10**). ¹³C{¹H} NMR (101 MHz, CDCl₃) δ (ppm): 159.51 (**C9**), 145.03 (**C4**), 140.84 (**C8**), 136.07 (**C5**), 128.77 (**C2**), 127.51 (**C6**), 126.89 (**C3**), 126.80 (**C1**), 122.81 (**C7**), 97.90 (**C11**), 21.02 (**C10**). MS (ESI⁺, MeOH) m/z calcd for C₂₉H₂₇N₂ [M+H]⁺: 403.2; found: 403.2 [M+H]⁺. Anal. Calcd for C₂₉H₂₆N₂·0.2H₂O: C, 85.76; H, 6.55; N, 6.90. Found: C, 85.70; H, 6.85; N, 7.07. The SC-XRD structure is shown in Figure S104.

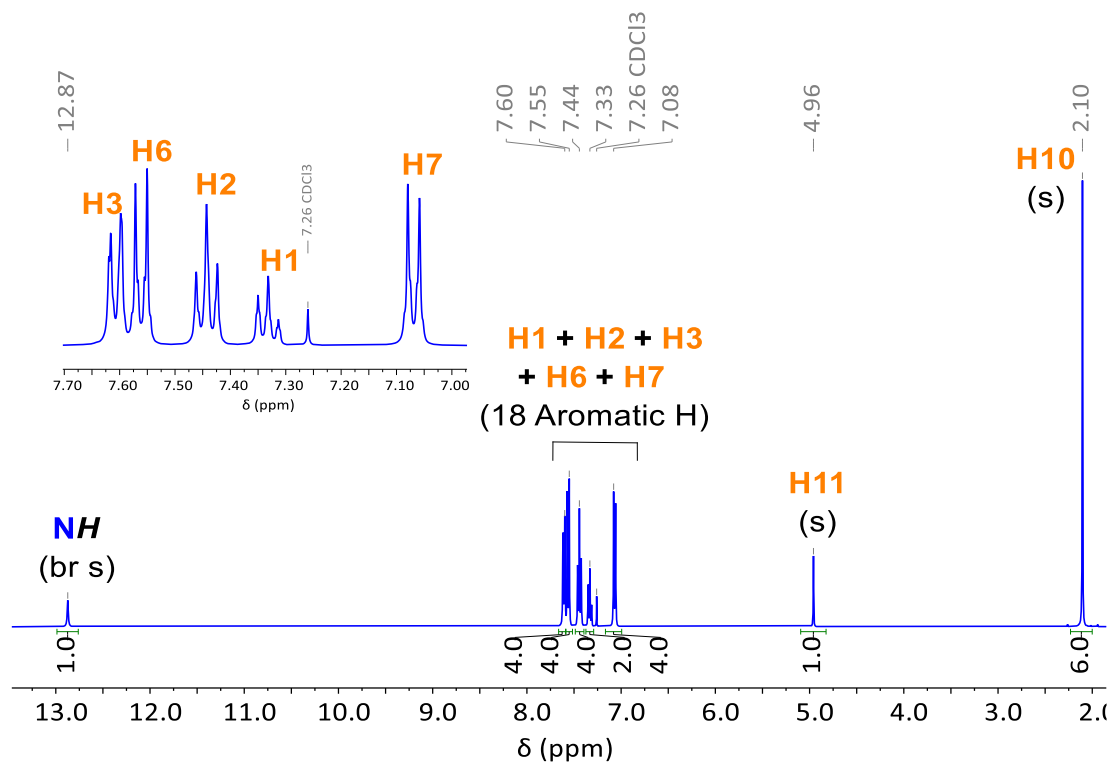


Figure S10. ^1H NMR spectrum (400 MHz, CDCl_3) of **HL3**.

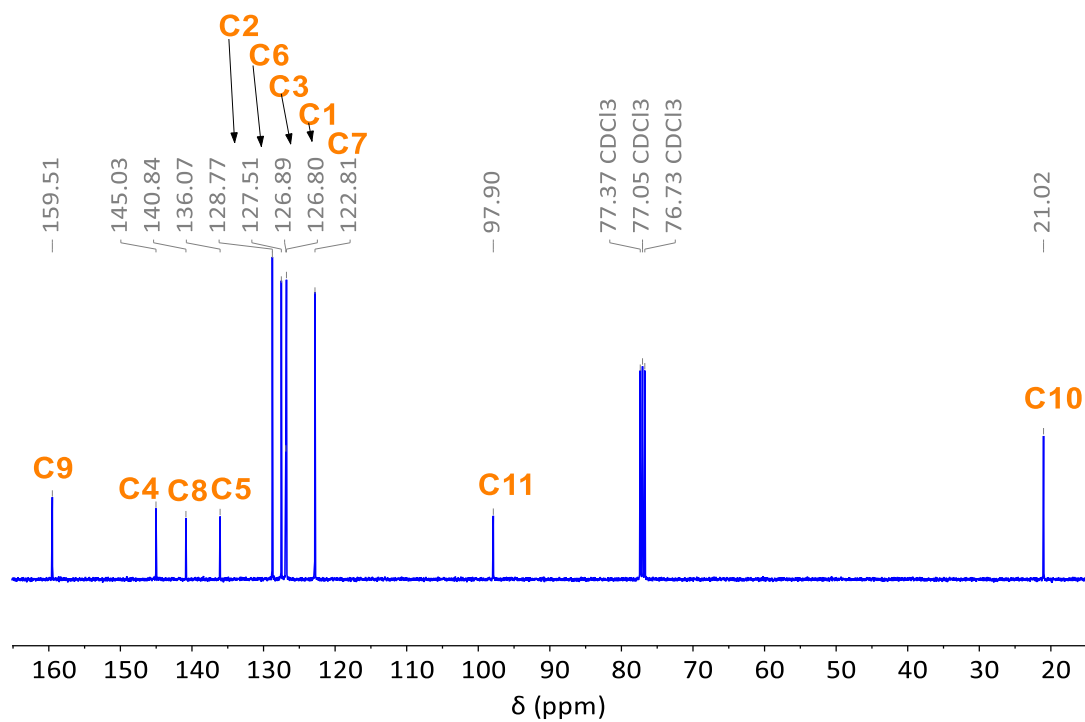
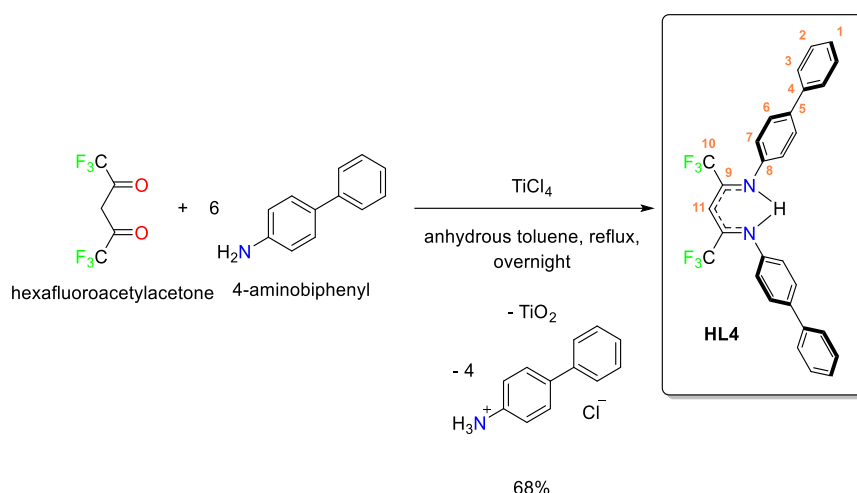


Figure S11. $^{13}\text{C}\{^1\text{H}\}$ NMR spectrum (101 MHz, CDCl_3) of **HL3**.

4.7. Preparation of **HL4**

Under an inert atmosphere, titanium tetrachloride (1.15 mL, 10.5 mmol) was added dropwise to a vigorously stirring solution of 4-aminobiphenyl (5.20 g, 30.1 mmol, 98%) at 0 °C in anhydrous toluene (25 mL). A dense brown precipitate formed immediately. The mixture was left to stir for 2 h at 80 °C. After cooling to RT, hexafluoroacetylacetone (0.72 mL, 50 mmol, 98%) was added, and additional toluene (25 mL) was added to assist stirring. The resulting mixture was refluxed overnight. The color of the reaction mixture lighter during the reaction. After cooling to RT, the precipitate was removed by vacuum filtration, and hexane was used to rinse the reaction flask. Then, the filtrate was washed with water (x 3) and brine (x 1). The organic layer was dried over anhydrous MgSO_4 , and the solvent was removed under reduced pressure to yield an orange solid residue. This residue was recrystallized from hexane (Bp/-35 °C), and shiny orange solid of **HL4** were obtained, which were washed with hexane and MeOH. The mother liquor was partially concentrated and kept at -35 °C to obtain a second crop of crystals. Total yield: 1.76 g, 3.4 mmol, 68%. $^1\text{H NMR}$ (400 MHz, C_6D_6) δ (ppm): 12.37 (br s, 1H, **NH**), 7.39 (d, $J_{\text{H}_3-\text{H}_2} = 8.5$ Hz, 4H, **H3**), 7.33 (d, $J_{\text{H}_6-\text{H}_7} = 8.5$ Hz, 4H, **H6**), 7.20 (t, $J_{\text{H}_2-\text{H}_3} = J_{\text{H}_2-\text{H}_1} = 8.5$ Hz t, 4H, **H2**), 7.13 (tt, $J_{\text{H}_1-\text{H}_2} = 8.5$ Hz, $J_{\text{H}_1-\text{H}_3} = 2.3$ Hz, tt, 2H, **H1**), 6.96 (d, $J_{\text{H}_7-\text{H}_6} = 8.5$ Hz, 4H, **H7**), 4.96 (s, 1H, **H11**), 2.10 (s, 6H, **H10**). $^{19}\text{F NMR}$ (376 MHz, C_6D_6) δ (ppm): -62.50 (s, **CF₃**). $^{13}\text{C}\{^1\text{H}\}$ NMR (75 MHz, C_6D_6) δ (ppm): 149.17, 148.77, 141.73, 140.24, 138.96, 128.73, 127.61, 127.28, 126.92, 122.85, 119.60 (low intensity q, $J_{\text{C}-\text{F}} = 284$ MHz, **CF₃**). **MS** (ESI⁺, MeOH) m/z calcd for $\text{C}_{29}\text{H}_{20}\text{F}_6\text{N}_2$ [$\text{M}+\text{H}$]⁺: 511.2; found: 511.1 [$\text{M}+\text{H}$]⁺. **MS** (ESI⁻, MeOH) m/z calcd for $\text{C}_{29}\text{H}_{20}\text{F}_6\text{N}_2$ [$\text{M}-\text{H}$]⁻: 509.2; found: 509.0. **Anal. Calcd** for $\text{C}_{29}\text{H}_{20}\text{F}_6\text{N}_2 \cdot 0.2\text{H}_2\text{O}$: C, 67.75; H, 4.00; N, 5.45. Found: C, 67.84; H, 4.21; N, 5.50. The **SC-XRD** structure is shown in Figure S105.

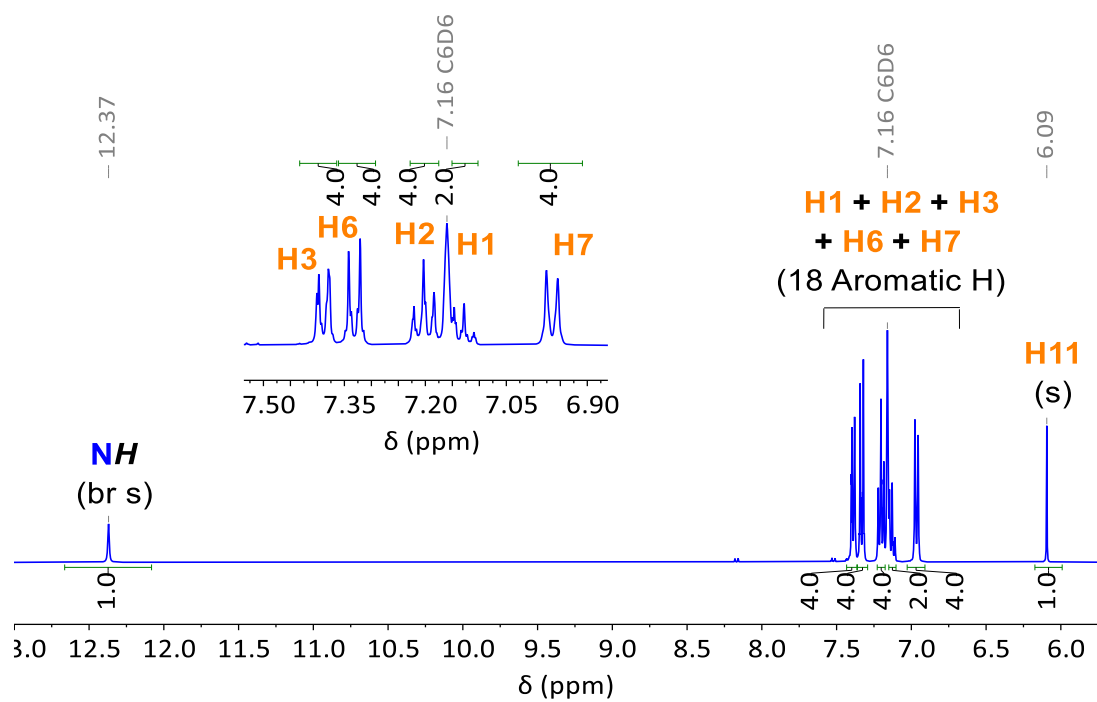


Figure S12. ^1H NMR spectrum (400 MHz, C_6D_6) of **HL4**.

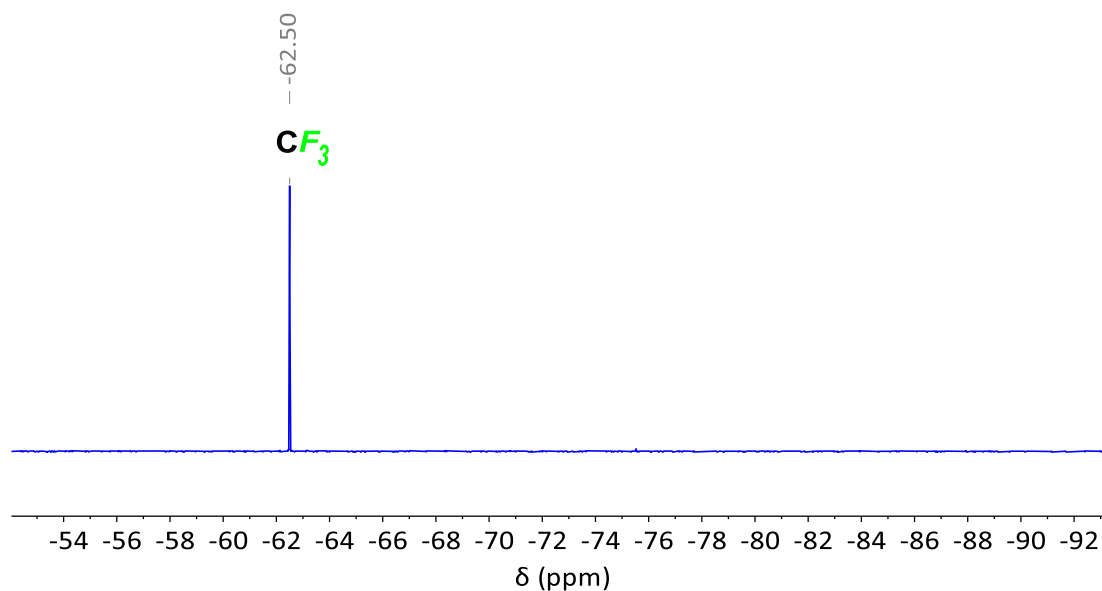
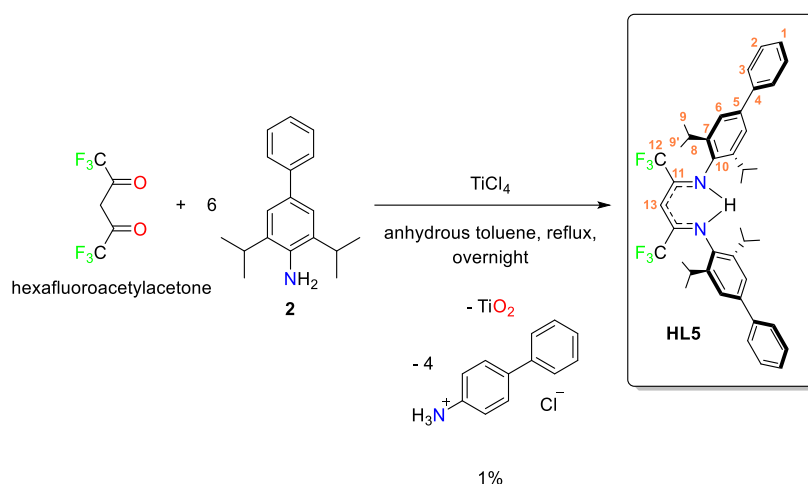


Figure S13. ^{19}F NMR spectrum (376 MHz, C_6D_6) of **HL4**.

4.8. Preparation of **HL5**

Under an inert atmosphere, titanium tetrachloride (1.45 mL, 13.2 mmol) was added dropwise to a vigorously stirring solution of **2** (9.62 g, 37.9 mmol) in anhydrous toluene (25 mL). The reaction mixture immediately turned dark red. After stirring the reaction mixture for 2 h at RT, hexafluoroacetylacetone (0.91 mL, 6.3 mmol, 98%) was added. The resulting reaction mixture was refluxed overnight, during which the color of the solution turned darker, and a significant amount of precipitate consisting of titanium dioxide and **P2** hydrochloride formed. The brown solution was isolated by vacuum filtration, and *n*-pentane was used to rinse the reaction flask. Then, the filtrate was washed with water (x 3) and brine (x 1). The orange layer was dried over anhydrous MgSO_4 , and the solvent was removed under reduced pressure to afford an orange oil. MeOH (25 mL) was added, and the mixture was left at $-35\text{ }^\circ\text{C}$ overnight to isolate the almost pure product as a light-yellow solid, which was recrystallized from hexane (Bp/ $-35\text{ }^\circ\text{C}$) to obtain pure **HL5** (60.8 mg, 0.9 mmol, 1%) as a shiny yellow solid. A second crop of crystals was not obtained from the mother liquor. $^1\text{H NMR}$ (400 MHz, CDCl_3) δ (ppm): 11.26 (br s, 1H, **NH**), 7.66-7.54 (d, 4H, **Ar**), 7.49-7.41 (t, 4H, **Ar**), 7.40-7.28 (m, 6H, **Ar**), 5.86 (s, 1H, **H13**), 3.02 (hept, $J_{\text{H8-H9}} = J_{\text{H8-H9}'} = 7.0\text{ Hz}$, **H8**), 1.29 (d, $J_{\text{H9-H8}} = 7.0\text{ Hz}$, 12H, **H9**), 1.18 (d, $J_{\text{H9'-H8}} = 7.0\text{ Hz}$, 12H, **H9'**). $^{19}\text{F NMR}$ (376 MHz, CDCl_3) δ (ppm): -65.52 (s, **CF₃**). $^{13}\text{C}\{^1\text{H}\}$ NMR (101 MHz, CDCl_3) δ (ppm): 142.15, 141.48, 139.57, 137.24, 128.85, 127.24, 122.32, 119.4 (low intensity q, $J_{\text{C-F}} = 280\text{ Hz}$, **CF₃**), 87.53, 28.83, 25.22, 22.96. **MS** (ESI⁺, MeOH) m/z calcd for $\text{C}_{41}\text{H}_{45}\text{F}_6\text{N}_2$ [$\text{M}+\text{H}$]⁺: 679.4; found: 679.3. **MS** (ESI, MeOH) m/z calcd for $\text{C}_{41}\text{H}_{43}\text{F}_6\text{N}_2$ [$\text{M}-\text{H}$]⁻: 677.3; found: 677.2. **Anal.** Calcd for $\text{C}_{41}\text{H}_{44}\text{F}_6\text{N}_2 \cdot 0.6\text{H}_2\text{O}$: C, 71.44; H, 6.61; N, 4.06. Found: C, 71.35; H, 6.92; N, 4.09. The **SC-XRD** structure is shown in Figure S106.

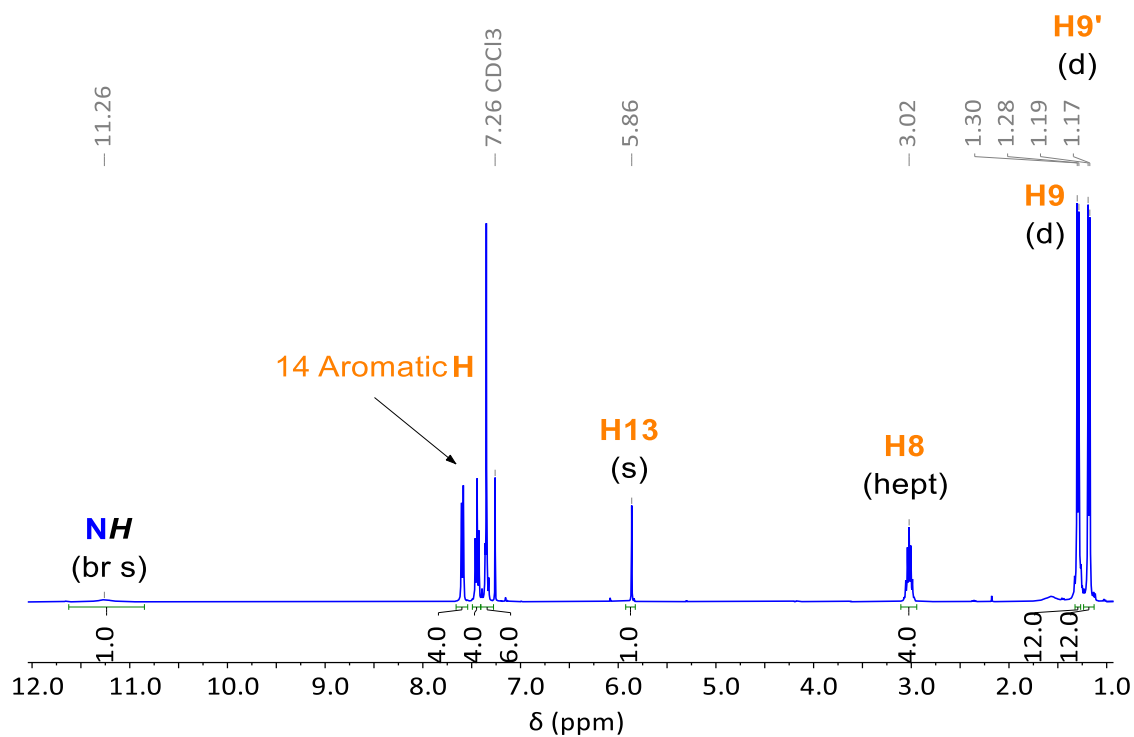


Figure S15. ^1H NMR spectrum (400 MHz, CDCl_3) of **HL5**.

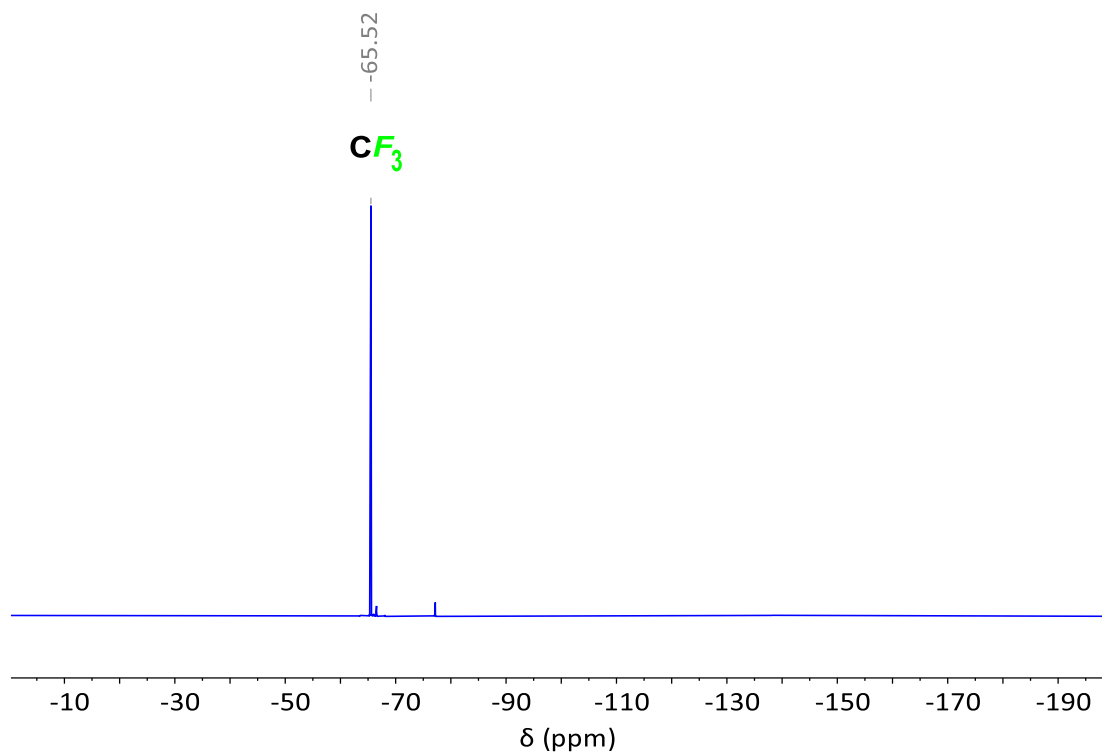


Figure S16. ^{19}F NMR spectrum (376 MHz, CDCl_3) of **HL5**.

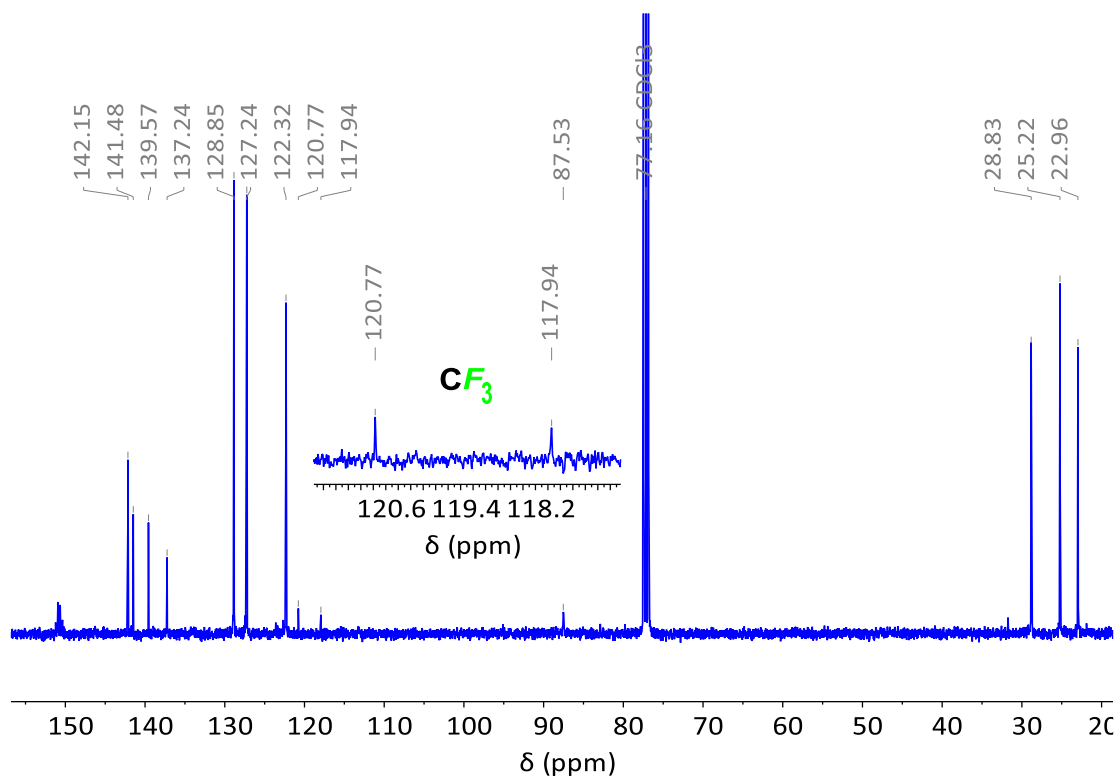
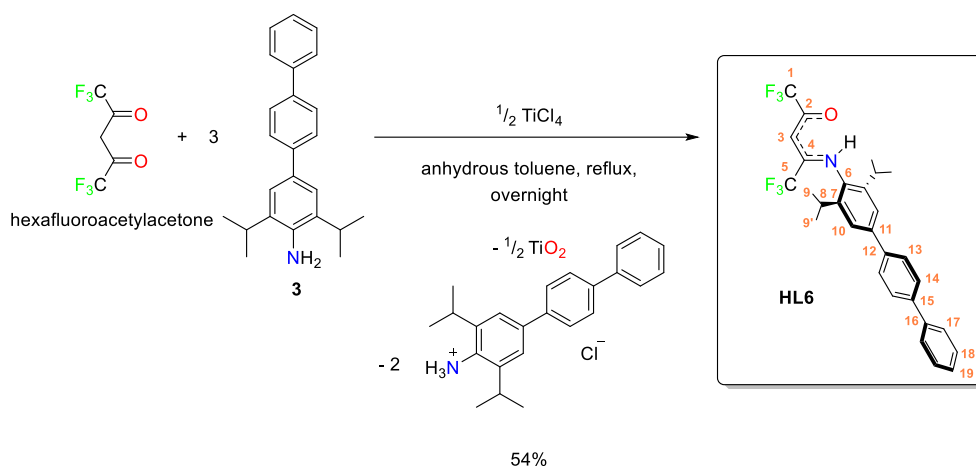
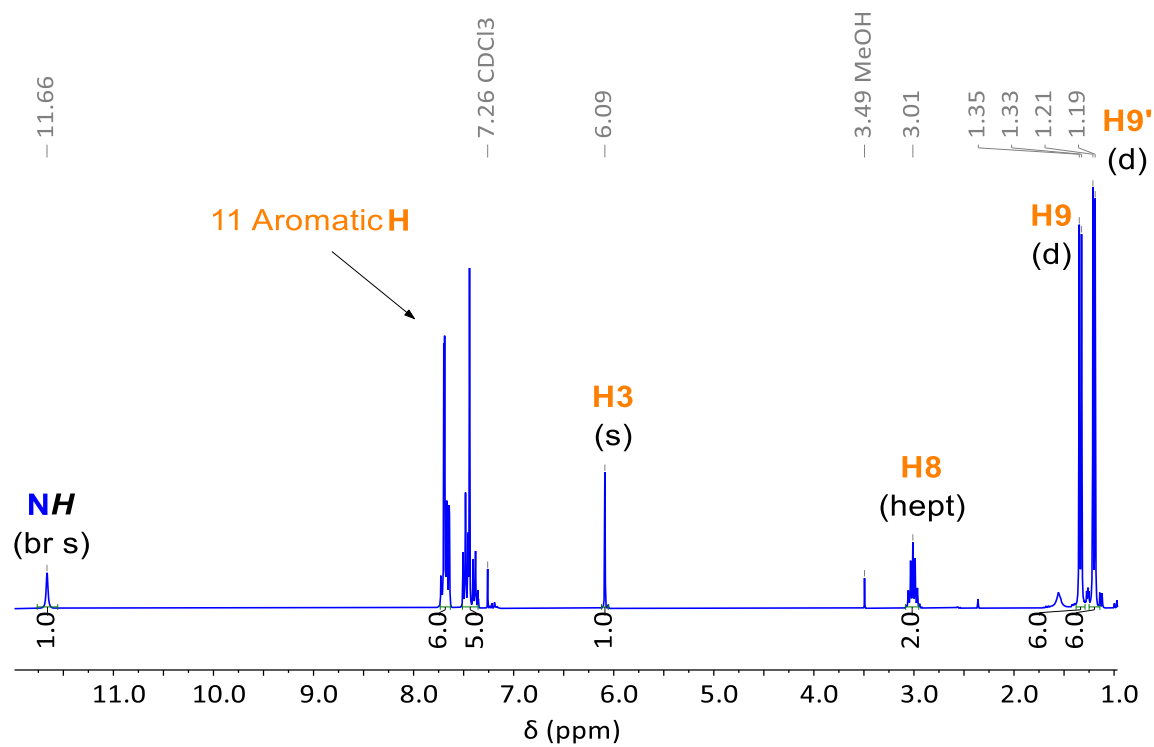
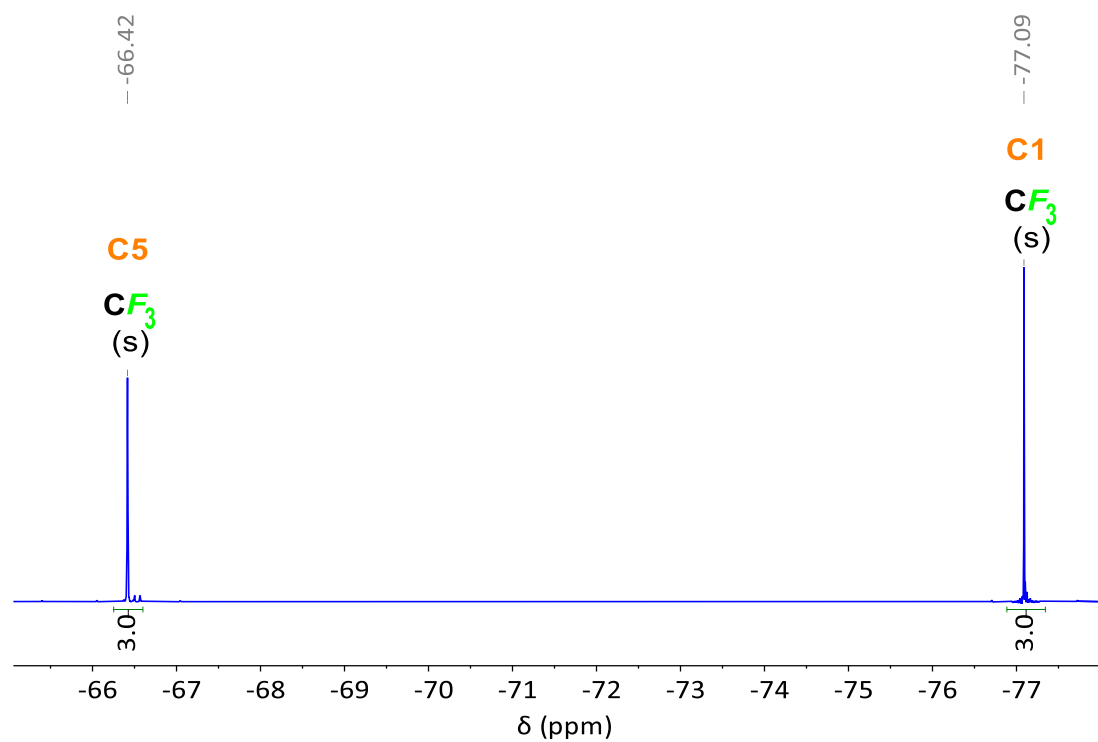


Figure S17. $^{13}\text{C}\{^1\text{H}\}$ NMR spectrum (101 MHz, CDCl_3) of **HL5**.

4.9. Preparation of HL6



Under an inert atmosphere, titanium tetrachloride (1.66 mL, 15.1 mmol) was added dropwise to a vigorously stirring solution of **3** (14.2 g, 43.1 mmol) in anhydrous toluene (150 mL) at 0 °C. The reaction mixture immediately turned dark and was stirred overnight at RT. Hexafluoroacetylacetone (1.04 mL, 7.2 mmol, 98%) was then added, and the mixture was stirred for 2 h at 90 °C. After this time, the color of the reaction mixture turned brown, and a significant amount of precipitate consisting of titanium dioxide and **P3** hydrochloride formed. A red solution was isolated by vacuum filtration, which was washed with water (x 3) and brine (x 1). The organic layer obtained was dried over anhydrous Na₂SO₄, and the solvent was removed under reduced pressure to afford a red oil. MeOH (100 mL) was added, and the mixture was stirred at RT to form a tan powder, which was isolated by vacuum filtration and washed with MeOH to yield **HL6** (2.02 g, 3.89 mmol, 54%). ¹H NMR (400 MHz, CDCl₃) δ (ppm): 11.66 (br s, 1H, **NH**), 7.71-7.62 (d, 12H, **Ar**), 7.75-7.31 (t, 4H, **Ar**), 7.44-7.34 (m, 6H, **Ar**), 6.09 (s, 1H, **H3**), 3.01 (hept, $J_{\text{H8-H9}} = J_{\text{H8-H9}'} = 7.0$ Hz, 2H, **H8**), 1.34 (d, $J_{\text{H9-H8}} = 7.0$ Hz, 12H, **H9**), 1.20 (d, $J_{\text{H9'-H8}} = 7.0$ Hz 12H, **H9'**). ¹⁹F NMR (282 MHz, CDCl₃) δ (ppm): -66.42 (s, 3F, **CF₃**, **C6**), -77.09 (s, 3F, **CF₃**, **C1**). ¹³C{¹H} NMR (101 MHz, CDCl₃) δ (ppm): 146.81, 142.10, 140.66, 139.66, 128.90 (low intensity q, $J_{\text{C-F}} = 286$ Hz, **CF₃**), 128.87, 127.64, 127.57, 127.09, 122.41, 29.06, 25.29, 21.76. **MS** (ESI, MeOH) m/z calcd for C₂₉H₂₆F₆NO [M-H]⁻: 518.2; found: 518.1. **Anal. Calcd** for C₂₉H₂₇F₆NO·0.3H₂O: C, 66.35; H, 5.30; N, 2.67. Found: C, 66.37; H, 5.57; N, 2.69.

Figure S18. ^1H NMR spectrum (300 MHz, CDCl_3) of **HL6**.Figure S19. ^{19}F NMR spectrum (282 MHz, CDCl_3) of **HL6**.

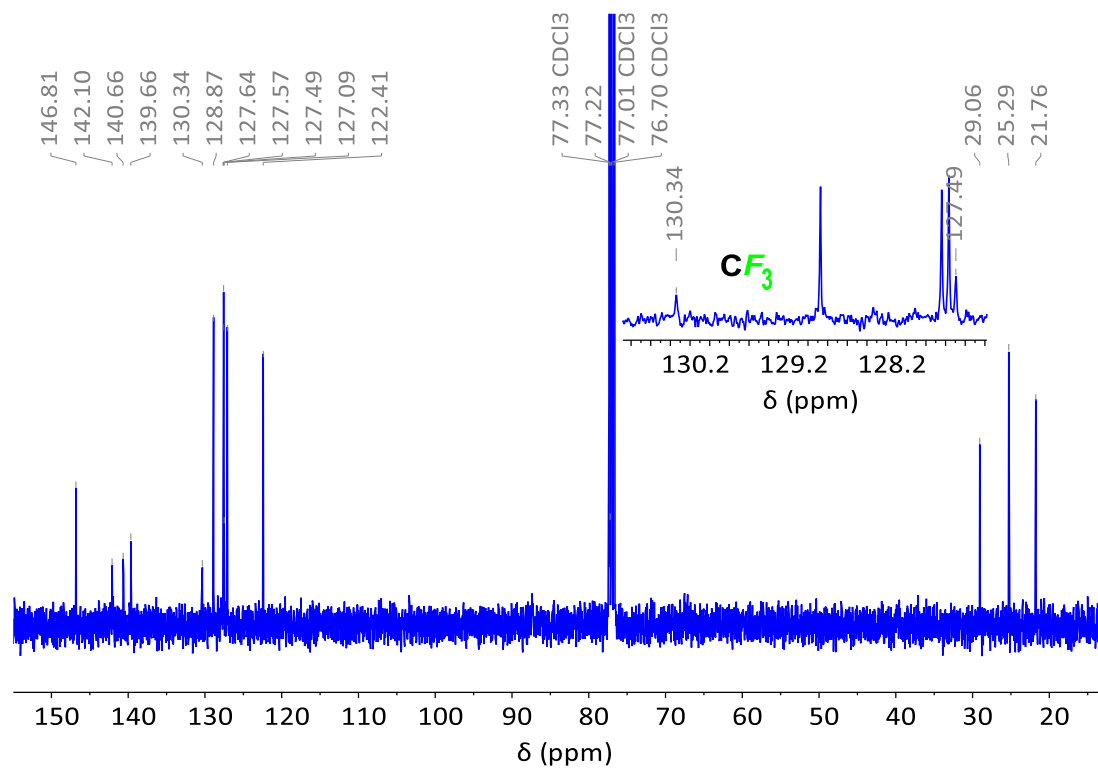
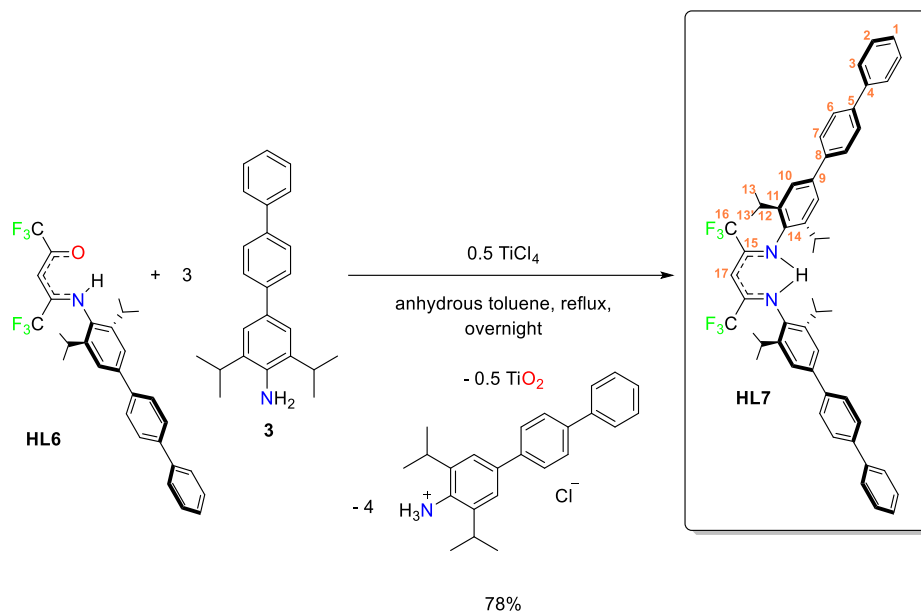


Figure S20. $^{13}\text{C}\{^1\text{H}\}$ NMR spectrum (101 MHz, CDCl_3) of **HL6**.

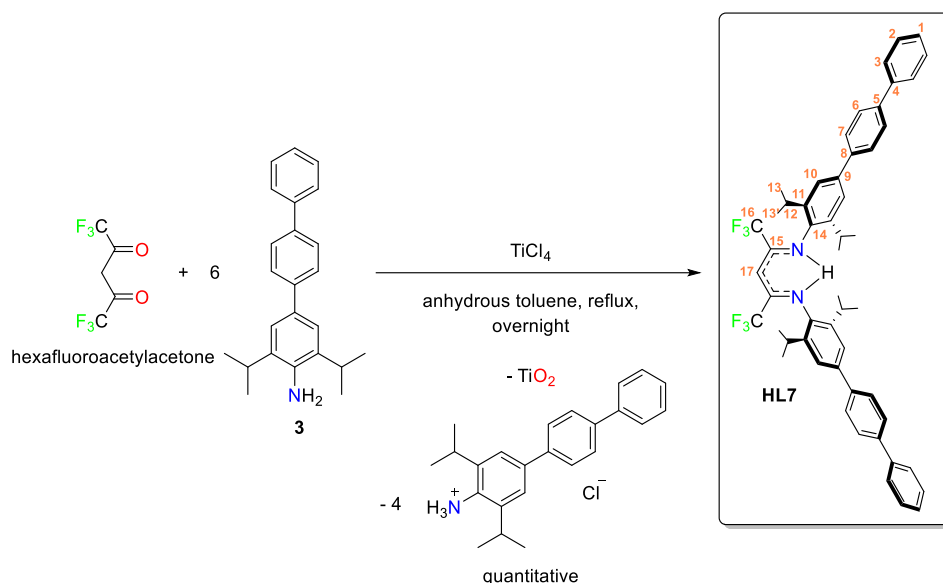
4.10. Preparation of **HL7**

Method A



Under an inert atmosphere, titanium tetrachloride (0.45 mL, 4.1 mmol) was added dropwise to a vigorously stirring solution of **3** (3.89 g, 11.8 mmol) in anhydrous toluene (20 mL) at RT. A dark brown precipitate formed immediately. After stirring the reaction mixture for 2 h at RT, a solution of **HL6** (1.03 g, 2.0 mmol) in anhydrous toluene (10 mL) was added. The resulting reaction mixture was refluxed overnight, during which time the color of the reaction mixture turned orange, and a significant amount of precipitate consisting of titanium dioxide and **P3** hydrochloride formed. A dark brown solution was isolated by vacuum filtration and washed with water (x 3) and brine (x 1). The organic layer was dried over anhydrous Na_2SO_4 , and the solvent was removed under reduced pressure to yield a solid residue. The residue was triturated with MeOH (100 mL), resulting in the isolation of **HL7** (1.27 g, 1.53 mmol, 78%) as a yellow solid. $^1\text{H NMR}$ (400 MHz, CDCl_3) δ (ppm): 11.27 (br s, 1H, **NH**), 7.81-7.58 (d, 12H, **Ar**), 7.51-7.44 (t, 4H, **Ar**), 7.44-7.28 (m, 6H, **Ar**), 5.88 (s, 1H, **H17**), 3.04 (hept, $J_{\text{H12-H13}} = J_{\text{H12-H13}'} = 7.0$ Hz, 4H, **H12**), 1.31 (d, $J_{\text{H13-H12}} = 7.0$ Hz, 12H, **H13**), 1.20 (d, $J_{\text{H13'-H12}} = 7.0$ Hz, 12H, **H13'**). $^{19}\text{F NMR}$ (376 MHz, CDCl_3) δ (ppm): -65.50 (s, **CF₃**).

Method B



Under an inert atmosphere, titanium tetrachloride (1.17 mL, 10.6 mmol) was added dropwise to a vigorously stirring solution of **3** (9.98 g, 30.3 mmol) in anhydrous toluene (80 mL) at RT. A dense yellow-brown precipitate formed immediately. After stirring the reaction mixture for 2 h at RT, hexafluoroacetylacetone (0.37 mL, 2.53 mmol, 98%) was added. The resulting mixture was refluxed overnight, during which the color of the solution turned orange-brown, and a significant amount of precipitate consisting of titanium dioxide and **3** hydrochloride formed. A dark brown solution was isolated by vacuum filtration and washed with water (x 3) and brine (x 1). The organic layer was dried over anhydrous Na_2SO_4 , and the solvent was removed under reduced pressure to yield a solid residue. The residue was purified by column chromatography (wet loading in DCM, silica gel deactivated with 3% TEA, hexane/EtAcO 9.5/0.5, $R_f \sim 0.7$) to afford **HL7** (2.09 g, 2.52 mmol, quantitative yield) as a yellow solid. $^1\text{H NMR}$ (400 MHz, CDCl_3) δ (ppm): 11.30 (br s, 1H, **NH**), 7.73-7.62 (m, 12H, **Ar**), 7.51-7.45 (t, 4H, **Ar**), 7.44-7.32 (m, 6H, **Ar**), 5.90 (s, 1H, **H17**), 3.06 (hept, $J_{\text{H12-H13}} = J_{\text{H12-H13}'} = 7.0$ Hz, 4H, **H12**), 1.33 (d, $J_{\text{H13-H12}} = 7.0$ Hz, 12H, **H13**), 1.22 (d, $J_{\text{H13'-H12}} = 7.0$ Hz 12H, **H13'**). $^{19}\text{F NMR}$ (376 MHz, CDCl_3) δ (ppm): -65.47 (s, **CF₃**).

$^{13}\text{C}\{^1\text{H}\}$ NMR (101 MHz, CDCl_3) δ (ppm): 142.12, 140.79, 140.26, 140.08, 138.94, 137.22, 128.85, 127.48, 127.46, 127.35, 127.08, 122.11, 119.40 (low intensity q, $J_{\text{C-F}} = 280$ Hz, **CF₃**), 87.41, 28.74, 25.12, 22.86. **MS** (ESI⁺, MeOH/FA) m/z calcd for $\text{C}_{53}\text{H}_{53}\text{F}_6\text{N}_2$ [$\text{M}+\text{H}$]⁺: 831.4; found: 831.4. **MS** (ESI⁻, MeOH/FA) m/z calcd for $\text{C}_{29}\text{H}_{51}\text{F}_6\text{N}_2$ [$\text{M}-\text{H}$]⁻: 829.4; found: 829.2. **Anal. Calcd** for $\text{C}_{53}\text{H}_{52}\text{F}_6\text{N}_2 \cdot 0.5\text{H}_2\text{O}$: C, 75.80; H, 6.36; N, 3.33. Found: C, 76.13; H, 6.77; N, 3.37. The SC-XRD structure is shown in Figure S107.

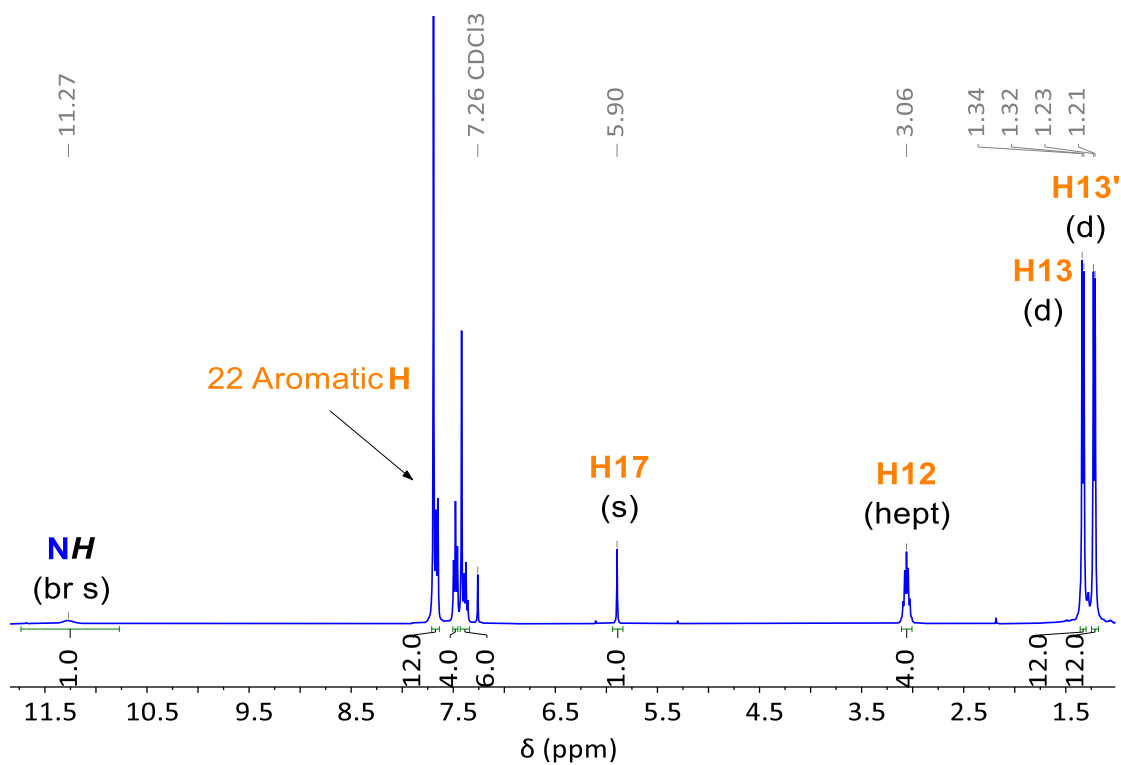


Figure S21. ^1H NMR spectrum (400 MHz, CDCl_3) of **HL7**.

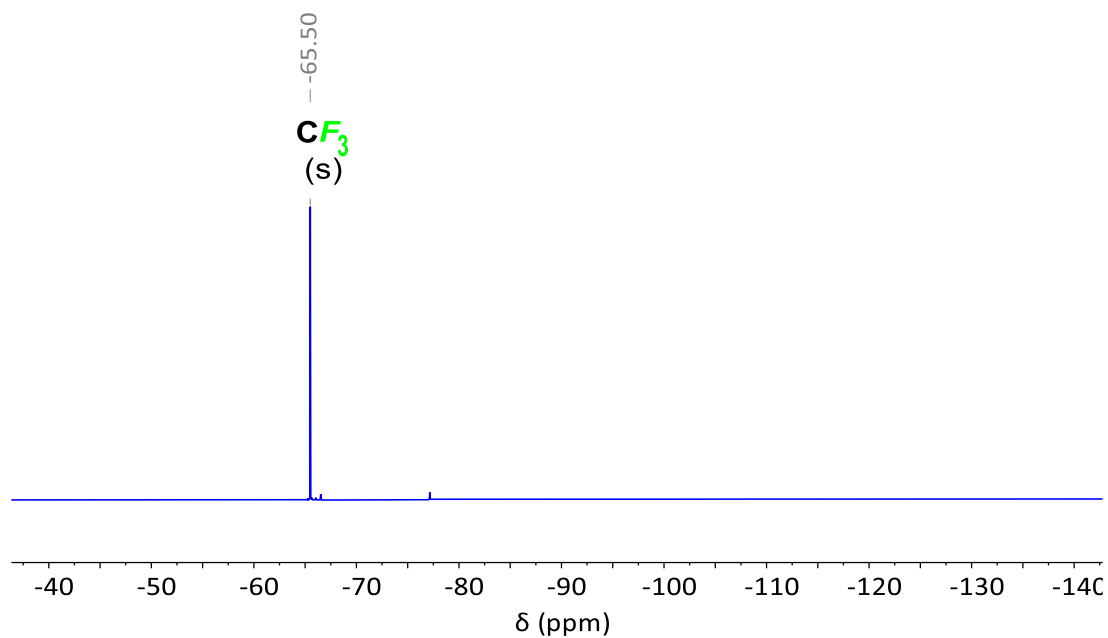


Figure S22. ^{19}F NMR spectrum (376 MHz, CDCl_3) of **HL7**.

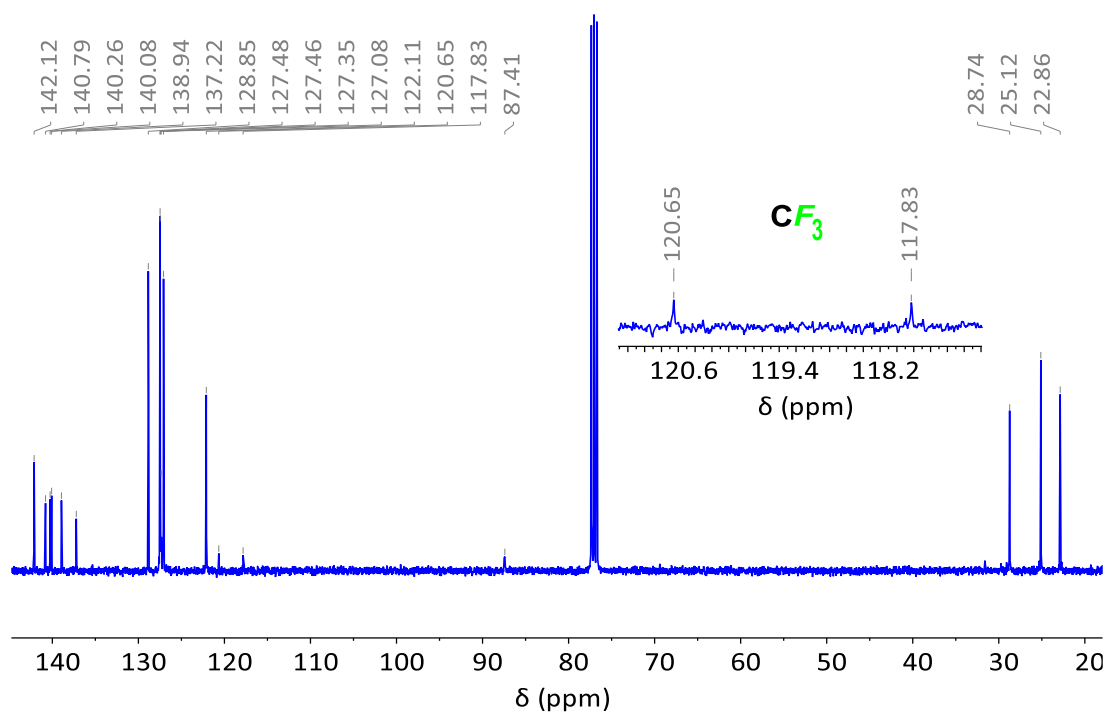
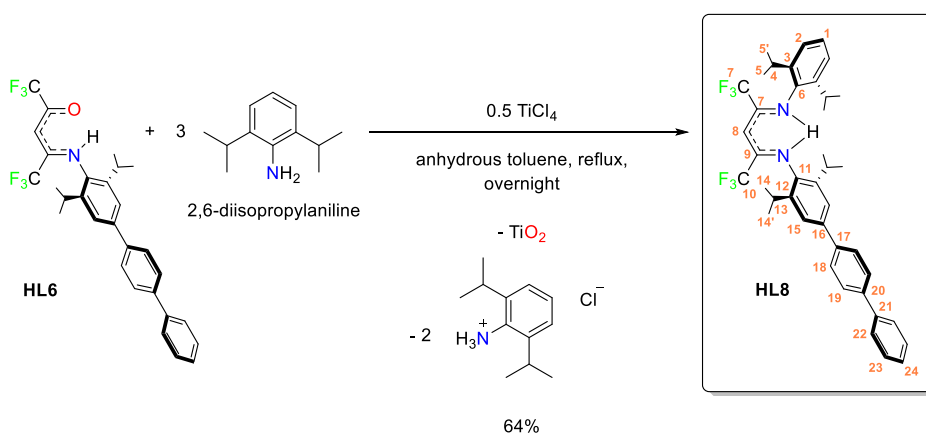
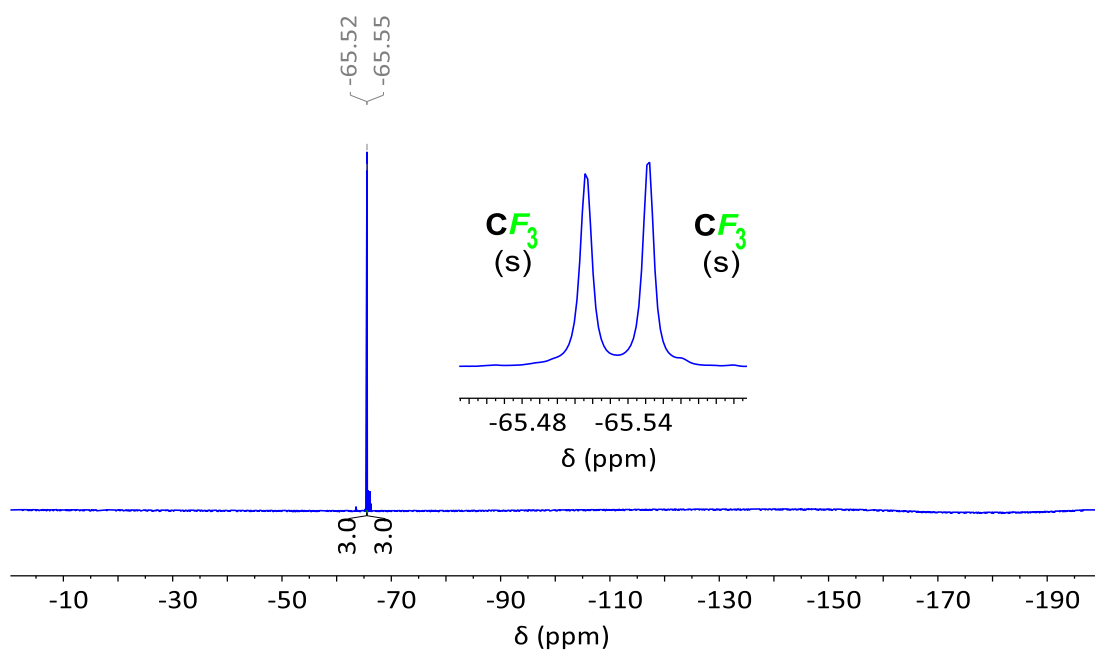
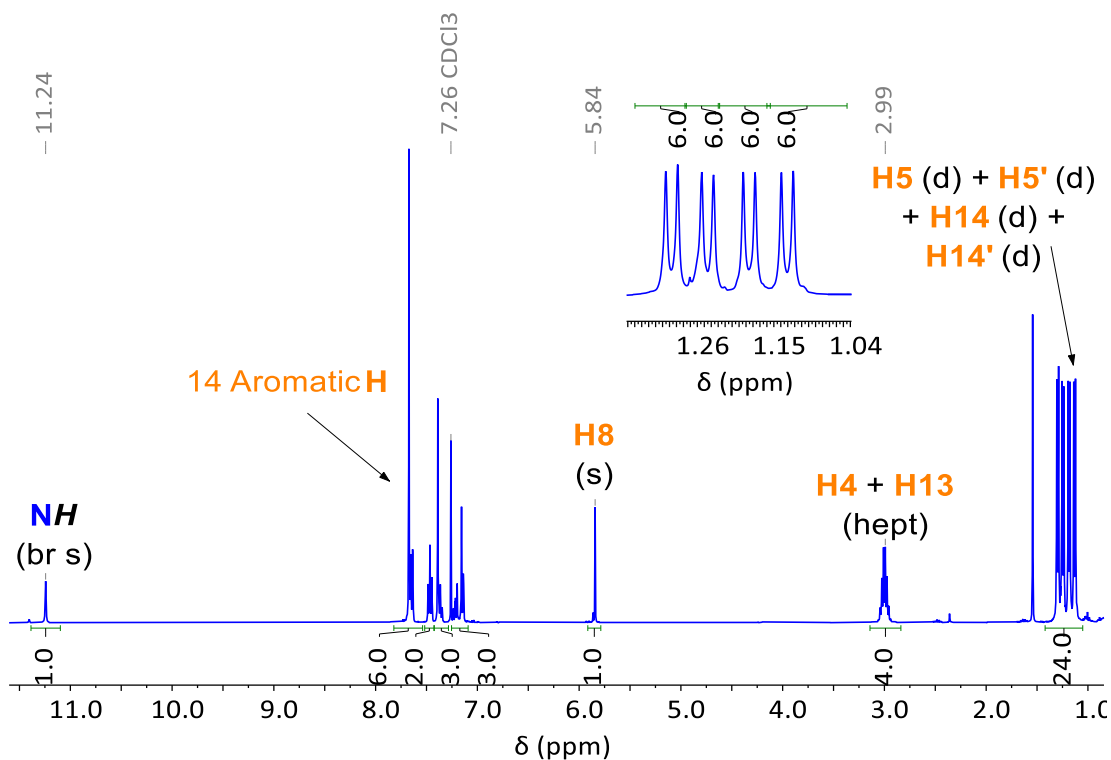


Figure S23. $^{13}\text{C}\{^1\text{H}\}$ NMR spectrum (101 MHz, CDCl_3) of **HL7**.

4.11. Preparation of **HL8**

Under an inert atmosphere, titanium tetrachloride (0.23 mL, 2.1 mmol) was added dropwise to a vigorously stirring solution of 2,6-diisopropylaniline (1.187 g, 6.0 mmol, 90%) in anhydrous toluene (5 mL) at RT. A dense orange precipitate formed immediately. After stirring the reaction mixture for 2 h at RT, a solution of **HL6** (519.7 mg, 1.0 mmol) in anhydrous toluene (5 mL) was added. The reaction mixture was refluxed overnight, during which the color of the solution turned dark brown, and a significant amount of precipitate consisting of titanium dioxide and 2,5-diisopropylanilinium chloride formed. A dark brown solution was isolated by vacuum filtration and washed with water (x 3) and brine (x 1). The organic layer was dried over anhydrous Na_2SO_4 , and the solvent was removed under reduced pressure to yield a solid residue. The residue was triturated with MeOH (10 mL) to obtain **HL8** (433 mg, 0.64 mmol, 64%) as shiny yellow crystals. $^1\text{H NMR}$ (400 MHz, CDCl_3) δ (ppm): 11.24 (br s, 1H, **NH**), 7.82-7.05 (m, 14H, **Ar**), 5.84 (s, 1H, **H8**), 2.99 (hept, $J_{\text{H4-H5}} = J_{\text{H4-H5}'} = J_{\text{H13-H14}} = J_{\text{H13-H14}'} = 7.0$ Hz, 4H, **H4 + H13**), 1.42-1.05 (d, d, d, d, $J_{\text{H5-H4}} = J_{\text{H5'-H4}} = J_{\text{H14-H13}} = J_{\text{H14'-H13}} = 7.0$ Hz, 24H, **H5 + H5' + H14 + H14'}**). $^{19}\text{F NMR}$ (376 MHz, CDCl_3) δ (ppm): -65.52 (s, 3F, **CF₃**), -65.55 (s, 3F, **CF₃**). $^{13}\text{C}\{^1\text{H}\}$ NMR (101 MHz, CDCl_3) δ (ppm): 142.26, 141.79, 140.93, 140.43, 140.17, 138.85, 137.87, 137.29, 128.97, 127.60, 127.57, 127.47, 127.20, 127.01, 123.40, 122.20, 28.82, 28.70, 25.23, 25.15, 23.01, 22.87. **MS** (ESI⁺, MeOH) m/z calcd for $\text{C}_{41}\text{H}_{45}\text{F}_6\text{N}_2$ $[\text{M}+\text{H}]^+$: 679.4; found: 679.3. **MS** (ESI⁻, MeOH) m/z calcd for $\text{C}_{41}\text{H}_{43}\text{F}_6\text{N}_2$ $[\text{M}-\text{H}]^-$: 677.3; found: 677.2. **Anal. Calcd** for $\text{C}_{41}\text{H}_{44}\text{F}_6\text{N}_2 \cdot 0.4\text{H}_2\text{O}$: C, 71.78; H, 6.58; N, 4.08. Found: C, 71.76; H, 7.06; N, 4.11. The **SC-XRD** structure is shown in Figure S108.



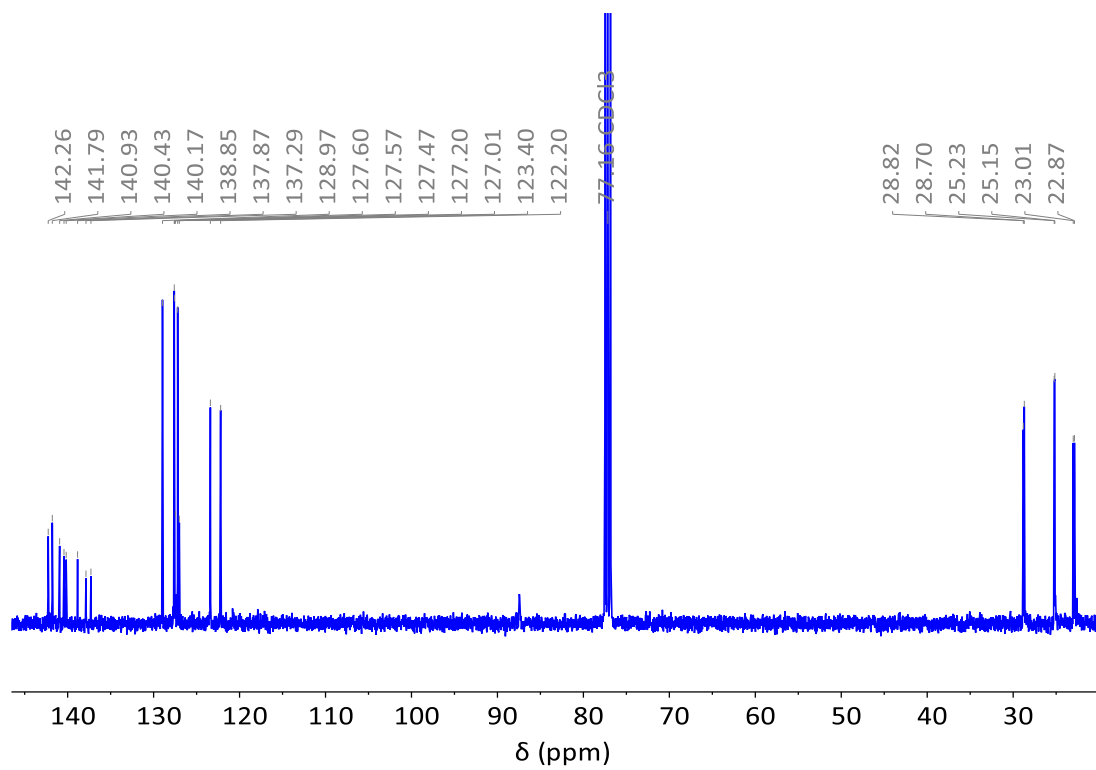
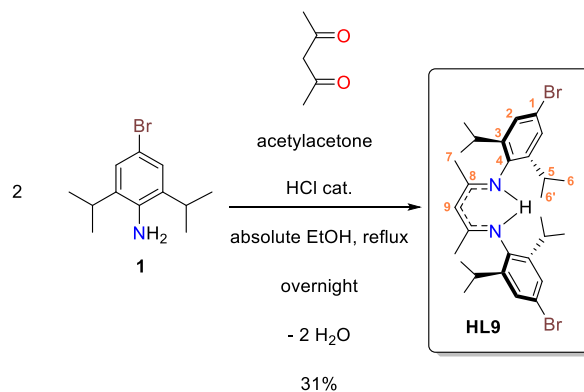
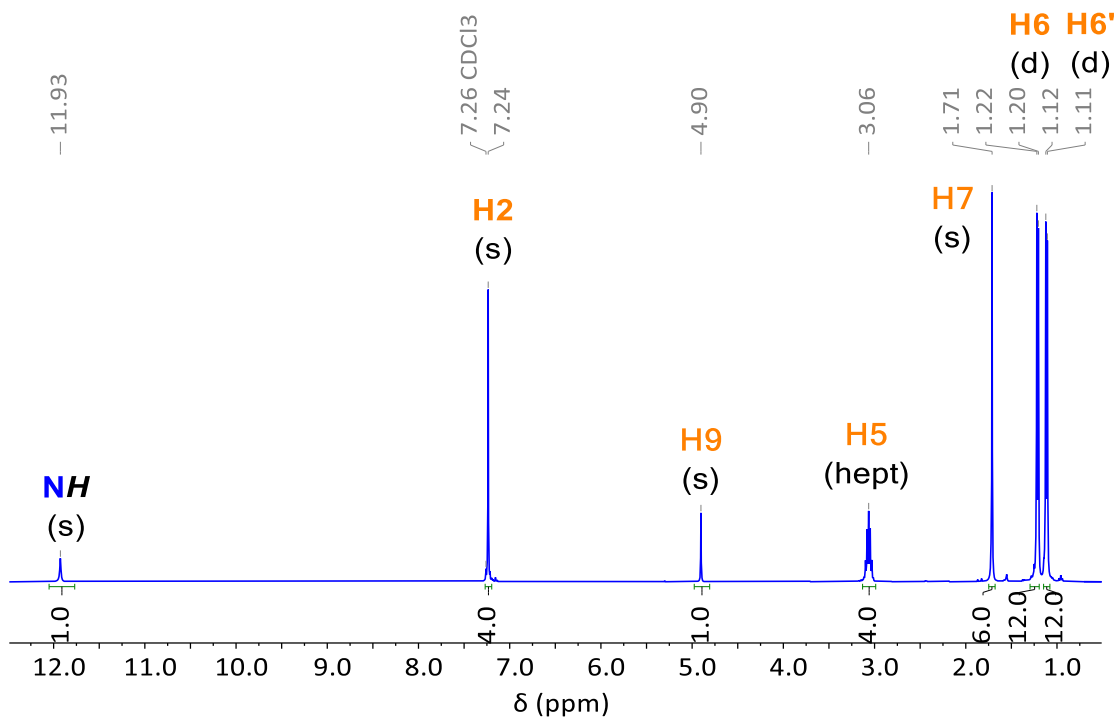
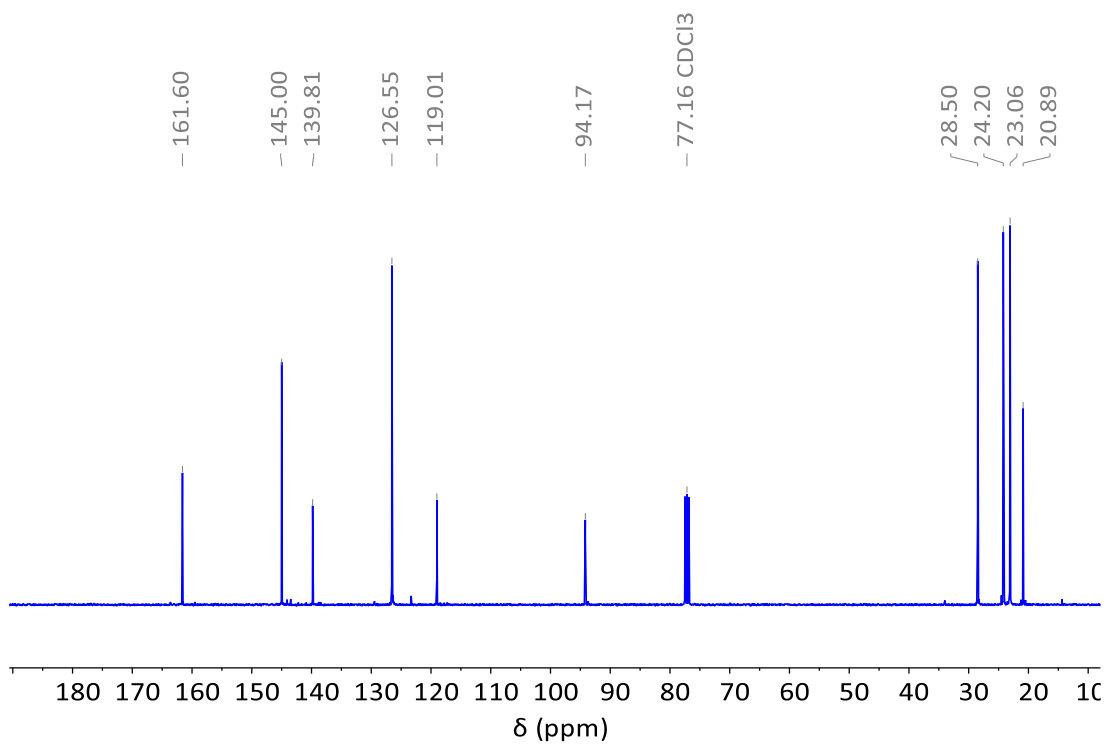
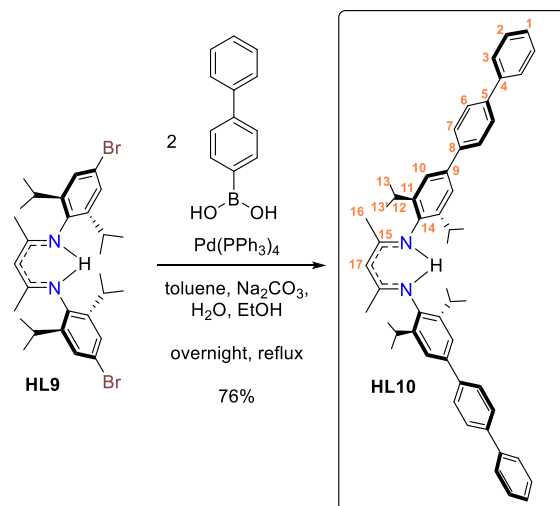


Figure S26. $^{13}\text{C}\{^1\text{H}\}$ NMR spectrum (101 MHz, CDCl_3) of **HL8**.

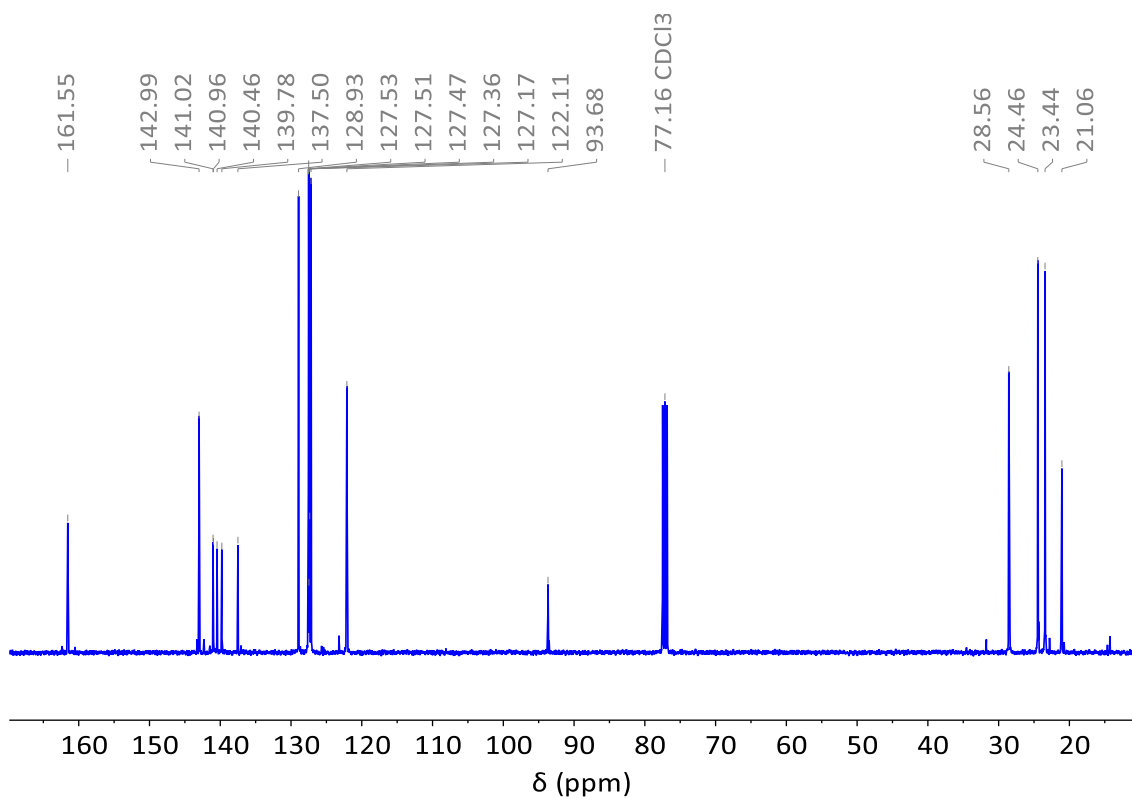
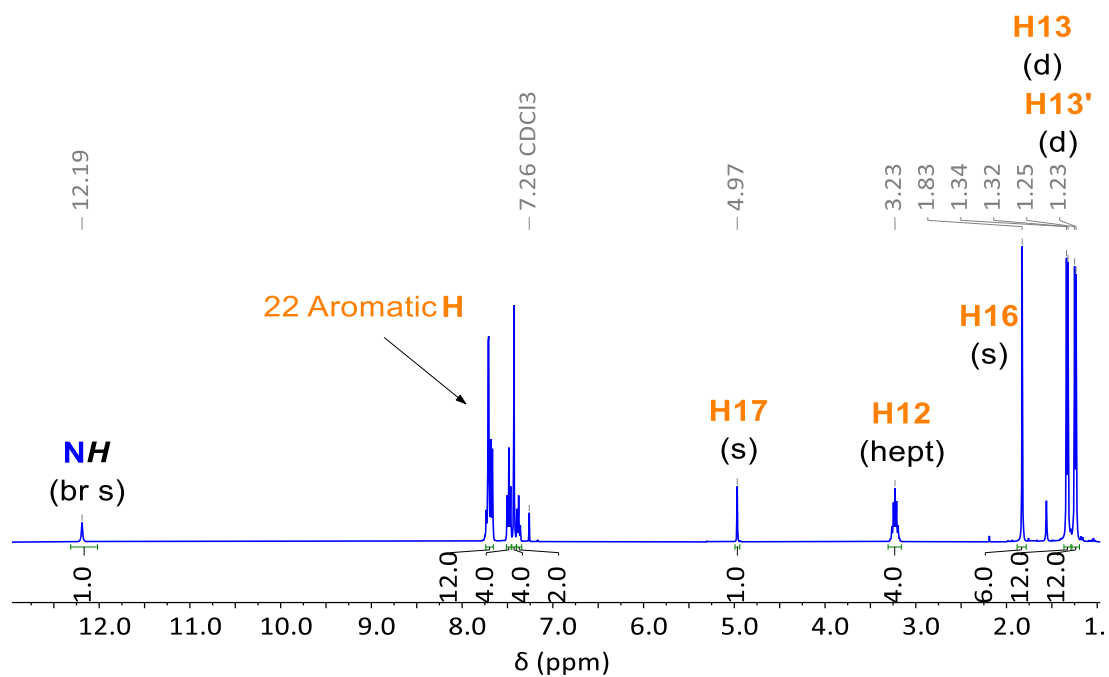
4.12. Preparation of **HL9**

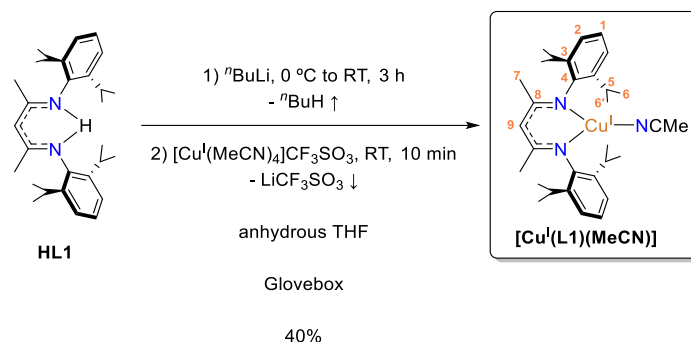
Concentrated HCl (4.6 mL, 55 mmol, 37%) was added dropwise to a solution of acetylacetone (5.8 mL, 56 mmol) and **1** (28.5 g, 111 mmol) in absolute EtOH (200 mL). The resulting mixture was refluxed overnight. After cooling the reaction mixture to RT, hydrochloride salt **HL9**·HCl formed as a white precipitate. The solvent was removed under vacuum, leaving an orange residue, which was refluxed with cyclohexane (300 mL) for 1 h. The resulting slurry was then allowed to cool to RT, filtered, and the solid was dissolved in DCM (300 mL). This solution was mixed with a saturated aqueous Na₂CO₃ solution (200 mL) and stirred until the solid dissolved. The organic layer was separated, washed with water (3 x 200 mL) and brine (200 mL), dried over anhydrous Na₂SO₄, and filtered. The solvent was removed under reduced pressure, yielding a pinkish residue, which was triturated with hexane and filtered to obtain **HL9** (10.11 g, 17.5 mmol, 31%) as a white solid. ¹H NMR (400 MHz, CDCl₃) δ (ppm): 11.93 (s, 1H, **NH**), 7.24 (s, 4H, **H2**), 4.90 (s, 1H, **H9**), 3.06 (hept, $J_{\text{H5-H6}} = J_{\text{H5-H6}'} = 7.0$ Hz, 4H, **H5**), 1.71 (s, **H7**), 1.21 (d, $J_{\text{H6-H5}} = 7.0$ Hz, 12H, **H6**), 1.11 (d, $J_{\text{H6'-H5}} = 7.0$ Hz, 12H, **H6'**). ¹³C{¹H} NMR (101 MHz, CDCl₃) δ (ppm): 161.60, 145.00, 139.81, 126.55, 119.01, 94.17, 28.50, 24.20, 23.06, 20.89. **MS** (ESI⁺, MeOH) m/z calcd for C₂₉H₄₁Br₂N₂ [M+H]⁺: 575.16; found: 577.1. **MS** (ESI⁻, MeOH) m/z calcd for C₂₉H₃₉Br₂N₂ [M-H]⁻: 573.15; found: 575.0. **Anal.** Calcd for C₂₉H₄₀Br₂N₂: C, 60.42; H, 7.00; N, 4.86. Found: C, 60.39; H, 7.46; N, 4.93. The SC-XRD structure is shown in Figure S109.

**Figure S27.** ^1H NMR spectrum (400 MHz, CDCl_3) of **HL9**.**Figure S28.** $^{13}\text{C}\{^1\text{H}\}$ NMR spectrum (101 MHz, CDCl_3) of **HL9**.

4.13. Preparation of **HL10**

HL9 (5.76 g, 10.0 mmol), 4-biphenylboronic acid (5.95 g, 30.0 mmol) and $\text{Pd}(\text{PPh}_3)_4$ (584 mg, 0.50 mmol) were mixed in toluene (100 mL) and EtOH (25 mL). The mixture was purged with inert gas for 30 min. Meanwhile, Na_2CO_3 (25 mL, 2 M solution in water) was also purged with inert gas for 30 min, and then added to the reaction mixture. The biphasic reaction mixture was refluxed overnight. After cooling to RT, the mixture was filtered through a toluene-rinsed Celite pad, and the dark organic layer was separated, washed with brine, and dried over anhydrous Na_2SO_4 and filtered. The solvent was removed under reduced pressure, yielding a brown solid residue. This residue was purified by column chromatography (wet loading in eluent, silica gel deactivated with 3% TEA, DCM/hexane 8:2, $R_f \sim 0.9$) and triturated with hexane to afford **HL10** (5.49 g, 7.6 mmol, 76%) as a white solid. $^1\text{H NMR}$ (400 MHz, CDCl_3) δ (ppm): 12.23 (s, 1H, **NH**), 7.80-7.35 (m, 12H, **Ar**), 5.00 (s, 1H, **H18**), (hept, $J_{\text{H12-H13}} = J_{\text{H12-H13}'} = 7.0$ Hz, 4H, **H12**), 1.86 (s, 6H, **H16**), 1.37 (d, $J_{\text{H13-H12}} = 7.0$ Hz, 12H, **H13**), 1.28 (d, $J_{\text{H13}'-H12} = 7.0$ Hz, 12H, **H13'**). $^{13}\text{C}\{^1\text{H}\}$ NMR (101 MHz, CDCl_3) δ (ppm): 161.55, 142.99, 141.02, 140.96, 140.46, 139.78, 137.50, 128.93, 127.53, 127.51, 127.47, 127.36, 127.17, 122.11, 93.68, 28.56, 24.46, 23.44, 21.06. **MS** (ESI⁺, MeOH): m/z calcd for $\text{C}_{53}\text{H}_{59}\text{N}_2$ $[\text{M}+\text{H}]^+$: 723.5; found: 723.3. **MS** (ESI⁻, MeOH) m/z calcd for $\text{C}_{29}\text{H}_{57}\text{N}_2$ $[\text{M}-\text{H}]^-$: 721.5; found: 721.2. **Anal. Calcd** for $\text{C}_{53}\text{H}_{58}\text{N}_2 \cdot 0.3\text{H}_2\text{O}$: C, 87.39; H, 8.11; N, 3.85. Found: C, 87.37; H, 8.37; N, 3.83. The **SC-XRD** structure is shown in Figure S110.



4.14. Preparation of $[\text{Cu}^{\text{I}}(\text{L1})(\text{MeCN})]$ 

The preparation of $[\text{Cu}^{\text{I}}(\text{L1})(\text{MeCN})]$ was based on previously reported procedures.^{10,11} Inside a glovebox ($[\text{H}_2\text{O}] < 0.1$ ppm, $[\text{O}_2] < 0.1$ ppm), a solution of $n\text{BuLi}$ (2.5 M in hexanes, 1.9 mL, 4.8 mmol) was carefully added dropwise at RT to a stirring solution of **HL1** (2.0 g, 4.8 mmol) in anhydrous THF (20 mL), avoiding overheating. The resulting yellow mixture was stirred at RT for 3 h. After this time, $[\text{Cu}^{\text{I}}(\text{MeCN})_4]\text{CF}_3\text{SO}_3$ (2.0 g, 4.8 mmol) was added to the reaction mixture, turning it dark. The mixture was stirred at RT for an additional 10 min. All volatiles were then removed under dynamic vacuum, leaving a green residue that was suspended in anhydrous n -pentane (3 x 20 mL) and filtered through a Celite plug. The volatiles of the filtrate were removed under dynamic vacuum, yielding a brown residue. This residue was recrystallized from n -pentane (RT/-40 °C) to afford $[\text{Cu}^{\text{I}}(\text{L1})(\text{MeCN})]$ (1.0 g, 1.9 mmol, 40%) as yellow crystals. ^1H NMR (400 MHz, C_6D_6) δ (ppm): 7.19 (m, 4H, **Ar**), 7.09 (m, 2H, **Ar**), 4.98 (s, 1H, **H9**), 3.55 (hept, $J_{\text{H5-H6}} = J_{\text{H5-H6}'} = 7.0$ Hz, 4H, **H5**), 1.85 (s, 6H, **H7**), 1.41 (d, $J_{\text{H6-H5}} = 7.0$ Hz, 12H, **H6**), 1.29 (d, $J_{\text{H6'-H5}} = 7.0$ Hz, 12H, **H6'**), 0.08 (s, 3H, **NCCH₃**).

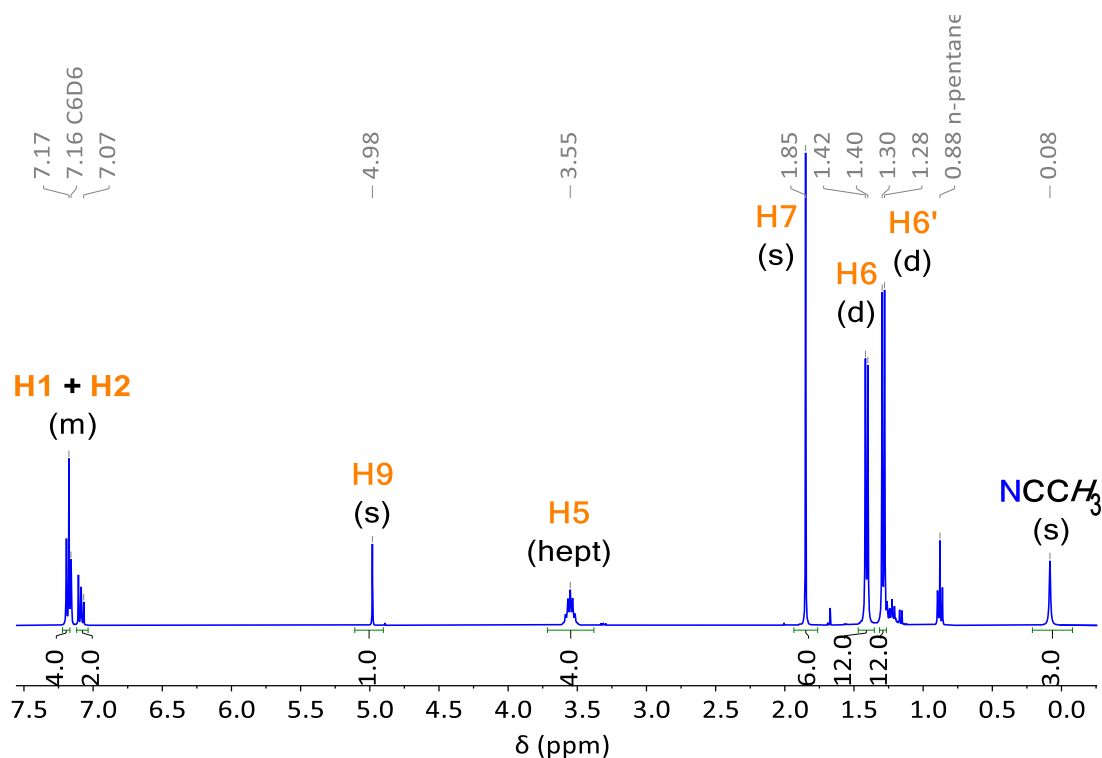
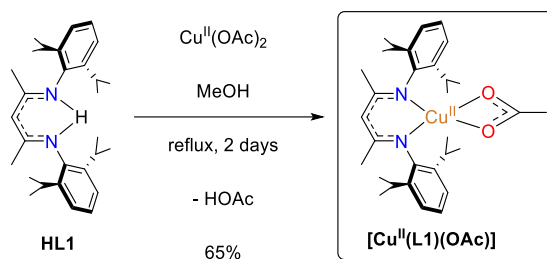


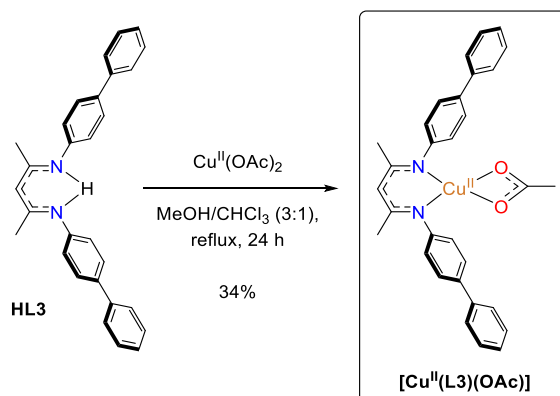
Figure S31. ^1H NMR spectrum (400 MHz, C_6D_6) of $[\text{Cu}^{\text{I}}(\text{L1})(\text{MeCN})]$.

4.15. Preparation of $[\text{Cu}^{\text{II}}(\text{L1})(\text{OAc})]$



The preparation of $[\text{Cu}^{\text{II}}(\text{L1})(\text{OAc})]$ was previously reported in the literature.¹² A MeOH solution (200 mL) containing **HL1** (41.9 mg, 0.1 mmol) and $\text{Cu}^{\text{II}}(\text{OAc})_2$ (18.7 mg, 0.1 mmol, 98%) was refluxed for 48 h under an inert atmosphere. After the solvent was evaporated under vacuum, a dark brown residue remained, from which $[\text{Cu}^{\text{II}}(\text{L1})(\text{OAc})]$ (352.7 mg, 0.65 mmol, 65%) was obtained as dark brown microcrystals from several crops of recrystallization from MeOH (Bp/-35 °C). **MS** (ESI⁺, MeOH, MeOH-FA, or MeCN-FA): $[\text{M}-\text{AcO}]^+$ or $[\text{M}+\text{H}]^+$ not found. **IR-ATR**: 1590 cm^{-1} (s, $\nu(\text{C}=\text{N})$) [reported]; 1551 cm^{-1} (s, $\nu(\text{C}=\text{N})$) [found]. **Anal. Calcd** for $\text{C}_{31}\text{H}_{44}\text{CuN}_2\text{O}_2 \cdot 1.2\text{H}_2\text{O}$: C, 66.30; H, 8.32; N, 4.99; Found: C, 66.30; H, 8.46; N, 5.05. **SC-XRD** shown in Figure S111 also confirmed the already reported structure.

4.16. Preparation of $[\text{Cu}^{\text{II}}(\text{L3})(\text{OAc})]$



A solution of **HL3** (40 mg, 0.1 mmol) in CHCl_3 (5 mL) was added to a stirring MeOH (15 mL) solution of $\text{Cu}^{\text{II}}(\text{OAc})_2$ (19 mg, 0.1 mmol, 98%). The resulting dark mixture was refluxed overnight. After this time, the solvent was removed under reduced pressure, and the residue was triturated with Et_2O (10 mL). The solid was filtered and washed with MeOH to yield $[\text{Cu}^{\text{II}}(\text{L3})(\text{OAc})]$ (18 mg, 0.034 mmol, 34%) as a dark brown powder. **Anal. Calcd** for $\text{C}_{31}\text{H}_{28}\text{CuN}_2\text{O}_2 \cdot 0.6\text{Cu}(\text{OAc})_2$: C, 60.92; H, 4.84; N, 4.25. Found: C, 60.85; H, 4.73; N, 4.40. The formulation $[\text{Cu}^{\text{II}}(\text{L3})(\text{OAc})]$ is the most likely structure formed under these conditions. The formation of $[\text{Cu}^{\text{II}}(\text{L3})_2]$ was not observed; instead, the product consistently appeared to contain a minor proportion of unreacted or co-precipitated $\text{Cu}^{\text{II}}(\text{OAc})_2$, supporting the assignment of a 1:1 Cu:L3 stoichiometry. Moreover, electrochemical studies show distinct redox behavior for this complex compared to that expected for a bis-chelated $[\text{Cu}^{\text{II}}(\text{L3})_2]$ species, further corroborating the proposed formulation (see Figures S54 and S55).

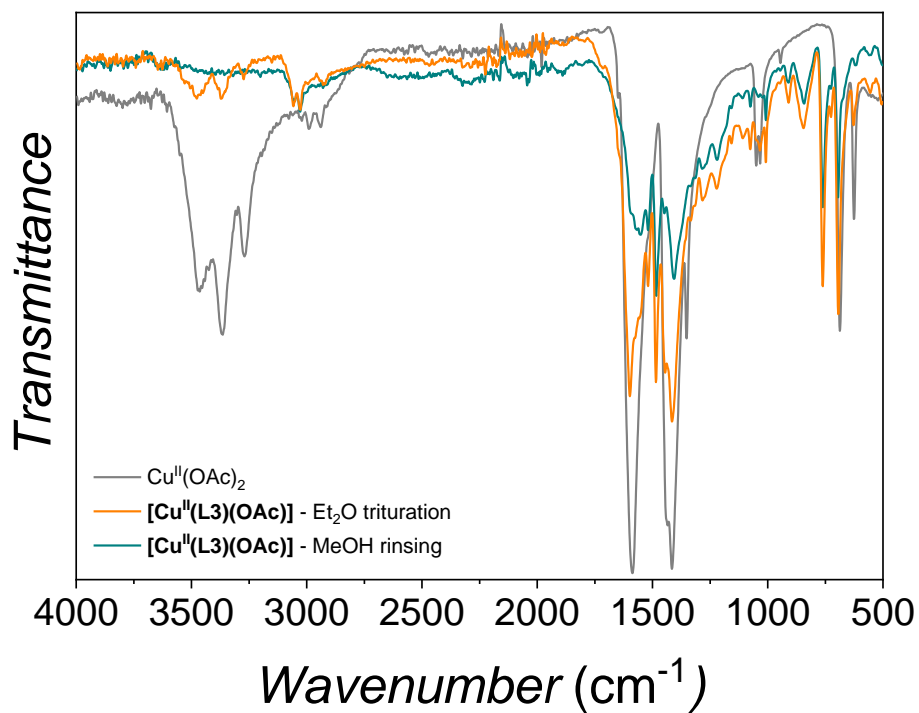


Figure S32. ATR-FTIR comparison between Cu^{II}(AcO)₂ and [Cu^{II}(L3)(AcO)] with/without MeOH rinsing.

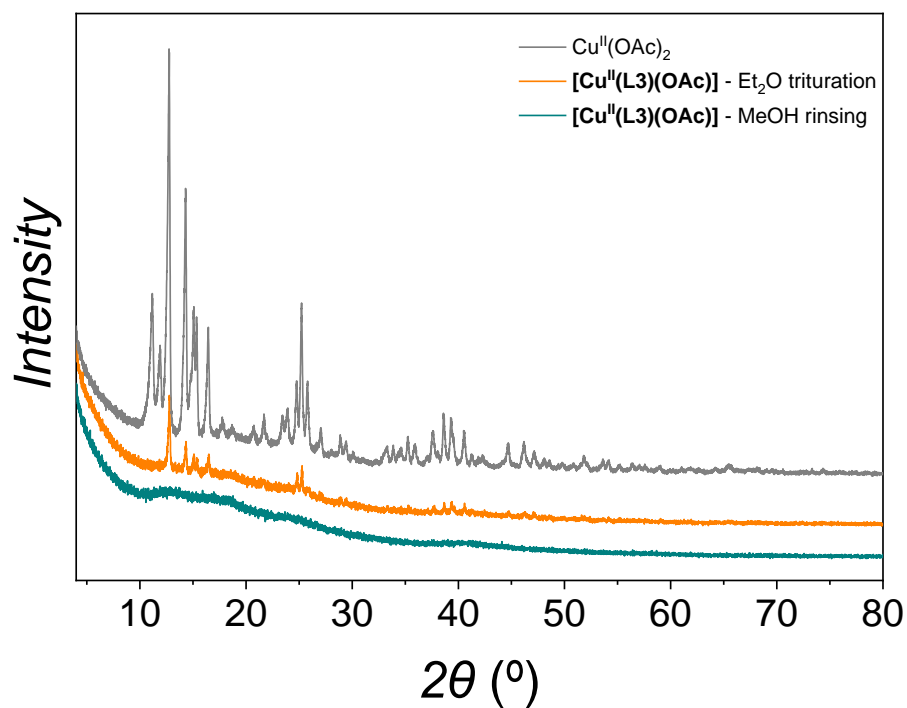
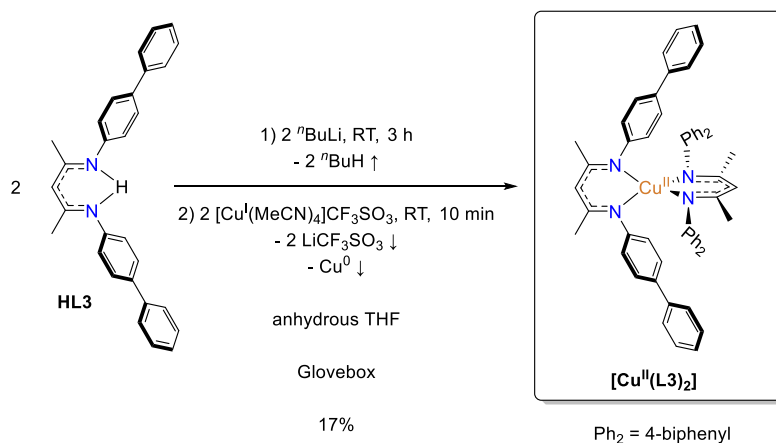


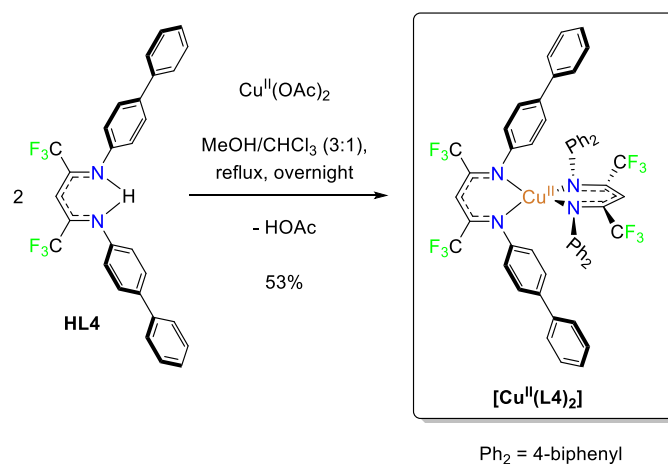
Figure S33. pXRD comparison between Cu^{II}(AcO)₂ and [Cu^{II}(L3)(AcO)] with/without MeOH rinsing. The crystallinity of the samples was coming from residual Cu^{II}(OAc)₂.

4.17. Preparation of $[\text{Cu}^{\text{II}}(\text{L3})_2]$

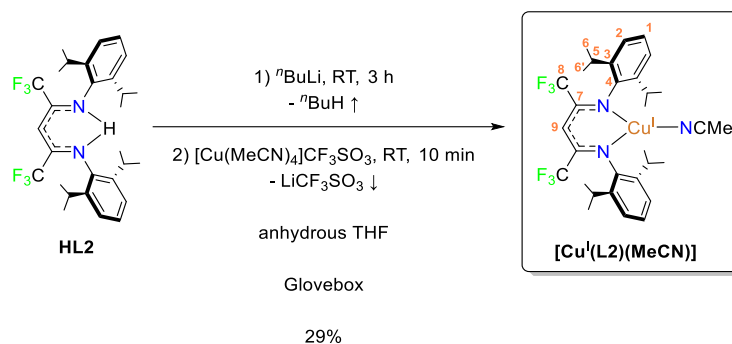


Inside a glovebox ($[\text{H}_2\text{O}] < 0.1 \text{ ppm}$, $[\text{O}_2] < 0.1 \text{ ppm}$), a solution of $n\text{BuLi}$ (2.5 M in hexanes, 0.24 mL, 0.60 mmol) was carefully added dropwise at RT to a stirring solution of **HL3** (200 mg, 0.50 mmol) in anhydrous THF (5 mL), avoiding overheating. The resulting orange mixture was stirred at RT for 3 h. After this time, $[\text{Cu}^{\text{I}}(\text{MeCN})_4]\text{CF}_3\text{SO}_3$ (189 mg, 0.50 mmol) was added to the reaction mixture, turning it dark. The mixture was stirred at RT for an additional 10 min. All volatiles were then removed under dynamic vacuum, leaving a red residue that was suspended in anhydrous n -pentane (3 x 20 mL) and filtered through a Celite plug. The volatiles of the filtrate were removed under dynamic vacuum, yielding a brown residue. This residue was recrystallized from n -pentane (RT/-40 $^\circ\text{C}$) to obtain $[\text{Cu}^{\text{II}}(\text{L3})_2]$ (37 mg, 0.042 mmol, 17%) as dark brown crystals. **Anal. Calcd** for $\text{C}_{58}\text{H}_{50}\text{CuN}_4 \cdot 2.4\text{H}_2\text{O}$: C, 76.57; H, 6.07; N, 6.16. Found: C, 76.57; H, 6.27; N, 6.09. The **SC-XRD** structure is shown in Figure S112.

4.18. Preparation of $[\text{Cu}^{\text{II}}(\text{L4})_2]$



A solution of **HL4** (102 mg, 0.1 mmol) in CHCl_3 (5 mL) was added to a stirring MeOH (15 mL) solution of $\text{Cu}^{\text{II}}(\text{AcO})_2$ (19 mg, 0.1 mmol). The resulting dark mixture was refluxed overnight. After this time, the reaction mixture was left to cool to RT, and dark brown precipitates formed. The solvent of the reaction mixture was removed under reduced pressure, and the residue was triturated with MeOH (10 mL) and filtered to yield $[\text{Cu}^{\text{II}}(\text{L4})_2]$ (57 mg, 0.053 mmol, 53%) as a dark brown powder. **Anal. Calcd** for $\text{C}_{58}\text{H}_{38}\text{CuF}_{12}\text{N}_4 \cdot 2.6\text{H}_2\text{O}$: C, 61.69; H, 3.86; N, 4.96. Found: C, 61.67; H, 3.75; N, 5.02. The **SC-XRD** structure is shown in Figure S113.

4.19. Preparation of $[\text{Cu}^{\text{I}}(\text{L2})(\text{MeCN})]$ 

Inside a glovebox ($[\text{H}_2\text{O}] < 0.1$ ppm, $[\text{O}_2] < 0.1$ ppm), a solution of $n\text{-BuLi}$ (2.5 M in hexanes, 1.00 mL, 1.25 mmol) was carefully added dropwise at RT to a stirring solution of **HL2** (1.258 g, 2.39 mmol) in anhydrous THF (10 mL), avoiding overheating. The resulting brown mixture was stirred at RT for 3 h. After this time, $[\text{Cu}^{\text{I}}(\text{MeCN})_4]\text{CF}_3\text{SO}_3$ (902 mg, 2.39 mmol) was added to the reaction mixture, turning it dark. The mixture was stirred at RT for an additional 10 min. All volatiles were then removed under dynamic vacuum, leaving a red residue that was suspended in anhydrous n -pentane (3 x 20 mL) and filtered through a Celite plug. The volatiles of the filtrate were removed under dynamic vacuum, yielding a red residue. This residue was recrystallized from MeCN (RT/ -40 °C) and washed with n -pentane to afford $[\text{Cu}^{\text{I}}(\text{L2})(\text{MeCN})]$ (440 mg, 0.70 mmol, 29%) as red crystals. NMR data corresponded to the one reported in the literature.¹³ ^1H NMR (400 MHz, CD_3CN) δ (ppm): 7.16-6.99 (m, 6H, **H1** + **H2**), 5.54 (s, 1H, **H8**), 3.06 (hept, $J_{\text{H4-H5}} = J_{\text{H4-H5}'} = 7.0$ Hz, 4H, **H4**), 1.96 (s, 3H, **NCCH₃**), 1.21 (d, $J_{\text{H5-H4}} = 7.0$ Hz, 12H, **H5**) 1.13 (d, $J_{\text{H5'-H4}} = 7.0$ Hz, 12H, **H5'**). ^{19}F NMR (376 MHz, CD_3CN) δ (ppm): -63.73 (s, **CF₃**).

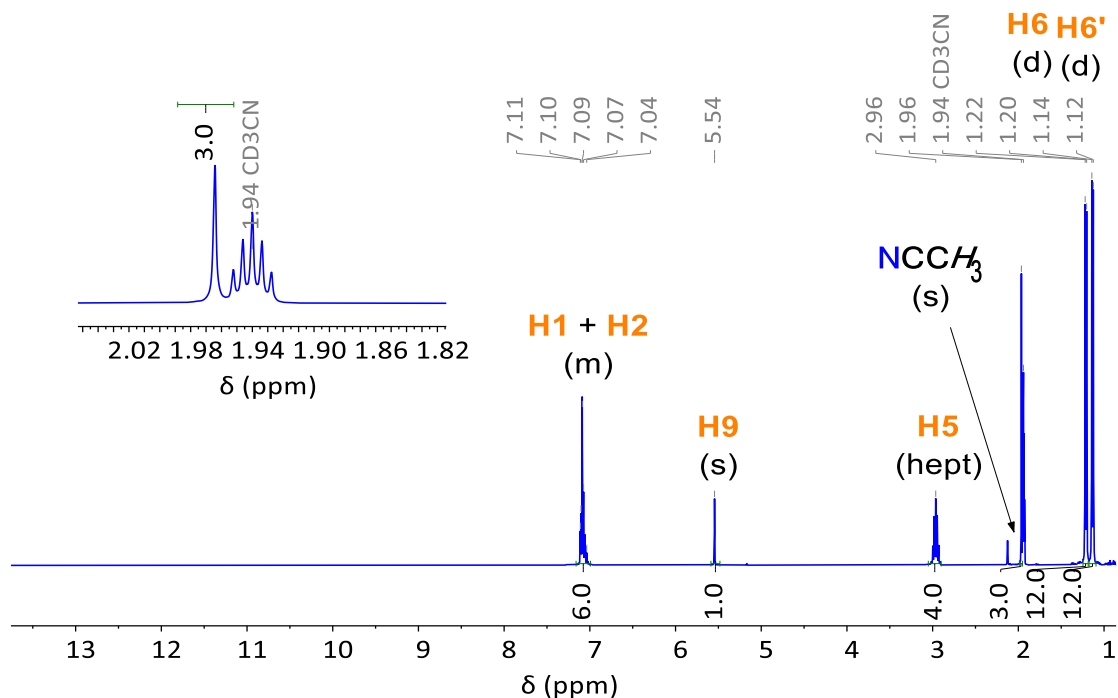


Figure S34. ^1H NMR spectrum (400 MHz, CD_3CN) of $[\text{Cu}^{\text{I}}(\text{L2})(\text{MeCN})]$.

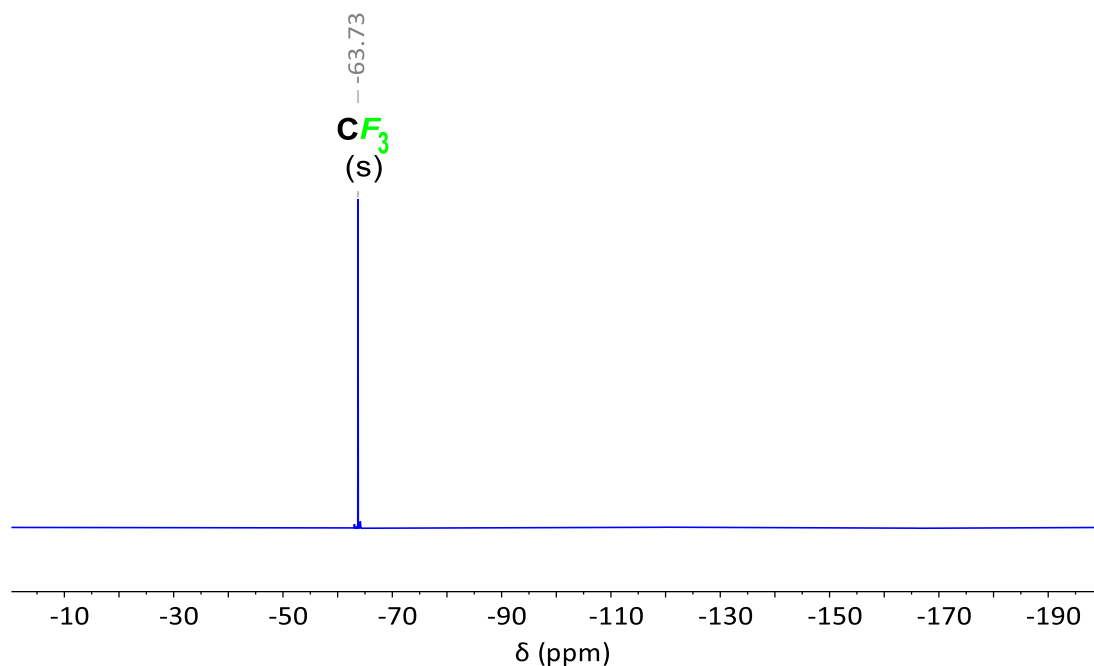


Figure S35. ^{19}F NMR spectrum (376 MHz, CD_3CN) of $[\text{Cu}^{\text{I}}(\text{L}2)(\text{MeCN})]$.

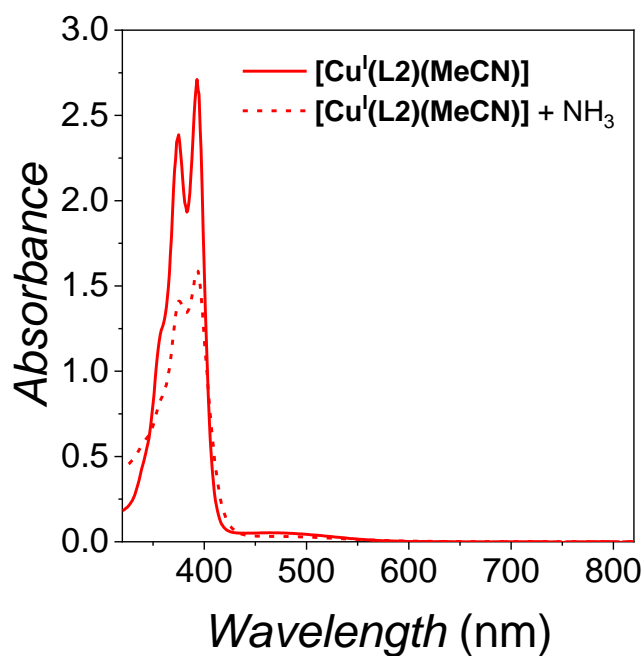
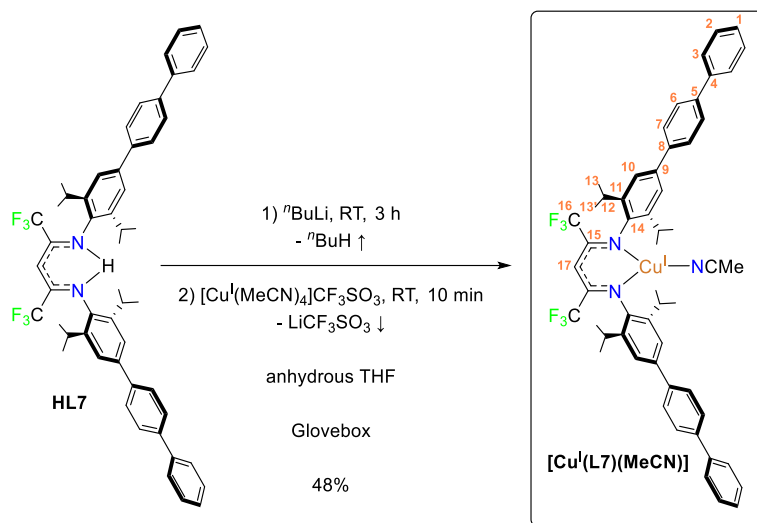
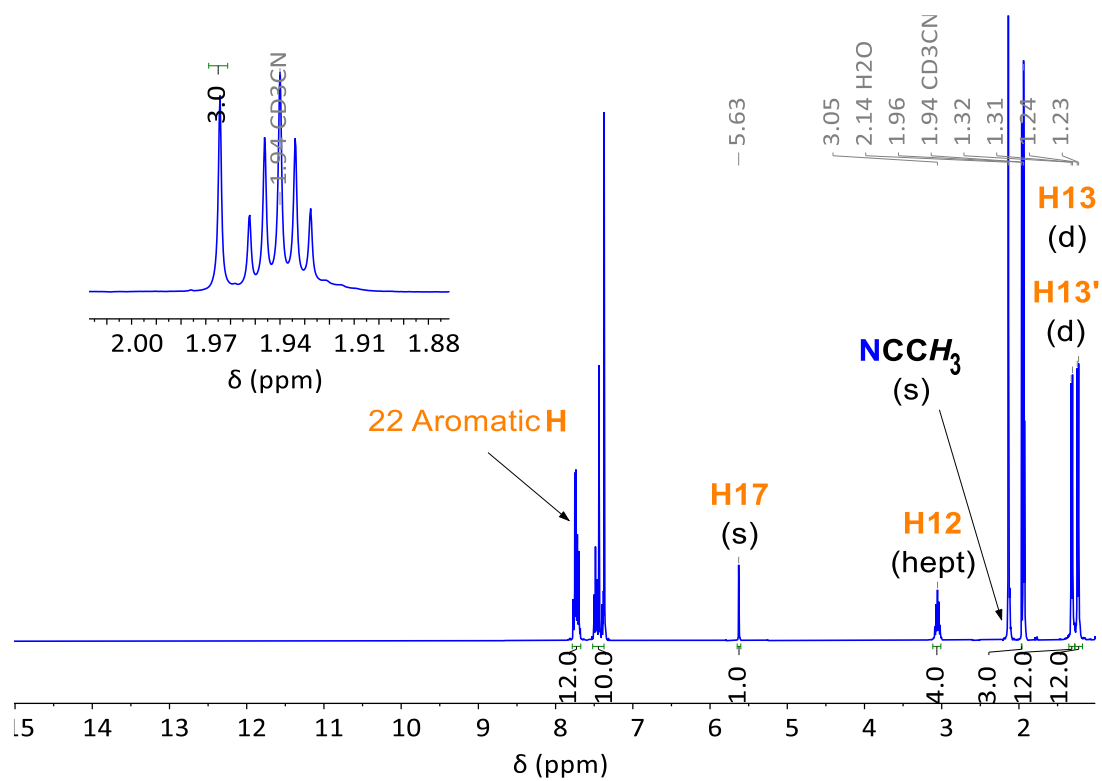
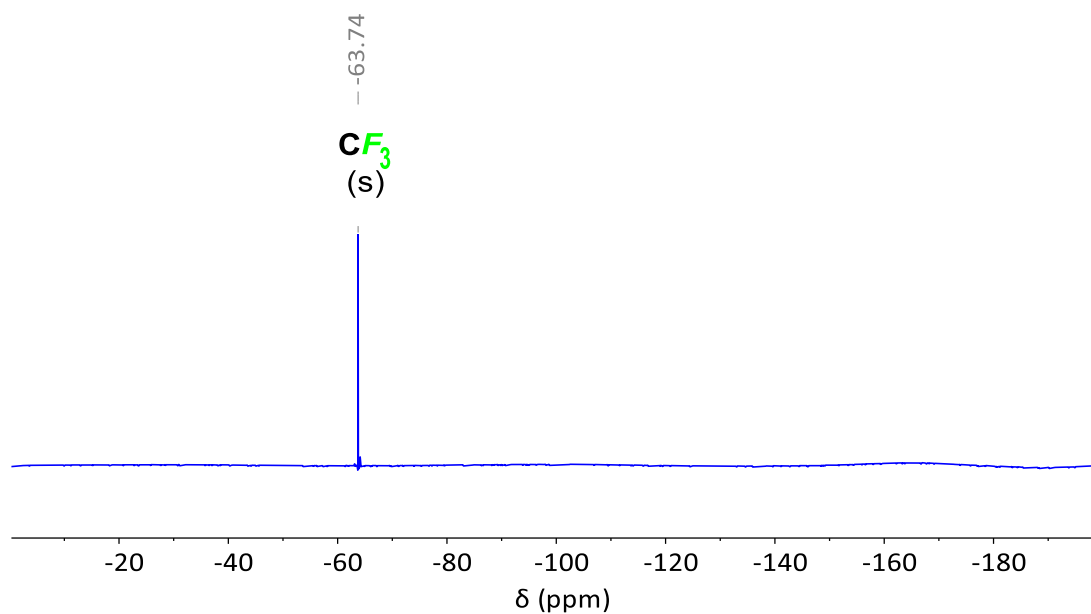


Figure S36. UV-vis spectrum of 0.1 mM $[\text{Cu}^{\text{I}}(\text{L}2)(\text{MeCN})]$ in MeCN under an inert atmosphere with/without 50 mM NH_3 . The presence of NH_3 initiates the equilibria described in the paper (Equations 8 and 9), leading to the formation of the colorless $[\text{Cu}^{\text{I}}(\text{NH}_3)_4]^+$ complex, which coexists in equilibrium with the red $[\text{Cu}^{\text{I}}(\text{L}2)(\text{NH}_3)]$ and $[\text{Cu}^{\text{I}}(\text{L}2)(\text{MeCN})]$ species.¹³ These equilibria are evidenced by the decrease in absorbance in the UV-vis spectra.

4.20. Preparation of $[\text{Cu}^{\text{I}}(\text{L7})(\text{MeCN})]$ 

Inside a glovebox ($[\text{H}_2\text{O}] < 0.1$ ppm, $[\text{O}_2] < 0.1$ ppm), a solution of $n\text{BuLi}$ (2.5 M in hexanes, 0.50 mL, 1.25 mmol) was carefully added dropwise at RT to a stirring solution of **HL7** (715 mg, 0.86 mmol) in anhydrous THF (5 mL), avoiding overheating. The resulting brown mixture was stirred at RT for 3 h. After this time, $[\text{Cu}^{\text{I}}(\text{MeCN})_4]\text{CF}_3\text{SO}_3$ (324 mg, 0.86 mmol) was added to the reaction mixture, turning it dark. The mixture was stirred at RT for an additional 10 min. All volatiles were then removed under dynamic vacuum, leaving a red residue that was suspended in anhydrous benzene (3 x 10 mL) and filtered through a Celite plug. The volatiles of the filtrate were removed under dynamic vacuum, yielding a red residue. This residue was recrystallized from MeCN (RT/ -40 °C) and washed with n pentane to afford $[\text{Cu}^{\text{I}}(\text{L7})(\text{MeCN})]$ (548 mg, 0.59 mmol, 48%) as red crystals. ^1H NMR (400 MHz, CD_3CN) δ (ppm): 7.80-7.66 (m, 12H, **Ar**), 7.53-7.35 (m, 10H, **Ar**), 5.63 (s, 1H, **H17**), 3.05 (hept, $J_{\text{H12-H13}} = J_{\text{H12-H13}'} = 7.0$ Hz, 4H, **H12**), 1.96 (s, 3H, **NCCCH₃**), 1.31 (d, $J_{\text{H13-H12}} = 7.0$ Hz, 12H, **H13**) 1.24 (d, $J_{\text{H13}'-H12} = 7.0$ Hz, 12H, **H13'**). ^{19}F NMR (376 MHz, CD_3CN) δ (ppm): -63.74 (s, **CF₃**). $^{13}\text{C}\{^1\text{H}\}$ NMR (101 MHz, CDCl_3) δ (ppm): 145.66, 141.37, 141.18, 140.30, 136.98, 129.95, 128.44, 128.27, 128.12, 127.77, 122.43, 118.31, 29.39, 24.85, 22.82, 22.70. **Anal. Calcd** for $\text{C}_{55}\text{H}_{54}\text{CuF}_6\text{N}_3 \cdot 0.4\text{H}_2\text{O}$: C, 70.14; H, 5.87; N, 4.46. Found: C, 70.17; H, 6.19; N, 4.21. The **SC-XRD** structure is shown in Figure S114.

Figure S37. ^1H NMR spectrum (400 MHz, CD_3CN) of $[\text{Cu}^{\text{I}}(\text{L7})(\text{MeCN})]$.Figure S38. ^{19}F NMR spectrum (376 MHz, CD_3CN) of $[\text{Cu}^{\text{I}}(\text{L7})(\text{MeCN})]$.

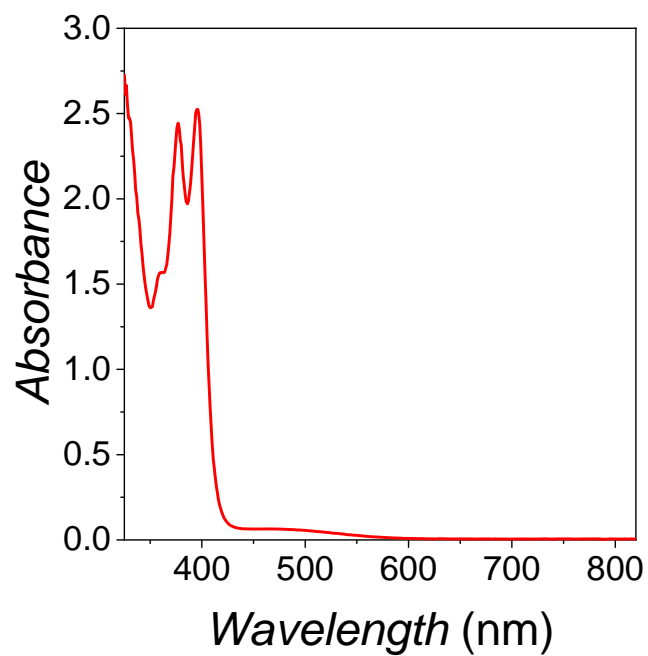
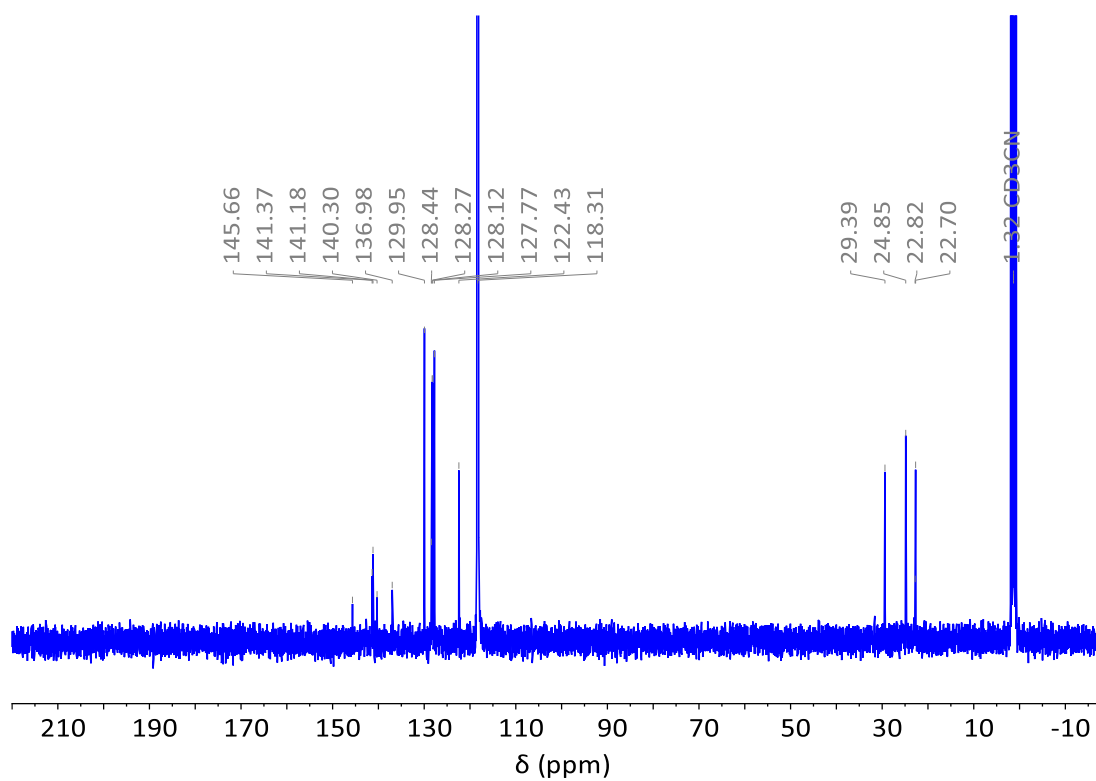
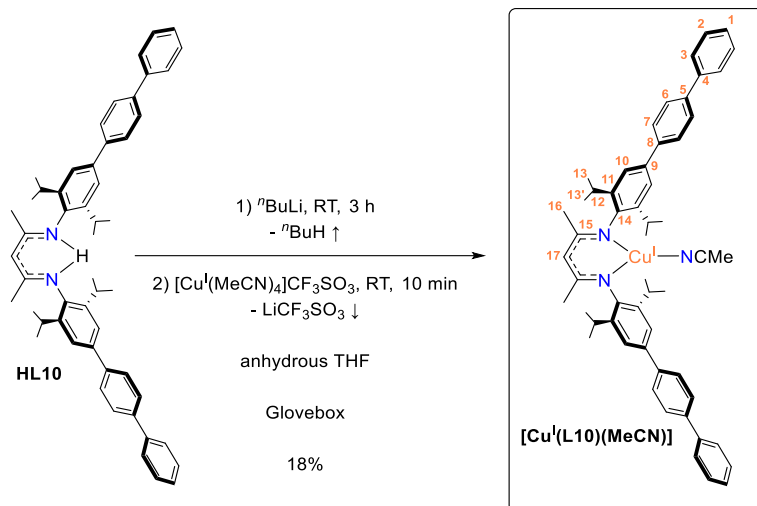


Table S1. Qualitative solubility test of [Cu^I(L7)(MeCN)] in various solvents commonly used in electrochemistry. The compound's solubility was evaluated visually by mixing small amounts of the solid with each solvent and observing whether it dissolved under gentle stirring. These results provide guidance for selecting suitable solvents for C_{FP} functionalization and also for determining the appropriate solvent in heterogeneous electrochemical experiments.

Solvent	Solubility at RT
1-(But-1-yl)-3-methyl-1H-imidazol-3-ium hexafluorophosphate	Insoluble
1,2-Dimethoxyethane	Soluble
2,2,2-Trifluoroethanol (TFE)	Insoluble
Benzene	Soluble
Benzonitrile	Soluble
Butyronitrile	Soluble
Dichloroethane (DCE)	Soluble
Dichloromethane (DCM)	Soluble
EtOH	Partially soluble
ⁱ PrOH	Partially soluble
MeCN	Soluble
MeOH	Partially soluble
N,N'-dimethylformamide (DMF)	Soluble
ⁿ BuOH	Partially soluble
Nitromethane	Soluble
N-methylpyrrolidinone (NMP)	Soluble
ⁿ pentane	Soluble
ⁿ PrOH	Partially soluble
Propylene carbonate (PC)	Partially soluble
THF	Soluble
Toluene	Soluble
Trifluoro-toluene	Soluble
γ -butyrolactone	Soluble

4.21. Preparation of $[\text{Cu}^{\text{I}}(\text{L10})(\text{MeCN})]$ 

Inside a glovebox ($[\text{H}_2\text{O}] < 0.1$ ppm, $[\text{O}_2] < 0.1$ ppm), a solution of $n\text{BuLi}$ (2.5 M in hexanes, 0.26 mL, 0.65 mmol) was carefully added dropwise at RT to a stirring solution of **HL10** (400 mg, 0.55 mmol) in anhydrous THF (10 mL), avoiding overheating. The resulting dark red mixture was stirred at RT for 3 h. After this time, $[\text{Cu}^{\text{I}}(\text{MeCN})_4]\text{CF}_3\text{SO}_3$ (452 mg, 1.20 mmol) was added to the reaction mixture, turning it yellow. The mixture was stirred at RT for an additional 10 min. All volatiles were then removed under dynamic vacuum, leaving a greenish yellow residue that was suspended in anhydrous n -pentane (3 x 10 mL) and filtered through a Celite plug. The volatiles of the filtrate were removed under dynamic vacuum, yielding a yellow residue. This residue was recrystallized from n -pentane (RT/ -40 °C) to afford $[\text{Cu}^{\text{I}}(\text{L10})(\text{MeCN})]$ (82 mg, 0.01 mmol, 18%) as yellow crystals. $^1\text{H NMR}$ (400 MHz, CD_3CN) δ (ppm): 7.78-7.69 (m, 12H, **Ar**), 7.51-7.35 (m, 10H, **Ar**), 4.76 (s, 1H, **H18**), 3.25 (hept, $J_{\text{H12-H13}} = J_{\text{H12-H13}'} = 7.0$ Hz, 4H, **H12**), 1.96 (s, 3H, **NCCCH**₃), 1.70 (s, 6H, **H16**), 1.30 (d, $J_{\text{H13-H12}} = 7.0$ Hz, 12H, **H13**), 1.24 (d, $J_{\text{H13}'-H12} = 7.0$ Hz, 12H, **H13'**). $^{13}\text{C}\{^1\text{H}\}$ NMR (101 MHz, CDCl_3) δ (ppm): 129.94, 128.22, 127.98, 127.74, 122.51, 118.31, 28.90, 24.24, 23.31. **Anal. Calcd** for $\text{C}_{55}\text{H}_{60}\text{CuN}_3 \cdot 3.9\text{H}_2\text{O}$: C, 73.65; H, 7.62; N, 4.69. Found: C, 73.69; H, 7.22; N, 4.04. The **SC-XRD** structure is shown in Figure S115.

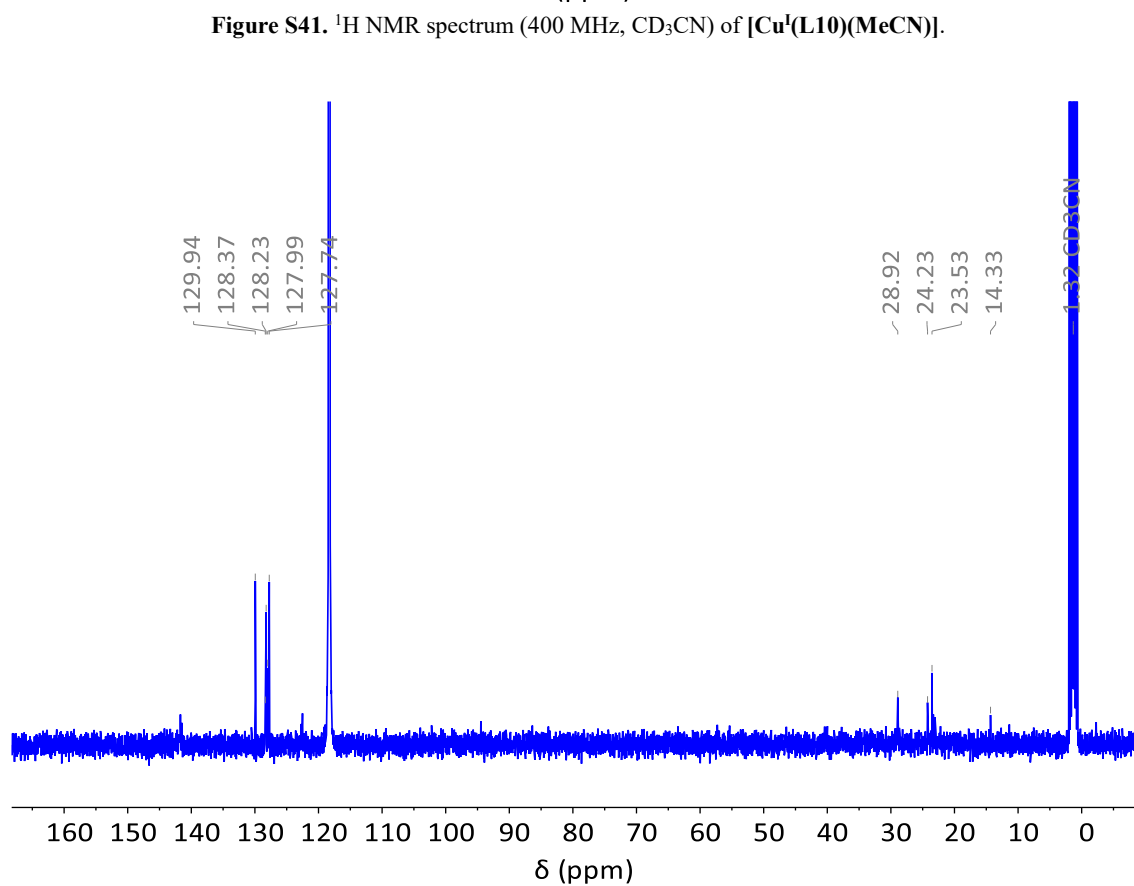
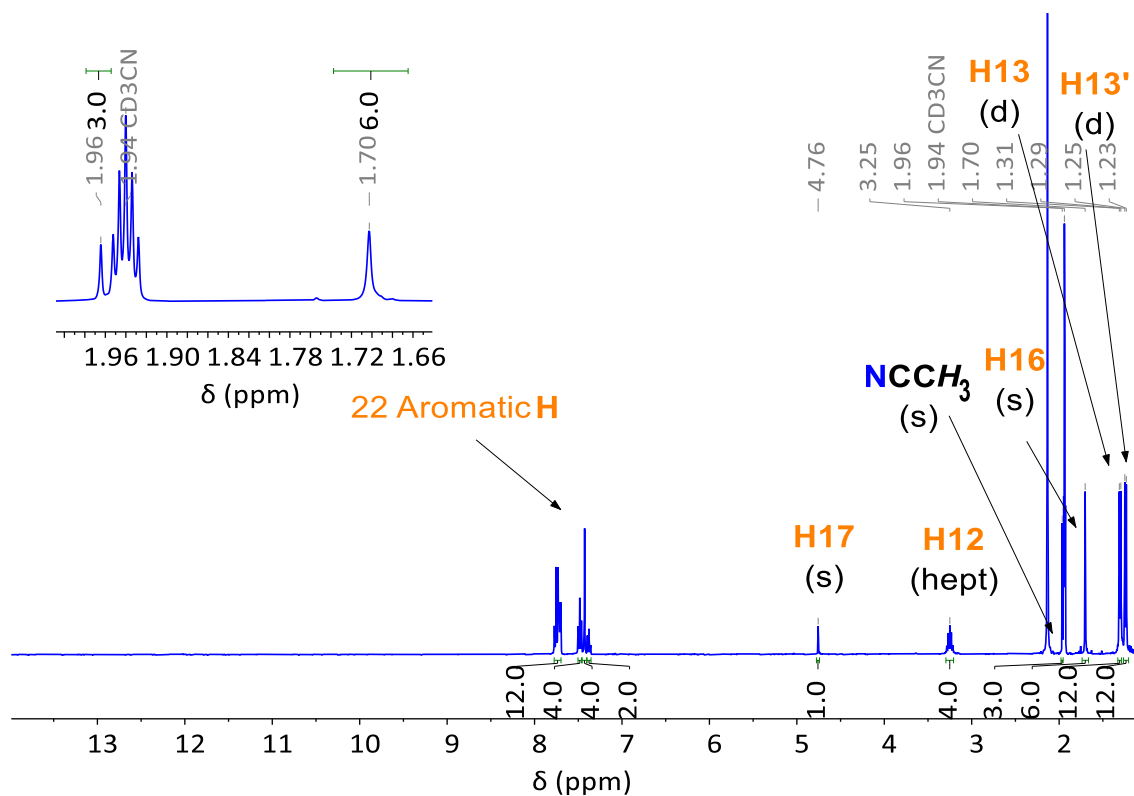
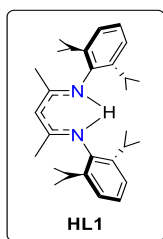


Table S2. Qualitative solubility test of [Cu^I(L10)(MeCN)] in various solvents commonly used in electrochemistry. The compound's solubility was evaluated visually by mixing small amounts of the solid with each solvent and observing whether it dissolved under gentle stirring. These results provide guidance for selecting suitable solvents for C_{FP} functionalization and also for determining the appropriate solvent in heterogeneous electrochemical experiments.

Solvent	Solubility at RT
1-(But-1-yl)-3-methyl-1H-imidazol-3-ium hexafluorophosphate	Insoluble
1,2-Dimethoxyethane	Soluble
2,2,2-Trifluoroethanol (TFE)	Insoluble
Benzene	Soluble
Benzonitrile	Soluble
Butyronitrile	Soluble
Dichloroethane (DCE)	Soluble
Dichloromethane (DCM)	Soluble
EtOH	Partially Soluble
ⁱ PrOH	Partially Soluble
MeCN	Partially soluble
MeOH	Partially soluble
N,N'-dimethylformamide (DMF)	Soluble
ⁿ BuOH	Partially Soluble
Nitromethane	Soluble
N-methylpyrrolidinone (NMP)	Soluble
ⁿ pentane	Partially soluble
ⁿ PrOH	Soluble
Propylene carbonate (PC)	Partially soluble
THF	Soluble
Toluene	Soluble
Trifluoro-toluene	Soluble
γ -butyrolactone	Partially Soluble

5. Electrochemical Studies

5.1. Electrochemistry of HL1



Homogeneous Electrochemistry of HL1 in THF

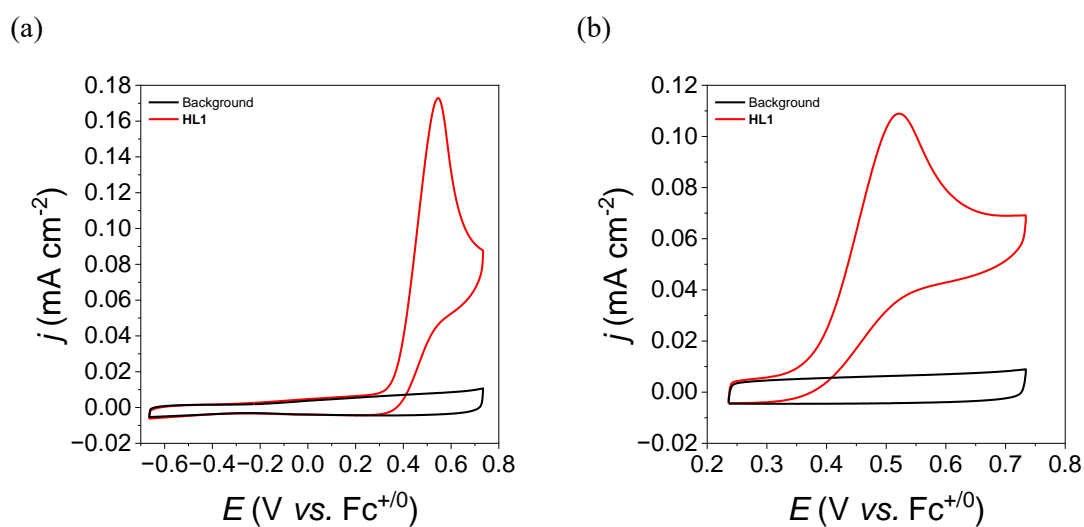


Figure S43. Cyclic voltammograms in THF ($\mu = 0.1$ M TBAPF₆) of 1 mM HL1. Conditions: under air, GC_{disk} ($S = 0.07$ cm²), WE; Pt disk, CE; Ag/AgCl wire, pseudo-RE; $\nu = 100$ mV s⁻¹.

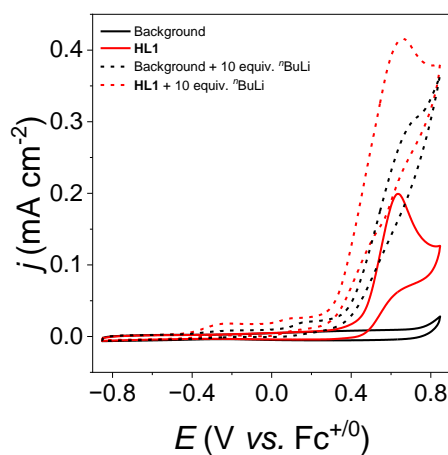
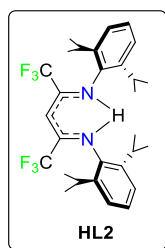


Figure S44. Cyclic voltammograms in THF ($\mu = 0.1$ M TBAPF₆) of 1 mM HL1 with 10 equiv. of ⁿBuLi. Conditions: under an inert atmosphere, GC_{disk} ($S = 0.07$ cm²), WE; Pt disk, CE; Ag/AgCl wire, pseudo-RE; $\nu = 100$ mV s⁻¹.

5.2. Electrochemistry of HL2



Homogeneous Electrochemistry of HL2 in THF

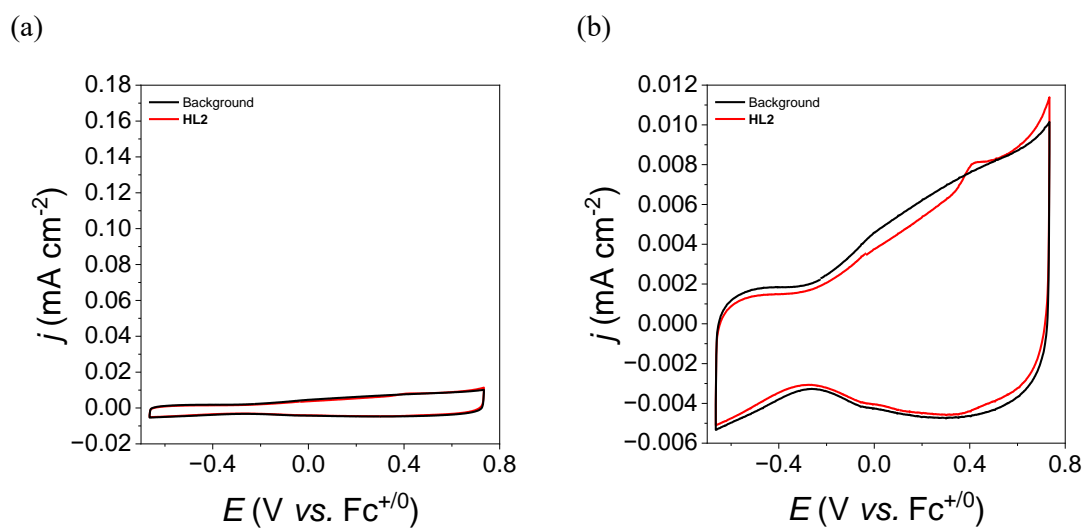


Figure S45. Cyclic voltammograms in THF ($\mu = 0.1$ M TBAPF₆) of 1 mM HL2. Conditions: under air, GC_{disk} ($S = 0.07$ cm²), WE; Pt disk, CE; Ag/AgCl wire, pseudo-RE; $\nu = 100$ mV s⁻¹.

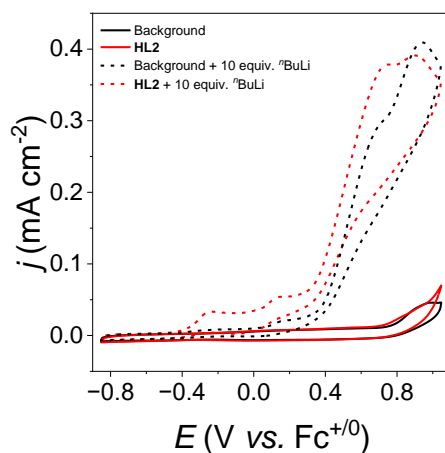


Figure S46. Cyclic voltammograms in THF ($\mu = 0.1$ M TBAPF₆) of 1 mM HL2 with 10 equiv. of ⁿBuLi. Conditions: under an inert atmosphere, GC_{disk} ($S = 0.07$ cm²), WE; Pt disk, CE; Ag/AgCl wire, pseudo-RE; $\nu = 100$ mV s⁻¹.

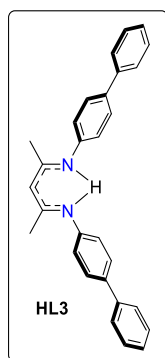
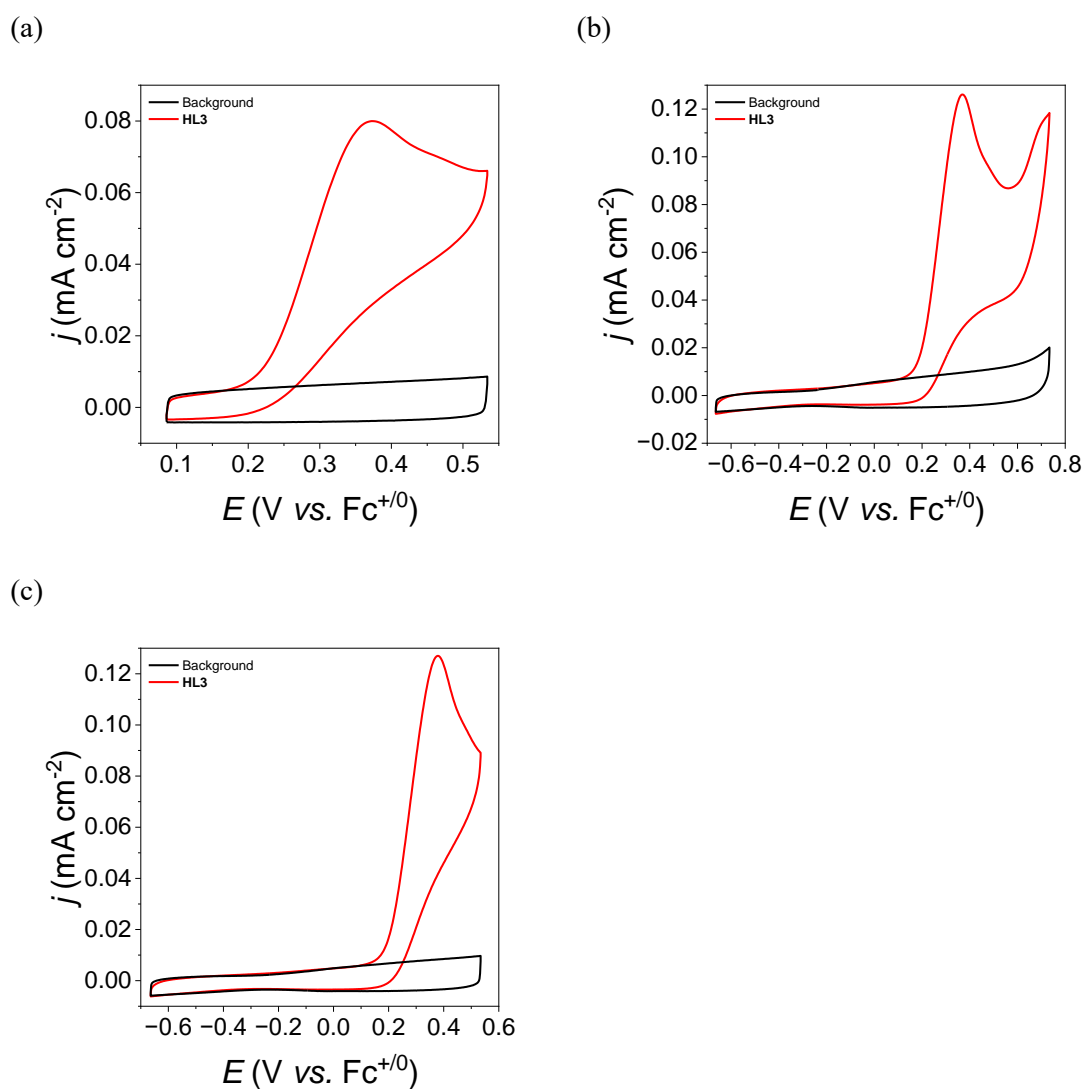
5.3. Electrochemistry of **HL3***Homogeneous Electrochemistry of HL3 in THF*

Figure S47. Cyclic voltammograms in THF ($\mu = 0.1$ M TBAPF₆) of 1 mM **HL3**. Conditions: under air, GC_{disk} ($S = 0.07$ cm²), WE; Pt disk, CE; Ag/AgCl wire, pseudo-RE; $\nu = 100$ mV s⁻¹.

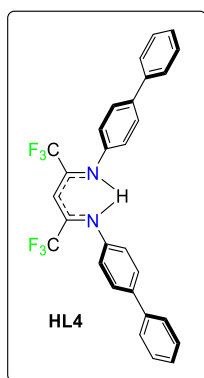
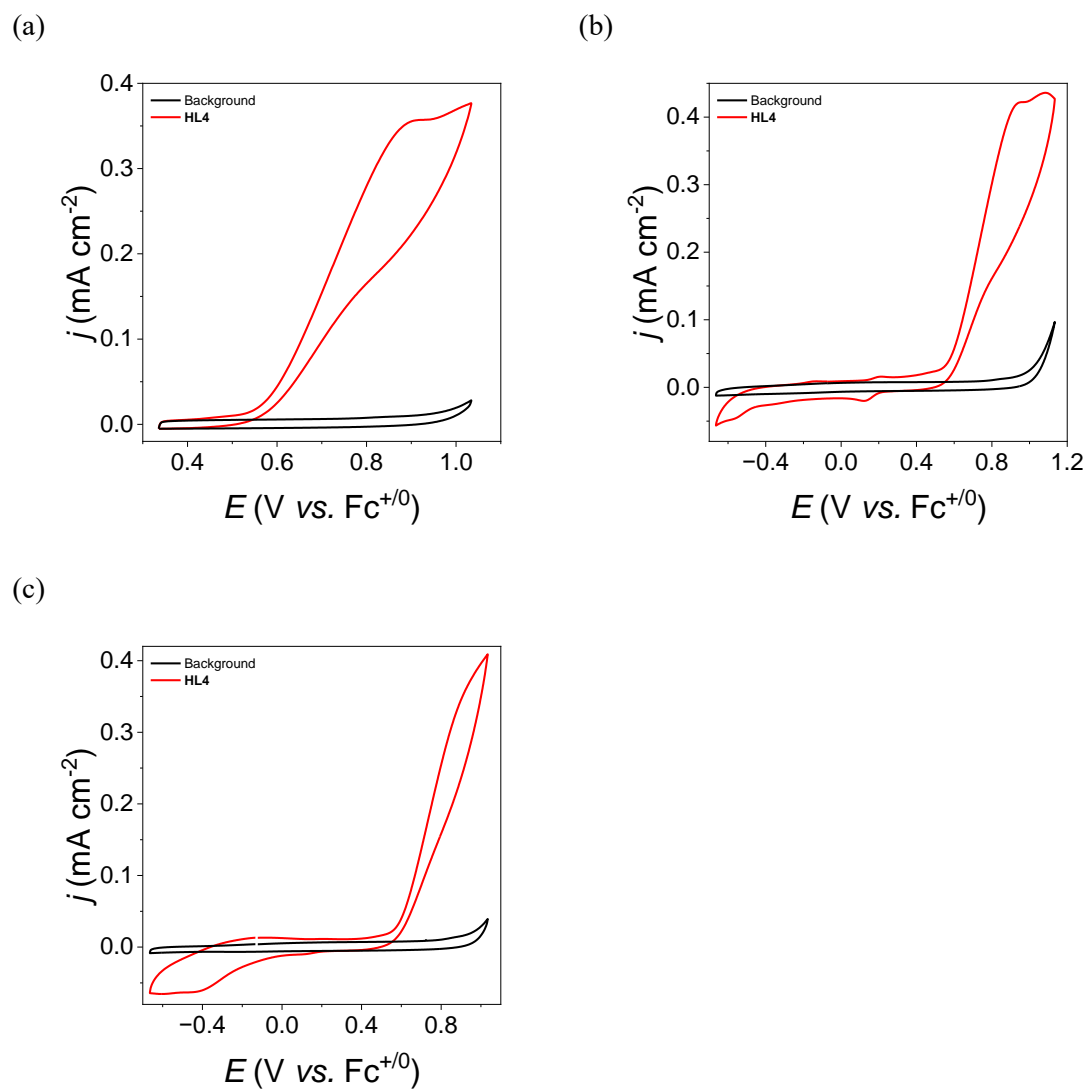
5.4. Electrochemistry of **HL4**Homogeneous Electrochemistry of **HL4** in THF

Figure S48. Cyclic voltammograms in THF ($\mu = 0.1$ M TBAPF₆) of 1 mM **HL4**. Conditions: under air, GC_{disk} ($S = 0.07$ cm²), WE; Pt disk, CE; Ag/AgCl wire, pseudo-RE; $\nu = 100$ mV s⁻¹.

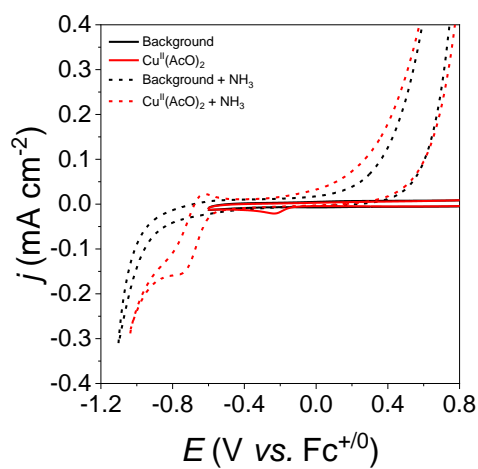
5.5. Electrochemistry of $\text{Cu}^{\text{II}}(\text{AcO})_2$ *Homogeneous Electrochemistry of $\text{Cu}^{\text{II}}(\text{AcO})_2$ in THF*

Figure S49. Cyclic voltammograms in THF ($\mu = 0.1$ M TBAPF_6) of 1 mM $\text{Cu}^{\text{II}}(\text{AcO})_2$ with/without 0.5 M NH_3 . Conditions: under air, GC_{disk} ($S = 0.07$ cm²), WE; Pt disk, CE; Ag/AgCl wire, pseudo-RE; $\nu = 100$ mV s⁻¹.

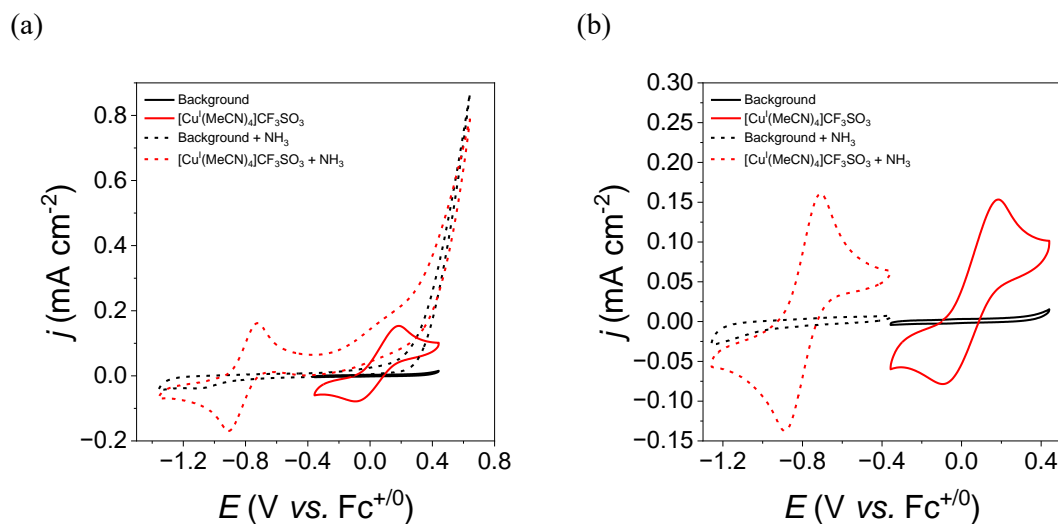
5.6. Electrochemistry of $[\text{Cu}^{\text{I}}(\text{MeCN})_4]\text{CF}_3\text{SO}_3$ *Homogeneous Electrochemistry of $[\text{Cu}^{\text{I}}(\text{MeCN})_4]\text{CF}_3\text{SO}_3$ in THF*

Figure S50. Cyclic voltammograms in THF ($\mu = 0.1$ M TBAPF₆) of 1 mM $[\text{Cu}^{\text{I}}(\text{MeCN})_4]\text{CF}_3\text{SO}_3$ with/without 0.5 M NH₃. *Conditions:* under an inert atmosphere, GC_{disk} ($S = 0.07$ cm²), WE; Pt disk, CE; Ag/AgCl wire, pseudo-RE; $\nu = 100$ mV s⁻¹.

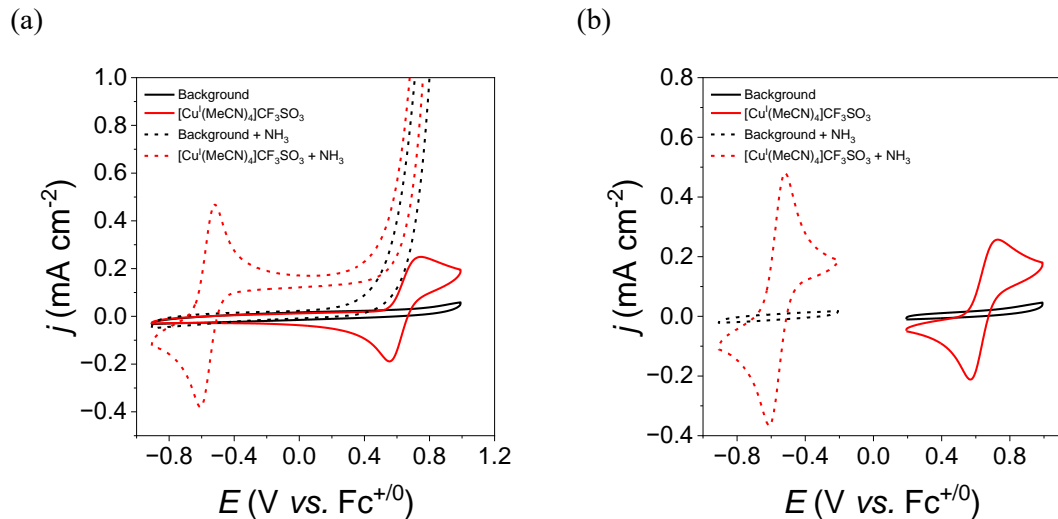
Homogeneous Electrochemistry of $[\text{Cu}^{\text{I}}(\text{MeCN})_4]\text{CF}_3\text{SO}_3$ in MeCN

Figure S51. Cyclic voltammograms in MeCN ($\mu = 0.1$ M TBAPF₆) of 1 mM $[\text{Cu}^{\text{I}}(\text{MeCN})_4]\text{CF}_3\text{SO}_3$ with/without 0.5 M NH₃. *Conditions:* under an inert atmosphere, GC_{disk} ($S = 0.07$ cm²), WE; Pt disk, CE; Ag/AgCl wire, pseudo-RE; $\nu = 100$ mV s⁻¹.

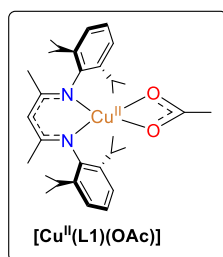
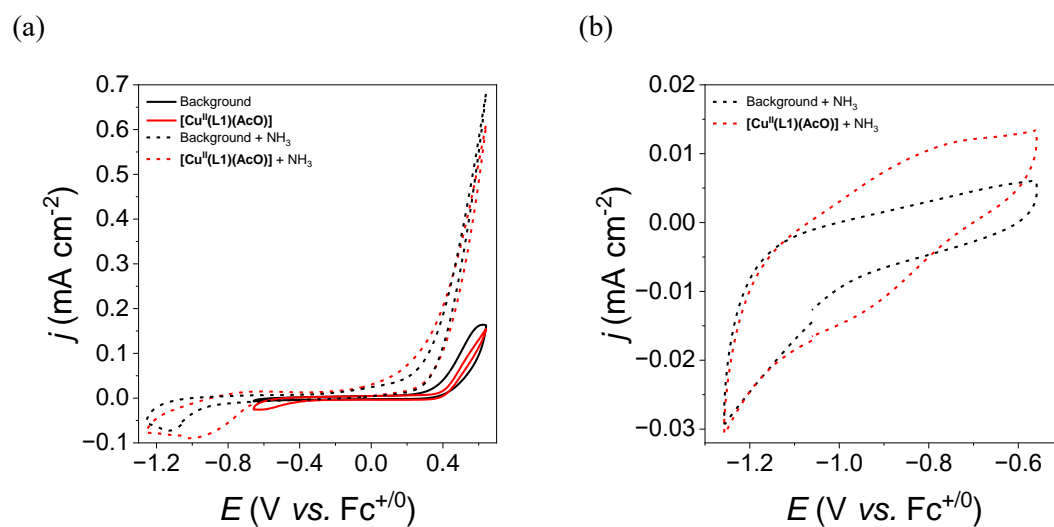
5.7. Electrochemistry of $[\text{Cu}^{\text{II}}(\text{L1})(\text{AcO})]$ Homogeneous Electrochemistry of $[\text{Cu}^{\text{II}}(\text{L1})(\text{AcO})]$ in THF

Figure S52. Cyclic voltammograms in THF ($\mu = 0.1$ M TBAPF₆) of 1 mM $[\text{Cu}^{\text{II}}(\text{L1})(\text{AcO})]$ with/without 0.5 M NH₃. Conditions: under air, GC_{disk} ($S = 0.07$ cm²), WE; Pt disk, CE; Ag/AgCl wire, pseudo-RE; $\nu = 100$ mV s⁻¹.

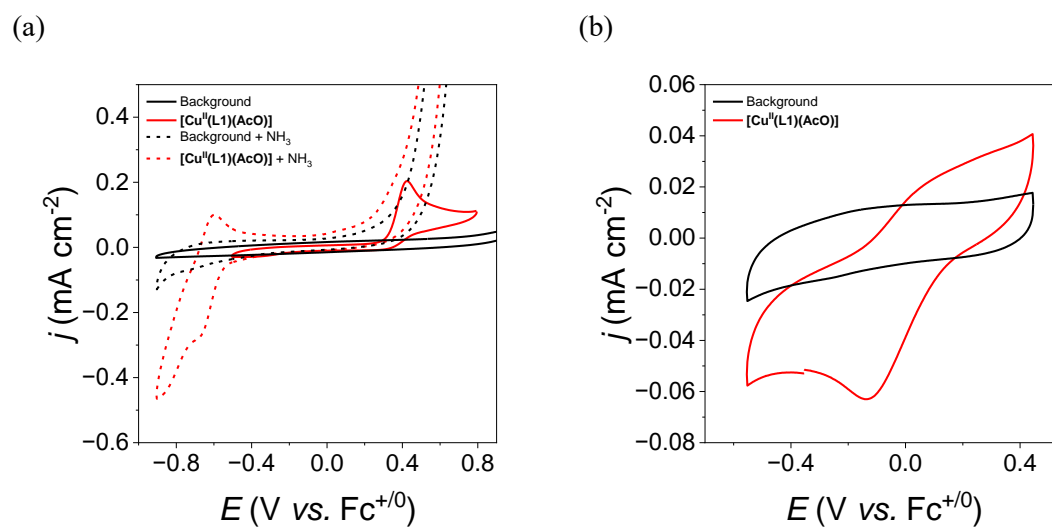
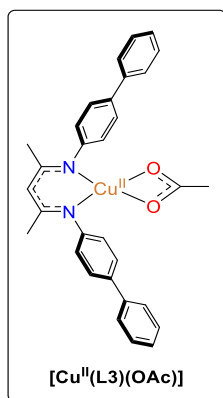
Homogeneous Electrochemistry of $[\text{Cu}^{\text{II}}(\text{L1})(\text{AcO})]$ in MeCN

Figure S53. (a) Cyclic voltammograms in MeCN ($\mu = 0.1 \text{ M TBAPF}_6$) of $1 \text{ mM } [\text{Cu}^{\text{II}}(\text{L1})(\text{AcO})]$ with/without 1.4 M NH_3 . Conditions: under an inert atmosphere, GC_{disk} ($S = 0.07 \text{ cm}^2$), WE; Pt disk, CE; Ag/AgCl wire, pseudo-RE; $\nu = 100 \text{ mV s}^{-1}$. (b) Cyclic voltammograms in THF ($\mu = 0.1 \text{ M NH}_4\text{CF}_3\text{SO}_3$) of $1 \text{ mM } [\text{Cu}^{\text{II}}(\text{L1})(\text{AcO})]$ with/without 1.4 M NH_3 . Conditions: under an inert atmosphere, GC_{disk} ($S = 0.07 \text{ cm}^2$), WE; Pt disk, CE; Ag/AgCl wire, pseudo-RE; $\nu = 100 \text{ mV s}^{-1}$.

5.8. Electrochemistry of $[\text{Cu}^{\text{II}}(\text{L3})(\text{AcO})]$



Homogeneous Electrochemistry of $[\text{Cu}^{\text{II}}(\text{L3})(\text{AcO})]$ in THF

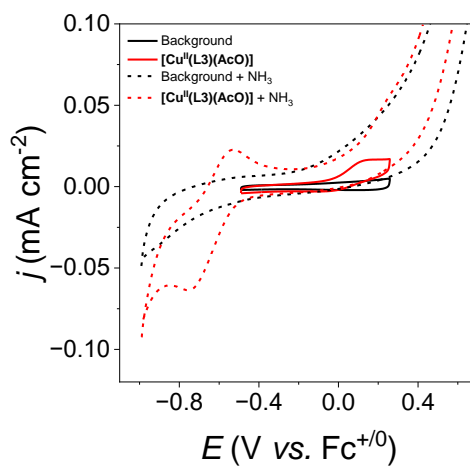


Figure S54. Cyclic voltammograms in THF ($\mu = 0.1 \text{ M TBAPF}_6$) of $1 \text{ mM } [\text{Cu}^{\text{II}}(\text{L3})(\text{AcO})]$ with/without 0.5 M NH_3 . Conditions: under air, GC_{disk} ($S = 0.07 \text{ cm}^2$), WE; Pt disk, CE; Ag/AgCl wire, pseudo-RE; $\nu = 100 \text{ mV s}^{-1}$.

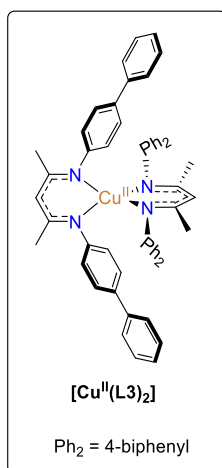
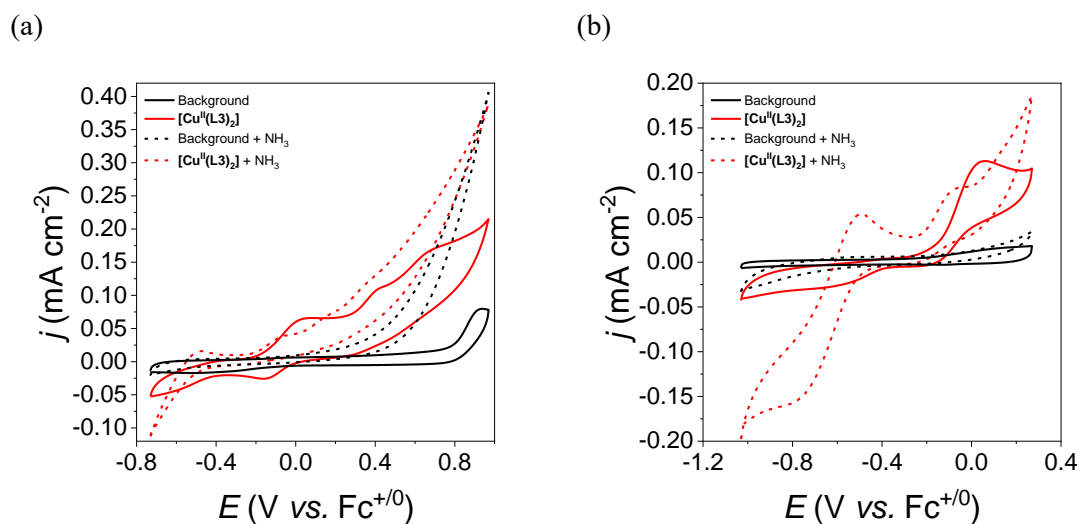
5.9. Electrochemistry of $[\text{Cu}^{\text{II}}(\text{L3})_2]$ *Homogeneous Electrochemistry of $[\text{Cu}^{\text{II}}(\text{L3})_2]$ in THF*

Figure S55. Cyclic voltammograms in THF ($\mu = 0.1 \text{ M TBAPF}_6$) of $1 \text{ mM } [\text{Cu}^{\text{II}}(\text{L3})_2]$ with/without 0.5 M NH_3 . Conditions: under air, GC_{disk} ($S = 0.07 \text{ cm}^2$), WE; Pt disk, CE; Ag/AgCl wire, pseudo-RE; $\nu = 100 \text{ mV s}^{-1}$.

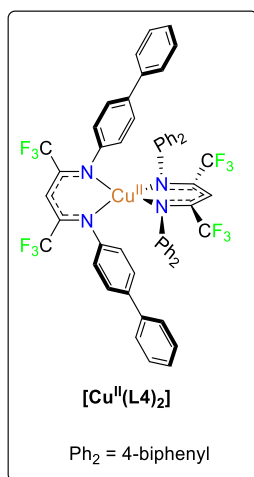
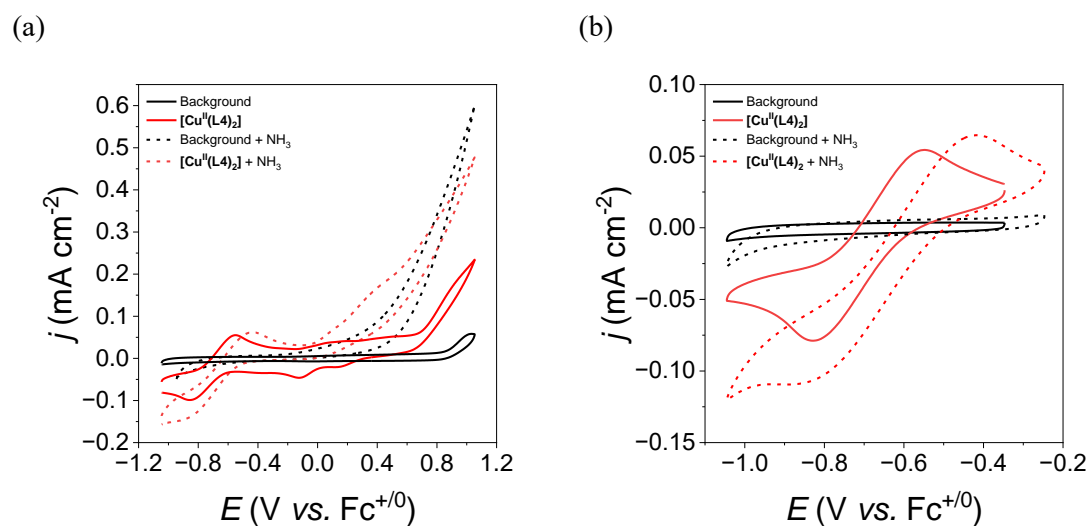
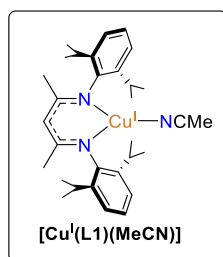
5.10. Electrochemistry of $[\text{Cu}^{\text{II}}(\text{L4})_2]$ *Homogeneous Electrochemistry of $[\text{Cu}^{\text{II}}(\text{L4})_2]$ in THF*

Figure S56. Cyclic voltammograms in THF ($\mu = 0.1 \text{ M TBAPF}_6$) of $1 \text{ mM } [\text{Cu}^{\text{II}}(\text{L4})_2]$ with/without 0.5 M NH_3 . Conditions: under air, GC_{disk} ($S = 0.07 \text{ cm}^2$), WE; Pt disk, CE; Ag/AgCl wire, pseudo-RE; $\nu = 100 \text{ mV s}^{-1}$.

5.11. Electrochemistry of $[\text{Cu}^{\text{I}}(\text{L1})(\text{MeCN})]$



Homogeneous Electrochemistry of $[\text{Cu}^{\text{I}}(\text{L1})(\text{MeCN})]$ in THF

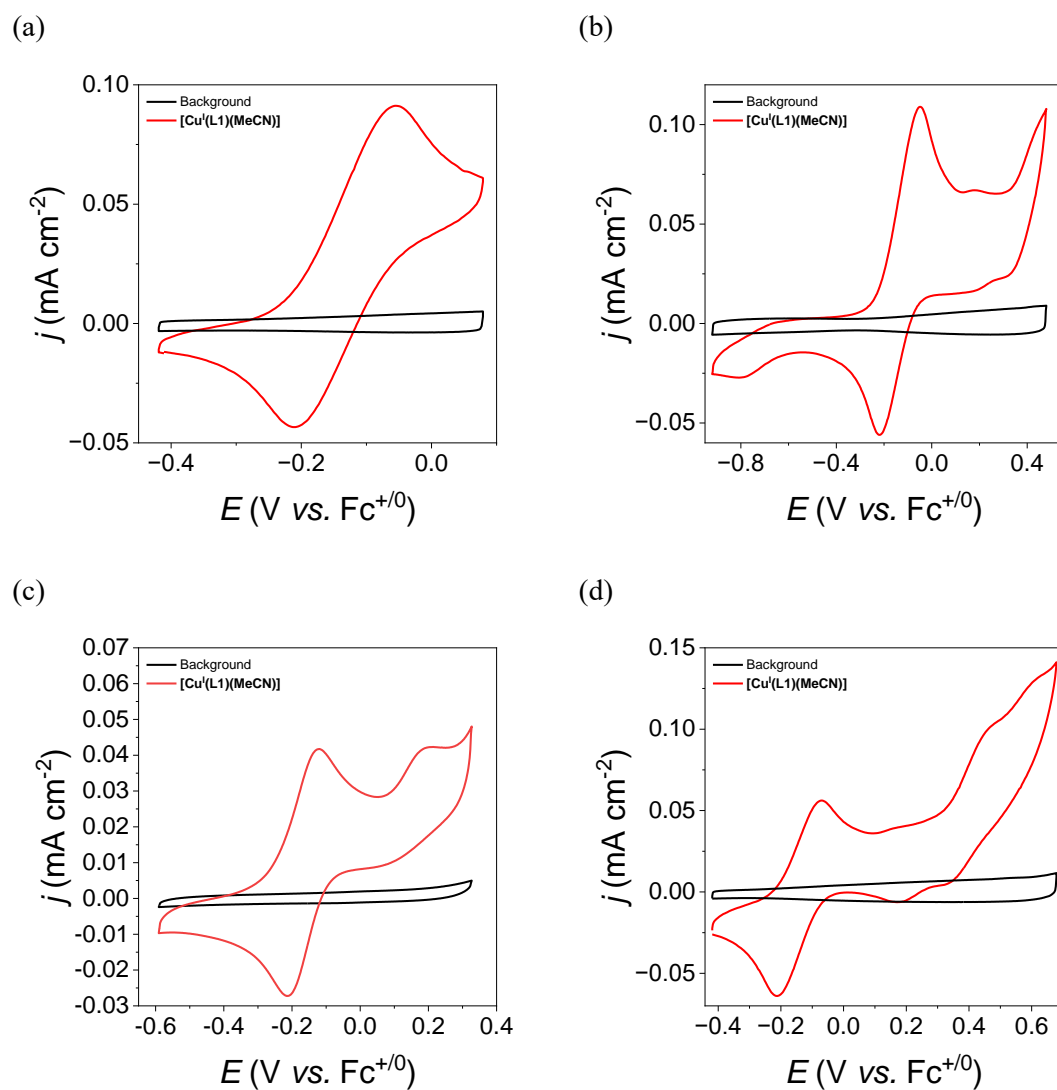


Figure S57. Cyclic voltammograms in THF ($\mu = 0.1 \text{ M TBAPF}_6$) of $1 \text{ mM } [\text{Cu}^{\text{I}}(\text{L1})(\text{MeCN})]$. Conditions: under an inert atmosphere, GC_{disk} ($S = 0.07 \text{ cm}^2$), WE; Pt disk, CE; Ag/AgCl wire, pseudo-RE; $\nu = 100 \text{ mV s}^{-1}$.

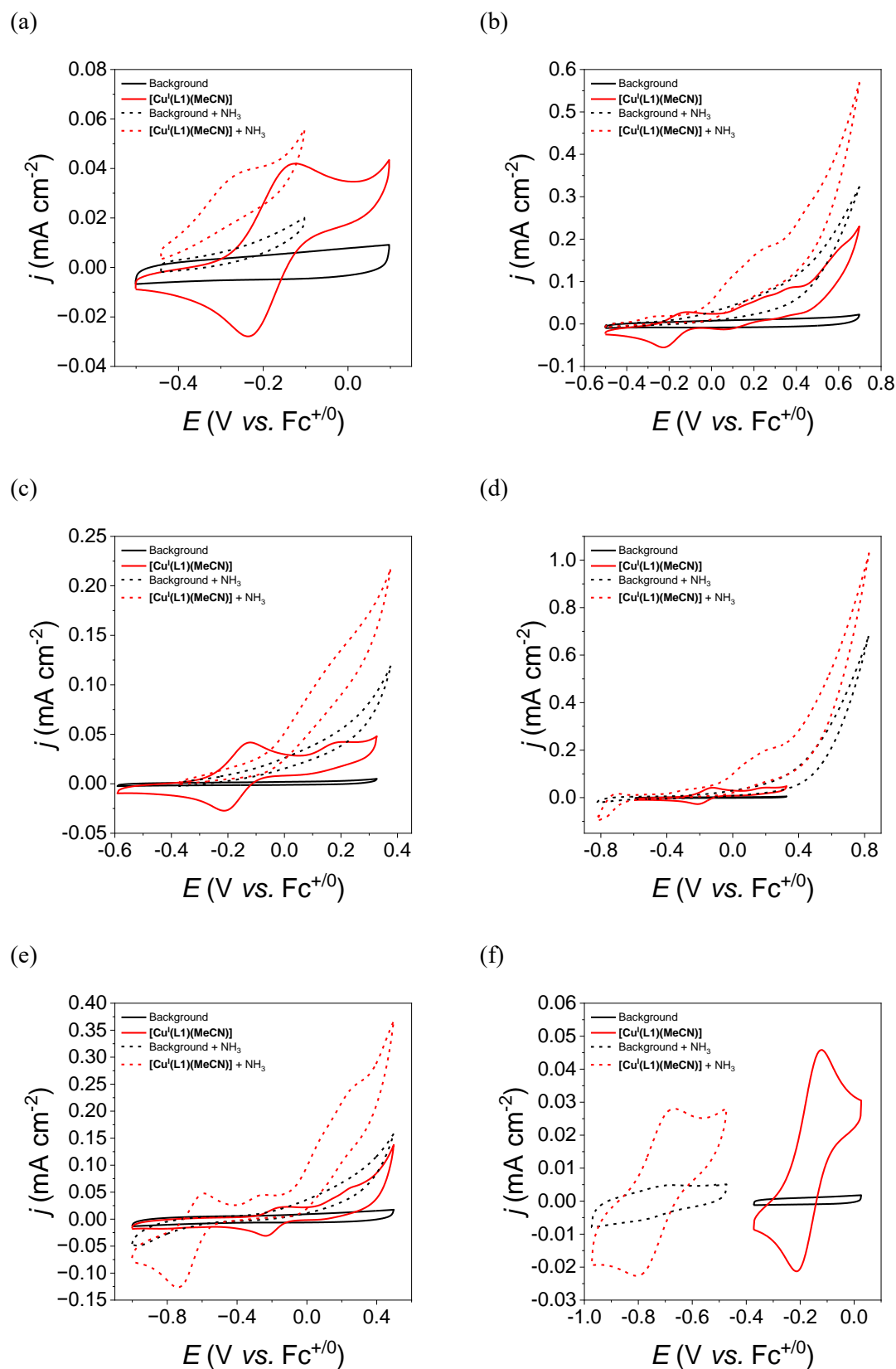


Figure S58. Cyclic voltammograms in THF ($\mu = 0.1$ M TBAPF₆) of 1 mM [Cu^I(L1)(MeCN)] with/without 0.5 M NH₃. Conditions: under an inert atmosphere, GC_{disk} ($S = 0.07$ cm²), WE; Pt disk, CE; Ag/AgCl wire, pseudo-RE; $\nu = 100$ mV s⁻¹.

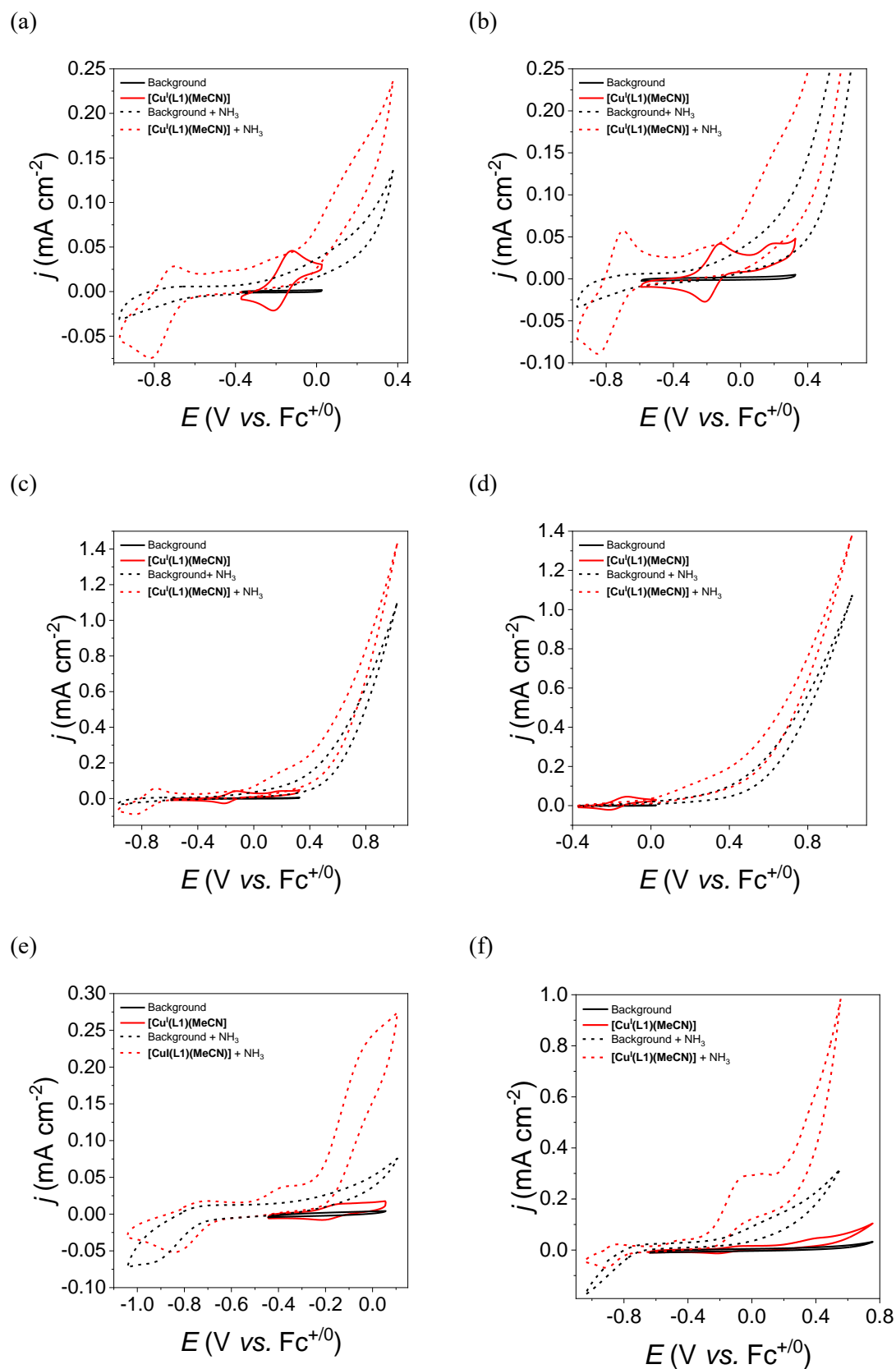
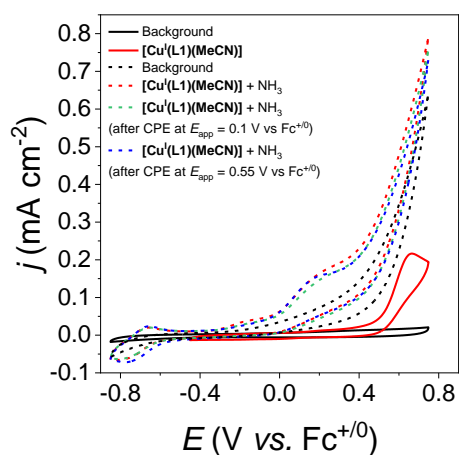
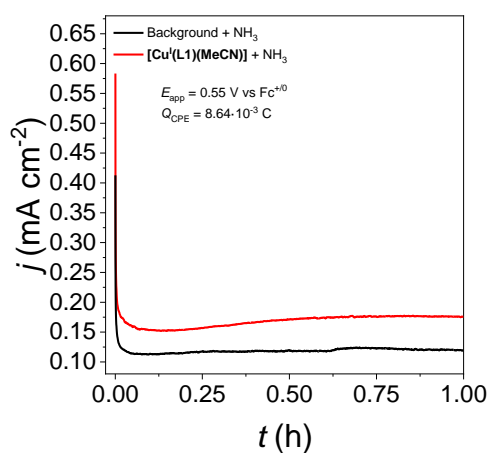


Figure S59. Cyclic voltammograms in THF ($\mu = 0.1$ M TBAPF_6) of 1 mM $[\text{Cu}^{\text{I}}(\text{L1})(\text{MeCN})]$ with/without 0.5 M NH_3 . Conditions: under an inert atmosphere, GC_{disk} ($S = 0.07$ cm^2), WE; Pt disk, CE; Ag/AgCl wire, pseudo-RE; $\nu = 100$ mV s^{-1} .

(a)



(b)



(c)

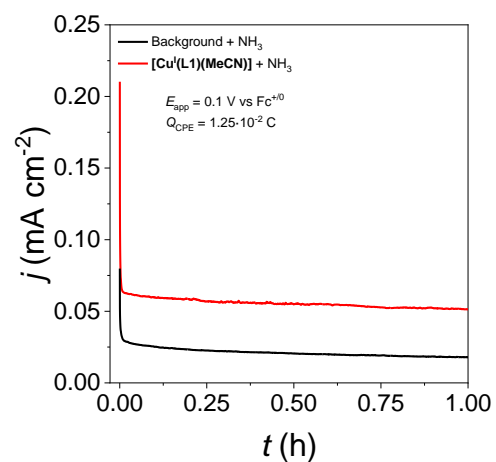


Figure S60. Cyclic voltammograms (a) and CPE (b and c) in THF ($\mu = 0.1$ M TBAPF₆) of 1 mM [Cu^I(L1)(MeCN)] with 0.5 M NH₃. *Conditions:* under an inert atmosphere, GC_{disk} ($S = 0.07$ cm²), WE; Pt coil, CE; Ag/AgCl wire, pseudo-RE; $\nu = 100$ mV s⁻¹; one-compartment cell. Oxidation done under substoichiometric conditions.

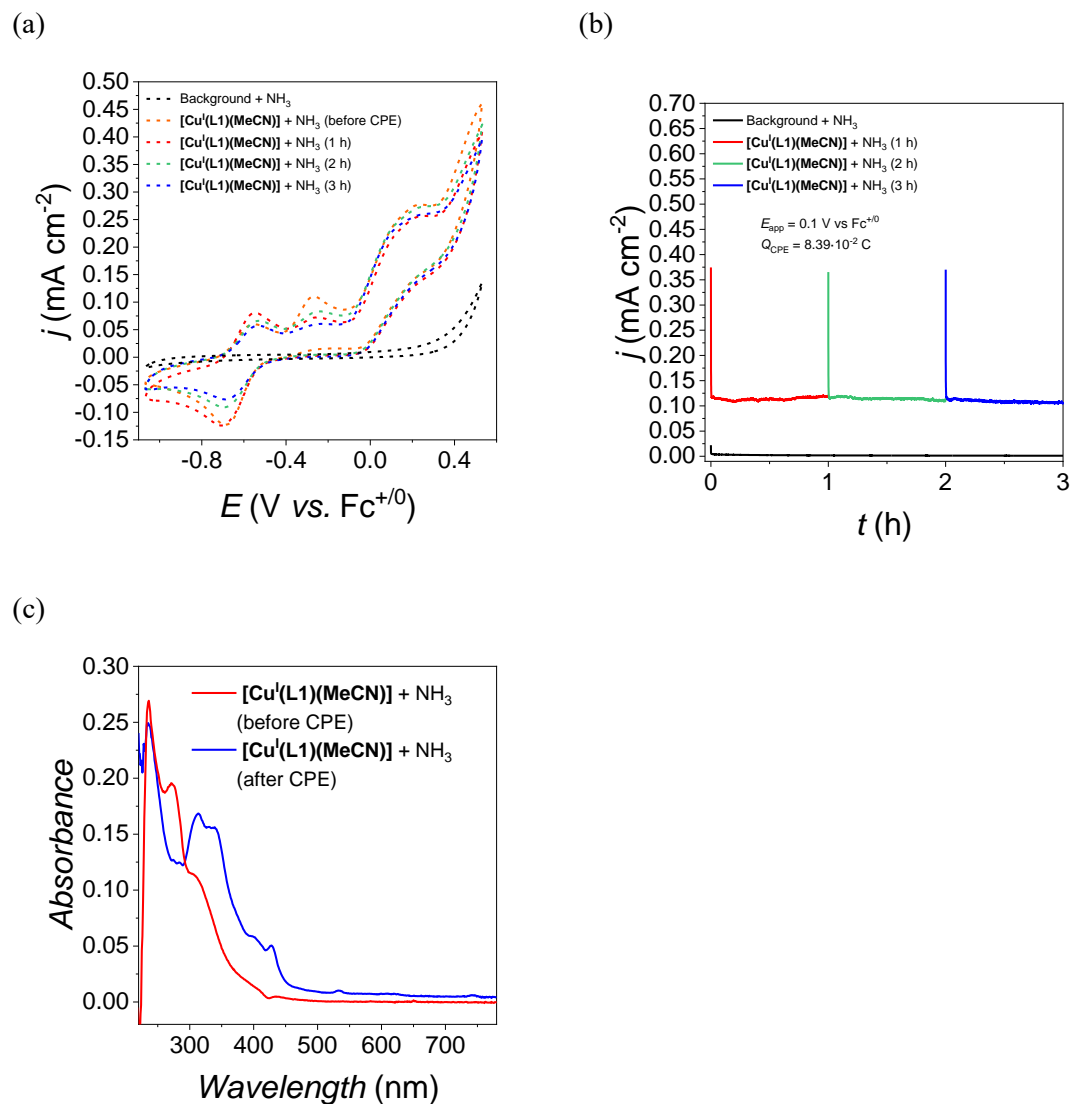


Figure S61. Cyclic voltammograms (a) and CPE (b) in THF ($\mu = 0.1 \text{ M TBAPF}_6$) of $1 \text{ mM } [\text{Cu}^{\text{I}}(\text{L1})(\text{MeCN})]$ with 0.5 M NH_3 . Conditions: under an inert atmosphere, GC_{disk} ($S = 0.07 \text{ cm}^2$), WE; Pt coil, CE; Ag/AgCl wire, pseudo-RE; $\nu = 100 \text{ mV s}^{-1}$; one-compartment cell. (c) UV-vis spectra were recorded before and after CPE by taking $20 \mu\text{L}$ aliquots of the electrolyte solution and diluting them in THF (3 mL). Oxidation done under substoichiometric conditions.

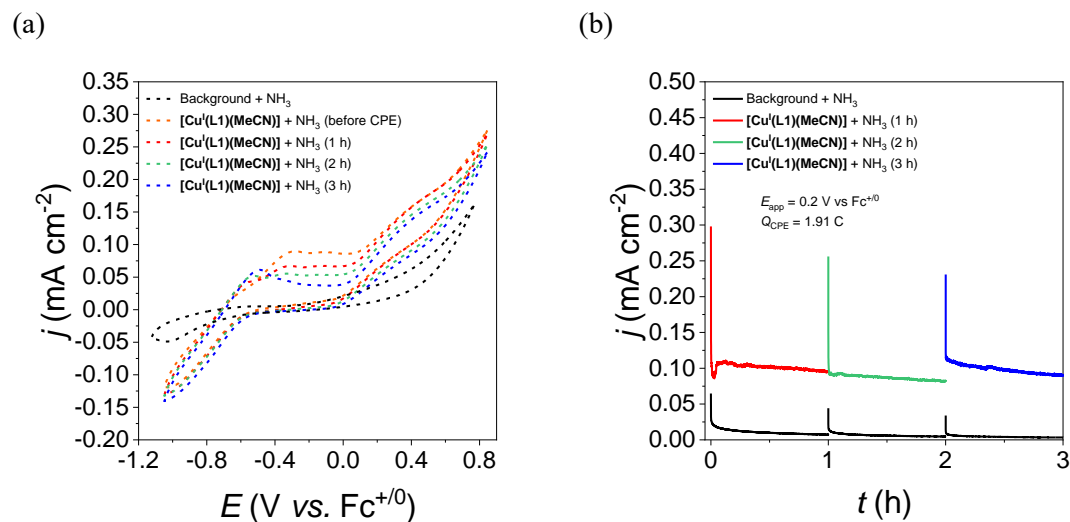


Figure S62. Cyclic voltammograms (a) and CPE (b) in THF ($\mu = 0.1$ M TBAPF₆) of 1 mM [Cu^I(L1)(MeCN)] with 0.5 M NH₃. *Conditions:* under an inert atmosphere, GC_{plate} ($S = 2$ cm²), WE; Pt coil, CE; Ag/AgCl wire, pseudo-RE; $\nu = 100$ mV s⁻¹; two-compartment cell. Oxidation done under substoichiometric conditions.

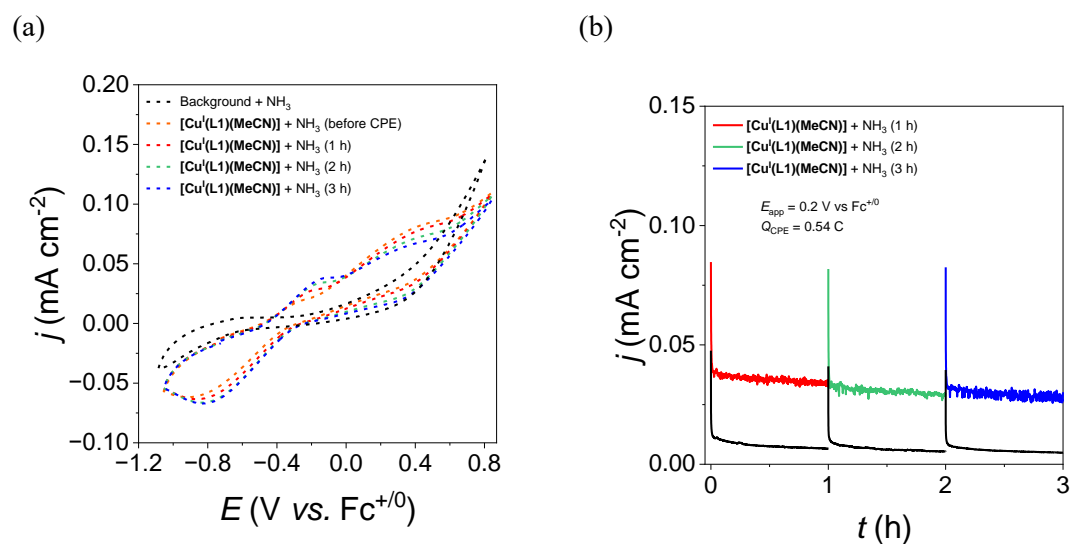


Figure S63. Cyclic voltammograms (a) and CPE (b) in THF ($\mu = 0.1$ M TBAPF₆) of 1 mM [Cu^I(L1)(MeCN)] with 0.5 M NH₃. *Conditions:* under an inert atmosphere, GC_{plate} ($S = 2$ cm²), WE; Pt coil, CE; Ag/AgCl wire, pseudo-RE; $\nu = 100$ mV s⁻¹; two-compartment cell. Oxidation done under substoichiometric conditions.

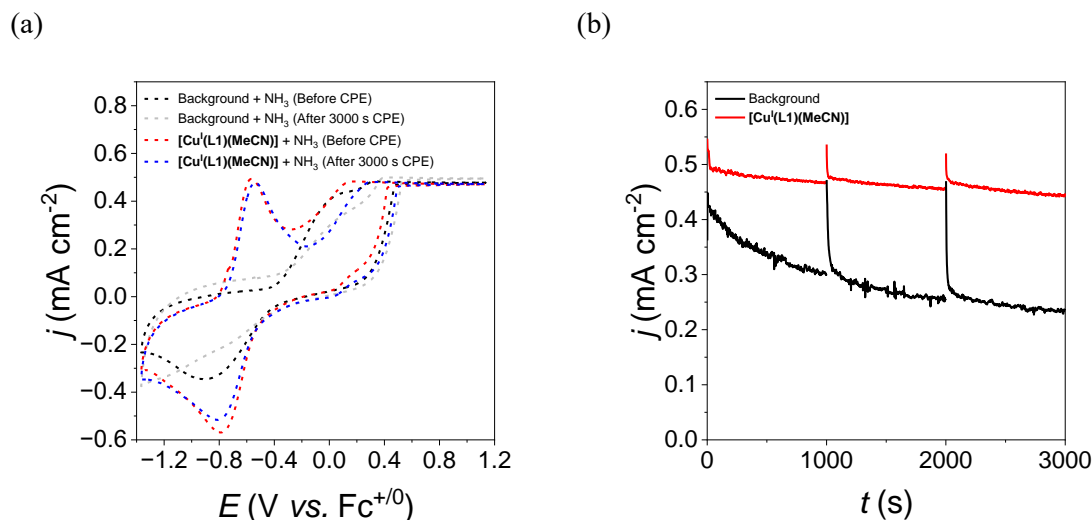


Figure S64. (a) Cyclic voltammograms in THF ($\mu = 0.1$ M TBAPF₆) of 1 mM [Cu^I(L1)(MeCN)] with 0.5 M NH₃. *Conditions:* under Ar, C_{FP} (S = 4 cm²; 4 x 1 cm), WE; Pt coil, CE; Ag/AgCl wire, pseudo-RE; $\nu = 100$ mV s⁻¹; two-compartment cell (with a glass frit of porosity grade 3). (b) Red trace, j vs. t graph for a CPE of a 35 mL solution of THF containing 500 mM NH₃, 1 mM of [Cu^I(L1)(MeCN)] and 100 mM TBAPF₆ as supporting electrolyte, at an $E_{app} = 0.63$ V vs. Fc⁺⁰ for 3000 s. *Conditions:* under Ar, C_{FP} (S = 4 cm²; 4 x 1 cm), WE; Pt coil, CE; Ag/AgCl wire, pseudo-RE; $\nu = 100$ mV s⁻¹; two-compartment cell with 15 mL headspace in each compartment. Black trace, the same without the Cu complex. In red, $Q = 5.58 - 3.47 = 2.11$ C. In black, $Q = 3.47$ C, for blank.

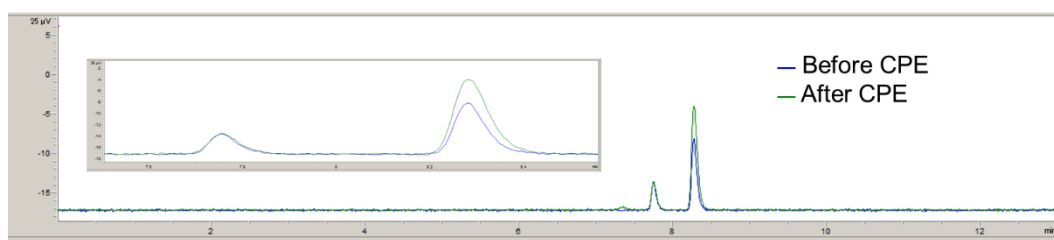


Figure S65. GC chromatograms of the anodic headspace compartment of the previous experiment in Figure S64 in the presence of catalyst [Cu^I(L1)(MeCN)]. Insets show enlargement of the $R_t = 7.5$ -8.5 min zone. R_t (O₂) = 7.8 min, R_t (N₂) = 8.3 min. Blue trace, before CPE showing the presence of adventitious air. Green trace, after CPE showing the increase of only N₂ from the NH₃ oxidation.

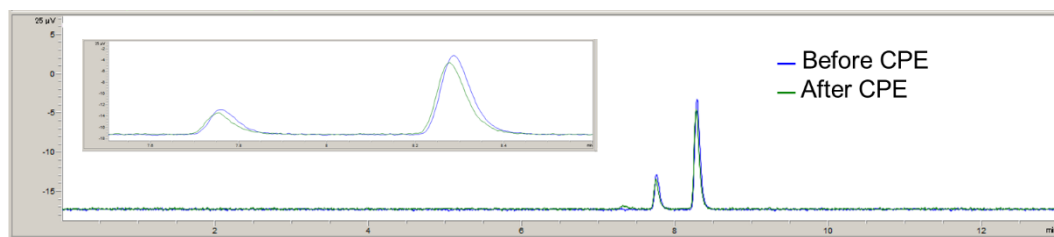


Figure S66. GC chromatograms of the anodic headspace compartment of the previous experiment in Figure S64 in the absence of catalyst [Cu^I(L1)(MeCN)]. Insets show enlargement of the $R_t = 7.5$ -8.5 min zone. R_t (O₂) = 7.8 min, R_t (N₂) = 8.3 min. Blue trace, before CPE showing the presence of adventitious air. Green trace, after CPE. Here no N₂ is observed except for the one obtained from adventitious air.

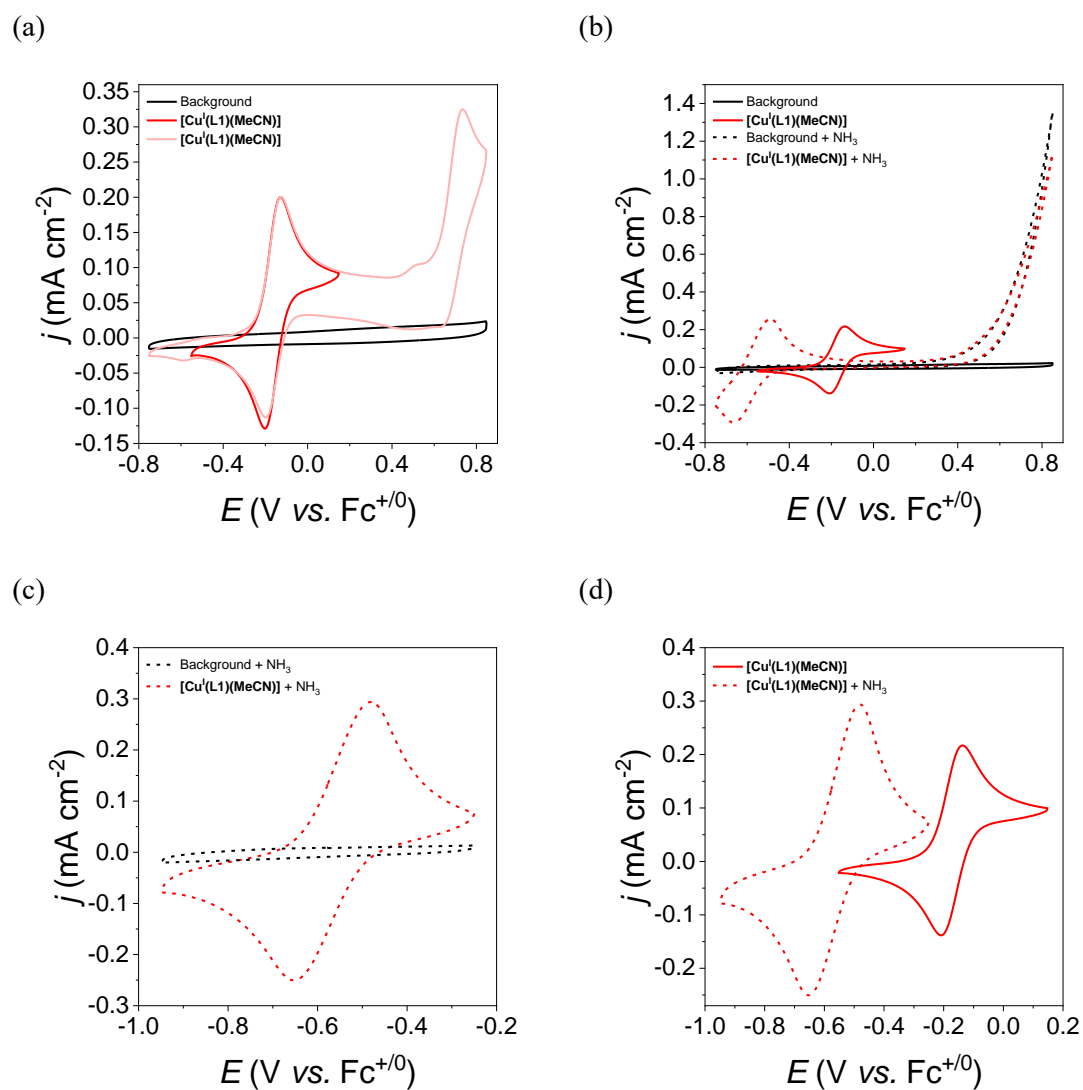
Homogeneous Electrochemistry of $[\text{Cu}^{\text{I}}(\text{L1})(\text{MeCN})]$ in MeCN

Figure S67. Cyclic voltammograms in MeCN ($\mu = 0.1$ M TBAPF_6) of 1 mM $[\text{Cu}^{\text{I}}(\text{L1})(\text{MeCN})]$ with/without 2 M NH_3 . Conditions: under an inert atmosphere, GC_{disk} ($S = 0.07$ cm 2), WE; Pt disk, CE; Ag/AgCl wire, pseudo-RE; $\nu = 100$ mV s $^{-1}$.

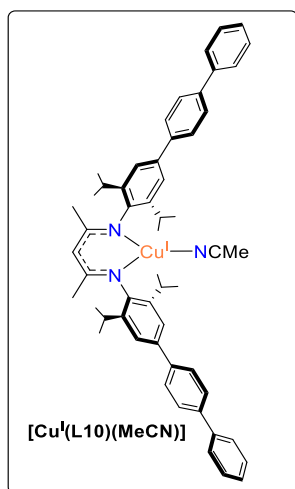
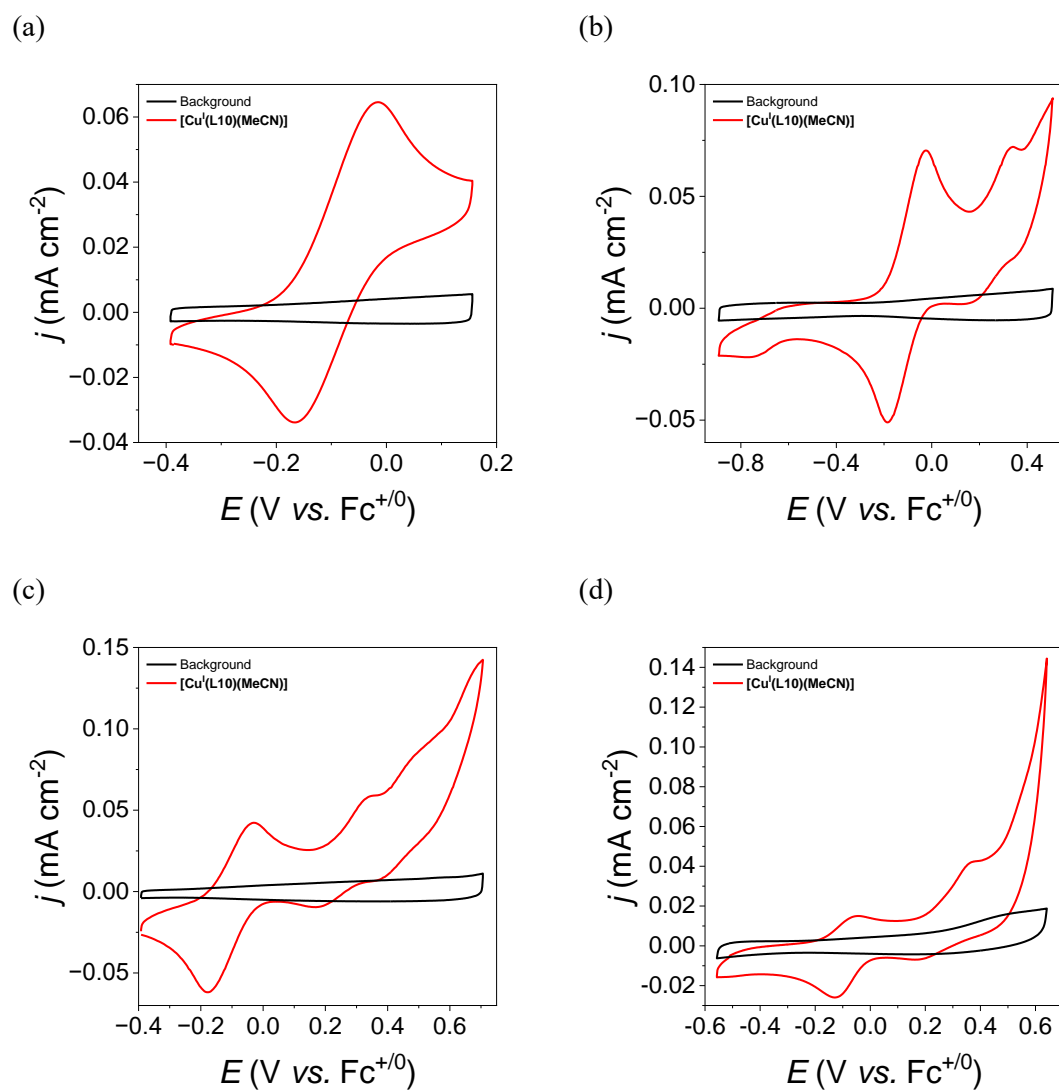
5.12. Electrochemistry of $[\text{Cu}^{\text{I}}(\text{L10})(\text{MeCN})]$ Homogeneous Electrochemistry of $[\text{Cu}^{\text{I}}(\text{L10})(\text{MeCN})]$ in THF

Figure S68. Cyclic voltammograms in THF ($\mu = 0.1$ M TBAPF₆) of 1 mM $[\text{Cu}^{\text{I}}(\text{L10})(\text{MeCN})]$. Conditions: under an inert atmosphere, GC_{disk} ($S = 0.07$ cm²), WE; Pt disk, CE; Ag/AgCl wire, pseudo-RE; $\nu = 100$ mV s⁻¹.

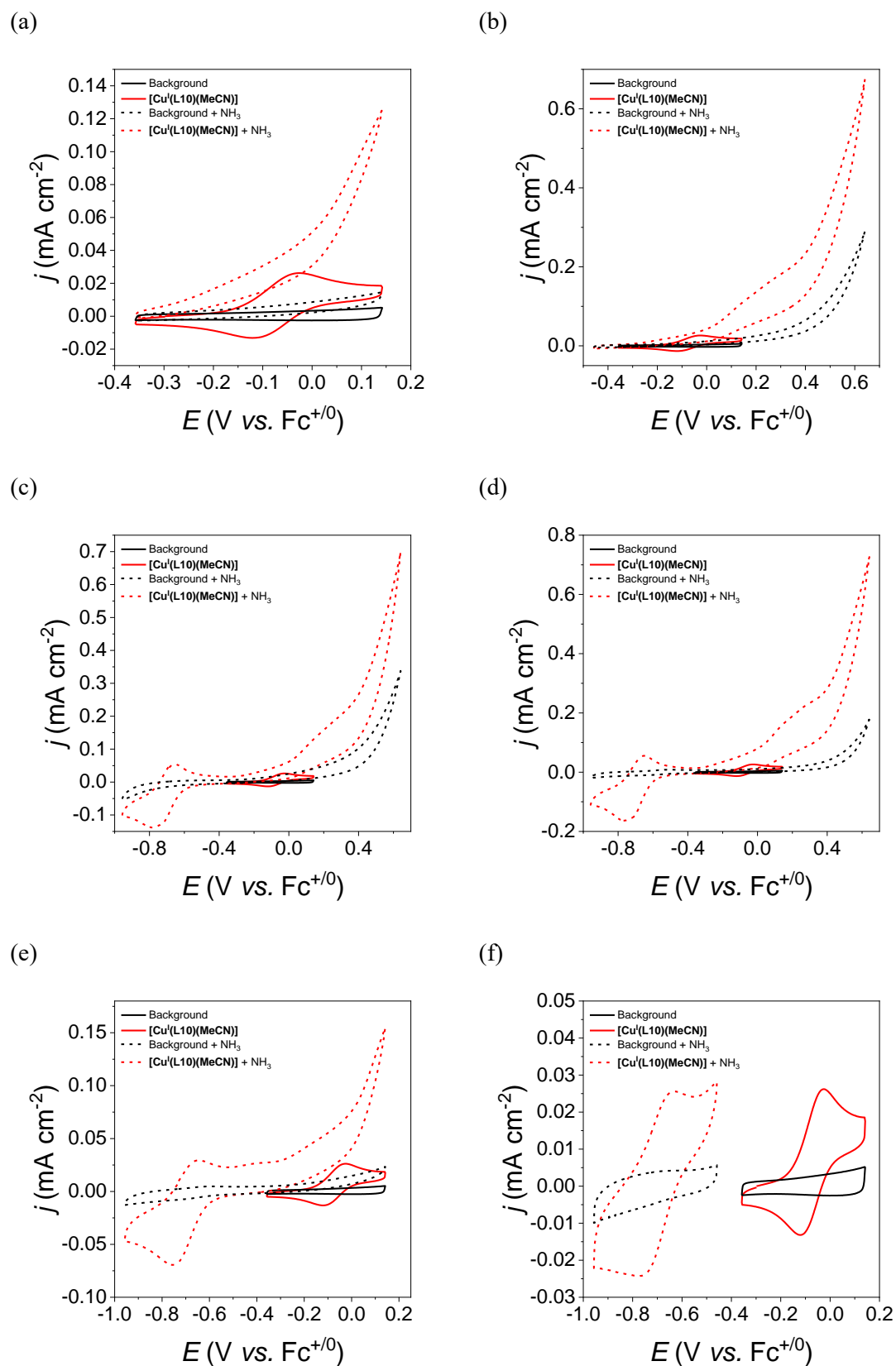


Figure S69. Cyclic voltammograms in THF ($\mu = 0.1$ M TBAPF₆) of 1 mM [Cu(L10)(MeCN)] with/without 0.5 M NH₃. Conditions: under an inert atmosphere, GC_{disk} ($S = 0.07$ cm²), WE; Pt disk, CE; Ag/AgCl wire, pseudo-RE; $\nu = 100$ mV s⁻¹.

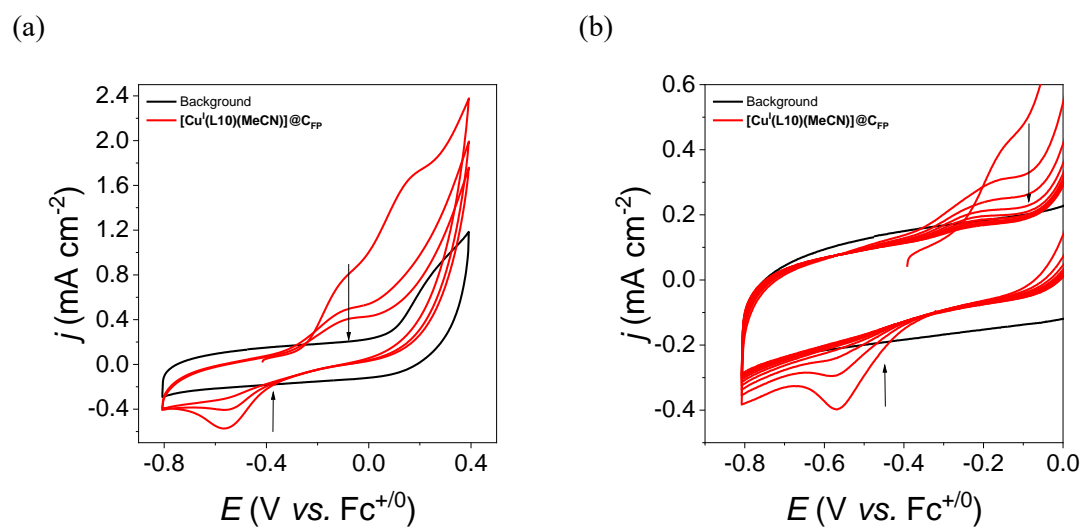
Heterogeneous Electrochemistry of $[\text{Cu}^{\text{I}}(\text{L10})(\text{MeCN})]$ in MeOH

Figure S70. Cyclic voltammograms in MeOH ($\mu = 0.1$ M TBAPF₆) of $[\text{Cu}^{\text{I}}(\text{L10})(\text{MeCN})]@\text{CFP}$ ($S = 0.25$ cm²). *Preparation:* $[\text{Cu}^{\text{I}}(\text{L10})(\text{MeCN})]@\text{CFP}$ electrodes were prepared by soaking for 1 h (a) or 1 s (b) C_{FP} into a solution of 1 mM $[\text{Cu}^{\text{I}}(\text{L10})(\text{MeCN})]$ in THF under an inert atmosphere. *Conditions:* under an inert atmosphere, Pt disk, CE; Ag/AgCl wire, pseudo-RE; $\nu = 100$ mV s⁻¹.

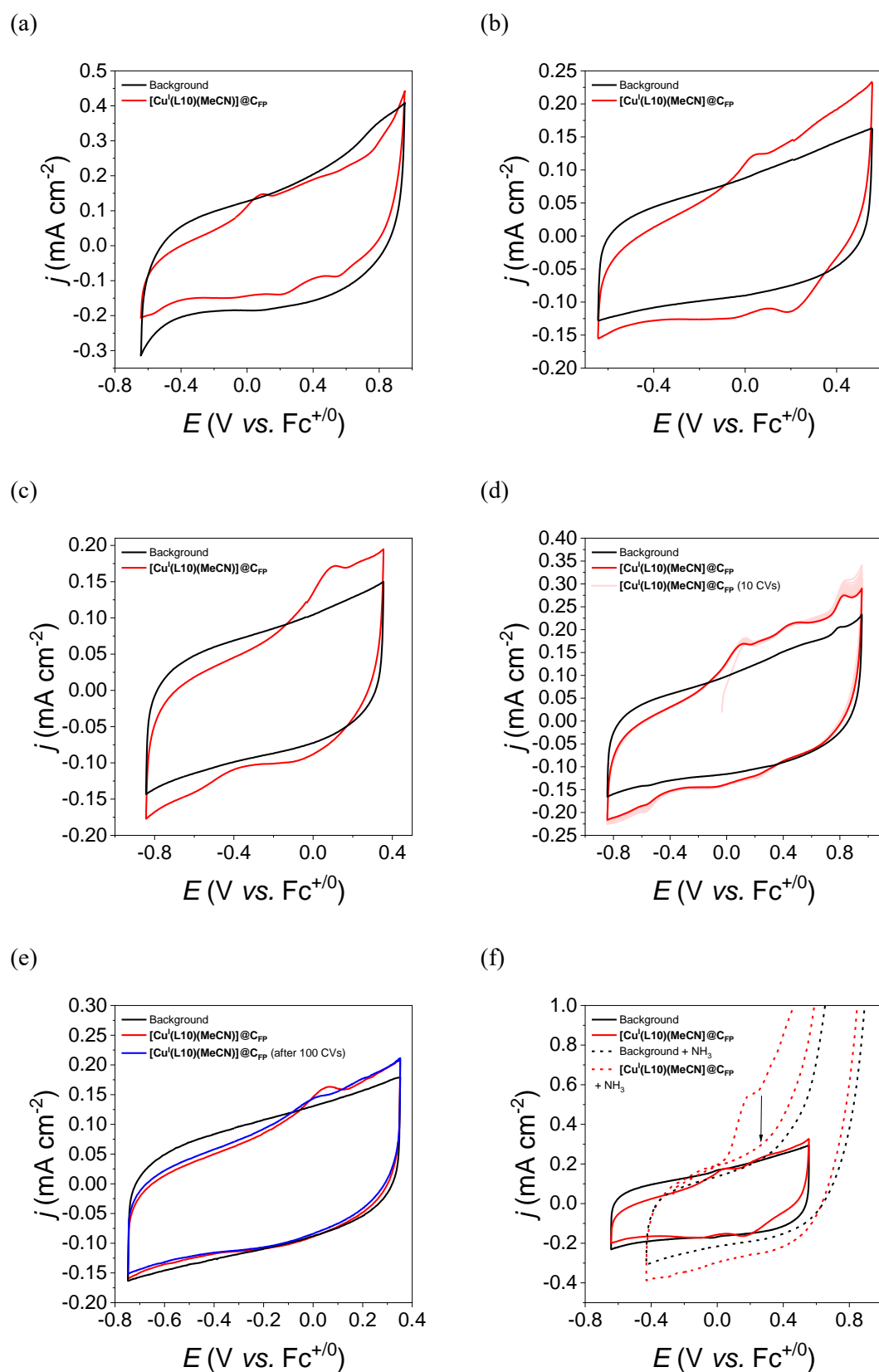
Heterogeneous Electrochemistry of $[\text{Cu}^{\text{I}}(\text{L10})(\text{MeCN})]$ in TFE

Figure S71. Cyclic voltammograms in TFE ($\mu = 0.1 \text{ M TBAPF}_6$) of $[\text{Cu}^{\text{I}}(\text{L10})(\text{MeCN})]$ @ C_{FP} ($S = 0.25 \text{ cm}^2$) with/without 0.93 M NH_3 . Preparation: $[\text{Cu}^{\text{I}}(\text{L10})(\text{MeCN})]$ @ C_{FP} electrodes were prepared by soaking for 1 s into a solution of $1 \text{ mM } [\text{Cu}^{\text{I}}(\text{L10})(\text{MeCN})]$ in THF under an inert atmosphere. Conditions: under an inert atmosphere, Pt disk, CE; Ag/AgCl wire, pseudo-RE; $\nu = 100 \text{ mV s}^{-1}$.

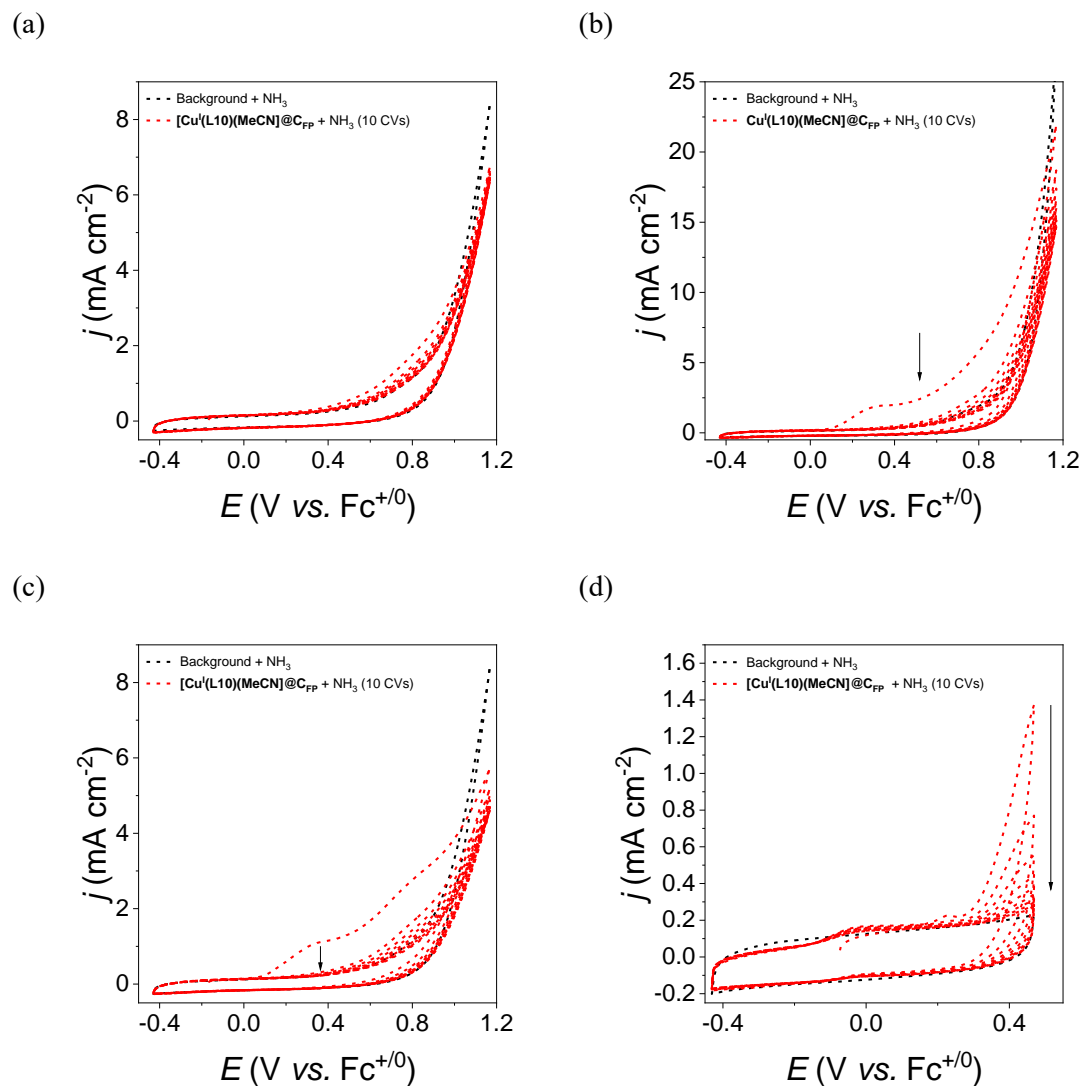


Figure S72. Cyclic voltammograms in TFE ($\mu = 0.1 \text{ M TBAPF}_6$) of $[\text{Cu}^{\text{I}}(\text{L10})(\text{MeCN})]@\text{CFP}$ ($S = 0.25 \text{ cm}^2$) with 0.93 M NH_3 . *Preparation:* $[\text{Cu}^{\text{I}}(\text{L10})(\text{MeCN})]@\text{CFP}$ electrodes were prepared by soaking for 1 s into a solution of $1 \text{ mM } [\text{Cu}^{\text{I}}(\text{L10})(\text{MeCN})]$ in THF under an inert atmosphere. *Conditions:* under an inert atmosphere, Pt disk, CE; Ag/AgCl wire, pseudo-RE; $\nu = 100 \text{ mV s}^{-1}$.

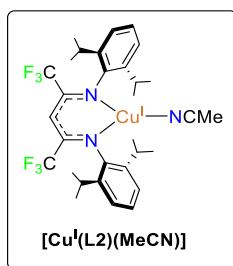
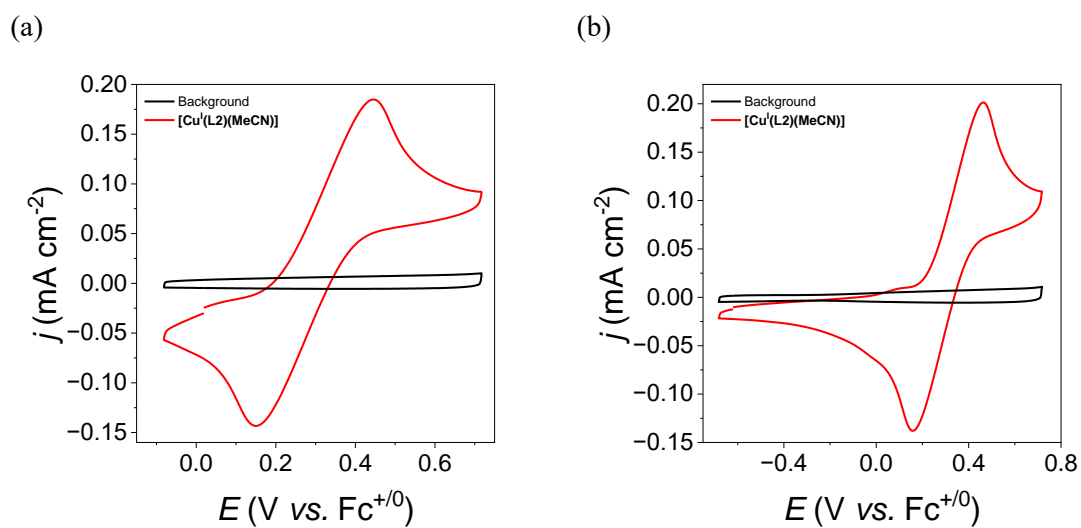
5.13. Electrochemistry of $[\text{Cu}^{\text{I}}(\text{L2})(\text{MeCN})]$ Homogeneous Electrochemistry of $[\text{Cu}^{\text{I}}(\text{L2})(\text{MeCN})]$ in THF

Figure S73. Cyclic voltammograms in THF ($\mu = 0.1$ M TBAPF₆) of 1 mM $[\text{Cu}^{\text{I}}(\text{L2})(\text{MeCN})]$. Conditions: under an inert atmosphere, GC_{disk} ($S = 0.07$ cm²), WE; Pt disk, CE; Ag/AgCl wire, pseudo-RE; $\nu = 100$ mV s⁻¹.

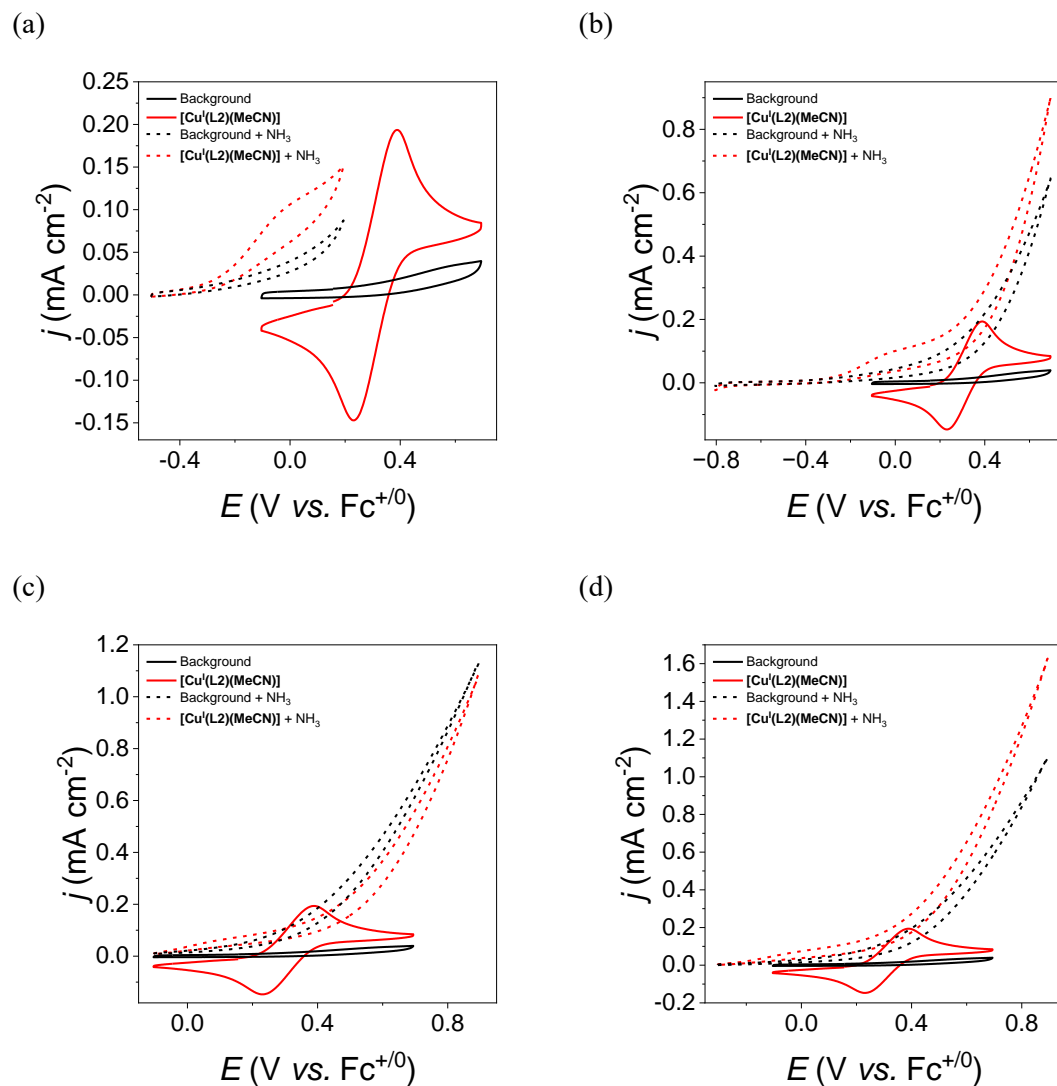


Figure S74. Cyclic voltammograms in THF ($\mu = 0.1$ M TBAPF₆) of 1 mM [Cu^I(L2)(MeCN)] with/without 0.5 M NH₃. Conditions: under an inert atmosphere, GC_{disk} ($S = 0.07$ cm²), WE; Pt disk, CE; Ag/AgCl wire, pseudo-RE; $\nu = 100$ mV s⁻¹.

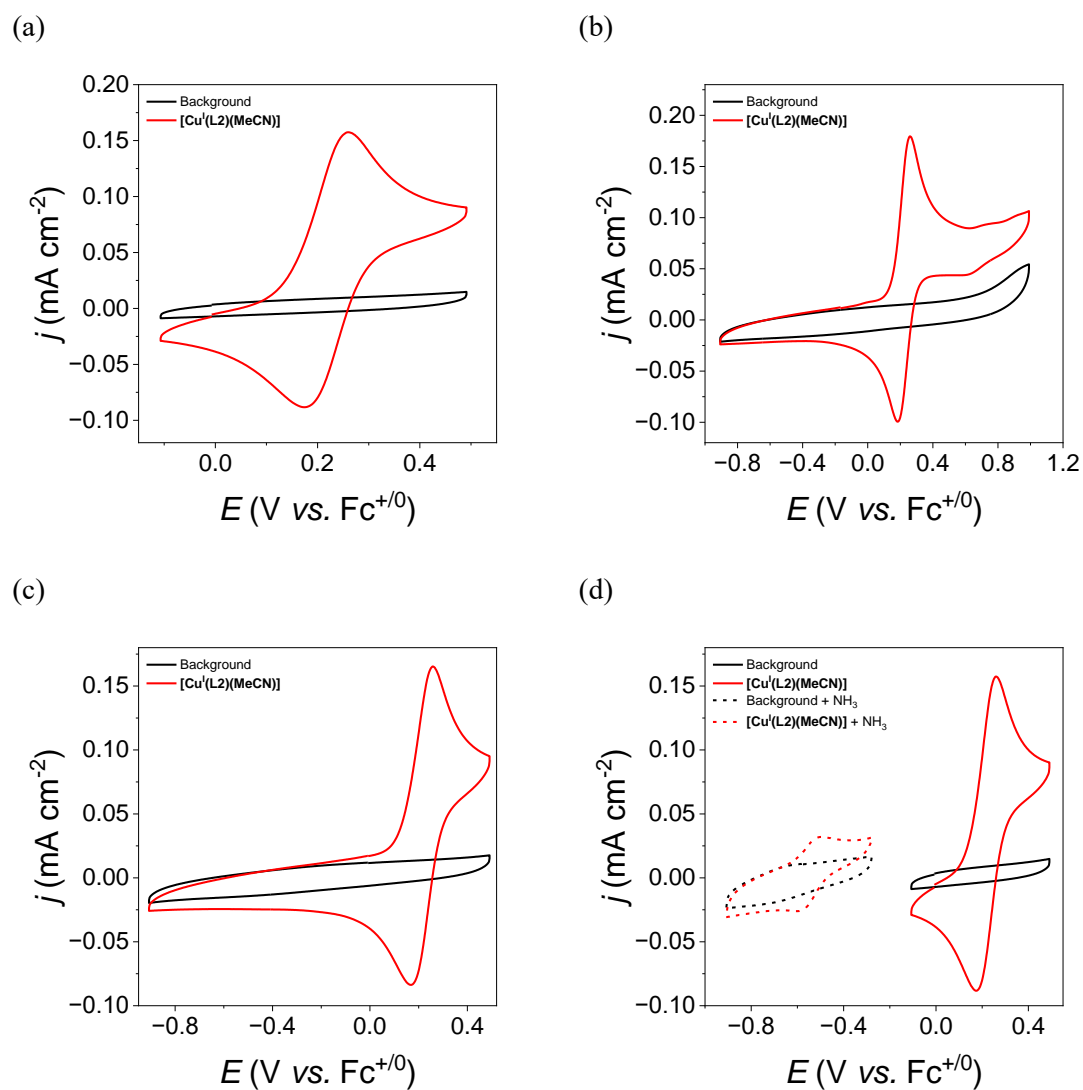
Homogeneous Electrochemistry of $[\text{Cu}^{\text{I}}(\text{L2})(\text{MeCN})]$ in MeCN

Figure S75. Cyclic voltammograms in MeCN ($\mu = 0.1$ M TBAPF₆) of 1 mM $[\text{Cu}^{\text{I}}(\text{L2})(\text{MeCN})]$ with/without 0.5 M NH₃. Conditions: under an inert atmosphere, GC_{disk} ($S = 0.07$ cm²), WE; Pt disk, CE; Ag/AgCl wire, pseudo-RE; $\nu = 100$ mV s⁻¹.

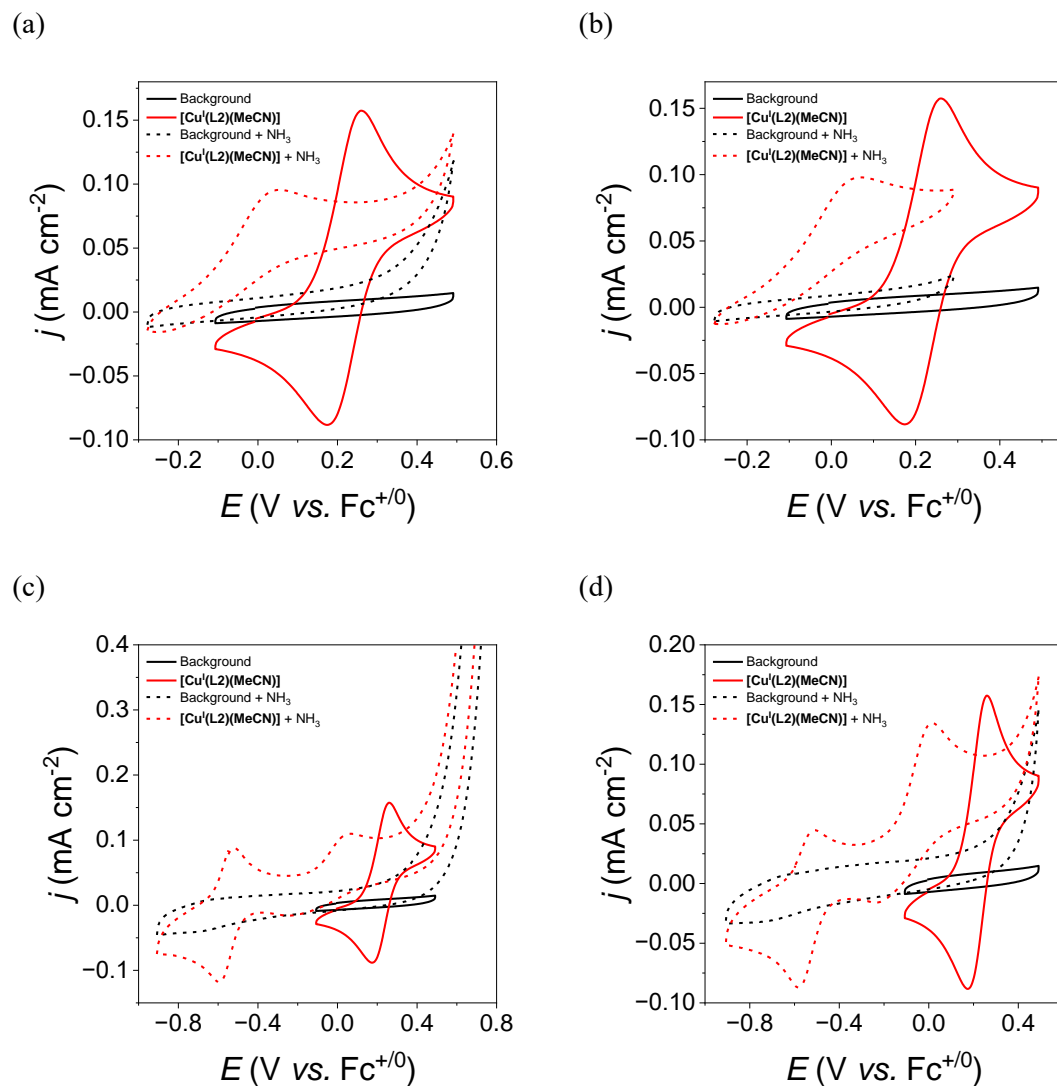


Figure S76. Cyclic voltammograms in MeCN ($\mu = 0.1$ M TBAPF₆) of 1 mM [Cu^I(L2)(MeCN)] with/without 0.5 M NH₃. Conditions: under an inert atmosphere, GC_{disk} ($S = 0.07$ cm²), WE; Pt disk, CE; Ag/AgCl wire, pseudo-RE; $\nu = 100$ mV s⁻¹.

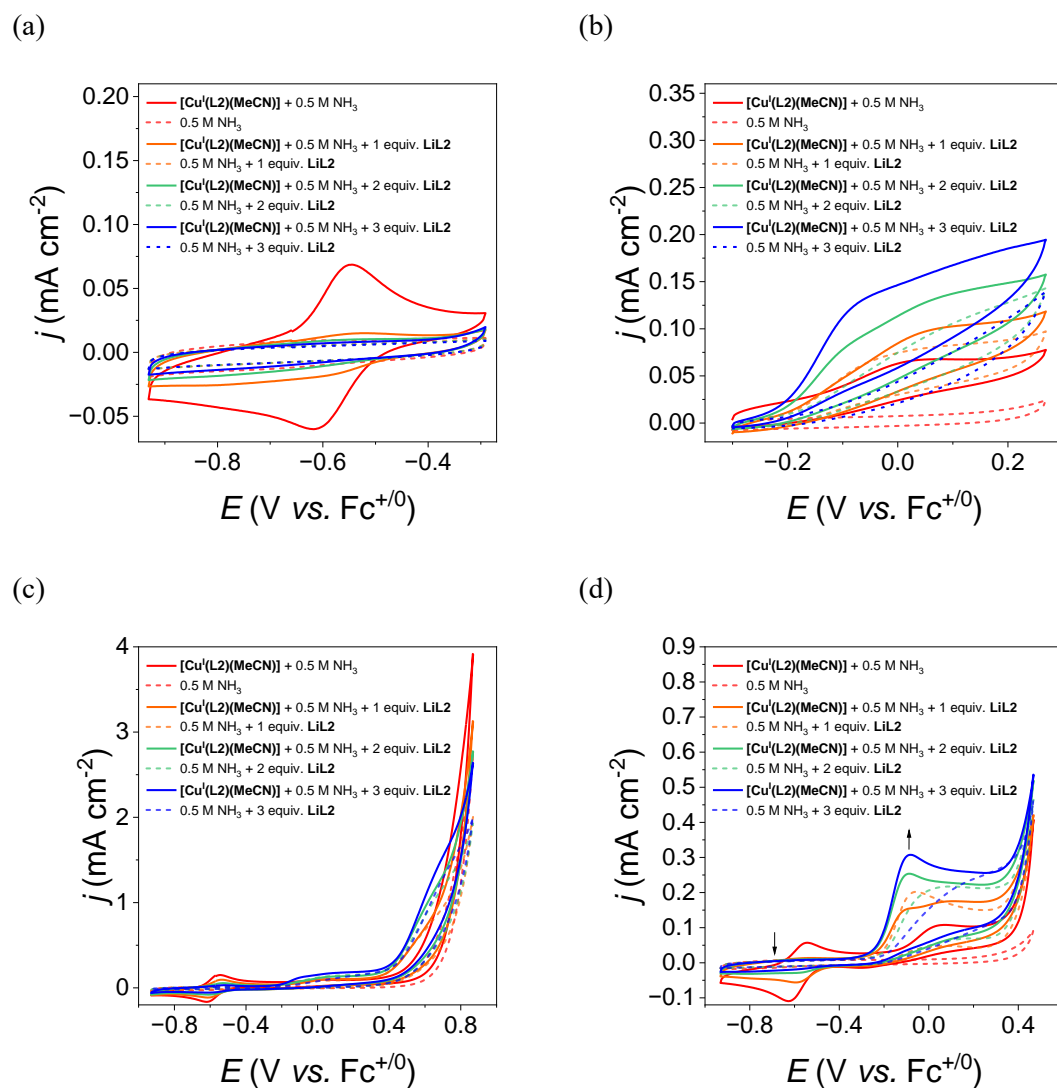


Figure S77. Cyclic voltammograms in MeCN ($\mu = 0.1$ M TBAPF₆) of 1 mM [Cu^I(L2)(MeCN)] with 0.5 M NH₃ and different equivalents of LiL2. A 300 mM LiL2 solution was prepared by adding ⁿBuLi (30 μ L, 2.5 M solution in hexanes) in MeCN (2.2 mL) containing HL2 (39.5 mg). Then, every LiL2 equivalent was added by adding 0.17 mL of the LiL2 solution into the electrolyte solution ($V_{\text{initial}} = 3$ mL). *Conditions:* under an inert atmosphere, GC_{disk} ($S = 0.07$ cm²), WE; Pt disk, CE; Ag/AgCl wire, pseudo-RE; $\nu = 100$ mV s⁻¹.

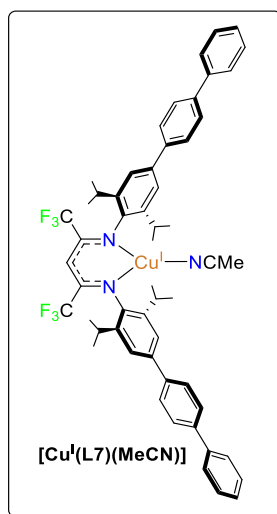
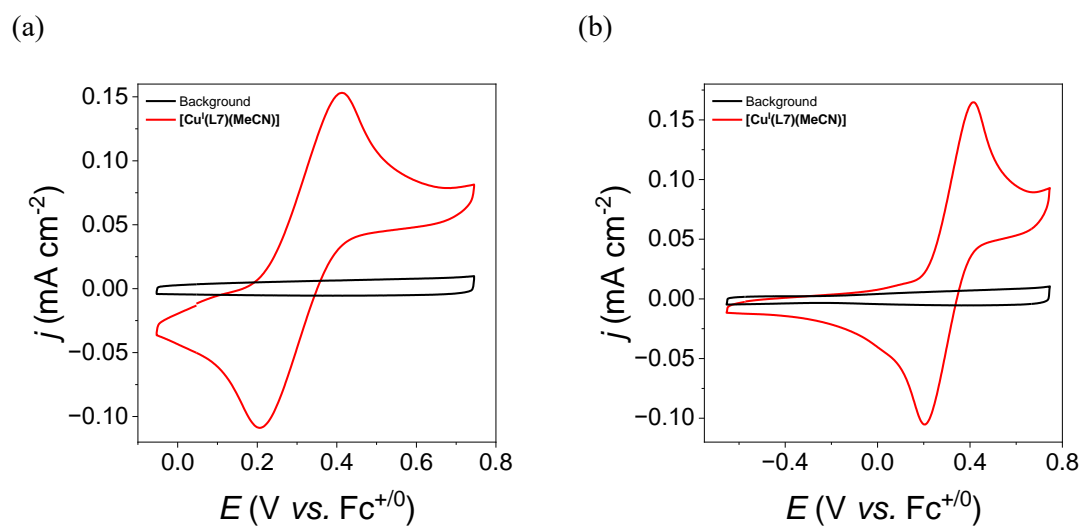
5.14. Electrochemistry of $[\text{Cu}^{\text{I}}(\text{L7})(\text{MeCN})]$ *Homogeneous Electrochemistry of $[\text{Cu}^{\text{I}}(\text{L7})(\text{MeCN})]$ in THF*

Figure S78. Cyclic voltammograms in THF ($\mu = 0.1 \text{ M TBAPF}_6$) of $1 \text{ mM } [\text{Cu}^{\text{I}}(\text{L7})(\text{MeCN})]$. Conditions: under an inert atmosphere, GC_{disk} ($S = 0.07 \text{ cm}^2$), WE; Pt disk, CE; Ag/AgCl wire, pseudo-RE; $\nu = 100 \text{ mV s}^{-1}$.

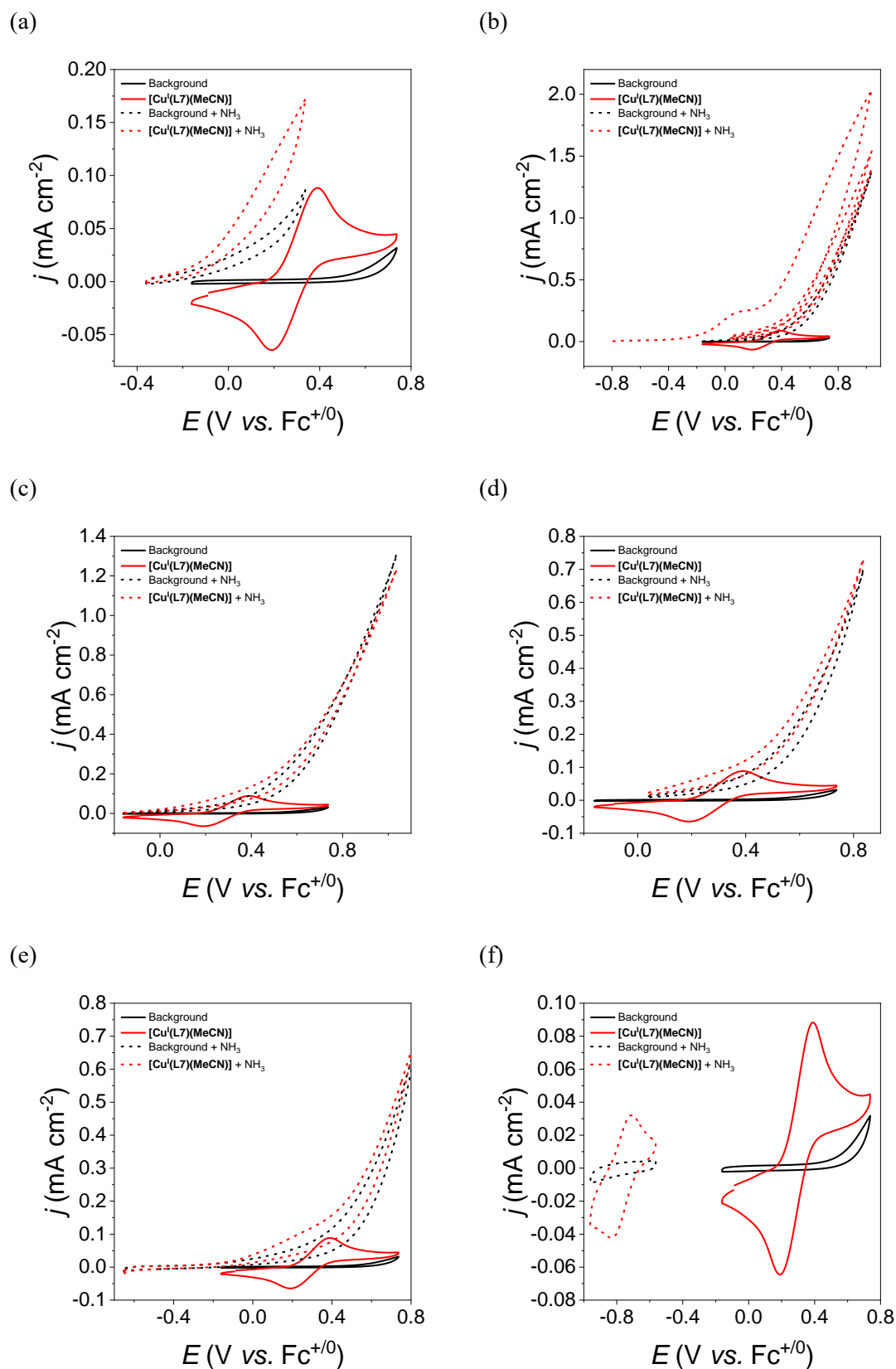


Figure S79. Cyclic voltammograms in THF ($\mu = 0.1$ M TBAPF₆) of 1 mM [Cu^I(L7)(MeCN)] with/without 0.5 M NH₃. Conditions: under an inert atmosphere, GC_{disk} ($S = 0.07$ cm²), WE; Pt disk, CE; Ag/AgCl wire, pseudo-RE; $\nu = 100$ mV s⁻¹.

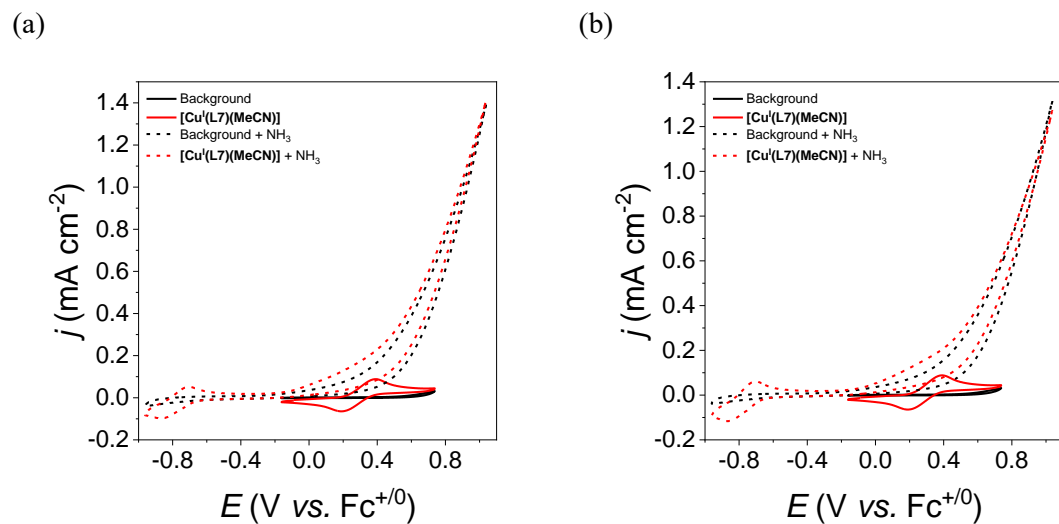


Figure S80. Cyclic voltammograms in THF ($\mu = 0.1$ M TBAPF₆) of 1 mM [Cu^I(L7)(MeCN)] with/without 0.5 M NH₃. Conditions: under an inert atmosphere, GC_{disk} ($S = 0.07$ cm²), WE; Pt disk, CE; Ag/AgCl wire, pseudo-RE; $\nu = 100$ mV s⁻¹.

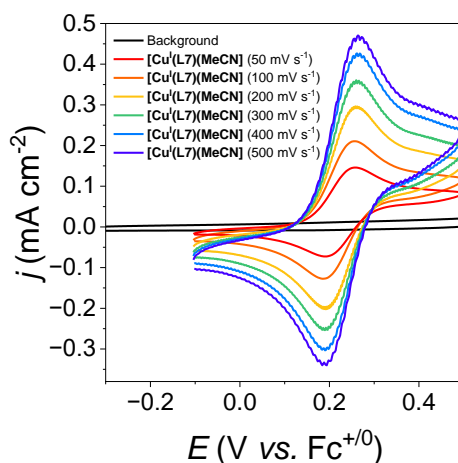
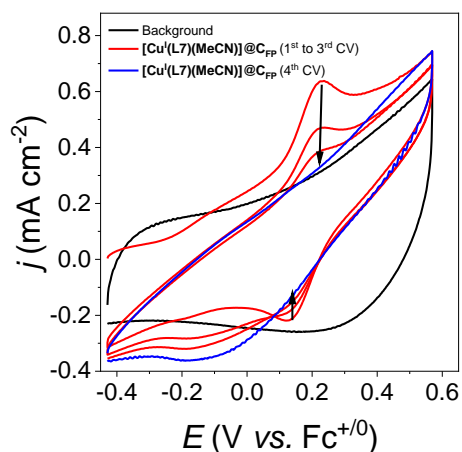
Homogeneous Electrochemistry of $[\text{Cu}^{\text{I}}(\text{L7})(\text{MeCN})]$ in MeCN

Figure S81. Cyclic voltammograms in MeCN ($\mu = 0.1$ M TBAPF₆) of 1 mM $[\text{Cu}^{\text{I}}(\text{L7})(\text{MeCN})]$. Conditions: under an inert atmosphere, GC_{disk} ($S = 0.07$ cm²), WE; Pt disk, CE; Ag/AgCl wire, pseudo-RE; $\nu = 100$ mV s⁻¹.

Heterogeneous Electrochemistry of $[\text{Cu}^{\text{I}}(\text{L7})(\text{MeCN})]$ in MeCN

(a)



(b)

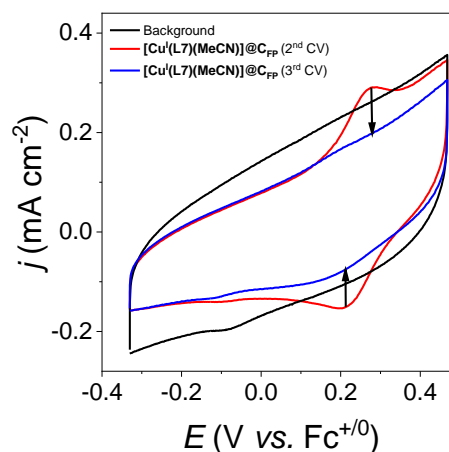


Figure S82. Cyclic voltammograms in MeCN ($\mu = 0.1$ M TBAPF₆) of $[\text{Cu}^{\text{I}}(\text{L7})(\text{MeCN})]@_{\text{CFP}}$ ($S = 0.25$ cm²). Preparation: (a) $[\text{Cu}^{\text{I}}(\text{L7})(\text{MeCN})]@_{\text{CFP}}$ electrodes were prepared by drop casting 200 μL of a solution of 0.5 mM $[\text{Cu}^{\text{I}}(\text{L7})(\text{MeCN})]$ in THF onto C_{FP} under an inert atmosphere. (b) $[\text{Cu}^{\text{I}}(\text{L7})(\text{MeCN})]@_{\text{CFP}}$ electrodes were prepared by soaking C_{FP} for 18 h into a solution of 0.5 mM $[\text{Cu}^{\text{I}}(\text{L7})(\text{MeCN})]$ in THF under an inert atmosphere. Conditions: under an inert atmosphere, Pt disk, CE; Ag/AgCl wire, pseudo-RE; $\nu = 100$ mV s⁻¹.

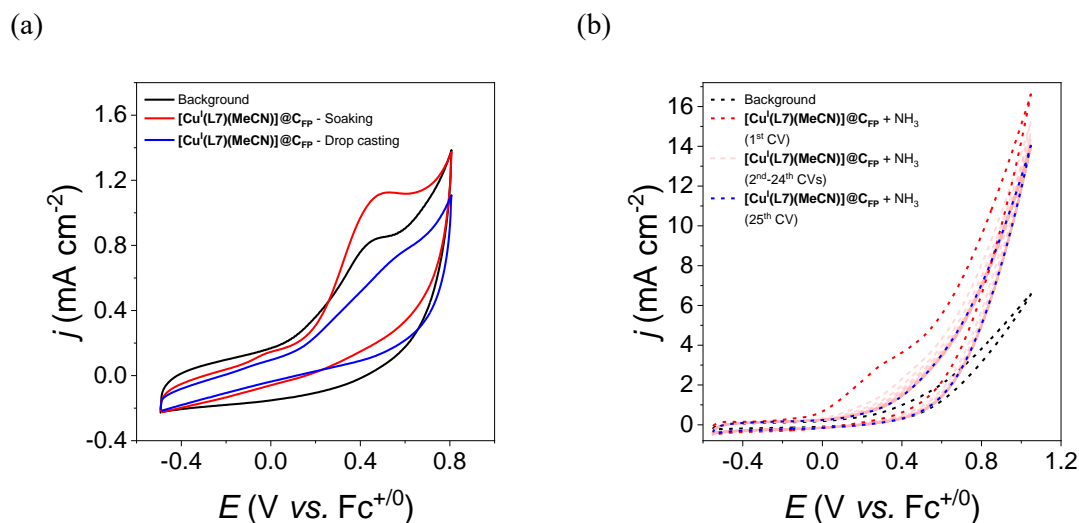
Heterogeneous Electrochemistry of $[\text{Cu}^{\text{I}}(\text{L7})(\text{MeCN})]$ in MeOH

Figure S83. (a) Cyclic voltammograms in MeOH ($\mu = 0.1 \text{ M NaClO}_4$) of $[\text{Cu}^{\text{I}}(\text{L7})(\text{MeCN})]@\text{CFP}$ ($S = 0.25 \text{ cm}^2$) with/without 2 M NH_3 . Preparation: $[\text{Cu}^{\text{I}}(\text{L7})(\text{MeCN})]@\text{CFP}$ electrodes were prepared by drop casting $100 \mu\text{L}$ of a solution of $0.5 \text{ mM } [\text{Cu}^{\text{I}}(\text{L7})(\text{MeCN})]$ in THF onto CFP or by soaking CFP for 18 h into a solution of $0.5 \text{ mM } [\text{Cu}^{\text{I}}(\text{L7})(\text{MeCN})]$ in THF under an inert atmosphere. (b) Cyclic voltammograms in MeOH ($\mu = 0.1 \text{ M NaClO}_4$) of $[\text{Cu}^{\text{I}}(\text{L7})(\text{MeCN})]@\text{CFP}$ ($S = 0.25 \text{ cm}^2$) with/without 2 M NH_3 . Preparation: $[\text{Cu}^{\text{I}}(\text{L7})(\text{MeCN})]@\text{CFP}$ electrodes were prepared by soaking CFP for 24 h into a solution of $0.5 \text{ mM } [\text{Cu}^{\text{I}}(\text{L7})(\text{MeCN})]$ in THF under an inert atmosphere. Conditions: under an inert atmosphere, Pt disk, CE; Ag/AgCl wire, pseudo-RE; $\nu = 100 \text{ mV s}^{-1}$.

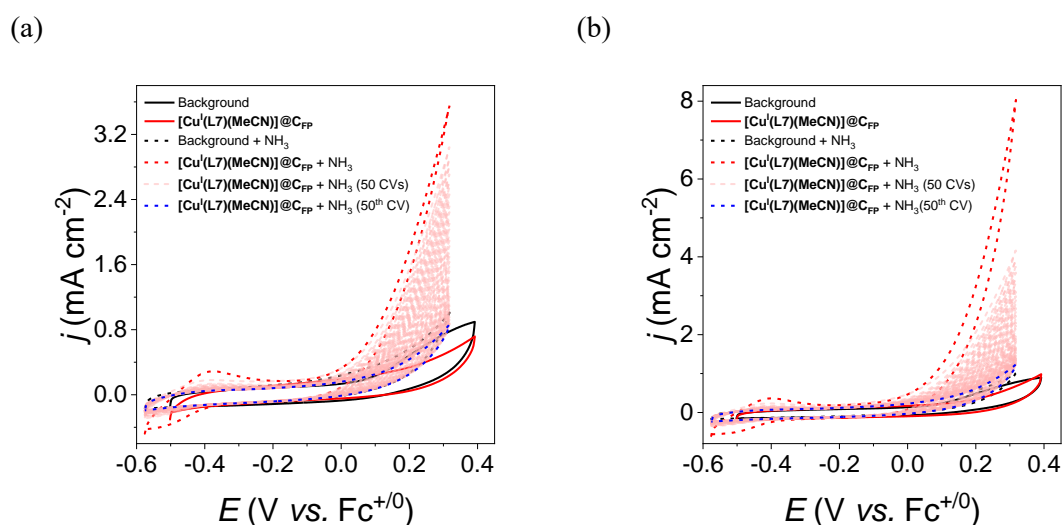


Figure S84. Cyclic voltammograms in MeOH ($\mu = 0.1 \text{ M TBAPF}_6$) of $[\text{Cu}^{\text{I}}(\text{L7})(\text{MeCN})]@\text{CFP}$ ($S = 0.25 \text{ cm}^2$) with/without 1.07 M NH_3 . Preparation: $[\text{Cu}^{\text{I}}(\text{L7})(\text{MeCN})]@\text{CFP}$ electrodes were prepared by soaking CFP for 8 days into a solution of $0.5 \text{ mM } [\text{Cu}^{\text{I}}(\text{L7})(\text{MeCN})]$ in THF under an inert atmosphere. After this time, the electrodes were dried at RT and rinsed (a) or not (b) once with MeOH. Conditions: under an inert atmosphere, Pt disk, CE; Ag/AgCl wire, pseudo-RE; $\nu = 100 \text{ mV s}^{-1}$.

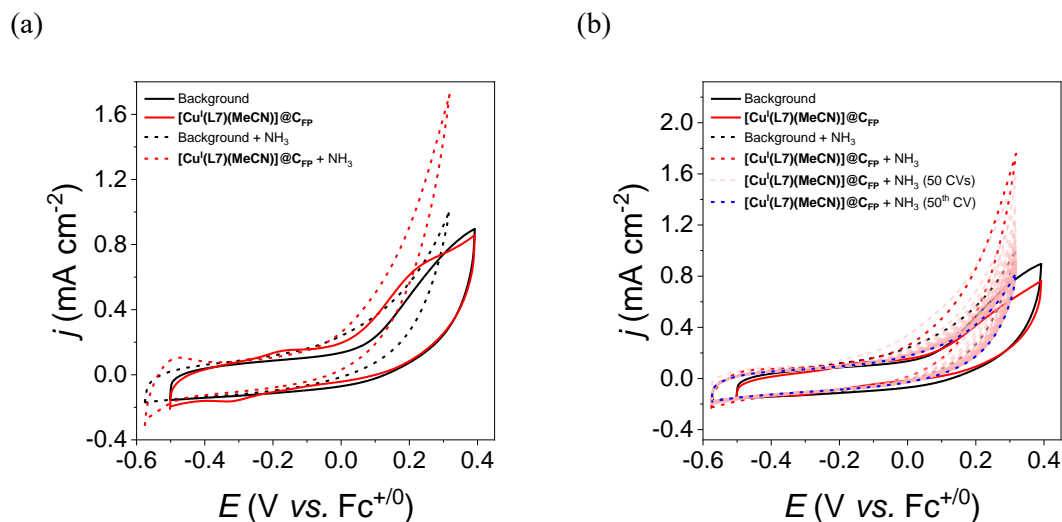


Figure S85. Cyclic voltammograms in MeOH ($\mu = 0.1$ M TBAPF₆) of [Cu^I(L7)(MeCN)]@C_{FP} ($S = 0.25$ cm²) with/without 1.07 M NH₃. *Preparation:* [Cu^I(L7)(MeCN)]@C_{FP} electrodes were prepared by soaking C_{FP} for 24 h into a solution of 0.5 mM [Cu^I(L7)(MeCN)] in THF under an inert atmosphere. *Conditions:* under an inert atmosphere, Pt disk, CE; Ag/AgCl wire, pseudo-RE; $\nu = 100$ mV s⁻¹.

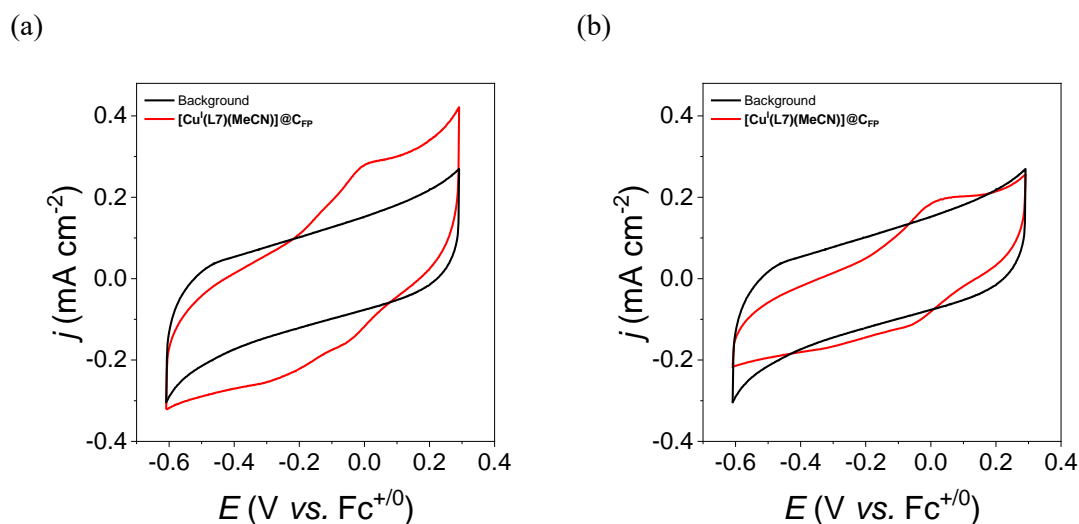


Figure S86. Cyclic voltammograms in MeOH ($\mu = 0.1$ M NH₄OTf) of [Cu^I(L7)(MeCN)]@C_{FP} ($S = 0.25$ cm²) with/without 1.07 M NH₃. *Preparation:* [Cu^I(L7)(MeCN)]@C_{FP} electrodes were prepared by drop casting (5 x 20 μ L) a solution of 1 mM [Cu^I(L7)(MeCN)] in MeCN under an inert atmosphere. *Conditions:* under an inert atmosphere, Pt disk, CE; Ag/AgCl wire, pseudo-RE; $\nu = 100$ mV s⁻¹.

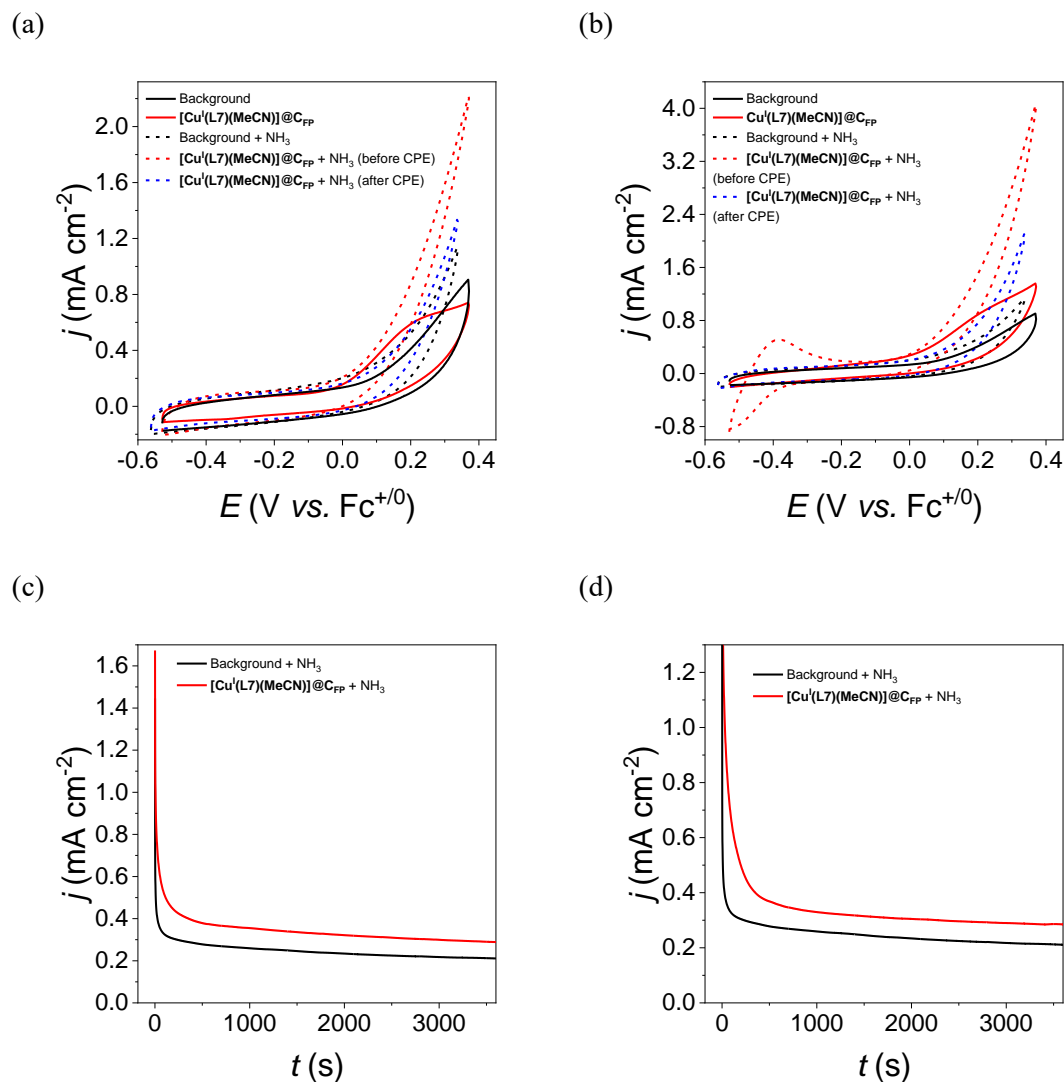


Figure S87. Cyclic voltammograms (a and b) and CPE (c and d) at $E_{\text{app}} = 0.24$ V vs $\text{Fc}^{+/0}$ without stirring in MeOH ($\mu = 0.1$ M TBAPF_6) of $[\text{Cu}^{\text{I}}(\text{L7})(\text{MeCN})]@\text{C}_{\text{FP}}$ ($S = 0.25$ cm²) with/without 0.43 M NH_3 . Preparation: $[\text{Cu}^{\text{I}}(\text{L7})(\text{MeCN})]@\text{C}_{\text{FP}}$ electrodes were prepared by soaking C_{FP} for 24 h into a solution of 0.5 mM $[\text{Cu}^{\text{I}}(\text{L7})(\text{MeCN})]$ in THF under an inert atmosphere. After this time, the electrodes were dried at RT and rinsed (a) or not (b) once with MeOH. *Conditions:* under an inert atmosphere, Pt disk, CE; Ag/AgCl wire, pseudo-RE; $\nu = 100$ mV s⁻¹. (a) $\Gamma = 1.2$ nmol cm⁻²; background subtracted $Q_{\text{CPE}} = 8.728 \cdot 10^{-2}$ C; TON = 520 assuming 100% FE. (b) $\Gamma = 0.53$ nmol cm⁻²; background subtracted $Q_{\text{CPE}} = 8.485 \cdot 10^{-2}$ C; TON = 1112 assuming 100% FE.

Example of calculation for surface loading, turnover number and turnover frequency from electrochemical data shown above between Figures S87a and S87c,

Considering one-electron transfer ... $[\text{Cu}^{\text{II}}(\text{L7})(\text{MeCN})]^+ + e^- = [\text{Cu}^{\text{I}}(\text{L7})(\text{MeCN})]$

$$\text{Surface loading } (\Gamma) = \frac{Q_{\text{integrated}}}{n * F} * \frac{1}{A_{\text{geometric}}} = \frac{2.80 \cdot 10^{-5} \text{ C}}{1 * 96485 \text{ C mol}^{-1}} * \frac{1}{0.5 \text{ cm} * 0.5 \text{ cm}} =$$

$$1.16 \cdot 10^{-9} \text{ mol } [\text{Cu}^{\text{I}}(\text{L7})(\text{MeCN})] \text{ cm}^{-2} = 1.2 \text{ nmol } [\text{Cu}^{\text{I}}(\text{L7})(\text{MeCN})] \text{ cm}^{-2}$$

Considering 100% FE ... $2 \text{ NH}_3 = \text{N}_2 + 6 \text{ H}^+ + 6 e^-$

$$\text{Turnover number } (TON) = \frac{n_{\text{electrons CPE}}}{n * n_{\text{catalyst}}} = \frac{Q_{\text{CPE}}}{6 * F * \Gamma * A_{\text{geometric}}} =$$

$$= \frac{8.728 \cdot 10^{-2} \text{ C}}{6 * 96485 \text{ C mol}^{-1} * 1.16 \cdot 10^{-9} \text{ mol } [\text{Cu}^{\text{I}}(\text{L7})(\text{MeCN})] \text{ cm}^{-2} * (0.5 \text{ cm} * 0.5 \text{ cm})} =$$

$$= 520$$

$$\text{Turnover frequency } (TOF) = \frac{TON}{t} = \frac{520}{3600 \text{ s}} = 0.14 \text{ s}^{-1} = 520 \text{ h}^{-1}$$

Example of calculation for surface loading, turnover number and turnover frequency from electrochemical data shown above between Figures S87b and S87d,

Considering one-electron transfer ... $[\text{Cu}^{\text{II}}(\text{L7})(\text{MeCN})]^+ + e^- = [\text{Cu}^{\text{I}}(\text{L7})(\text{MeCN})]$

$$\text{Surface loading } (\Gamma) = \frac{Q_{\text{integrated}}}{n * F} * \frac{1}{A_{\text{geometric}}} = \frac{1.27 \cdot 10^{-5} \text{ C}}{1 * 96485 \text{ C mol}^{-1}} * \frac{1}{0.5 \text{ cm} * 0.5 \text{ cm}} =$$

$$5.27 \cdot 10^{-10} \text{ mol } [\text{Cu}^{\text{I}}(\text{L7})(\text{MeCN})] \text{ cm}^{-2} = 0.53 \text{ nmol } [\text{Cu}^{\text{I}}(\text{L7})(\text{MeCN})] \text{ cm}^{-2}$$

Considering 100% FE ... $2 \text{ NH}_3 = \text{N}_2 + 6 \text{ H}^+ + 6 e^-$

$$\text{Turnover number } (TON) = \frac{n_{\text{electrons CPE}}}{n * n_{\text{catalyst}}} = \frac{Q_{\text{CPE}}}{6 * F * \Gamma * A_{\text{geometric}}} =$$

$$= \frac{8.485 \cdot 10^{-2} \text{ C}}{6 * 96485 \text{ C mol}^{-1} * 5.27 \cdot 10^{-10} \text{ mol } [\text{Cu}^{\text{I}}(\text{L7})(\text{MeCN})] \text{ cm}^{-2} * (0.5 \text{ cm} * 0.5 \text{ cm})} =$$

$$= 1112$$

$$\text{Turnover frequency } (TOF) = \frac{TON}{t} = \frac{1112}{3600 \text{ s}} = 0.31 \text{ s}^{-1} = 1112 \text{ h}^{-1}$$

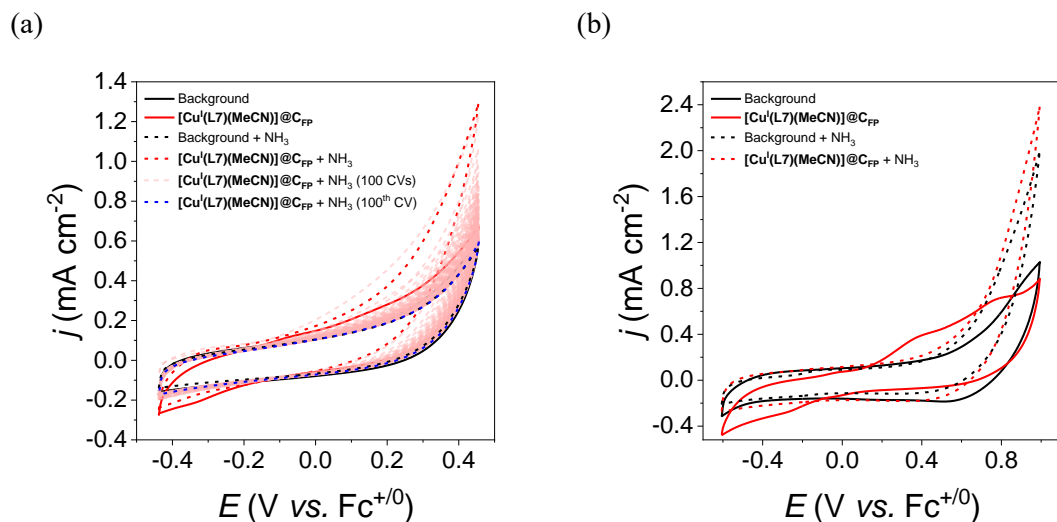


Figure S88. Cyclic voltammograms (a) in MeOH/TFE (1:1) ($\mu = 0.1$ M TBAPF₆) and (b) in MeOH/TFE (1:9) ($\mu = 0.1$ M TBAPF₆) of [Cu^I(L7)(MeCN)]@C_{FP} ($S = 0.25$ cm²) with/without 0.25 M NH₃. Preparation: [Cu^I(L7)(MeCN)]@C_{FP} electrodes were prepared by soaking C_{FP} for 24 h into a solution of 0.5 mM [Cu^I(L7)(MeCN)] in THF under an inert atmosphere. *Conditions:* under an inert atmosphere, Pt disk, CE; Ag/AgCl wire, pseudo-RE; $\nu = 100$ mV s⁻¹.

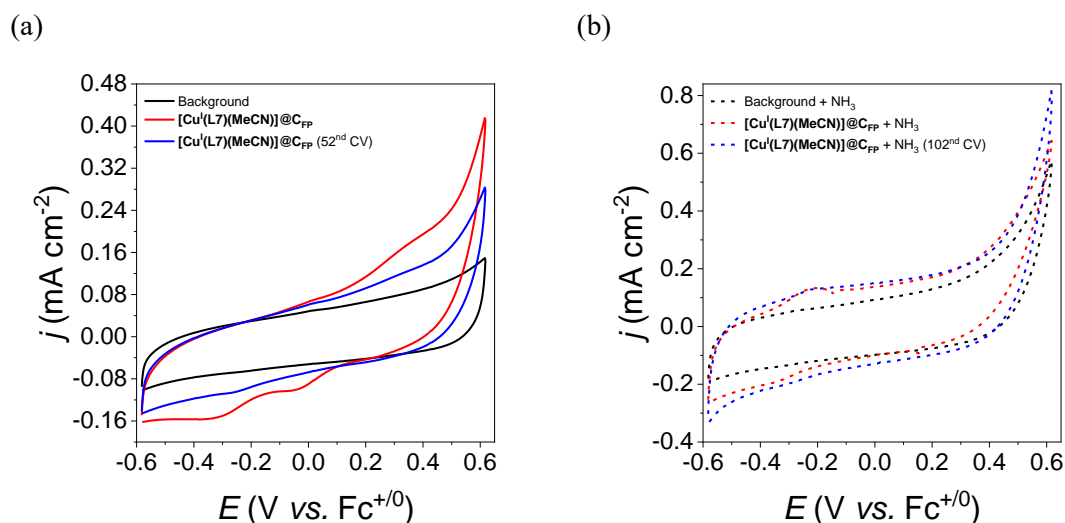


Figure S89. Cyclic voltammograms in TFE ($\mu = 0.1$ M TBAPF₆) of [Cu^I(L7)(MeCN)]@C_{FP} ($S = 0.25$ cm²) and cyclic voltammograms in 0.5 M NH₃ in MeOH. Preparation: [Cu^I(L7)(MeCN)]@C_{FP} electrodes were prepared by soaking C_{FP} for 24 h into a solution of 0.5 mM [Cu^I(L7)(MeCN)] in THF under an inert atmosphere. *Conditions:* under an inert atmosphere, Pt disk, CE; Ag/AgCl wire, pseudo-RE; $\nu = 100$ mV s⁻¹.

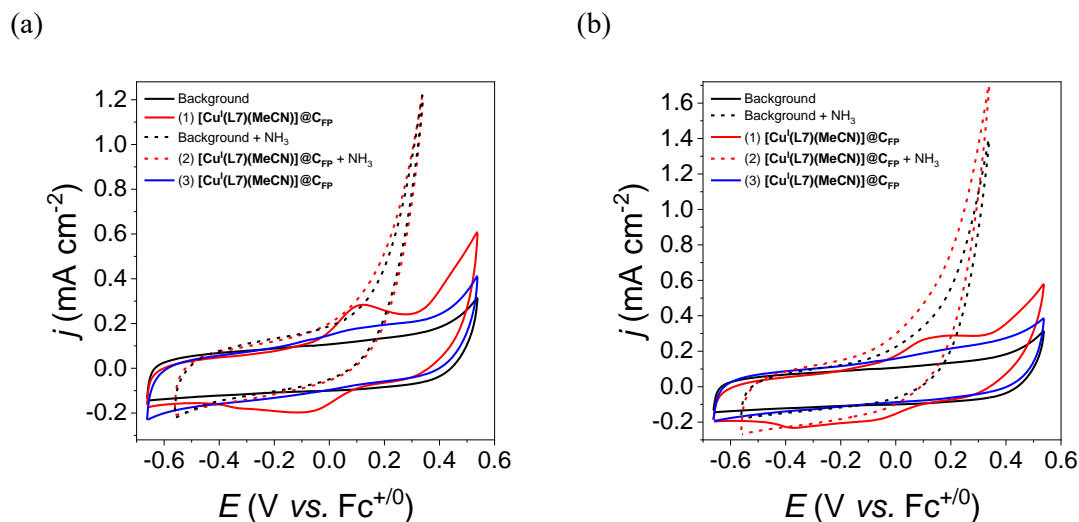


Figure S90. (a) Cyclic voltammograms in (1) TFE ($\mu = 0.1$ M TBAPF₆), (2) 2 M NH₃ in MeOH ($\mu = 0.1$ M TBAPF₆) and (3) TFE ($\mu = 0.1$ M TBAPF₆) of [Cu^I(L7)(MeCN)]@C_{FP} ($S = 0.25$ cm²). (b) Cyclic voltammograms in (1) TFE ($\mu = 0.1$ M TBAPF₆), (2) 1 M NH₃ in MeOH ($\mu = 0.1$ M TBAPF₆) and (3) TFE ($\mu = 0.1$ M TBAPF₆) of [Cu^I(L7)(MeCN)]@C_{FP} ($S = 0.25$ cm²). Preparation: [Cu^I(L7)(MeCN)]@C_{FP} electrodes were prepared by soaking C_{FP} for 24 h into a solution of 0.5 mM [Cu^I(L7)(MeCN)] in THF under an inert atmosphere. Conditions: under an inert atmosphere, Pt disk, CE; Ag/AgCl wire, pseudo-RE; $\nu = 100$ mV s⁻¹. The average integrated charge of the main cathodic wave of [Cu^I(L7)(AcO)]@C_{FP} electrodes in TFE was $Q_{\text{integrated}} = 2.00 \cdot 10^{-5}$ C considering different replicates, corresponding to $\Gamma = 0.83$ nmol cm⁻².

Example of calculation for surface Loading, turnover number and turnover frequency from electrochemical data shown above,

Considering one-electron transfer ... [Cu^{II}(L7)(MeCN)]⁺ + e⁻ = [Cu^I(L7)(MeCN)]

$$\text{Surface loading } (\Gamma) = \frac{Q_{\text{integrated}}}{n * F} * \frac{1}{A_{\text{geometric}}} = \frac{2.00 \cdot 10^{-5} \text{ C}}{1 * 96485 \text{ C mol}^{-1}} * \frac{1}{0.5 \text{ cm} * 0.5 \text{ cm}} =$$

$$8.29 \cdot 10^{-10} \text{ mol [Cu}^{\text{I}}(\text{L7})(\text{MeCN})] \text{ cm}^{-2} = 0.83 \text{ nmol [Cu}^{\text{I}}(\text{L7})(\text{MeCN})] \text{ cm}^{-2}$$

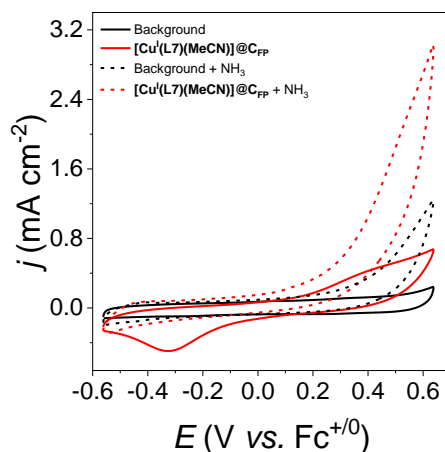
Heterogeneous Electrochemistry of $[\text{Cu}^{\text{I}}(\text{L7})(\text{MeCN})]$ in TFE

Figure S91. Cyclic voltammograms in TFE ($\mu = 0.1$ M TBAPF₆) of $[\text{Cu}^{\text{I}}(\text{L7})(\text{MeCN})]$ @C_{FP} ($S = 0.25$ cm²) with/without bubbled NH₃ gas. *Preparation:* $[\text{Cu}^{\text{I}}(\text{L7})(\text{MeCN})]$ @C_{FP} electrodes were prepared by soaking C_{FP} for 24 h into a solution of 0.5 mM $[\text{Cu}^{\text{I}}(\text{L7})(\text{MeCN})]$ in THF under an inert atmosphere. After this time, the electrodes were dried at RT and rinsed once with MeOH. *Conditions:* under an inert atmosphere, Pt disk, CE; Ag/AgCl wire, pseudo-RE; $\nu = 100$ mV s⁻¹.

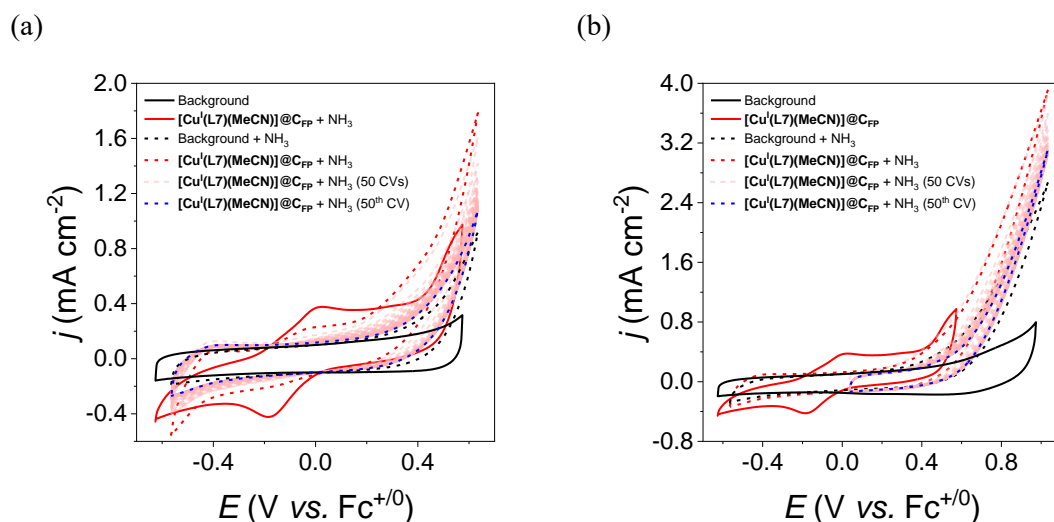


Figure S92. Cyclic voltammograms in TFE ($\mu = 0.1$ M TBAPF₆) of $[\text{Cu}^{\text{I}}(\text{L7})(\text{MeCN})]$ @C_{FP} ($S = 0.25$ cm²) with/without 6.7 M NH₃ at different potential windows. *Preparation:* $[\text{Cu}^{\text{I}}(\text{L7})(\text{MeCN})]$ @C_{FP} electrodes were prepared by drop casting some drops of a solution of 0.5 mM $[\text{Cu}^{\text{I}}(\text{L7})(\text{MeCN})]$ in MeCN onto C_{FP}. *Conditions:* under an inert atmosphere, Pt disk, CE; Ag/AgCl wire, pseudo-RE; $\nu = 100$ mV s⁻¹.

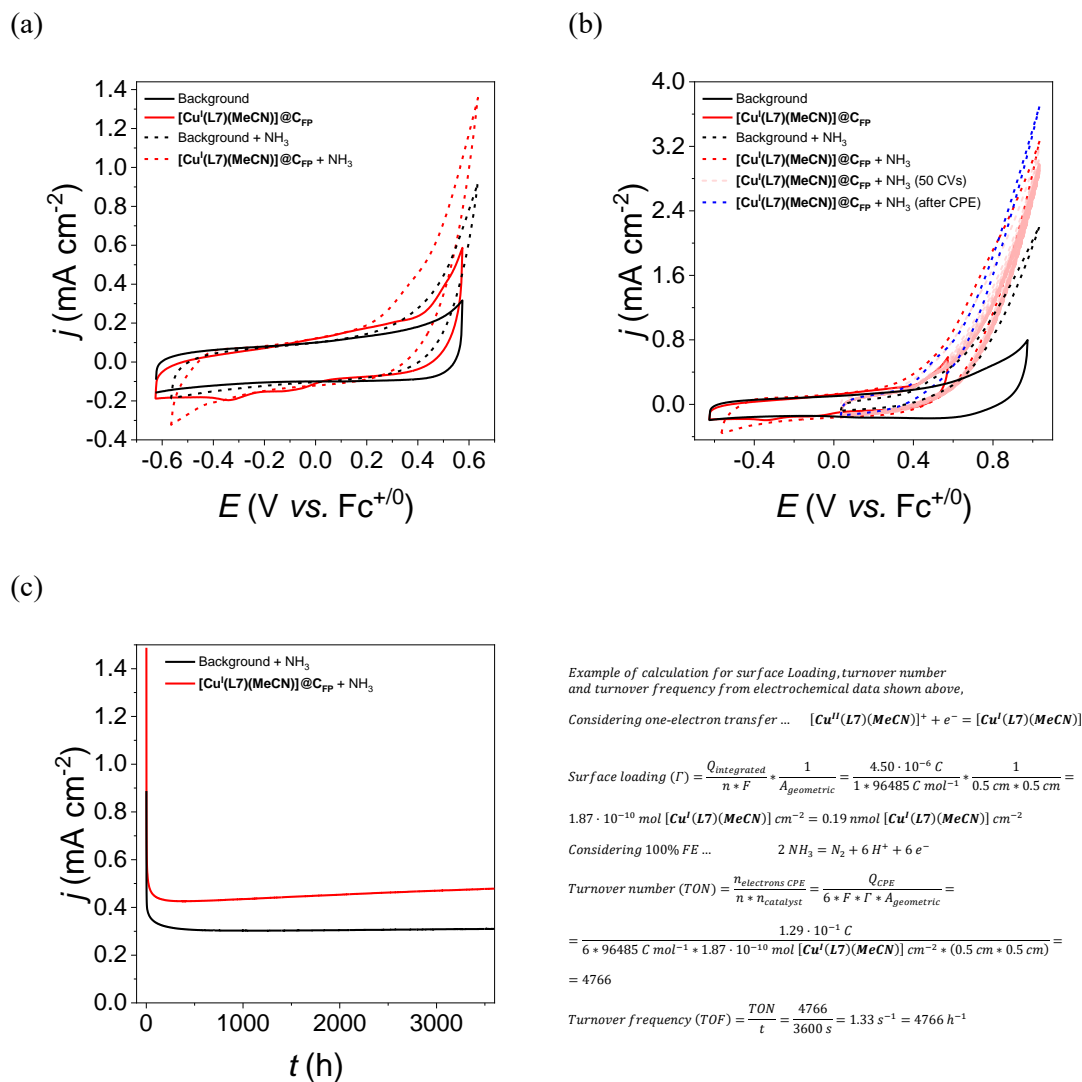


Figure S93. Cyclic voltammograms and CPE at $E_{\text{app}} = 0.64 \text{ V vs Fc}^{+/0}$ with stirring in TFE ($\mu = 0.1 \text{ M TBAPF}_6$) of $[\text{Cu}^{\text{I}}(\text{L7})(\text{MeCN})]@\text{C}_{\text{FP}}$ ($S = 0.25 \text{ cm}^2$) with/without 6.7 M NH_3 . Preparation: $[\text{Cu}^{\text{I}}(\text{L7})(\text{MeCN})]@\text{C}_{\text{FP}}$ electrodes were prepared by soaking C_{FP} for 24 h into a solution of $0.5 \text{ mM } [\text{Cu}^{\text{I}}(\text{L7})(\text{MeCN})]$ in MeCN under an inert atmosphere. Conditions: under an inert atmosphere, Pt disk, CE; Ag/AgCl wire, pseudo-RE; $\nu = 100 \text{ mV s}^{-1}$. $\Gamma = 0.19 \text{ nmol cm}^{-2}$; background subtracted. $Q_{\text{CPE}} = 1.29 \cdot 10^{-1} \text{ C}$; TON = 4766 assuming 100% FE.

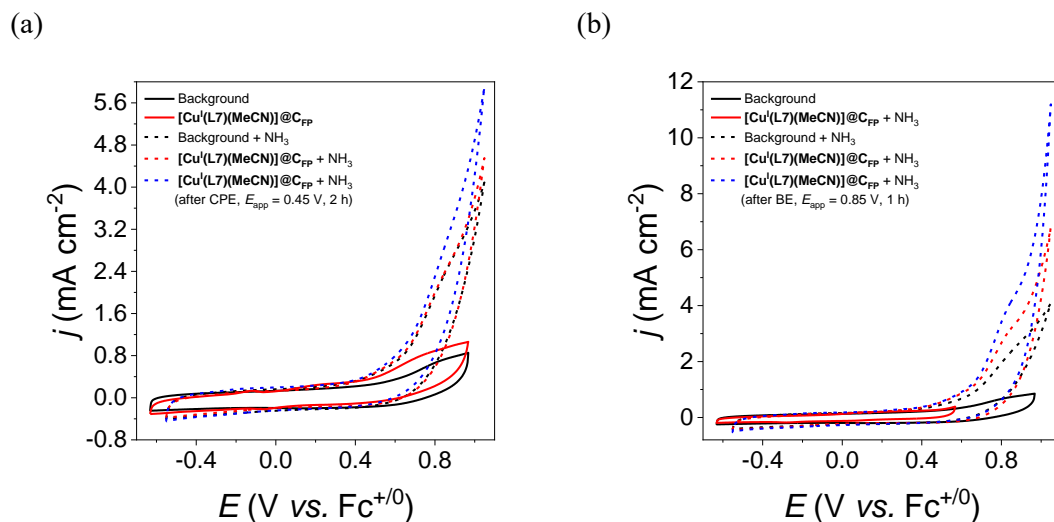


Figure S94. Cyclic voltammograms in TFE ($\mu = 0.1$ M TBAPF₆) of [Cu^I(L7)(MeCN)]@C_{FP} ($S = 0.25$ cm²) with/without 3.4 M NH₃. *Preparation:* [Cu^I(L7)(MeCN)]@C_{FP} electrodes were prepared by soaking C_{FP} for 24 h into a solution of 0.5 mM [Cu^I(L7)(MeCN)] in MeCN under an inert atmosphere. *Conditions:* under an inert atmosphere, Pt disk, CE; Ag/AgCl wire, pseudo-RE; $\nu = 100$ mV s⁻¹.

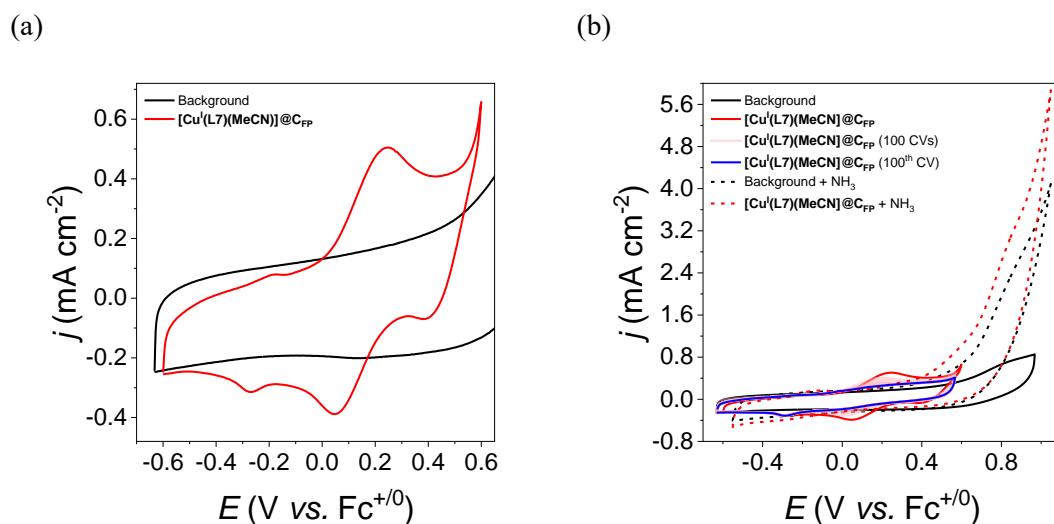


Figure S95. Cyclic voltammograms in TFE ($\mu = 0.1$ M TBAPF₆) of [Cu^I(L7)(MeCN)]@C_{FP} ($S = 0.25$ cm²) with/without 3.4 M NH₃. *Preparation:* [Cu^I(L7)(MeCN)]@C_{FP} electrodes were prepared by drop casting a solution of 1 mM [Cu^I(L7)(MeCN)] in MeCN (5 x 40 μ L) onto C_{FP} under an inert atmosphere. *Conditions:* under an inert atmosphere, Pt disk, CE; Ag/AgCl wire, pseudo-RE; $\nu = 100$ mV s⁻¹.

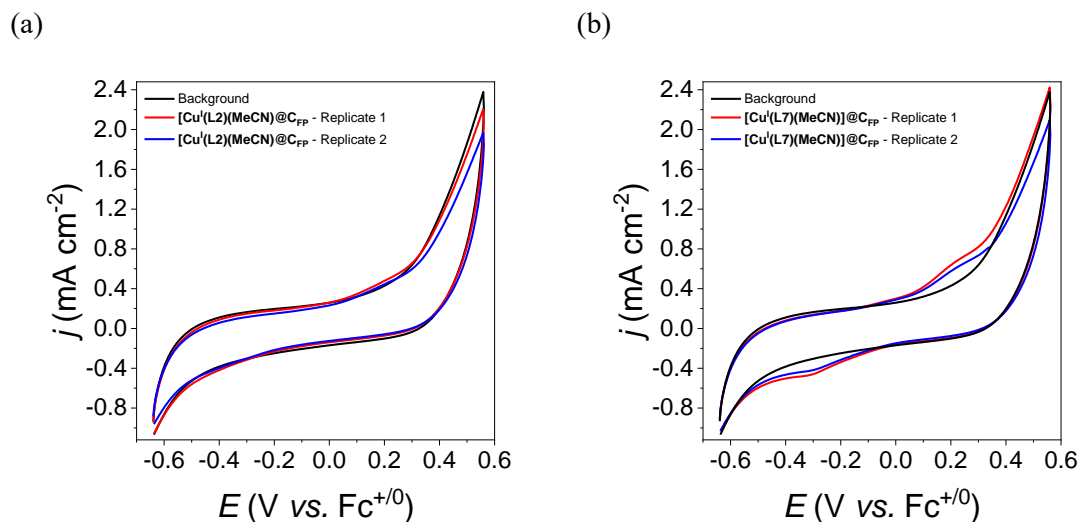


Figure S96. Cyclic voltammograms in TFE ($\mu = 0.1$ M TBAPF₆) of (a) [Cu^I(L2)(MeCN)]@CFP ($S = 0.25$ cm²) and (b) [Cu^I(L7)(MeCN)]@CFP ($S = 0.25$ cm²). *Preparation:* [Cu^I(L2)(MeCN)]@CFP and [Cu^I(L7)(MeCN)]@CFP electrodes were prepared by soaking for 1 s C_{FP} into a solution of 1 mM [Cu^I(L2)(MeCN)] or [Cu^I(L7)(MeCN)] in THF under an inert atmosphere, respectively. *Conditions:* under an inert atmosphere, Pt disk, CE; Ag/AgCl wire, pseudo-RE; $\nu = 100$ mV s⁻¹.

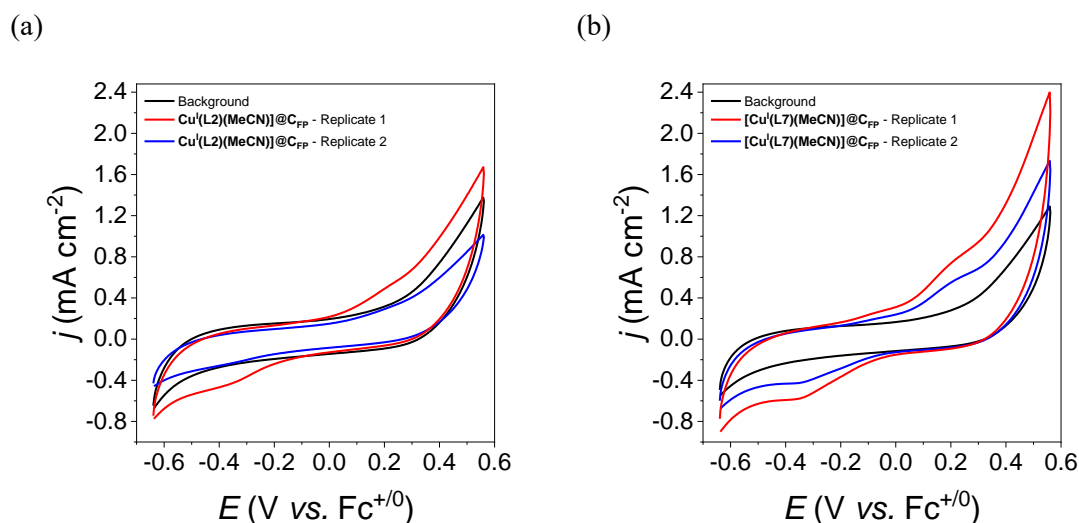


Figure S97. Cyclic voltammograms in TFE ($\mu = 0.1$ M TBAPF₆) of (a) [Cu^I(L2)(MeCN)]@CFP ($S = 0.25$ cm²) and (b) [Cu^I(L7)(MeCN)]@CFP ($S = 0.25$ cm²). *Preparation:* [Cu^I(L2)(MeCN)]@CFP and [Cu^I(L7)(MeCN)]@CFP electrodes were prepared by soaking for 1 h C_{FP} into a solution of 1 mM [Cu^I(L2)(MeCN)] or [Cu^I(L7)(MeCN)] in THF under an inert atmosphere, respectively. *Conditions:* under an inert atmosphere, Pt disk, CE; Ag/AgCl wire, pseudo-RE; $\nu = 100$ mV s⁻¹.

Heterogeneous Electrochemistry of [Cu^I(L7)(MeCN)] in 1-(But-1-yl)-3-methyl-1H-imidazol-3-ium hexafluorophosphate

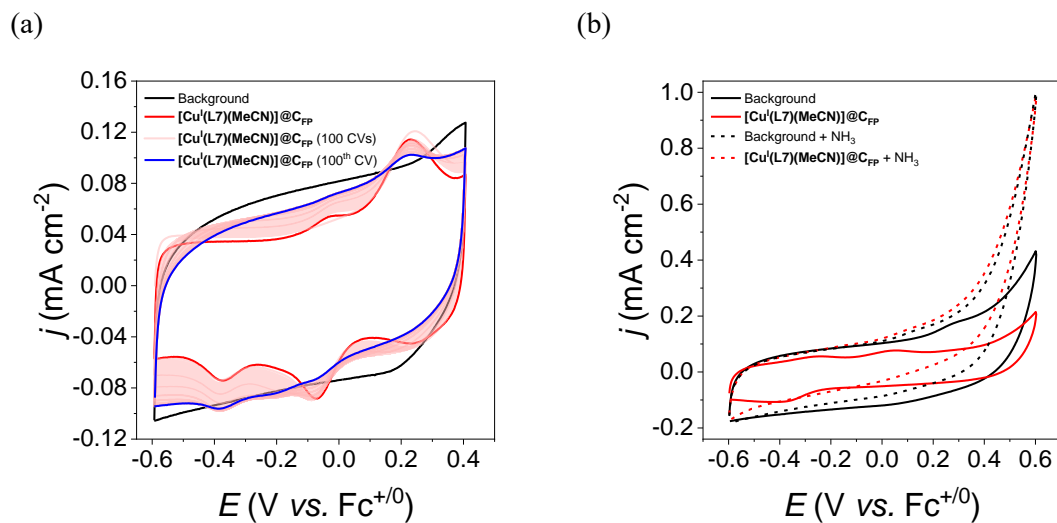


Figure S98. (a) Cyclic voltammograms in 1-(But-1-yl)-3-methyl-1H-imidazol-3-ium hexafluorophosphate of [Cu^I(L2)(MeCN)]@CFP ($S = 0.25 \text{ cm}^2$). Preparation: [Cu^I(L7)(MeCN)]@CFP electrodes were prepared by soaking CFP for 24 h into a solution of 0.5 mM [Cu^I(L7)(MeCN)]@CFP in THF under an inert atmosphere. After this time, the electrodes were dried at RT and rinsed once with MeOH. (b) Cyclic voltammograms in 1-(But-1-yl)-3-methyl-1H-imidazol-3-ium hexafluorophosphate of [Cu^I(L2)(MeCN)]@CFP ($S = 0.25 \text{ cm}^2$) with/without bubbled NH₃. Preparation: [Cu^I(L7)(MeCN)]@CFP electrodes were prepared by soaking CFP for 24 h into a solution of 0.5 mM [Cu^I(L7)(MeCN)]@CFP in THF under an inert atmosphere. Conditions: under an inert atmosphere, Pt disk, CE; Ag/AgCl wire, pseudo-RE; $\nu = 100 \text{ mV s}^{-1}$.

5.15. Comparative Studies

Comparison between Homogeneous Electrochemistry of $[\text{Cu}^{\text{I}}(\text{L}2)(\text{MeCN})]$ and $[\text{Cu}^{\text{I}}(\text{MeCN})_4]\text{CF}_3\text{SO}_3$ in THF with 0.5 NH_3

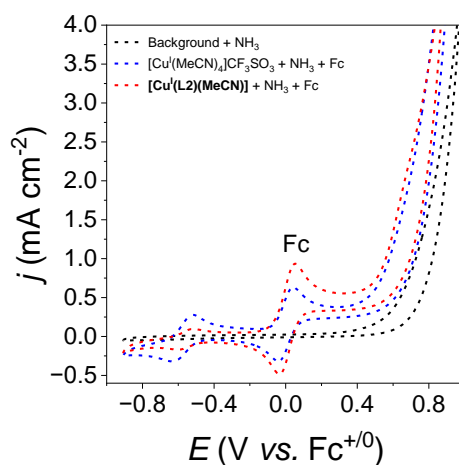


Figure S99. Cyclic voltammograms in MeCN ($\mu = 0.1$ M TBAPF₆) of 1 mM $[\text{Cu}^{\text{I}}(\text{MeCN})_4]\text{CF}_3\text{SO}_3$ (blue dashed line) and 1 mM $[\text{Cu}^{\text{I}}(\text{L}2)(\text{MeCN})]$ (red dashed line) with 0.5 M NH_3 and Fc, showing a coinciding wave at cathodic potentials. Conditions: under an inert atmosphere, GC_{disk} ($S = 0.07$ cm²), WE; Pt disk, CE; Ag/AgCl wire, pseudo-RE; $\nu = 100$ mV s⁻¹.

Comparison between Homogeneous Electrochemistry of $[\text{Cu}^{\text{I}}(\text{L}1)(\text{MeCN})]$, $[\text{Cu}^{\text{I}}(\text{L}2)(\text{MeCN})]$, $[\text{Cu}^{\text{I}}(\text{L}7)(\text{MeCN})]$ and $[\text{Cu}^{\text{I}}(\text{L}10)(\text{MeCN})]$ in THF

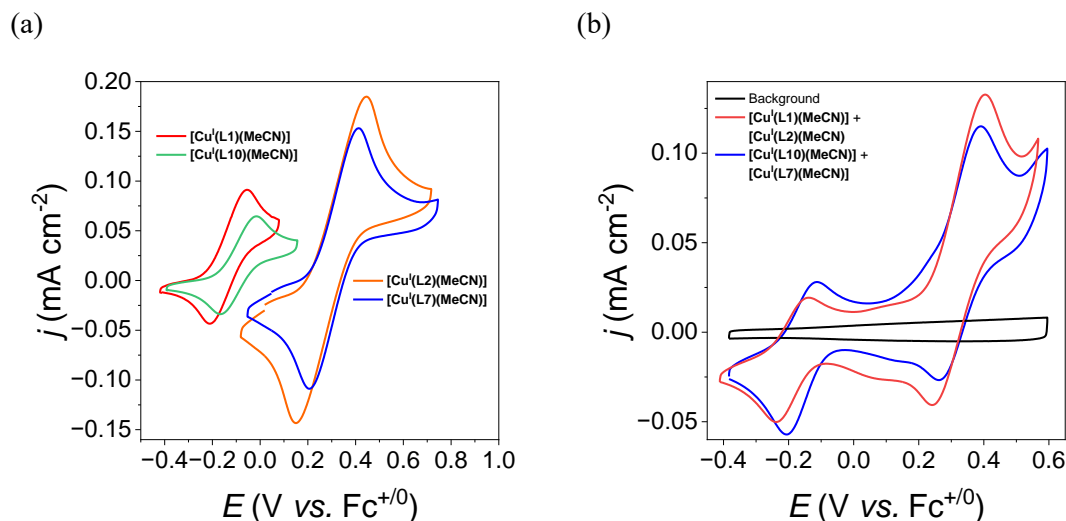


Figure S100. (a) Cyclic voltammograms in THF ($\mu = 0.1$ M TBAPF₆) of 0.5 mM $[\text{Cu}^{\text{I}}(\text{L}1)(\text{MeCN})]$ and 0.5 mM $[\text{Cu}^{\text{I}}(\text{L}2)(\text{MeCN})]$ (red line) and 0.5 mM $[\text{Cu}^{\text{I}}(\text{L}1)(\text{MeCN})]$ and 0.5 mM $[\text{Cu}^{\text{I}}(\text{L}2)(\text{MeCN})]$ (blue line). (b) Cyclic voltammograms in THF ($\mu = 0.1$ M TBAPF₆) of 1 mM $[\text{Cu}^{\text{I}}(\text{LX})(\text{MeCN})]$ (LX = 1, 2, 7, 10) complexes. Conditions: under an inert atmosphere, GC_{disk} ($S = 0.07$ cm²), WE; Pt disk, CE; Ag/AgCl wire, pseudo-RE; $\nu = 100$ mV s⁻¹.

6. Spectroscopical Studies

6.1. UV-Vis Studies

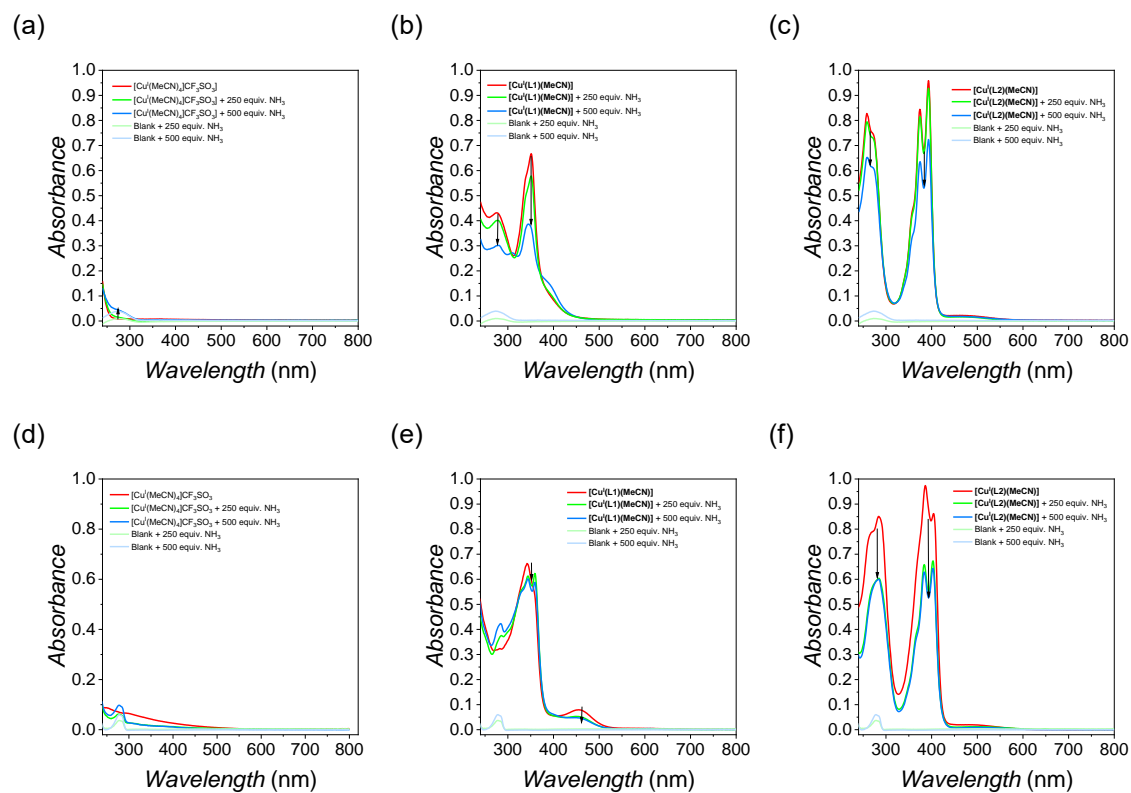
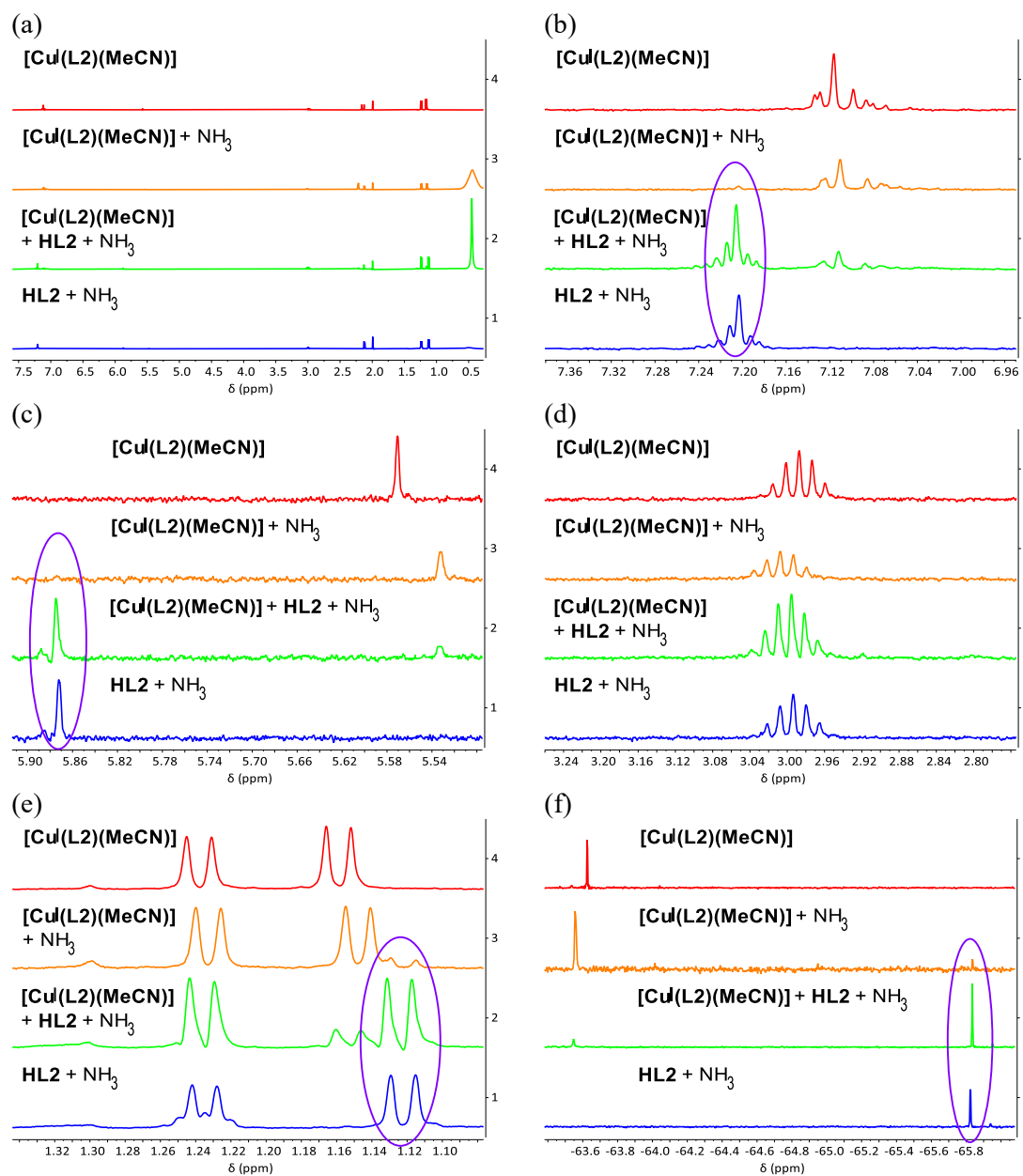


Figure S101. UV-Vis spectra in MeCN (top) and THF (bottom) of $[\text{Cu}^{\text{I}}(\text{MeCN})_4]^+$ (a and d), $[\text{Cu}^{\text{I}}(\text{L1})(\text{MeCN})]$ (b and e), and $[\text{Cu}^{\text{I}}(\text{L2})(\text{MeCN})]$ (c and f) under an inert atmosphere with different equivalents of NH_3 . *Procedure:* 1 mM complex stock solutions were prepared with varying concentration of NH_3 and subsequently added (150 μL) to THF (3.15 mL) under an inert atmosphere.

6.2. NMR Studies



7. Crystallographic Details

CIF files can be found on CCDC with deposition number 2410168-2410180.

Structure	CCDC Number
3	2410175
HL3	2410178
HL4	2410177
HL5	2410173
HL7	2410168
HL8	2410172
HL9	2410180
HL10	2410176
[Cu^{II}(L1)(OAc)]	2410174
[Cu^{II}(L3)₂]	2410170
[Cu^{II}(L4)₂]	2410171
[Cu^I(L7)(MeCN)]	2410179
[Cu^I(L10)(MeCN)]	2410169

7.1. Data Collection

Crystal structure determinations for compounds **HL4**, **HL5**, **HL10**, **[Cu^I(L3)₂]**, **[Cu^I(L4)₂]**, **[Cu^I(L7)(MeCN)]** and **[Cu^I(L10)(MeCN)]** were performed using a Rigaku diffractometer equipped with a Pilatus 200K area detector, a Rigaku MicroMax-007HF microfocus rotating anode with MoK α radiation, Confocal Max Flux optics, and an Oxford Cryosystems Cryostream 700 plus low-temperature device ($T = -173$ °C). Full-sphere data collection was conducted with ω and φ scans. *Programs used:* The data collection and data reduction was performed using CrysAlisPro,¹⁴ and absorption correction was applied using the Scale3 Abspack scaling algorithm.¹⁵

Crystal structure determinations for **3**, **HL3**, **HL7**, **HL8**, **HL9** and **[Cu^{II}(L1)(AcO)]** were performed with an Apex DUO Kappa 4-axis goniometer, equipped with an APEX 2 4K CCD area detector, a Microfocus Source E025 IuS using MoK α radiation, Quazar MX multilayer Optics as a monochromator, and an Oxford Cryosystems Cryostream 700 plus low-temperature device ($T = -173$ °C). Full-sphere data collection was employed with ω and φ scans. *Programs used:* The data collection was conducted using APEX-2,¹⁶ data reduction was done using Bruker Saint¹⁷ V/.60A, and absorption correction was applied using SADABS.¹⁸

7.2. Structure Solution and Refinement

The crystal structures were solved using the SHELXT program.¹⁹ Visualization and processing were performed with OLEX2 program.²⁰ Missing atoms were subsequently located from difference Fourier synthesis and added to the atom list. Least-squares refinement on F^2 using all measured intensities was carried out using the SHELXL 2015 program.²¹ All non-hydrogen atoms were refined including anisotropic displacement parameters.

7.3. ORTEP Structures and Comments

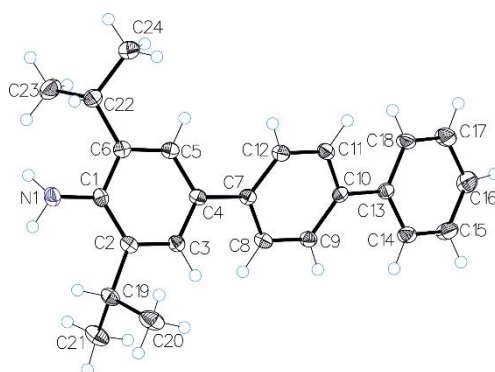


Figure S103. ORTEP drawing (50%) showing compound **3**. Solvent molecules and disordered atoms have been omitted for the sake of clarity. Monocrystals were formed by slow evaporation at RT of a solution in MeOH. *Comments:* The asymmetric unit contains one molecule of the organic compound. The terminal aromatic ring (C13-C18) is disordered in two orientations (ratio: 62:38).

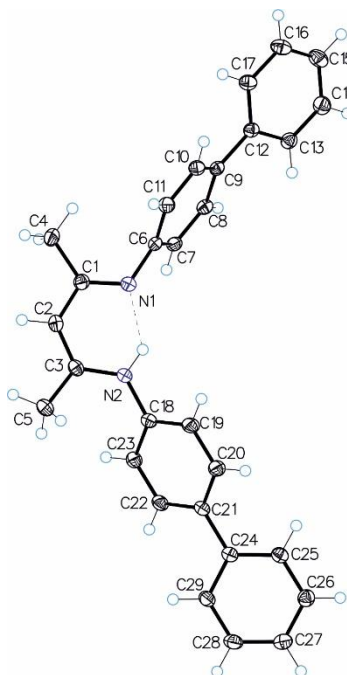


Figure S104. ORTEP drawing (50%) showing compound **HL3**. Solvent molecules and disordered atoms have been omitted for the sake of clarity. Monocrystals were formed by slow evaporation at RT of a saturated solution in THF. *Comments:* The asymmetric unit contains one molecule of the organic compound.

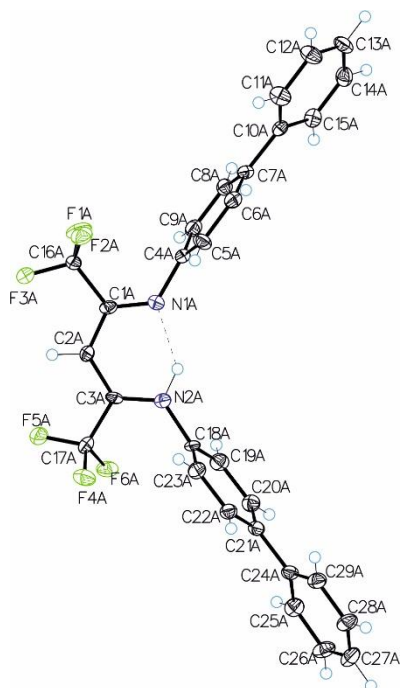


Figure S105. ORTEP drawing (50%) showing compound **HL4**. Solvent molecules and disordered atoms have been omitted for the sake of clarity. Monocrystals were formed by slow evaporation at RT in deuterated benzene. *Comments:* The asymmetric unit contains two independent molecules of the same organic compound and two molecules of benzene. One of the benzene molecules is disordered in two orientations (ratio 60:40). The measured sample was a multi-component crystal in which two domains could be indexed and integrated consistently (twin ratio 69:31). The two crystals identified were processed using Scale3 Abspack, accounting for overlapping reflections.²²

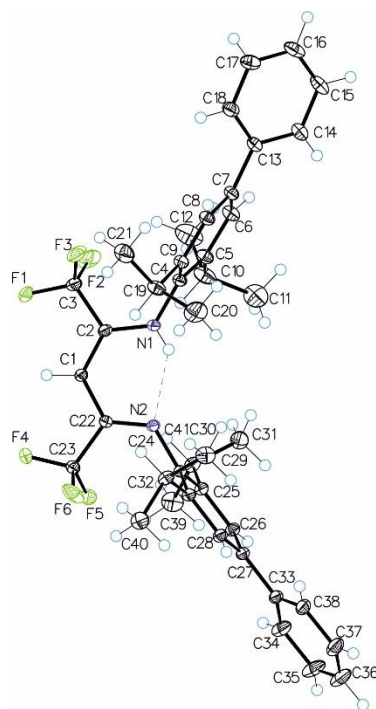


Figure S106. ORTEP drawing (50%) showing compound **HL5**. Solvent molecules and disordered atoms have been omitted for the sake of clarity. Monocrystals were formed by slow evaporation at RT in CHCl_3 . *Comments:* The asymmetric unit contains one molecule of the organic compound and one solvent molecule. For the solvent molecule there is a positional disorder in which 86% corresponds to chloroform and 14% to dichloromethane. In the main organic molecule one of the CF_3 groups is disordered in two orientations (ratio 93:7). The hydrogen atom located at N1 was localized experimentally from the residual electron density.

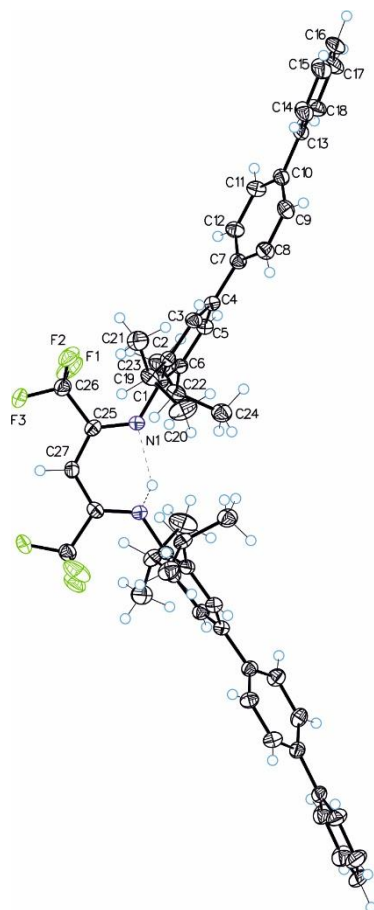


Figure S107. ORTEP drawing (50%) showing compound **HL7**. Solvent molecules and disordered atoms have been omitted for the sake of clarity. Monocrystals were formed by slow evaporation at RT in CHCl_3 . *Comments:* The asymmetric unit contains two molecules of the same organic compound. Both molecules are partially disordered in two orientations.

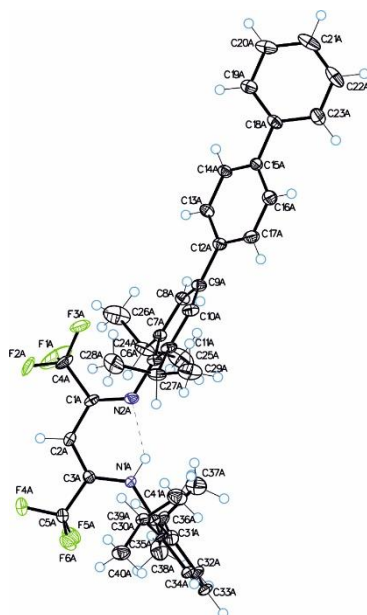


Figure S108. ORTEP drawing (50%) showing compound **HL8**. Solvent molecules and disordered atoms have been omitted for the sake of clarity. Monocrystals were formed by slow evaporation at RT in acetone. *Comments:* The asymmetric unit contains half molecule of the organic compound which is located on a 2-fold axis. The hydrogen atom coordinated to N1 is disordered in two orientations around the two-fold axes (ratio 0.5:0.5). The CF_3 -groups are disordered in two orientations (ratio 91:9).

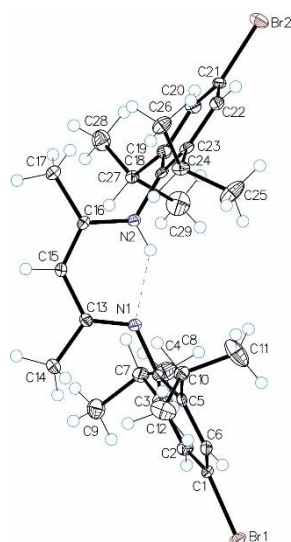


Figure S109. ORTEP drawing (50%) showing compound **HL9**. Solvent molecules and disordered atoms have been omitted for the sake of clarity. Monocrystals were formed by recrystallization from acetone (Bp/RT). *Comments:* The asymmetric unit contains one molecule of the organic compound. Two of the isopropyl groups present in the molecule are disordered in two orientations with a ratio of 58:42.

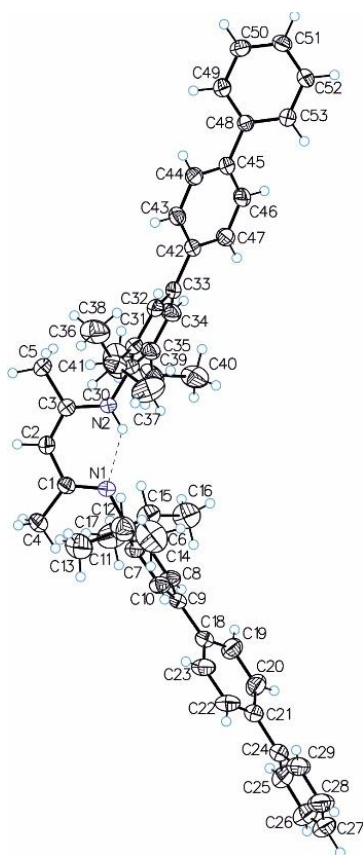


Figure S110. ORTEP drawing (50%) showing compound **HL10**. Solvent molecules and disordered atoms have been omitted for the sake of clarity. Monocrystals were formed by recrystallization from hexane (Bp/-35 °C). *Comments:* The asymmetric unit contains one molecule of the organic compound. Some of the isopropyl groups and one of the terminal benzene rings present in the molecule are disordered in two orientations.

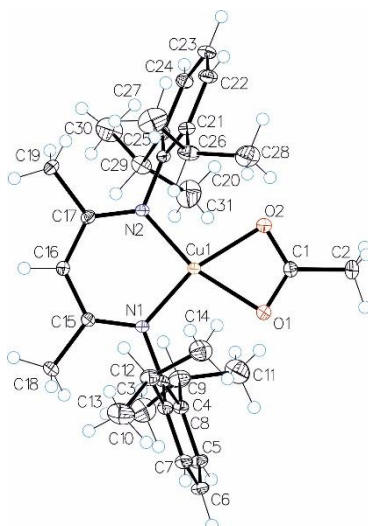


Figure S111. ORTEP drawing (50%) showing compound $[\text{Cu}^{\text{II}}(\text{L1})(\text{AcO})]$. Monocrystals were formed by recrystallization from MeOH (Bp/-35 °C). The structure is already resolved in the literature.²³ *Comments:* The asymmetric unit contains one molecule of the copper metal complex. The measured sample was a multi-component crystal in which two domains could be indexed and integrated consistently (twin ratio 50:50). The two crystals identified were processed with TWINABS taking in account overlapping reflections.²⁴

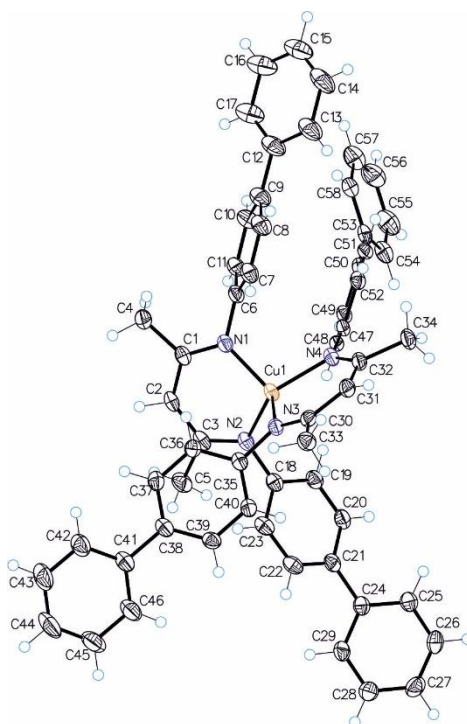


Figure S112. ORTEP drawing (50%) showing compound $[\text{Cu}^{\text{II}}(\text{L3})_2]$. Solvent molecules and disordered atoms have been omitted for the sake of clarity. Monocrystals were formed by recrystallization from *n*-pentane (RT/-35 °C). *Comments:* The asymmetric unit contains one molecule of the organometallic compound and one molecule of *n*-pentane. In the main molecule one of the ligands is disordered in two orientations (ratio 70:30). The *n*-pentane molecule is disordered in five orientations with a ratio 0.25:0.25:0.15:0.20:0.15.

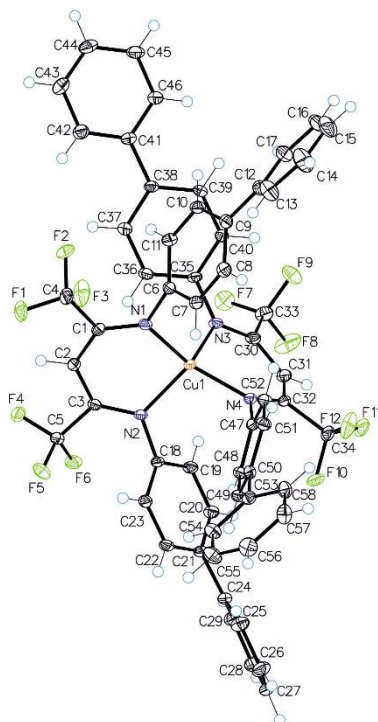


Figure S113. ORTEP drawing (50%) showing compound $[\text{Cu}^{\text{II}}(\text{L4})_2]$. Monocrystals were formed by recrystallization from DCM/MeOH 1:1 at RT. *Comments:* The sample measured was a multi-component crystal from which only one crystal could be indexed. The asymmetric unit contains one molecule of the organometallic compound. Despite of being a multi-component crystal, the structure is of good quality.

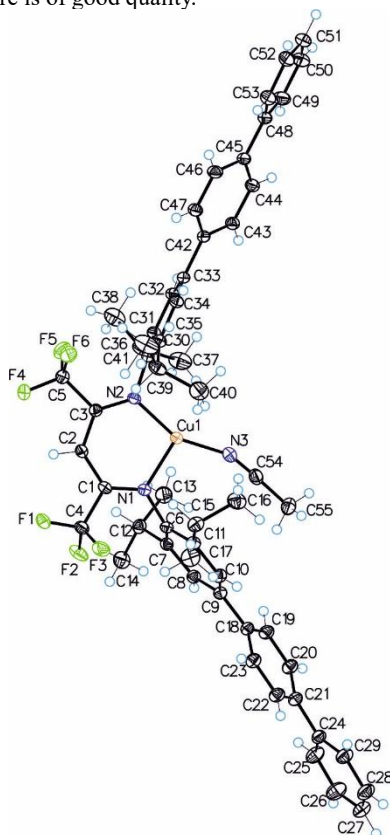


Figure S114. ORTEP drawing (50%) showing compound $[\text{Cu}^{\text{I}}(\text{L7})(\text{MeCN})]$. Solvent molecules and disordered atoms have been omitted for the sake of clarity. Monocrystals were formed by recrystallization from MeCN (RT/-40 °C). *Comments:* The asymmetric unit contains one molecule of the organometallic compound and half molecule of non-coordinated acetonitrile. The non-coordinated MeCN molecule is disordered in two orientations (ratio 50:50).

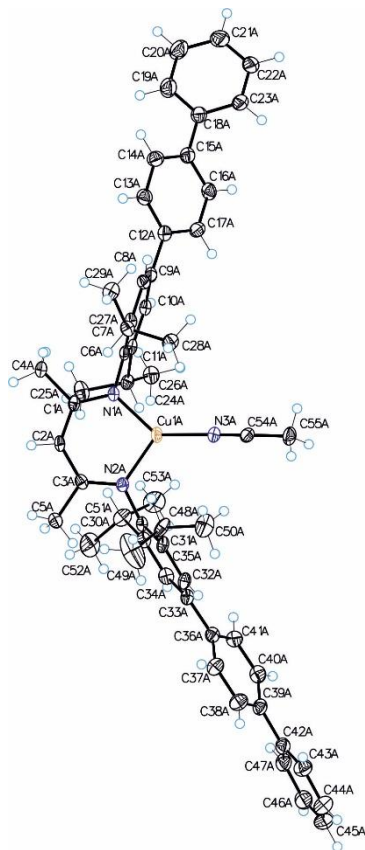


Figure S115. ORTEP drawing (50%) showing compound $[\text{Cu}^{\text{I}}(\text{L10})(\text{MeCN})]$. Solvent molecules and disordered atoms have been omitted for the sake of clarity. Monocrystals were formed by recrystallization from MeCN (Bp/-40 °C). *Comments:* The asymmetric unit contains two independent molecules of the same copper metal complex and one molecule of acetonitrile. The acetonitrile molecule is disordered in four positions with a ratio 0.37:0.37:0.13:0.13.

8. Computational Studies

8.1. General Procedure

All structures were modelled using the AMS2021 software package with the DFT functional BP86-D3²⁵ (Becke exchange functional²⁶ with gradient correction provided by the Perdew expression²⁷ and Grimme's D3 dispersion²⁸) with a DZP basis set for the elements H, C, N, and F and a TZP for Cu, including ZORA²⁹⁻³¹ scalar relativistic corrections. The calculations were performed using THF or MeOH as solvent employing the COSMO^{32,33} solvent model. Weak interactions were analysed using the Non-Covalent Interactions (NCIs) approach.^{34,35} The interactions were computed with a coarse grid, and depicted using an isosurface value of 0.3 and a density threshold for detection of weak interaction regions of 0.02. A data set collection of input and output files is available in the ioChem-BD repository.³⁶

8.2. Structure Optimization and Anchoring

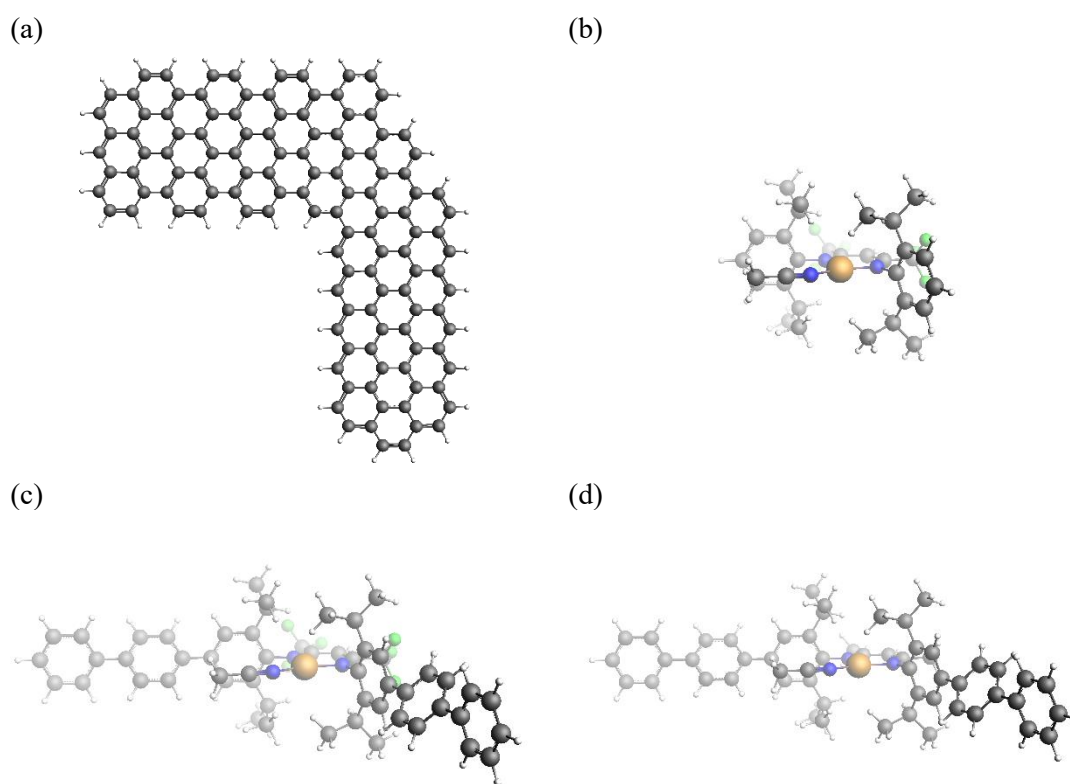


Figure S116. Optimized structures of (a) graphene surface (C₁₂₄H₃₈), (b) [Cu^I(L2)(MeCN)], (c) [Cu^I(L7)(MeCN)], (d) and [Cu^I(L10)(MeCN)] in MeOH. Color code: Gray (C), blue (N), white (H), green (F), orange (Cu).

Before conducting the anchoring study, the conformation of the complex in solution was evaluated (Figure S116). Achieving full π - π stacking along the entire triphenyl group could significantly enhance immobilization stability onto a graphene layer. However, the isopropyl groups on the first ring may hinder this due to the high steric hindrance with the β -diketiminato ring. To assess this, the rotation energy barrier of the ortho-substituted ring was calculated, as shown in Figure S117. The results indicate that the barrier is too high for the ring to adopt a flat orientation, preventing complete π - π stacking.

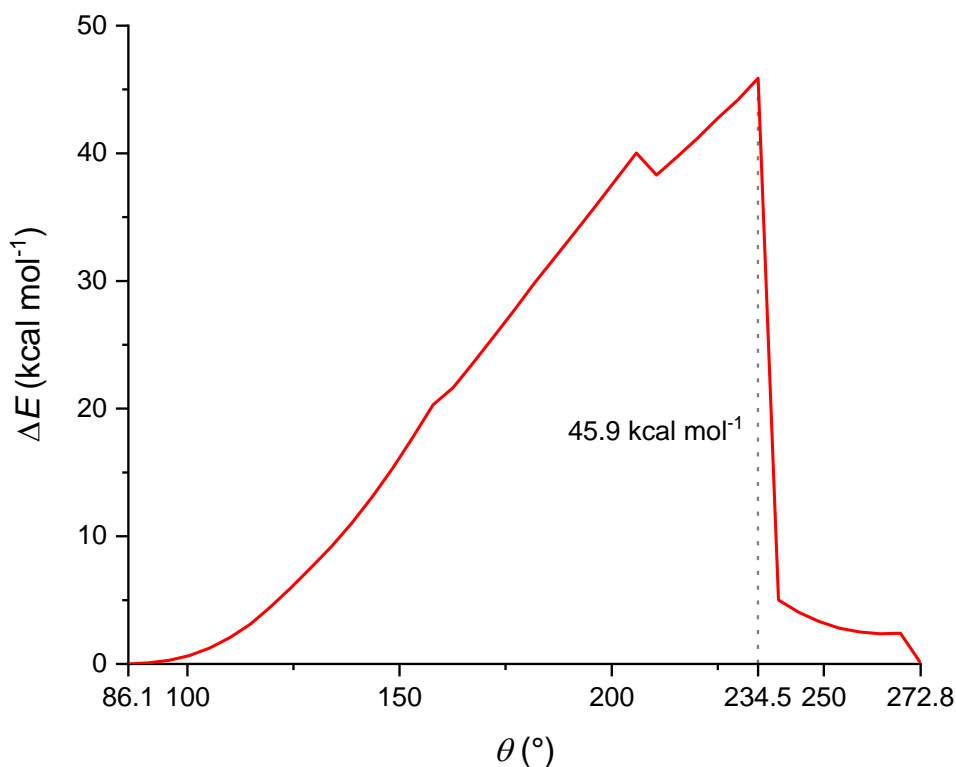


Figure S117. Energy barrier for the rotation of the triphenyl group around the β -diketiminato ring.

While the rotation of the isopropyl-substituted ring requires significant energy, the barrier for adjusting the angle between the phenyl rings within the triphenyl unit of $[\text{Cu}^{\text{I}}(\text{L7})(\text{MeCN})]$ and $[\text{Cu}^{\text{I}}(\text{L10})(\text{MeCN})]$ is relatively low, making this adjustment feasible.

Figures S118, S119, and S120 display the structures of the immobilized complexes and highlight the interactions responsible for anchoring them onto the surface via only CH- π interactions. The complex-graphene distances are provided in Figures S119, S111, and S113.

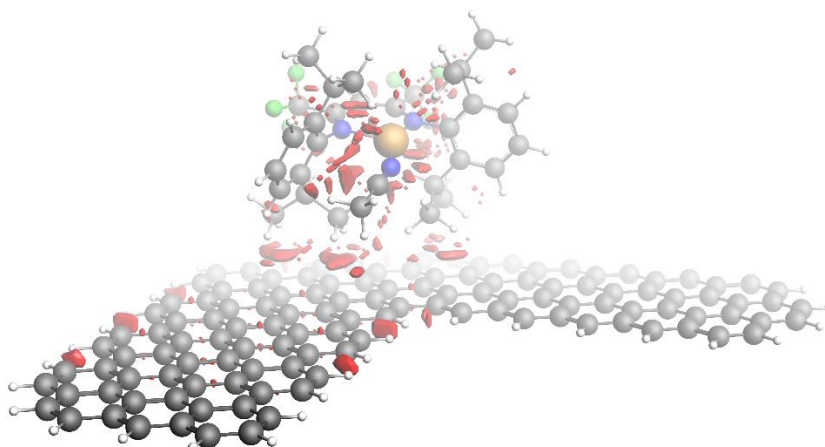


Figure S118. Optimized structure of $[\text{Cu}^{\text{I}}(\text{L2})(\text{MeCN})]$ anchored via sole CH- π interactions onto a graphene layer. The supramolecular interactions are indicated in red. Color code: Gray (C), blue (N), white (H), green (F), orange (Cu).

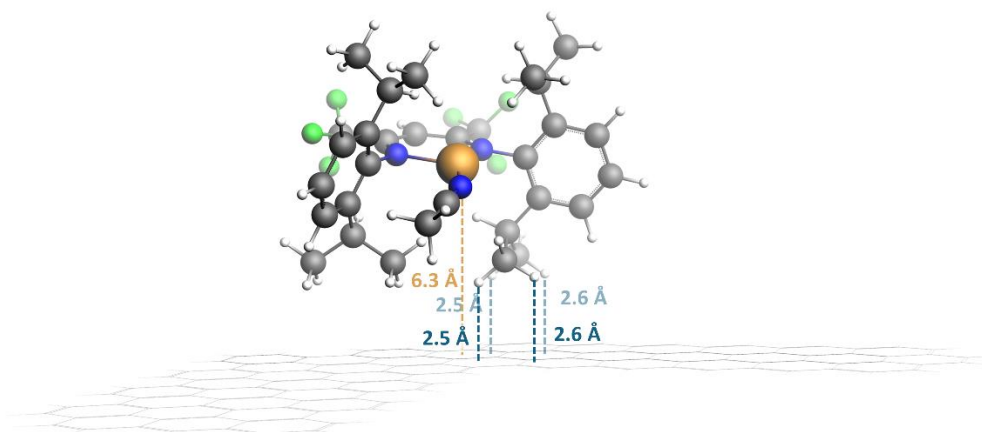


Figure S119. Complex-graphene distances for structure $[\text{Cu}^{\text{I}}(\text{L2})(\text{MeCN})]$ anchored via sole CH- π interactions onto a graphene layer. Color code: orange (Cu-graphene), blue (CH- π isopropyl-graphene).

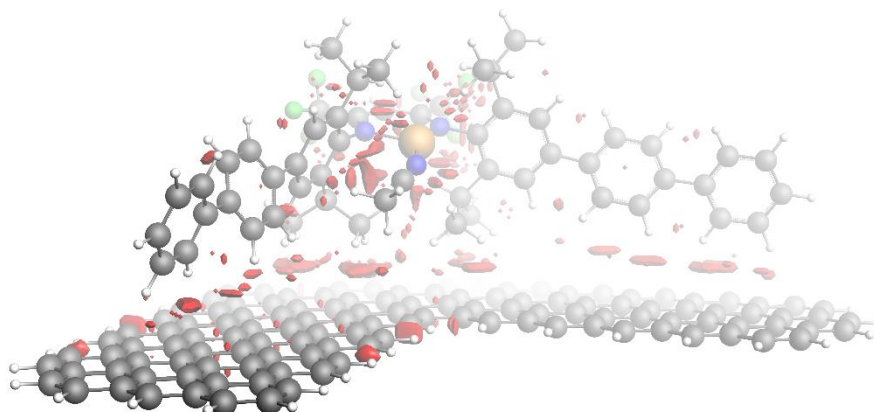


Figure S120. Optimized structure of $[\text{Cu}^{\text{I}}(\text{L7})(\text{MeCN})]$ anchored via sole CH- π interactions onto a graphene layer. The supramolecular interactions are indicated in red. Color code: Gray (C), blue (N), white (H), green (F), orange (Cu).

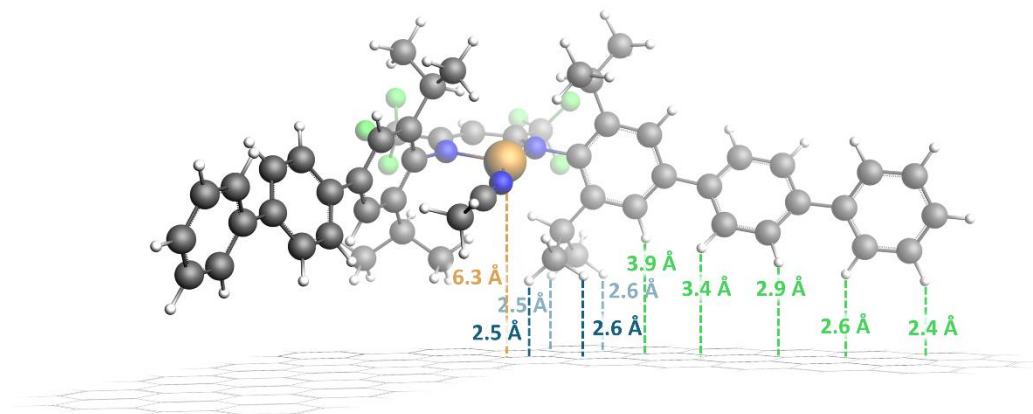


Figure S121. Complex-graphene distances for structure $[\text{Cu}^{\text{I}}(\text{L7})(\text{MeCN})]$ anchored via sole CH- π interactions onto a graphene layer. Color code: orange (Cu-graphene), blue (CH- π isopropyl-graphene), green (CH- π phenyl-graphene).

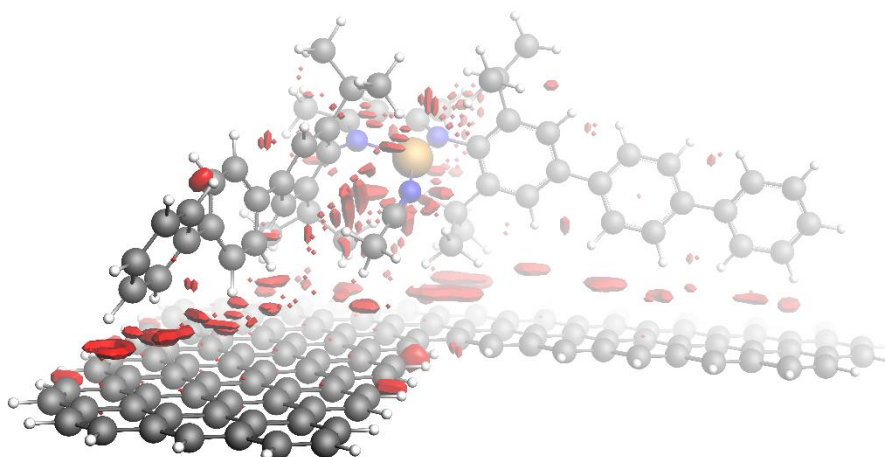


Figure S122. Optimized structure of $[\text{Cu}^{\text{I}}(\text{L10})(\text{MeCN})]$ anchored via sole CH- π interactions onto a graphene layer. The supramolecular interactions are indicated in red. Color code: Gray (C), blue (N), white (H), orange (Cu).

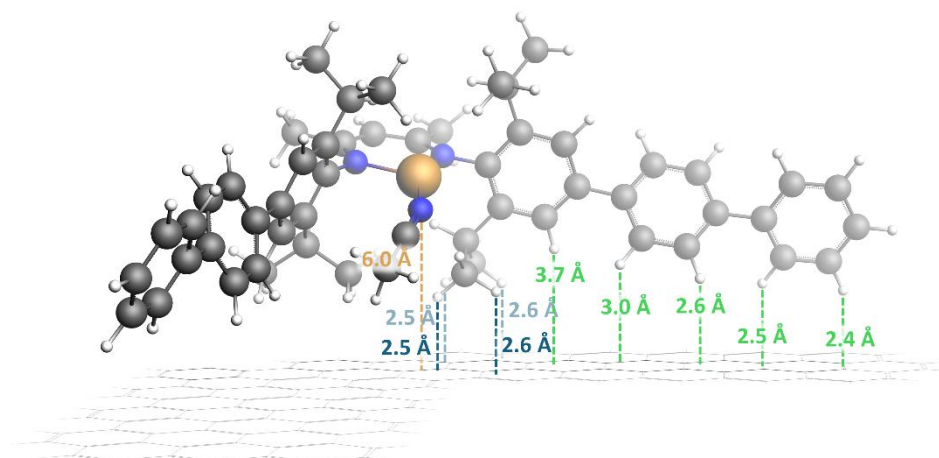


Figure S123. Complex-graphene distances for structure $[\text{Cu}^{\text{I}}(\text{10})(\text{MeCN})]$ anchored via sole CH- π interactions onto a graphene layer. Color code: orange (Cu-graphene), blue (CH- π isopropyl-graphene), green (CH- π phenyl-graphene).

Figures S124-S127 show the structures of the immobilized complexes stabilized by a combination of CH- π and π - π interactions. The advantage of mixed CH- π and π - π anchoring is evident in the enhanced anchoring energy compared to CH- π interactions alone. The anchoring energy values in MeOH and THF are reported in Tables S3 and S4, respectively.

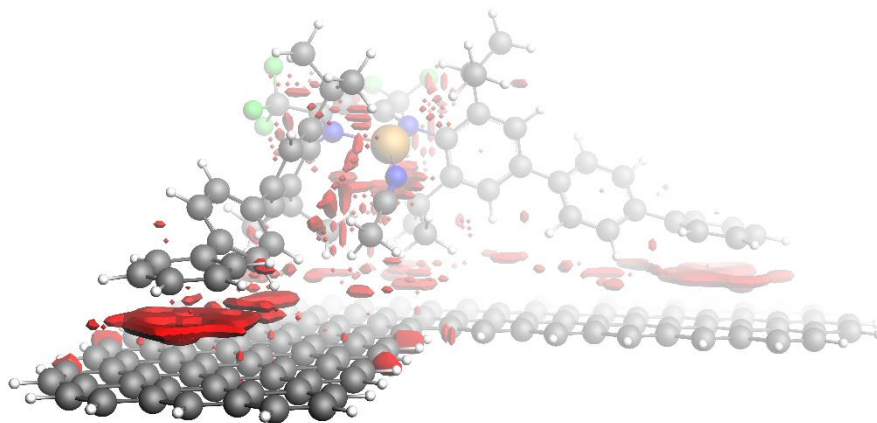


Figure S124. Optimized structure of $[\text{Cu}^{\text{I}}(\text{L7})(\text{MeCN})]$ anchored via mixed CH- π interactions and π - π stacking onto a graphene layer. The supramolecular interactions are indicated in red. Gray (C), blue (N), white (H), green (F), orange (Cu).

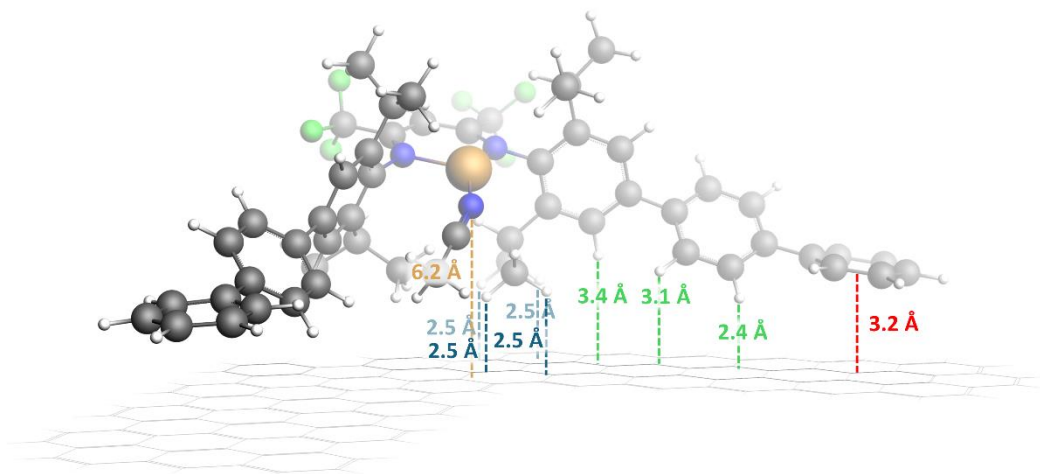


Figure S125. Complex-graphene distances for structure $[\text{Cu}^{\text{I}}(\text{L7})(\text{MeCN})]$ anchored via mixed CH- π interactions and π - π stacking onto a graphene layer. Color code: orange (Cu-graphene), blue (CH- π isopropyl-graphene), green (CH- π phenyl-graphene), red (π - π stacking).

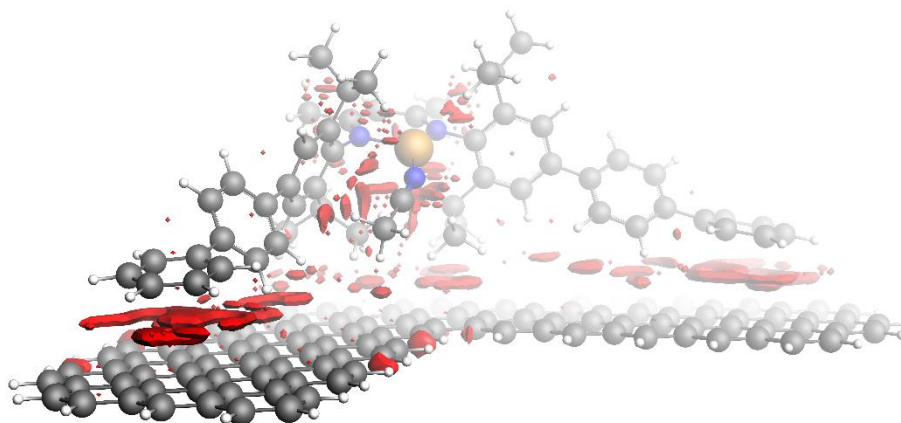


Figure S126. Optimized structure of $[\text{Cu}^{\text{I}}(\text{L10})(\text{MeCN})]$ anchored via mixed CH- π interactions and π - π stacking onto a graphene layer. The supramolecular interactions are indicated in red. Color code: Gray (C), blue (N), white (H), orange (Cu).

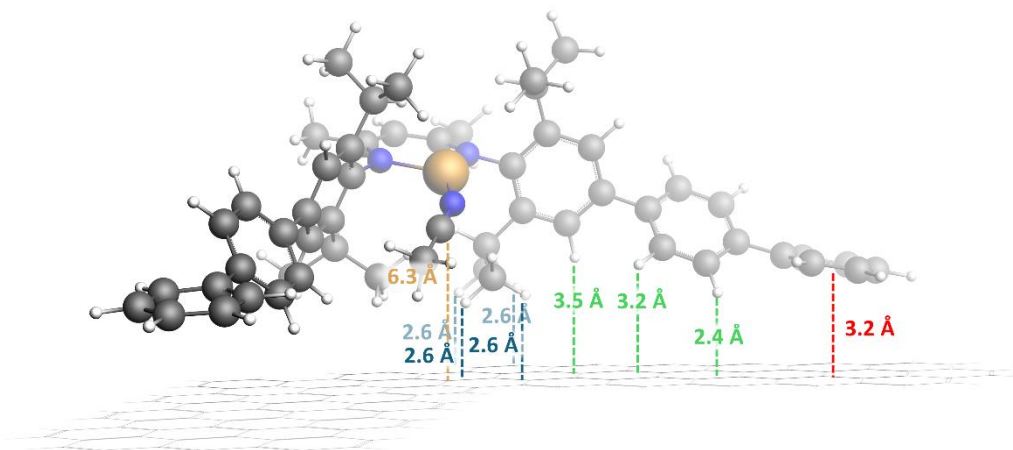


Figure S127. Complex-graphene distances for structure $[\text{Cu}^{\text{I}}(10)(\text{MeCN})]$ anchored via mixed CH- π interactions and π - π stacking onto a graphene layer. Color code: orange (Cu-graphene), blue (CH- π isopropyl-graphene), green (CH- π phenyl-graphene), red (π - π stacking).

The energies obtained from the calculations were used to quantify the anchoring energy, as described by Equation 1:

$$E_{\text{anchoring}} = TBE_{\text{assembled}} - (TBE_{\text{graphene}} + TBE_{\text{cat}}) \quad (1)$$

The anchoring energy ($E_{\text{anchoring}}$) represents the energy contribution responsible for the deposition of the complex onto the graphene layer. TBE_{cat} , TBE_{graphene} , and $TBE_{\text{assembled}}$ are the energies provided by the software for the complex, graphene and the assembled system, respectively.

Since the complexes $[\text{Cu}^{\text{I}}(\text{L7})(\text{MeCN})]$ and $[\text{Cu}^{\text{I}}(\text{L10})(\text{MeCN})]$ have multiple possible anchoring geometries, several values for the anchoring energy were obtained, each corresponding to a different geometry. The energy difference between each anchoring geometry and the most stable one was calculated and expressed as relative energy (E_{rel}), using Equation 2:

$$E_{\text{rel}} = E_i - E_{\text{most stable}} \quad (2)$$

Table S3. Anchoring energies of [Cu^I(L2)(MeCN)], [Cu^I(L7)(MeCN)], and [Cu^I(L10)(MeCN)] on the electrode surface in MeOH as solvent.

Structure	$E_{\text{anchoring}}$ (kcal mol ⁻¹)	E_{rel} (kcal mol ⁻¹)
[Cu ^I (L2)(MeCN)]	-32.9	67.9
[Cu ^I (L7)(MeCN)] (CH- π)	-66.8	34.0
[Cu ^I (L7)(MeCN)] (π - π)	-100.8	0
[Cu ^I (L10)(MeCN)] (CH- π)	-75.0	25.8
[Cu ^I (L10)(MeCN)] (π - π)	-97.6	3.2

Table S4. Anchoring energies of [Cu^I(L2)(MeCN)], [Cu^I(L7)(MeCN)], and [Cu^I(L10)(MeCN)] on the electrode surface in THF as solvent.

Structure	$E_{\text{anchoring}}$ (kcal mol ⁻¹)	E_{rel} (kcal mol ⁻¹)
[Cu ^I (L2)(MeCN)]	-33.2	68.4
[Cu ^I (L7)(MeCN)] (CH- π)	-67.3	34.3
[Cu ^I (L7)(MeCN)] (π - π)	-101.6	0
[Cu ^I (L10)(MeCN)] (CH- π)	-75.5	26.1
[Cu ^I (L10)(MeCN)] (π - π)	-98.2	3.4

The calculations performed in MeOH and in THF show very similar values of the anchoring energies. As expected, ligand **L2** is less suitable for immobilization, as the only anchoring sites are the two isopropyl groups. In contrast, ligands **L7** and **L10** exhibit greater stabilization due to their larger surface area, which allows for more interactions. Additionally, the triphenyl group in these ligands can rotate to lie parallel to the surface, promoting stronger π - π stacking and further enhancing the anchoring energy.

Building on the catalytic cycle proposed by Warren and coworkers in homogeneous conditions,¹² where ammonia replaces acetonitrile in-situ on the copper center, we also calculated the stability of the immobilized structure for the resulting complex. The structures and energy values are presented in Figures S128-S132 and Tables S5 and S6. Comparison of the anchoring energies for the ammonia-substituted complex indicates that the solvent replacement has minimal impact, as the energy values remain virtually unchanged.

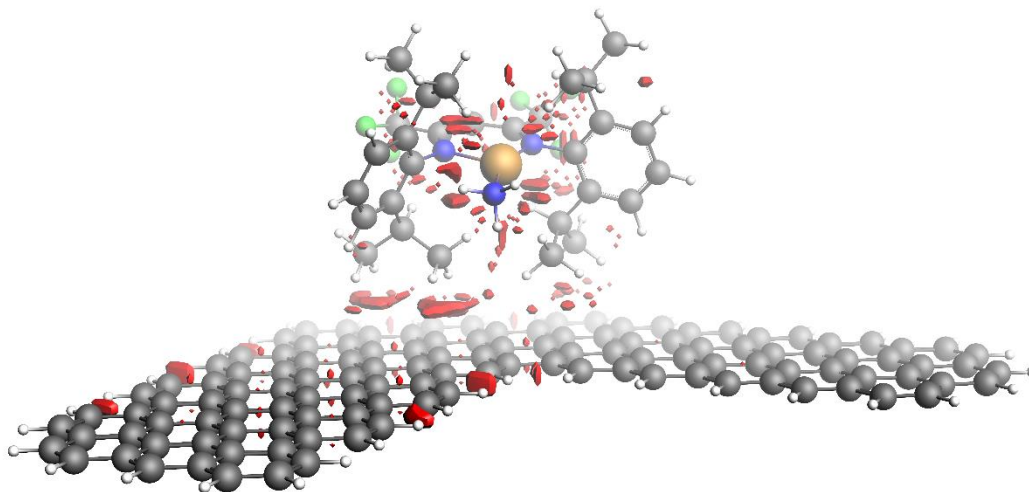


Figure S128. Optimized structure of $[\text{Cu}^{\text{I}}(\text{L2})(\text{NH}_3)]$ anchored via CH- π interactions onto a graphene layer. The supramolecular interactions are indicated in red. Color code: Gray (C), blue (N), white (H), green (F), orange (Cu).

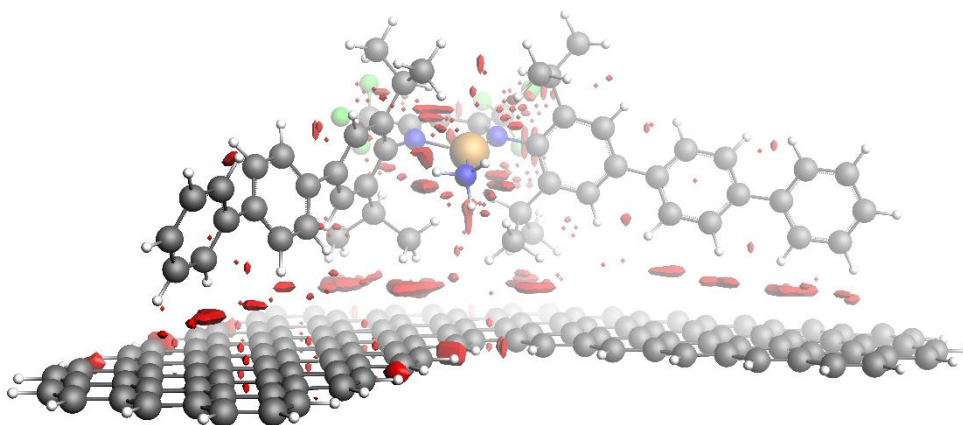


Figure S129. Optimized structure of $[\text{Cu}^{\text{I}}(\text{L7})(\text{NH}_3)]$ anchored via CH- π interactions onto a graphene layer. The supramolecular interactions are indicated in red. Color code: Gray (C), blue (N), white (H), green (F), orange (Cu).

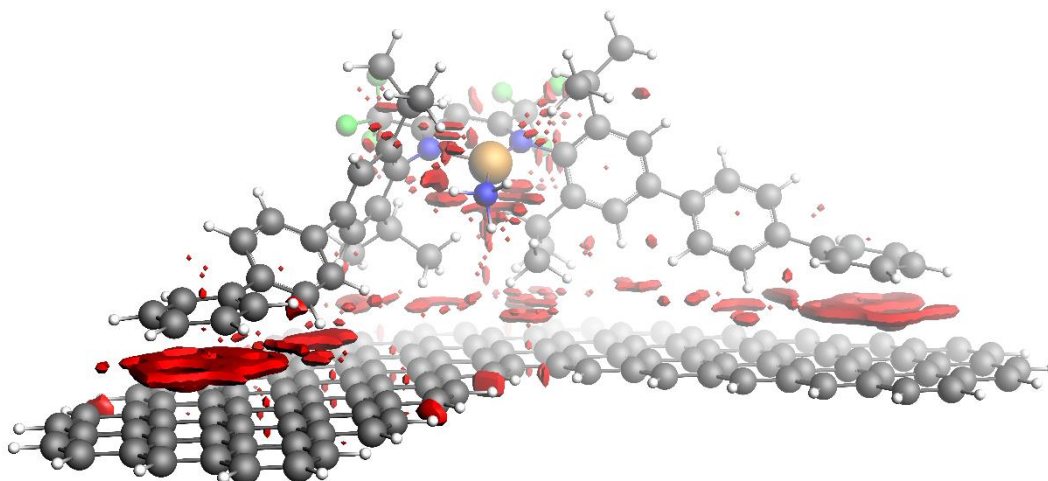


Figure S130. Optimized structure of $[\text{Cu}^{\text{I}}(\text{L7})(\text{NH}_3)]$ anchored via mixed CH- π interactions and π - π stacking onto a graphene layer. The supramolecular interactions are indicated in red. Color code: Gray (C), blue (N), white (H), green (F), orange (Cu).

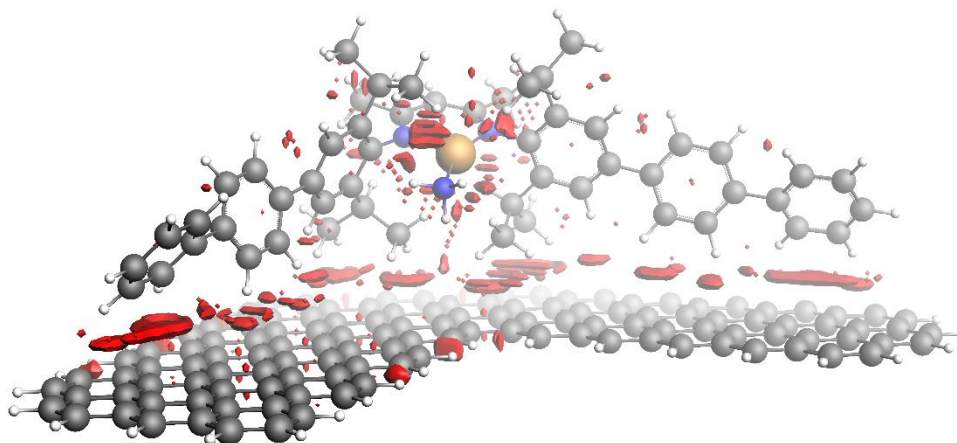


Figure S131. Optimized structure of $[\text{Cu}^{\text{I}}(\text{L7})(\text{NH}_3)]$ anchored via CH- π interactions onto a graphene layer. The supramolecular interactions are indicated in red. Color code: Gray (C), blue (N), white (H), orange (Cu).

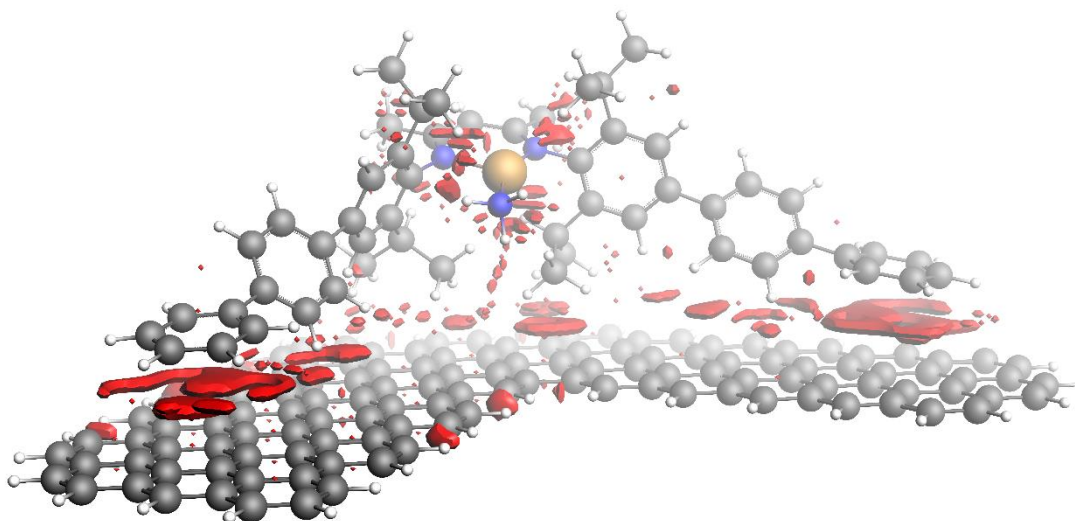


Figure S132. Optimized structure of $[\text{Cu}^{\text{I}}(\text{L7})(\text{NH}_3)]$ anchored via mixed CH- π interactions and π - π stacking onto a graphene layer. The supramolecular interactions are indicated in red. Color code: Gray (C), blue (N), white (H), orange (Cu).

Table S5. Anchoring energies of [Cu^I(L2)(NH₃)], [Cu^I(L7)(NH₃)], and [Cu^I(L10)(NH₃)] on the electrode surface in MeOH as solvent.

Structure	$E_{\text{anchoring}}$ (kcal mol ⁻¹)	E_{rel} (kcal mol ⁻¹)
[Cu ^I (L2)(NH ₃)]	-32.0	66.7
[Cu ^I (L7)(NH ₃)] (CH- π)	-67.5	31.2
[Cu ^I (L7)(NH ₃)] (π - π)	-98.8	0
[Cu ^I (L10)(NH ₃)] (CH- π)	-78.9	19.9
[Cu ^I (L10)(NH ₃)] (π - π)	-96.3	2.5

Table S6. Anchoring energies of [Cu^I(L2)(NH₃)], [Cu^I(L7)(NH₃)], and [Cu^I(L10)(NH₃)] on the electrode surface in THF as solvent.

Structure	$E_{\text{anchoring}}$ (kcal mol ⁻¹)	E_{rel} (kcal mol ⁻¹)
[Cu ^I (L2)(NH ₃)]	-32.3	67.3
[Cu ^I (L7)(NH ₃)] (CH- π)	-68.0	31.5
[Cu ^I (L7)(NH ₃)] (π - π)	-99.5	0
[Cu ^I (L10)(NH ₃)] (CH- π)	-79.2	20.3
[Cu ^I (L10)(NH ₃)] (π - π)	-96.8	2.8

9. References

- 1 Molecular sieve, *ScienceDirect Topics*, <https://www.sciencedirect.com/topics/chemistry/molecular-sieve> (accessed November 22, 2024).
- 2 D. B. G. Williams and M. Lawton, Drying of Organic Solvents: Quantitative Evaluation of the Efficiency of Several Desiccants, *J. Org. Chem.*, 2010, **75**, 8351–8354.
- 3 A. M. Beiler, A. Denisiuk, J. Holub, F.-J. Sánchez-Baygual, M. Gil-Sepulcre, M. Z. Ertem, D. Moonshiram, A. Piccioni and A. Llobet, Heterogeneous Electrochemical Ammonia Oxidation with a Ru-bda Oligomer Anchored on Graphitic Electrodes via CH- π Interactions, *ACS Energy Lett.*, 2023, **8**, 172–178.
- 4 C. Yang, L. Zhang, H. Li, Y. Guo, C. Jia, W. Zhu, F. Mo and X. Guo, Single-Molecule Electrical Spectroscopy of Organocatalysis, *Matter*, 2021, **4**, 2874–2885.
- 5 R. J. Lewis, M. Koy, M. Macino, M. Das, J. H. Carter, D. J. Morgan, T. E. Davies, J. B. Ernst, S. J. Freakley, F. Glorius and G. J. Hutchings, N-Heterocyclic Carbene Modified Palladium Catalysts for the Direct Synthesis of Hydrogen Peroxide, *J. Am. Chem. Soc.*, 2022, **144**, 15431–15436.
- 6 F. Wang, R. Tanaka, Z. Cai, Y. Nakayama and T. Shiono, Room-Temperature Suzuki–Miyaura Cross-Coupling Reaction with α -Diimine Pd(II) Catalysts, *Appl. Organomet. Chem.*, 2015, **29**, 771–776.
- 7 R. B. Muterle, F. Fabri, R. Buffon, W. de Oliveira and U. Schuchardt, Synthesis of a Bis(Diketiminato)Bromosamarium(III) Complex and Its Activity in the Polymerization of Methyl Methacrylate, *Appl. Catal., A*, 2007, **317**, 149–153.
- 8 D. T. Carey, E. K. Cope-Eatough, E. Vilaplana-Mafé, F. S. Mair, R. G. Pritchard, J. E. Warren and R. J. Woods, Structures and Reactions of Monomeric and Dimeric Lithium Diazapentadienyl Complexes with Electrophiles: Synthesis of α -C,C'-Dialkyl- β -Diimines, and Dissolution-Reversible Synthesis of an α -Alkoxyolithium- β -Diimine, *Dalton Trans.*, 2003, 1083–1093.
- 9 Z. Sakhaei, S. Kundu, J. M. Donnelly, J. A. Bertke, W. Y. Kim and T. H. Warren, Nitric Oxide Release via Oxygen Atom Transfer from Nitrite at Copper(II), *Chem. Commun.*, 2017, **53**, 549–552.
- 10 D. J. E. Spencer, N. W. Aboeella, A. M. Reynolds, P. L. Holland and W. B. Tolman, β -Diketiminato Ligand Backbone Structural Effects on Cu(I)/O₂ Reactivity: Unique Copper–Superoxo and Bis(μ -Oxo) Complexes, *J. Am. Chem. Soc.*, 2002, **124**, 2108–2109.
- 11 A. Bakhoda, O. E. Okoromoba, C. Greene, M. R. Boroujeni, J. A. Bertke and T. H. Warren, Three-Coordinate Copper(II) Alkynyl Complex in C–C Bond Formation: The Sesquicentennial of the Glaser Coupling, *J. Am. Chem. Soc.*, 2020, **142**, 18483–18490.
- 12 C. Shimokawa, J. Teraoka, Y. Tachi and S. Itoh, A Functional Model for pMMO (Particulate Methane Monooxygenase): Hydroxylation of Alkanes with H₂O₂ Catalyzed by β -Diketiminatocopper(II) Complexes, *J. Inorg. Biochem.*, 2006, **100**, 1118–1127.
- 13 M. E. Ahmed, M. Raghibi Boroujeni, P. Ghosh, C. Greene, S. Kundu, J. A. Bertke and T. H. Warren, Electrocatalytic Ammonia Oxidation by a Low-Coordinate Copper Complex, *J. Am. Chem. Soc.*, 2022, **144**, 21136–21145.
- 14 *Data Reduction with CrysAlisPro 1.171.43.130*, Rigaku Oxford Diffraction, 2018.
- 15 *Empirical Absorption Correction Using Spherical Harmonics Implemented in SCALE3 ABSPACK Scaling Algorithm*, *CrysAlisPro 1.171.43.130*, Rigaku Oxford Diffraction, 2018.
- 16 *Data Collection with APEX II Version V2013.4-1*, Bruker AXS Inc., Madison, Wisconsin, USA, 2007.
- 17 *Data Reduction with Bruker SAINT Version V8.30c*, Bruker, 2007, Bruker AXS Inc., Madison, Wisconsin, USA.
- 18 *Bruker AXS Inc., SADABS*, version 2012/1, Madison, Wisconsin, USA, 2001; R. H. Blessing, *Acta Crystallogr., Sect. A*, 1995, **51**, 33–38.
- 19 SHELXT; V2018/2, Sheldrick, G. M., *Acta Cryst.*, 2015, **A71**, 3–8.

- 20 OLEX2 Version 1.5-Ac5-024, Dolomanov, O. V.; Bourhis, L. J.; Gildea, R. J.; Howard, J. A. K.; Puschmann, H., *J. Appl. Cryst.*, 2009, **42**, 339–341.
- 21 SHELXL; SHELXL-2018/3, Sheldrick, G. M., *Acta Cryst.*, 2015, **C71**, 3–8.
- 22 CrysAlisPro 1.171.43.114a, Rigaku Oxford Diffraction, 2022. Empirical Absorption Correction Using Spherical Harmonics, Implemented in SCALE3 ABSPACK Scaling Algorithm.
- 23 Inosako, M.; Kunishita, A.; Shimokawa, C.; Teraoka, J.; Kubo, M.; Ogura, T.; Sugimoto, H.; Itoh, S. Reaction of β -Diketiminato Copper(II) Complexes and Na_2S_2 . *Dalton Trans.*, 2008, **44**, 6250–6256.
- 24 TWINABS: Version 2008/4, Bruker AXS Inc., Madison, Wisconsin, USA; Blessing, R. H., *Acta Cryst.*, 1995, **A51**, 33–38.
- 25 O. Salomon, M. Reiher and B. A. Hess, Assertion and Validation of the Performance of the B3LYP* Functional for the First Transition Metal Row and the G2 Test Set. *J. Chem. Phys.*, 2002, **117**, 4729–4737.
- 26 A. D. Becke, Density-Functional Exchange-Energy Approximation with Correct Asymptotic Behavior, *Phys. Rev. A*, 1988, **38**, 3098–3100.
- 27 J. P. Perdew and W. Yue, Accurate and Simple Density Functional for the Electronic Exchange Energy: Generalized Gradient Approximation, *Phys. Rev. B*, 1986, **33**, 8800–8802.
- 28 E. Caldeweyher, S. Ehlert, A. Hansen, H. Neugebauer, S. Spicher, C. Bannwarth and S. Grimme, A Generally Applicable Atomic-Charge Dependent London Dispersion Correction. *J. Chem. Phys.*, 2019, **150**, 154122.
- 29 E. van Lenthe, E. J. Baerends and J. G. Snijders, Relativistic Regular Two-component Hamiltonians, *J. Chem. Phys.*, 1993, **99**, 4597–4610.
- 30 E. van Lenthe, E. J. Baerends and J. G. Snijders, Relativistic Total Energy Using Regular Approximations, *J. Chem. Phys.*, 1994, **101**, 9783–9792.
- 31 E. van Lenthe, A. Ehlers and E.-J. Baerends, Geometry Optimizations in the Zero Order Regular Approximation for Relativistic Effects, *J. Chem. Phys.*, 1999, **110**, 8943–8953.
- 32 A. Klamt, Conductor-like Screening Model for Real Solvents: A New Approach to the Quantitative Calculation of Solvation Phenomena, *J. Phys. Chem.*, 1995, **99**, 2224–2235.
- 33 C. C. Pye and T. Ziegler, An Implementation of the Conductor-like Screening Model of Solvation within the Amsterdam Density Functional Package, *Theor Chem Acc*, 1999, **101**, 396–408.
- 34 E. R. Johnson, S. Keinan, P. Mori-Sánchez, J. Contreras-García, A. J. Cohen and W. Yang, Revealing Noncovalent Interactions, *J. Am. Chem. Soc.*, 2010, **132**, 6498–6506.
- 35 J. Contreras-García, E. R. Johnson, S. Keinan, R. Chaudret, J.-P. Piquemal, D. N. Beratan and W. Yang, NCIPLLOT: A Program for Plotting Noncovalent Interaction Regions, *J. Chem. Theory Comput.*, 2011, **7**, 625–632.
- 36 (a) M. Álvarez-Moreno, C. de Graaf, N. López, F. Maseras, J. M. Poblet and C. Bo, Managing the computational chemistry big data problem: the ioChem-BD platform, *J. Chem. Inf. Model.*, 2015, **55**, 95–103. (b) The data set collection associated with this work is available under the reference DOI: 10.19061/iochem-bd-1-363.